The Chiral Phase Transition of QCD with 2+1 Flavors

A lattice study on
Goldstone modes and universal scaling

Dissertation
zur Erlangung des Doktorgrades
an der Fakultät für Physik
der Universität Bielefeld

vorgelegt von
Wolfgang Unger

August 2010

Gedruckt auf alterungsbeständigem Papier °° ISO 9706

Abstract

This PhD thesis is concerned with the chiral phase transition of QCD with two degenerate light quark masses and a strange quark mass close to its physical value. We analyze the quark mass dependence of the chiral condensate and chiral susceptibilities close to the transition temperature. The analysis is twofold:

First we provide evidence for the influence of thermal fluctuations of Goldstone modes on the chiral condensate at finite temperature. We show that at temperatures below but close to the chiral phase transition at vanishing quark mass this leads to a characteristic dependence of the light quark chiral condensate on the square root of the light quark mass m_l. As a consequence the chiral susceptibility shows a strong quark mass dependence for all temperatures below T_c and diverges like $m_l^{-1/2}$ in the chiral limit. We separately examine the divergence of disconnected and connected parts of the light quark susceptibility and discuss the volume as well as cut-off dependence of susceptibilities and chiral condensates.

Second we analyze the critical behavior of the chiral transition with a scaling analysis based on the O(N) scaling functions. We find strong evidence for 2nd order O(N) scaling in the chiral limit of the light quark mass and with physical strange quark mass. Z(2) scaling is disfavored for finite values of the m_l^c, which indicates that the physical strange quark mass is above the tricritical mass, $m_s^{\rm phys} > m_s^{\rm tric}$. The scaling fits are based on the magnetic equation of state for the chiral condensate. We compare these fit results also with the corresponding scaling functions for the chiral susceptibilities and identify the Goldstone contributions and attempt to identify the connected and disconnected susceptibility contributions. We discuss the deviations from scaling and compare results for two different lattice spacings. Finally we present the result on the pseudocritical line for zero chemical potential and the curvature of the critical line for non-zero chemical potential to lowest order.

Contents

Chapter 1

Introduction: The Phase Diagram of QCD

> "There is a philosophy that says that if something is unobservable – unobservable in principle – it is not part of science. If there is no way to falsify or confirm a hypothesis, it belongs to the realm of metaphysical speculation, together with astrology and spiritualism. By that standard, most of the universe has no scientific reality – it's just a figment of our imaginations." (Leonard Susskind)

Quantum chromodynamics (QCD) describes the interaction of the quarks and gluons, which are the constituents of the hadrons. Since it is a nonabelian gauge theory with gauge group SU(3), also the gluons interact with each other, leading to a rather complex dynamics of the gauge fields. The bare masses of the quarks are small in comparison to the masses of the hadrons that they constitute. Most of the energy that makes hadrons heavy is binding energy. It is stored in the gauge fields and in so-called sea quarks, which are virtual quark-antiquark pairs that are produced and annihilated incessantly.

Hadron physics, the physics of bounded states of quarks, cannot be studied perturbatively. This is because the strong interaction is "strong", which manifests in a comparatively large coupling constant at low energies. Moreover, the coupling increases as the energy scale decreases, leading to the confinement of colors: no individual quarks can be observed, only color neutral combinations of them. On the contrary, for high energies the color charge is anti-screened, as was shown by Gross, Wilzek, and Politzer, which leads to asymptotic freedom, the statement that at high energies the coupling becomes weak. Only at high energies it is possible to study QCD via perturbation theory: The momentum scale has to be large compared to the scale $\Lambda_{\mathrm{QCD}} \simeq 200\mathrm{MeV}$, which is the scale where the gauge coupling $g(Q^2)$ is of order $\mathcal{O}(1)$. At low energies, perturbation theory breaks down as the gauge coupling becomes large. Hence, non-perturbative methods, most prominently lattice QCD, play a crucial role in our understanding of low-energy QCD. This also includes QCD at moderate temperatures.

QCD at finite temperature and density is an interesting subject because hadronic matter is assumed to undergo a phase transition to a new phase of matter, the *quark-gluon plasma* (QGP). We shortly describe the most widely expected scenario of the QCD phase diagram for physical quark masses, as illustrated in Fig. 1: At high temperatures, the quarks are deliberated from confinement and can travel through the strongly interacting plasma without being bound in hadrons. The transition is expected to be a rapid crossover. This transition is expected to become even more pronounced for finite baryon chemical potential μ_B and might eventually reach a critical point $(\mu_{B,c}, T_c)$, where

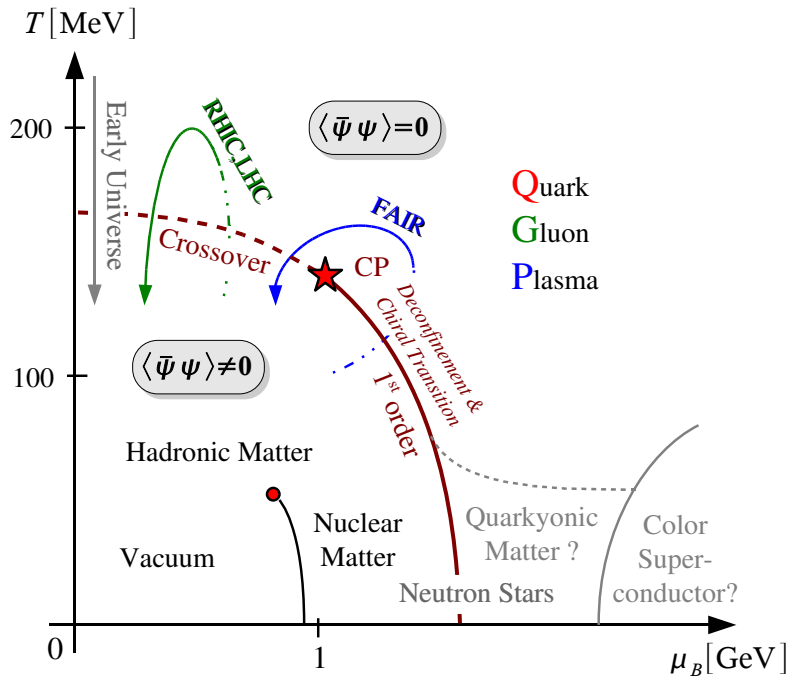

Figure 1.1: Phase diagram of QCD for physical quark masses. Highlighted is the deconfinement and chiral phase transition, which is a crossover for small baryon chemical potential μ_B, and a first order transition for large μ_B. The location of the critical point (CP) is aimed for in lattice simulations as well as experiment (FAIR).

a second order transition takes place. It is believed to be the endpoint of a first order transition for temperatures below T_c along a line $\mu_B^{1st}(T)$, which may extend to zero temperature. At large baryon densities a color superconducting phase is expected which may play a role in the physics of neutron stars. At intermediate densities, even more exotic new states of quark matter have been suggested, for instance *quarkyonic matter* at intermediate densities, which is characterized in the large N_c limit by the dominance of gluons and may lead to "confined" quarks which do not form hadrons.

The investigation of the QCD phase transition is of special interest for at least two reasons:

1. It plays an important role in the physics of the early universe. At the end of the electroweak epoch at about 10^{-12} seconds after the Big Bang, when the fundamental interactions took the form
$$\mathrm{SU}(3) \times \mathrm{SU}(2) \times \mathrm{U}(1), \tag{1.0.1}$$
the QGP dominated the universe. About 10^{-6} seconds after the Big Bang this quark epoch ended and hadronic matter formed.

2. Nuclear matter can be heated up to form a QGP in heavy ion collisions. Such experiments are conducted nowadays at the *Relativistic Heavy Ion Collider* (RHIC) in Brookhaven, the *Large Hadron Collider* (LHC) in Geneva, and will also be performed at the *Facility for Antiproton and Ion Research* (FAIR) in Darmstadt for high baryon densities. At these colliders, the properties of the QGP can be probed. Also the freeze out temperature T_f has been determined, which is the temperature where hadronization takes place and which is a lower bound for the transition temperature.

In fact, in principle there could be two separate phase transitions in QCD:

1. The *confinement-deconfinement transition*, which is characterized by the liberation of quark degrees of freedom, and with the Polyakov loop $\langle L \rangle$ as its order parameter.

2. The *chiral transition*, which is characterized by the restoration of chiral symmetry, and with the chiral condensate $\langle \bar{\psi}\psi \rangle$ as its order parameter. For temperatures below T_ch, chiral symmetry is spontaneously broken, resulting in a non-zero expectation value of $\langle \bar{\psi}\psi \rangle$

There are plenty of speculations that both aspects are linked to each other, and lattice simulations for physical masses indicate that the transition temperatures are very close to each other and may even coincide, $\mathrm{T_{ch}} \simeq T_{\mathrm{dec}}$.

1.1 The Confinement-Deconfinement Transition

The *Polyakov loop*

$$\langle L \rangle = \frac{1}{N_{\mathrm{c}}} \left\langle \mathrm{Tr}\, P \exp\left(i \int_0^{1/T} d\tau A_4(\boldsymbol{x}, \tau) \right) \right\rangle \simeq \exp\left(-F_q(T)/T\right) \tag{1.1.1}$$

represents a static quark, and its logarithm is proportional to the free energy $F_q(T)$ induced by a static quark source. In the quenched limit $m_q \to \infty$, where no dynamical quarks are present, the Polyakov loop becomes a true order parameter: In the confined phase at $T < T_{\mathrm{dec}}$ one finds that $F_q(T)$ is infinite because a colored quark can not be screened. In the deconfined phase at $T > T_{\mathrm{dec}}$, $F_q(T) < \infty$, hence $\langle L \rangle \neq 0$. The deconfinement transition at zero chemical potential for the gauge group SU(3) is expected to be of first order: the center symmetry is Z(3) and it turns out that the transition is of the same order as the three state Potts model. Indeed a first order transition was verified numerically for SU(3) pure gauge theory. However, the global $\mathrm{Z}(N_{\mathrm{c}})$ symmetry gets lost when dynamical quarks are present, the Polyakov loop is no longer a true order parameter but remains non-zero for all temperatures.

The Polyakov loop susceptibility $\chi_L = \langle L^2 \rangle - \langle L \rangle^2$ is not well suited for a precise determination of T_{dec}. Other important observables signaling the confinement-denconfinement transition are the *quark number susceptibilities*, which strongly rise in the transition region. In particular the strange quark number susceptibility is often calculated on the lattice: Strange quarks are suppressed below T_{dec}, as nuclear matter is exclusively composed from up and down quarks, but are pair produced and annihilated as much as the light quarks for high temperatures, leading to a non-zero susceptibility.

The MIT bag model [113] can be used for a rough estimate of the deconfinement transition temperature . It is based on the assumption that hadrons have a constant energy density B (known as the *bag constant*) within the spherical "bag". The ansatz for the full hadron energy is

$$E_H = \frac{4\pi}{3} R^3 B + \frac{C}{R} \tag{1.1.2}$$

with C/R the quark self energy estimated in a harmonic oscillator basis. By minimizing E_H w.r.t. R one obtains the equilibrium radius R_{eq} which is related to the hadron mass M as follows:

$$R_{\mathrm{eq}} = \left(\frac{C}{4\pi B} \right)^{1/4}, \qquad M = \frac{16\pi}{3} R_{\mathrm{eq}}^3 B. \tag{1.1.3}$$

By assuming that the degrees of freedom in the hadronic phase is given by $\nu_{b,\pi} = N_{\mathrm{f}}^2 - 1$ massless pions, and in the plasma phase by $\nu_{b,g} = 2(N_{\mathrm{c}}^2 - 1) = 16$ (spin ± 1) gluons plus $\nu_f = 2N_{\mathrm{c}}N_{\mathrm{f}}$ massless (anti-)quarks, one obtains with $B^{1/4} \simeq 200$ MeV (estimated from the hadron mass) for $N_{\mathrm{c}} = 3$ and $N_{\mathrm{f}} = 2, 3$ a prediction of the critical temperature by equating the pressures of both phases:

$$P = \nu_{b,\pi} \frac{\pi^2 T_{\mathrm{dec}}^4}{90} \stackrel{!}{=} \left(\nu_{b,g} + \frac{7}{4} \nu_f \right) \frac{\pi^2 T_{\mathrm{dec}}^4}{90} - \epsilon_B \quad \Longrightarrow \quad T_{\mathrm{dec}}^{N_{\mathrm{f}}=2} = \left(\frac{45\epsilon_B}{17\pi^2} \right)^{1/4} \simeq 144\mathrm{MeV} \tag{1.1.4}$$

$$T_{\mathrm{dec}}^{N_{\mathrm{f}}=3} = \left(\frac{180\epsilon_B}{79\pi^2} \right)^{1/4} \simeq 139\mathrm{MeV}. \tag{1.1.5}$$

These numbers provide already a good estimate of the transition temperature when compared to lattice results which range between 150 and 190 MeV. It can be compared with the chemical freezeout temperature $T_{\mathrm{f}} = 176(8)$ MeV [27], which is expected to be somewhat smaller than T_{dec}.

1.2 The Chiral Transition

In this work, we will focus on the chiral phase transition for zero baryon chemical potential. For physical quark masses (m_u, m_d, m_s), chiral symmetry is explicity broken. However, the light quark masses turn out to be small enough such that the light quark chiral condensate remains an approximate order parameter. In lattice simulations they are usually taken to be degenerate, $m_l \equiv m_u = m_d$. For these masses, no true phase transition has been found on the lattice, but a rapid crossover. Although the chiral transition temperature $T_{\rm ch}$ for physical quark masses has been investigated extensively in the past by different groups, no quantitative agreement in its precise value has been reached so far (for a recent discussion see [19]). The main focus of this work however is not the precise determination of $T_{\rm ch}$, but the *universality class* of the transition in the chiral limit of the light quarks, based on a scaling analysis.

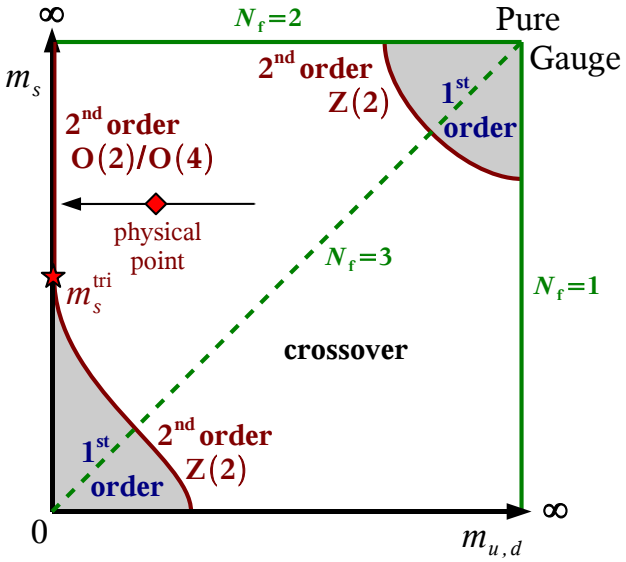

Figure 1.2: Columbia plot: The expected phase diagram in the plane of quark masses for zero chemical potential. The physical point is characterized by the physical masses (m_l, m_s) and is located in the crossover region. The arrow indicates the chiral limit in m_l we are interested in.

It is well known that the order of the transition crucially depends on the quark masses. The famous Columbia plot, Fig. 1.2, sketches the expected behavior for zero chemical potential [21]. The current understanding of this phase diagram is as follows:

- A first order transition is expected for $N_{\rm f} = 3$ degenerate massless quarks [100].
- The first order behavior of the transition for three light quarks should end at some critical quark mass $m_s^c(m_{u,d})$, where a *second order transition* occurs. Beyond this *critical line*, the transition becomes a crossover. It was shown [75] that for $N_f = 3$ the second order transition at m_q^c belongs to the universality class of the Ising model, controlled by a global $Z(2)$ symmetry. However, the location of this point in terms of the physical mass is not well determined yet.
- The physical point of realistic quark masses is expected to be in the crossover regime.
- In the chiral limit of $N_{\rm f} = 2$ the global symmetry group is most likely $\mathrm{SU}(2)_L \times \mathrm{SU}(2)_R \simeq \mathrm{O}(4)$, in analogy with the σ model a second order transition is expected. However, the O(4) critical exponents could not yet be verified unambiguously.
- The location of the tricritical point $m_s^{\rm tric}$, separating a regime of Z(2) critical behavior from a regime of O(4) behavior, is unknown, and it is not even clear whether it exists or whether the Z(2) critical line extends to infinite m_s. O(4) critical behavior is still expected if the strange quark mass is larger than $m_s^{\rm tric}$. It is one of the key questions whether $m_s^{\rm tric} < m_s^{\rm phys}$.

In this work, we will investigate the universality class of the chiral transition for physical strange quark mass and vanishing light quark masses. In lattice simulations with staggered fermions we actually expect to find O(2) instead of O(4) scaling for reasons discussed in Sec. 2.1.3 and Sec. 4.4.2.

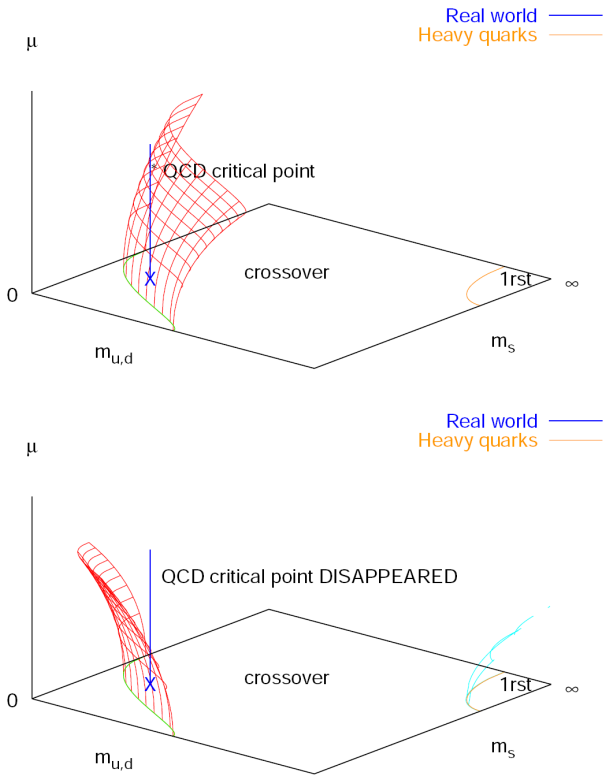

Figure 1.3: The critical surface at finite density: region of second order transition. Two scenarios: positive curvature (top), negative curvature (down). Taken from [46].

For *nonzero quark chemical potential* $\mu = \mu_B/3$ the critical line extends to a *critical surface*. The standard scenario is that for physical masses, there is a critical point at some finite value of μ_c as the critical surface bends towards the physical point (see top of Fig. 1.3). The search for this critical point is one of the goals for lattice QCD at finite density, at present only rough estimates exist $\mu_B/T_c \simeq 1-2$, it is however not clear whether the method (estimate of the radius of convergence) is under control. The FAIR collider is assumed to reach temperatures and baryon densities close to the critical point. It may be possible to measure the location of the critical point by an analysis of fluctuations.

It is however not clear whether a chiral critical point exists. The standard scenario has been questioned by de Forcrand and Philipsen [46]. Simulations of staggered fermions for imaginary chemical potential μ and analytic continuation have indicated that the curvature of the critical surface bends away from the physical point and hence there might be no chiral critical point at the physical point for any μ, as is illustrated in the bottom of Fig. 1.3.

The scaling analysis in this work has also implications for the quest of locating the critical point for physical quark masses and non-zero density: if it turns out that the physical strange quark mass is heavy compared to the strange quark mass characterizing the tricritical point, the argument by de Forcrand and Philipsen might be irrelevant as the physical point is too far away from the Z(2) critical line.

1.3 Outline

This thesis is organized as follows: in Chap. 2 we give a short introduction into finite temperature lattice QCD, with special emphasize on the staggered fermion formulation, the improved actions we made use of, and on the RHMC algorithm.

In Chap. 3 we introduce the concepts and methods of the physics of critical phenomena, in particular w.r.t. the O(N) symmetric spin models. We explain the Goldstone effect and the magnetic equation of state and give the parameterization of the O(2) and O(4) scaling functions used in the scaling analysis.

In Chap. 4 we discuss expectations from continuum chiral perturbation theory for QCD with $N_{\rm f} = 2 + 1$ flavors at zero and non-zero temperature, and present calculations of chiral observables within staggered chiral perturbation theory.

In Chap. 5 we present our results on Goldstone scaling and critical scaling for $N_{\rm f} = 2+1$ staggered fermions in the chiral limit of the light quark mass and with a realistic strange quark mass. The analysis is based on two lattice spacings, corresponding to $N_\tau = 4$ and $N_\tau = 8$. The lattice results on Goldstone scaling will be compared with the predictions from staggered chiral perturbation theory. We present fits of the chiral condensate to the O(2) scaling function via the magnetic equation of state and provide evidence that QCD at zero temperature with massless light quarks and a physical strange quark lies in the O(N) universality class. We determine a QCD specific parameter $z_0(m_s)$ and study its impact on the pseudo-critical line.

Chapter 2

Lattice QCD at Finite Temperature

Lattice quantum chromodynamics (LQCD), which was initiated by Wegner [118] and Wilson [124] in the first half of the 1970ties, is one of the important approaches to study the low energy regime of QCD. In the last decades, a rich body of methods has been developed to improve on the numerical results obtained from Monte Carlo simulations, which established the field in particle physics. Important physical quantities such as the masses of the hadron spectrum or the string tension [29] have been successfully determined on the lattice and some have reached an accuracy that allows comparison with experiment.

Finite temperature lattice QCD is an active field in LQCD which investigates the qualitatively new behavior of QCD matter at temperatures comparable or larger than the typical hadron scale. In this chapter, we will give a short introduction into LQCD with emphasis on the thermal aspects.

2.1 Discretization of QCD

We introduce the hypercubic Euclidean lattice by

$$\Gamma_{N_\sigma,N_\tau} = \{n_\mu \in \mathbb{N}^3 \times \mathbb{N} \,|\, n_i < N_\sigma (i = 1 \ldots 3), n_4 < N_\tau\} \tag{2.1.1}$$

and define the *lattice spacing* a as the distance between two neighboring lattice sites. We restrict ourselves to isotropic lattices, i.e. the lattice spacing is independent of the direction. Γ_{N_σ,N_τ} corresponds to the physical volume and inverse temperature

$$V = (aN_\sigma)^3, \qquad T^{-1} = aN_\tau. \tag{2.1.2}$$

The quantum fields live on a torus (Fig. 2.1), since $N_\tau \ll N_\sigma$ they strongly feel the boundary conditions in the temporal direction.

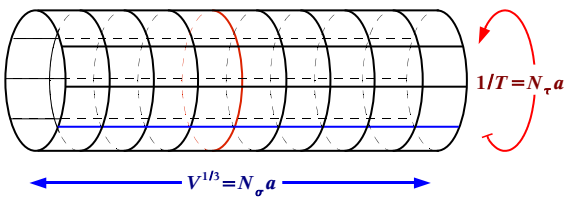

Figure 2.1: Lattice discretization for finite temperature QCD, here only shown in 1+1 dimensions. Periodicity in N_σ is not shown.

In lattice calculations we are forced to use only dimensionless quantities, and thus we need a scheme which translates the lattice quantities into physical quantities. The physical unit at hand for this task is the lattice spacing a, which sets a scale for length and mass quantities:

$$\begin{aligned} x_\mu &\leftrightarrow n_\mu = x_\mu/a, & m &\leftrightarrow \hat{m} = ma, \\ A_\mu(x) &\leftrightarrow \hat{A}_\mu(n) = A_\mu(an)a, & \psi_\alpha(x) &\leftrightarrow \hat{\psi}_\alpha(n) = \psi_\alpha(an)a^{3/2}, \\ \int d^4x \circ &\leftrightarrow a^4 \sum_n \circ & \mathcal{D}\psi &\leftrightarrow \prod_n d\hat{\psi}_\mu(n) \equiv [d\hat{\psi}]. \end{aligned} \tag{2.1.3}$$

Quantities in lattice units will be denoted with a hat in order to distinguish them from their continuum counterparts. Moreover, we will indicate directions on the lattice by the unit vector $\hat{\mu} = \hat{e}_\mu$. The lattice spacing will depend on the gauge coupling, characterized by a renormalization group equation which we will discuss in detail in Sec. 5.2.2.

2.1.1 The Lattice QCD Partition Function

LQCD can be regarded as a regularized version of continuum QCD, based on a hypercubic lattice in position space on which the degrees of freedom are distributed. The inverse lattice spacing provides the momentum cut-off. However, the lattice is not only an approximation to the continuum.[1] Rather one should adopt the point of view of the Wegner/Wilson formulation and consider LQCD as a statistical model of a classical theory. This is evident within the path integral formalism by making use of analytic continuation from Minkowski space to Euclidean space, which transforms the path integral into a partition function:

$$\mathcal{Z}(V,T) = \int [dU][d\hat{\psi}][d\bar{\hat{\psi}}] e^{-S_E[U,\hat{\psi},\bar{\hat{\psi}}]}, \qquad [dU] = \prod_{n,\mu} dU_\mu(n), \tag{2.1.4}$$

$$S_E[U,\hat{\psi},\bar{\hat{\psi}}] = \int_0^{1/T} d\tau \int_V d^3x \mathcal{L}_E(U,\hat{\psi},\bar{\hat{\psi}}) = S_G[U] + S_F[U,\hat{\psi},\bar{\hat{\psi}}] \tag{2.1.5}$$

where the *link variables* $U_\mu(n) \in \mathrm{SU}(N_\mathrm{c})$ given by

$$U_\mu(n) \equiv \exp\left(i\hat{A}_\mu(n)\right) = \overset{n \quad n+\hat{\mu}}{\bullet\longrightarrow\bullet}\,, \qquad U_\mu^\dagger(n) = \overset{n \quad n+\hat{\mu}}{\bullet\longleftarrow\bullet}\,, \qquad U_\mu(n)U_\mu^\dagger(n) = \mathbb{1} \tag{2.1.6}$$

are the parallel transports between two neighboring sites $(n, n+\hat{\mu})$ and are placed on the edges of the lattice, whereas the fermionic degrees of freedom $\bar{\hat{\psi}}(n)$, $\hat{\psi}(n)$ live on the sites. This partition function enables us to do calculations on a computer. Eq. (2.1.4) is a finite multiple integral. Clearly it is not feasible to evaluate these integrals by ordinary numerical methods because of the immense number of degrees of freedom of $\mathcal{O}\left(10^6\right)$. Hence the integrals are evaluated via statistical methods explained in Sec. 2.3.

It is not straight forward to put fermions on a computer due to the Grassmanian nature of the fermionic degrees of freedom in the path integral. Luckily the fermionic degrees of freedom can be integrated out such that the fermionic action becomes a function of the link variables only:

$$S_F[U,\hat{\psi},\bar{\hat{\psi}}] = \int_0^{1/T} d\tau d^3x \sum_{q=u,d,s} \bar{\hat{\psi}}_q M_q[U] \hat{\psi}_q = \int_0^{1/T} d\tau d^3x \sum_{q=u,d,s} \log\left(\det M_q[U]\right), \tag{2.1.7}$$

$$\mathcal{Z}(V,T) = \int [dU] \prod_{q=u,d,s} \det M_q[U] e^{-S_G[U]} \tag{2.1.8}$$

where $M_q = \not{D} + m_q$ is called the *fermion matrix*. The resulting action is non-local, which makes it very expensive to calculate. The determinant is evaluated by making use of the pseudo-fermion method discussed in Sec. 2.1.3.

2.1.2 The Wilson Action

The lattice action for the gauge part is constructed to reproduce the Euclidean continuum action

$$S_G = \frac{1}{2g^2} \int d^4x \,\mathrm{Tr}\left(F_{\mu\nu}F_{\mu\nu}\right). \tag{2.1.9}$$

[1] It is not always clear whether the continuum limit of a lattice formulation exists.

In order to obtain a gauge invariant[2] lattice action from Eq. (2.1.9), Wilson introduced the so-called *Wilson loop*, which is the color trace over a path ordered product for an integral along the closed path $\mathcal{P}$:

$$U_{\mathcal{P}}(x) = \mathrm{Tr}\left(\mathrm{P}e^{\oint_{\mathcal{P}} A_\mu(x+s\hat{\mu})ds}\right) \tag{2.1.10}$$

The Wilson loop is gauge invariant due to the cyclic property of the trace. The lattice analogue of the Wilson loop is constructed in terms of the link variables $U_\mu(n)$. The smallest non-trivial closed loop on the lattice is the so-called *elementary plaquette*

$$P_{\mu\nu}(n) = U_\mu(n)U_\nu(n+\hat{\mu})U_\mu^\dagger(n+\hat{\nu})U_\nu^\dagger(n) = \quad \hat{\nu} \tag{2.1.11}$$

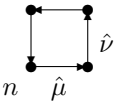

which obeys $P_{\mu\nu}^\dagger = P_{\nu\mu}$. The operator which is invariant under the local gauge transformation

$$U_\mu(n) \xrightarrow{\text{g.t.}} \Lambda(n)U_\mu(n)\Lambda^{-1}(n+\hat{\mu}), \quad \Lambda(n) \in \mathrm{SU}(N_\mathrm{c}) \tag{2.1.12}$$

is the elementary Wilson loop, obtained by taking the color trace

$$W_{\mu\nu}(n) = \mathrm{Tr}\, P_{\mu\nu}(n) \xrightarrow{\text{g.t.}} W_{\mu\nu}(n), \tag{2.1.13}$$

which serves to define the lattice gauge action. This can be seen by expanding $P_{\mu\nu}(n)$ via the Baker-Campbell-Hausdorff formula $e^A e^B = e^{A+B+\frac{1}{2}[A,B]+\cdots}$:

$$P_{\mu\nu}(n) = \mathbb{1} + iga^2 F_{\mu\nu}(an) - \tfrac{1}{2}g^2a^4F_{\mu\nu}(an)F_{\mu\nu}(an) + \mathcal{O}(a^6), \tag{2.1.14}$$

$$W_{\mu\nu}(n) = N_c - \tfrac{1}{2}g^2a^4\,\mathrm{Tr}\,(F_{\mu\nu}(an)F_{\mu\nu}(an)) + \mathcal{O}(a^6). \tag{2.1.15}$$

Based on these expansions, the *Wilson gauge action* is defined as

$$S_G^{\mathrm{Wil}}[U] = \frac{1}{2g^2}\sum_{n,\mu,\nu} 2\,\mathrm{Tr}\,(\mathbb{1} - P_{\mu\nu}(n)) = \beta\sum_{n,\mu<\nu}\left(1 - \frac{1}{N_\mathrm{c}}\mathrm{Re}W_{\mu\nu}(n)\right), \qquad \beta = \frac{2N_\mathrm{c}}{g^2}, \tag{2.1.16}$$

where β is introduced in order to adopt the notation of statistical physics. This action has indeed the correct continuum limit and lattice artifacts of $\mathcal{O}\left(a^2\right)$:

$$S_G[U] = S_G^{\mathrm{Wil}}[U] + \mathcal{O}(a^2). \tag{2.1.17}$$

2.1.3 Staggered Fermions

Fermion Doubling Problem

Due to their spin 1/2 Dirac structure, fermions are difficult to put on the lattice. The naive discretization of the Euclidean action for **free fermions** of mass m_q

$$S_F = \int d^4x\bar{\psi}(x)(\gamma_\mu\partial_\mu + m_q)\psi(x), \tag{2.1.18}$$

based on the replacements given in Eq. (2.1.3), leads to the *naive lattice action*

$$\begin{aligned} S_F[\bar{\hat{\psi}},\hat{\psi}] &= \sum_{n,\mu;\alpha,\beta}\bar{\hat{\psi}}_\alpha(n)(\gamma_\mu)_{\alpha\beta}\frac{1}{2}\left[\hat{\psi}_\beta(n+\hat{\mu}) - \hat{\psi}_\beta(n-\hat{\mu})\right] + \sum_{n,\alpha}\hat{m}_q\bar{\hat{\psi}}_\alpha(n)\hat{\psi}_\alpha(n) \\ &\equiv \sum_{n,n';\alpha,\beta}\bar{\hat{\psi}}_\alpha(n)\left(M_q(n,n')\right)_{\alpha\beta}\hat{\psi}_\beta(n') \end{aligned} \tag{2.1.19}$$

[2] Wilson required that gauge invariance must not depend on the lattice spacing. This is essential because otherwise it would not be granted that gauge invariance also holds in the continuum limit. Moreover, a gauge invariant formulation is attractive because it does not require any gauge fixing.

where α, β are spinor indices and the derivative is replaced by a symmetric lattice derivative. The second line defines the *fermion matrix* M_q. Problems arise when calculating the free propagator in momentum space, given by the Fourier transform of the inverse of M_q:

$$\tilde{M}_q^{-1}(p) \sim \frac{-i\sum_\mu \gamma_\mu \sin(p_\mu a)/a + m_q}{m_q^2 + \sum_\mu \gamma_\mu \sin^2(p_\mu a)/a^2}. \tag{2.1.20}$$

This propagator has poles in all corners of the Brillouin zone: we do not find excitations only at $(0,0,0,0)$ corresponding to $p_\mu \ll 1/a$, but at all other corners $(\pi/a,0,0,0)$, $(0,\pi/a,0,0),\dots(\pi/a,\pi/a,\pi/a,\pi/a)$ as well. This is called the *fermion doubling problem*: the number of fermions is double for each dimension.

It has been proven by the famous "no go" theorem of Nielsen and Ninomiya [96] that it is impossible to put chiral fermions on the lattice without producing doublers, because it is required that for each quantum number both left- and right-handed fermions are present. There are several lattice fermion formulations which attempt to circumvent the problem, in particular Wilson fermions[3] [32], Ginsparg-Wilson fermions [95], domain wall fermions [48] and Kogut-Susskind or *staggered fermions* [78], which we will consider here.

Staggered Fermion Formulation

The staggered fermion formulation attempts to solve the fermion doubling problem by redistributing the 16 doublers over the adjacent lattice sites of the 2^4 hypercube in a way that reflects the Dirac structure of fermions. Consider the following local transformation of the fermion field:

$$\hat{\psi}(n) = T(n)\chi(n), \qquad \bar{\hat{\psi}}(n) = \bar{\chi}(n)T^\dagger(n), \qquad T(n) = \gamma_1^{n_1}\gamma_2^{n_2}\gamma_3^{n_3}\gamma_4^{n_4} \tag{2.1.21}$$

with γ_μ the Euclidean gamma matrices and $T^\dagger(n)T(n) = \mathbb{1}$. The matrices T allow to diagonalize the gamma matrices via the transformation

$$T^\dagger(n)\gamma_\mu T(n+\hat{\mu}) = \eta_\mu(n)\mathbb{1}, \tag{2.1.22}$$

where $\eta_\mu(n)$ is called the *staggered phase*. In terms of the new fields, the fermion action Eq. (2.1.19) can be rewritten as

$$S_F^{\mathrm{stag}(16)}[\bar{\chi}_\alpha, \chi_\alpha] = \frac{1}{2}\sum_{n,\mu;\alpha}\eta_\mu(n)\bar{\chi}_\alpha(n)\left[\chi_\alpha(n+\hat{\mu}) - \chi_\alpha(n-\hat{\mu})\right] + \sum_{n,\alpha}\hat{m}_q\bar{\chi}_\alpha(n)\chi_\alpha(n), \tag{2.1.23}$$

$$S_F^{\mathrm{stag}(4)}[\bar{\chi}, \chi] = \frac{1}{2}\sum_{n,\mu}\eta_\mu(n)\bar{\chi}(n)\left[\chi(n+\hat{\mu}) - \chi(n-\hat{\mu})\right] + \sum_{n}\hat{m}_q\bar{\chi}(n)\chi(n). \tag{2.1.24}$$

In the second row the Lorentz index $\alpha = 1,\dots 4$ is dropped because the spin diagonalization decouples the four components. This reduces the number of degrees of freedom from 16 to 4 Dirac fermions. The new fermionic fields $\chi(n)$ are one-component fields, the spin structure is reflected by the staggered phases $\eta_\mu(n)$ which are located at the links between the sites and take different values within the 2^4 hypercube which naturally divides the lattice in even and odd sites (sites of even and odd parity):

$$\eta_1(n) = 1, \quad \eta_2(n) = (-1)^{n_1}, \quad \eta_3(n) = (-1)^{n_1+n_2}, \quad \eta_4(n) = (-1)^{n_1+n_2+n_3}. \tag{2.1.25}$$

In the chiral limit, the action (2.1.24) exhibits a residual U(1) symmetry given by the transformation

$$\chi \to e^{i\Gamma_5\theta}\chi, \quad \bar{\chi} \to \bar{\chi}e^{i\Gamma_5\theta}, \qquad \Gamma_5 = (-1)^{n_1+n_2+n_3+n_4} = \begin{cases} 1 & \text{for } n \text{ even} \\ -1 & \text{for } n \text{ odd} \end{cases}. \tag{2.1.26}$$

[3] Wilson fermions are characterized by an irrelevant additional term $S_F^{\mathrm{Wil}} = -\frac{ar}{2}\sum_{n,\nu}\bar{\hat{\psi}}(n)\Delta_\nu\hat{\psi}(n)$ which adds to the doublers a mass term of the cutoff scale $1/a$, hence they become inaccessibly heavy in the continuum limit. r is usually set to 1. The Wilson fermion action is often rewritten in terms of the *hopping parameter* $\kappa = 1/(8+2ma)$ which controls the quark mass m.

The four tastes labeled by the index $t = 1, \dots 4$ can be expressed in the staggered fermion spin⊗taste basis:

$$\hat{\psi}^{\alpha t}(N) = \frac{1}{8}\sum_{\rho}(T(\rho))^{\alpha t}\chi(N+\rho), \qquad n_\mu = N_\mu + \rho_\mu, \qquad \rho_\mu \in \{0,1\}. \tag{2.1.27}$$

Also the fermion action can be rewritten in this basis:

$$S_F[\bar{\hat{\psi}},\hat{\psi}] = \sum_{N,\mu} 8\bar{\hat{\psi}}(N)\left[(\gamma_\mu\otimes\mathbb{1})\hat{\Delta}_\mu + \frac{1}{2}(\gamma_5\otimes\gamma_\mu^*\gamma_5)\hat{\Box}_\mu\right]\hat{\psi}(N) + 16\hat{m}_q\sum_N \bar{\hat{\psi}}(\mathbb{1}\otimes\mathbb{1})\hat{\psi}(N), \tag{2.1.28}$$

$$\text{with} \qquad \hat{\Delta}_\mu\hat{\psi}(N) = \frac{1}{2}\left(\hat{\psi}(N+2\hat{\mu}) - \hat{\psi}(N-2\hat{\mu})\right), \tag{2.1.29}$$

$$\hat{\Box}_\mu\hat{\psi}(N) = \hat{\psi}(N+2\hat{\mu}) + \hat{\psi}(N-2\hat{\mu}) - 2\hat{\psi}(N). \tag{2.1.30}$$

The $\gamma_5\otimes\gamma_\mu^*\gamma_5$ term breaks taste symmetry explicitly at non-zero lattice spacing. The lattice spacing is effectively doubled. However, the fermion doubling problem is only partially solved: The residual four doublers for a given flavor, called the *tastes*, need to be eliminated by an additional trick (see next section).

For **interacting fermions**, the discretization for the covariant derivative results in

$$S_F^{\text{stag}}[\bar{\chi},\chi,U] = \sum_{n,n'}\bar{\chi}_i(n)M_q(n,n';i,j)[U]\chi_j(n'), \tag{2.1.31}$$

$$M_q(n,n';i,j)[U] = \hat{m}_q\delta_{n,n'}\delta_{ij} + \frac{1}{2}\sum_\mu \eta_\mu(n)\left((U_\mu(n))_{i,j}\delta_{n',n+\hat{\mu}} - (U_\mu^\dagger(n))_{i,j}\delta_{n,n'+\hat{\mu}}\right) \tag{2.1.32}$$

with the color indices $i, j = 1, \dots N_c$. The fermion matrix M given above corresponds to the standard action which will need improvement to reduce lattice artifacts. The discussion given here also holds for interacting fermions, only the corresponding expression for the action in the spin⊗spin basis Eq. (2.1.28) is more complicated and involves additional taste symmetry breaking terms.

Rooting and the Pseudo-Fermion Method

As the doubling problem is only partially solved, the four tastes have to be reduced to one to obtain a single flavor of mass m_q. To this end we apply the *fourth root trick*, i.e. we take the fourth root of the fermion determinant in the partition function Eq. (2.1.8), which for $N_\text{f} = 2+1$ flavors with $\hat{m}_l \equiv \hat{m}_u = \hat{m}_d$ results in:

$$\mathcal{Z}(V,T) = \int [dU](\det M_l[U])^{1/2}(\det M_s[U])^{1/4}e^{-S_G[U]}. \tag{2.1.33}$$

Taking the fourth root of the fermion determinant is permissible in the continuum, but on the lattice the method is controversial: it may lead to a partition function which is not in the universality class of the one of QCD. In particular, it averages over left-handed and right-handed modes [30]. However, for 2 light flavors only the square root has to be taken, the number of left-and right handed fermions is equal, and the strange quark might be too heavy to pose serious problems.

The partition function is evaluated by making use of the so-called *pseudo-fermion method*, where the fermion determinant is reexpressed by a path integral over pseudo-fermions, i.e. a bosonic 3-component color field $\boldsymbol{\phi}$:

$$(\det M_q[U])^{N_q/4} = \int [d\boldsymbol{\phi}^\dagger][d\boldsymbol{\phi}]\exp\left(-\boldsymbol{\phi}^\dagger M_q^{-N_q/4}[U]\boldsymbol{\phi}\right) \tag{2.1.34}$$

$$= \int [d\boldsymbol{\phi_e}^\dagger][d\boldsymbol{\phi_e}]\exp\left(-\boldsymbol{\phi_e}^\dagger (M_q^\dagger M_q)^{-N_q/4}\boldsymbol{\phi_e}\right) \tag{2.1.35}$$

with $q = l, s$ and $N_l = 2$, $N_s = 1$. The second identity is based on γ_5-Hermiticity $D^\dagger = \gamma_5 D \gamma_5$, which for staggered fermions implies that the Dirac operator is anti-Hermitian, all eigenvalues are paired or are zero:

$$\not{D}\hat{\psi}_i = i\lambda_i \hat{\psi}_i, \quad \not{D}\gamma_5\hat{\psi}_i = -i\lambda_i\gamma_5\hat{\psi}_i \tag{2.1.36}$$

$$\implies \quad \det M_q = \prod_i (i\lambda_i + m_q) = m_q^\nu \prod_{\text{pairs}} (\lambda_j^2 + m_q^2) \tag{2.1.37}$$

with ν the number of zero-modes. Since the combination $M_q^\dagger M_q$ only connects sites of the same parity, it suffices to restrict the pseudofermion field on the even sites, $\boldsymbol{\phi} \to \boldsymbol{\phi_e}$ (or alternatively odd sites) only. The method allows to make use of the heatbath update for the pseudo-fermion field.

2.2 Improved Actions

In practice, lattice simulations at finite temperature are performed on rather coarse lattices due to the high computational costs: The choice of the lattice spacing $a = 1/(N_\tau T)$ is constrained by the range of the temperature to be considered (here, $T \approx T_{\text{ch}}$) and N_τ. However, the aspect ratio should not be too small on isotropic lattices, $N_\sigma/N_\tau \geq 4$, and the typical correlation lengths should fit on the lattice to avoid finite size effects, i.e. $L = N_\sigma a > \xi$. Hence, to reduce the lattice spacing at a given temperature often requires to increase the number of lattice points drastically, which is limited by computer resources. Coarse lattices however are problematic because one might be outside the region where continuum extrapolations on a set of given N_τ data would yield reasonable results. Hence it is mandatory to reduce lattice artifacts in the lattice action.

There are two types of improvements: (1) Breaking of rotational symmetry, which affects the dispersion relation and needs improvement both in the gauge and fermionic part of the action, and (2) taste breaking for staggered fermions, which needs improvement in the fermionic part. There are also other types of lattice artifacts which cannot be addressed by improvement, but are related to renormalization, such as additional UV divergent contributions to lattice observables. They are discussed in Sec. 5.2.3.

2.2.1 Gauge Part: Tree-level Improved Symanzik Action

The Wilson gauge action has lattice artifacts at order $\mathcal{O}\left(a^2\right)$. In our simulations we make use of the tree-level improved Symanzik action, which has lattice artifacts of order $\mathcal{O}\left(a^4\right)$. The basic idea of the so-called *tree-level improved actions*[4] is to add a linear combination of gauge invariant terms to the action Eq. (2.1.16), typically Wilson loops of size $n \times m$ in lattice units, which make the lattice artifacts vanish up to the desired order. The Symanzik action [114] is the considerably simplest improved action consisting of two Wilson loops of size 1×1 and 2×1:

$$S_G = \beta \sum_{n,\mu<\nu} \left\{ \frac{5}{3}\left(1 - \frac{1}{N_{\text{c}}}\text{Re}\,\text{Tr}\left(\right.\right.\right. \right. \tag{2.2.1}$$

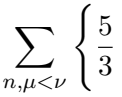

$$\left.\left.\left.\left.\right)\right)\right) - \frac{1}{6}\left[1 - \frac{1}{2N_{\text{c}}}\text{Re}\,\text{Tr}\left(\right.\right.\right.$$

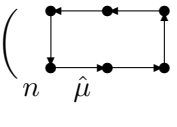

$$\left.\left.\left.\right)\right]\right\}$$

The coefficients $\frac{5}{3}$ and $-\frac{1}{6}$ are chosen such that at tree-level the lattice artifacts vanish at order $\mathcal{O}\left(a^2\right)$.

2.2.2 Fermionic Part: p4fat3 Action

Lattice discretization leads to lattice artifacts which explicitly break the taste- and rotational symmetry. Hence we make use of an improved lattice action, the p4fat3 action. It belongs to the class

[4] The improvement is designed for the classical action but does not account for quantum corrections of higher order.

of tree-level improved actions which lead to small cut-off effects at the one-loop level.[5] Let us first consider taste symmetry: Taste breaking occurs because of the unphysical one-gluon exchange of high momenta $q \approx \pi/a$ between the quarks of a specific taste. This exchange can be reduced by the suppression of high momentum gluons. The strategy used here is a smearing method which consists of *fattening the 1-links gauge terms*: The fat3 actions are flavor improved by fattening the 1-link gauge term in the fermion action with all possible 3-link staples which connect the same neighboring lattice sites:

$$U_\mu^{\text{fat}}(n) = \frac{1}{1+6\omega}\left\{U_\mu(n) + \omega\sum_{\nu\neq\mu} U_\nu(n)U_\mu(n+\hat{\nu})U_\nu^\dagger(n+\hat{\mu}) \right. \\ \left. + U_\nu^\dagger(n-\hat{\nu})U_\mu(n-\hat{\nu})U_\nu^\dagger(n+\hat{\mu}-\hat{\nu})\right\}. \tag{2.2.2}$$

The parameter ω can be adjusted to control the degree of fattening. The improvement achieved hereby is $\mathcal{O}\left(g^2a^2\right)$, and the reduction of taste breaking is of importance to recover the hadronic spectrum (see also Sec. 4.4.1 for details on the so-called taste splittings in the pseudoscalar meson spectrum). We did set $\omega = 0.2$.

But also the rotation symmetry has to be improved, in particular to improve on the dispersion relation $E(\boldsymbol{p})$. At high temperatures, this improvement will be important to reach the Stefan Boltzmann limit for the equation of state faster in the continuum limit. The improvement is achieved via 3-link paths called the Naik term $U_\mu^{(3,0)}$ [93] and the knight moves $U_{\mu\nu}^{(1,2)}$:

$$\begin{aligned} U_\mu^{(3,0)}(n) &= U_\mu(n)U_\mu(n+\hat{\mu})U_\mu(n+2\hat{\mu}), \\ U_{\mu\nu}^{(1,2)}(n) &= \frac{1}{2}\left(U_\mu(n)U_\nu(n+\hat{\mu})U_\nu(n+\hat{\mu}+\hat{\nu}) + U_\mu(n)U_\nu(n+\hat{\nu})U_\nu(n+2\hat{\nu})\right), \\ U_{\mu\nu}^{(1,-2)}(n) &= \frac{1}{2}\left(U_\mu(n)U_\nu^\dagger(n+\hat{\mu}-\hat{\nu})U_\nu^\dagger(n+\hat{\mu}-2\hat{\nu}) + U_\mu^\dagger(n-\hat{\nu})U_\nu^\dagger(n-2\hat{\nu})U_\nu(n-2\hat{\nu})\right). \end{aligned} \tag{2.2.3}$$

With these terms one can construct the fermion action [67]

$$\begin{aligned} S_F = \hat{m}_q\sum_n \bar{\chi}(n)\chi(n) + \sum_{n,\mu}\eta_\mu(n)\bar{\chi}(n)\left\{c_{10}\left[U_\mu^{\text{fat}}(n)\chi(n+\hat{\mu}) - \left(U_\mu^{\text{fat}}\right)^\dagger(n-\hat{\mu})\chi(n-\hat{\mu})\right]\right. \\ +c_{30}\left[U_\mu^{(3,0)}(n)\chi(n+3\hat{\mu}) - \left(U_\mu^{(3,0)}\right)^\dagger(n-3\hat{\mu})\chi(n-3\hat{\mu})\right] \\ +c_{12}\sum_{\nu\neq\mu}\left[U_{\mu\nu}^{(1,2)}(n)\chi(n+\hat{\mu}+2\hat{\nu}) - \left(U_{\mu\nu}^{(1,2)}\right)^\dagger(n-\hat{\mu}-2\hat{\nu})\chi(n-\hat{\mu}-2\hat{\nu})\right. \\ \left.\left. +U_{\mu\nu}^{(1,-2)}(n)\chi(n+\hat{\mu}-2\hat{\nu}) - \left(U_{\mu\nu}^{(1,-2)}\right)^\dagger(n-\hat{\mu}+2\hat{\nu})\chi(n-\hat{\mu}+2\hat{\nu})\right]\right\}. \end{aligned} \tag{2.2.4}$$

In order to get the correct continuum limit, at tree level the coefficients have to fulfill the relation

$$2c_{10} + 6c_{30} + 12c_{12} = 1. \tag{2.2.5}$$

Another condition is obtained by requiring that the free fermion propagator is rotationally invariant up to $\mathcal{O}\left(p^4\right)$:

$$c_{10} + 27c_{30} + 6c_{12} = 24c_{12}. \tag{2.2.6}$$

[5] Fully 1-loop improved (perfect) actions generate a large number of terms, including 4-fermion operators, and are impractical for numerical calculations.

The *p4-action* is characterized by the choice:

$$c_{10} = \frac{3}{8}, \qquad c_{12} = \frac{1}{48}, \qquad c_{30} = 0, \tag{2.2.7}$$

whereas the *Naik-action* is given by the choice:

$$c_{10} = \frac{9}{4}, \qquad c_{12} = 0, \qquad c_{30} = -\frac{1}{48}. \tag{2.2.8}$$

Compared to other improved actions for staggered fermions, such as the stout action [92], the asqtad action [98] and the HISQ action [45], the inversion of the fermion matrix for the p4fat3 action is comparatively expensive. This is because of the large number of knight move hopping terms. We emphasize that the improvement of p4fat3 is focused on the dispersion relation — even the $\mathcal{O}\left(a^4\right)$ violations are small [99] — at the expense of flavor symmetry improvement. The various actions are compared in Tab. 2.1.

fermionic	terms		improvement		computational	
action	add. terms	fattening	rotation	taste	costs	remarks
p4fat7	knight	fat7	high	medium	very high	
p4fat3	**knight**	**fat3**	**high**	**low**	**high**	
HISQ	Naik	multilevel	medium	high	high	tadpole imp., reunit.
asqtad	Naik	fat7	medium	medium	medium	tadpole improved
Naikfat3	Naik	fat3	medium	low	medium	
stout	none	multilevel	none	none	low	reunitarization
standard	none	none	none	none	low	

Table 2.1: Comparison of some improved actions for staggered fermions, rough estimates of computational costs, which however depend on the chosen quark masses. Multilevel smearing applies the fattening procedure more than once. The HISQ and stout action reunitarize the fattened link to an SU(3) element.

2.3 The RHMC Algorithm

We make use of the *Rational Hybrid Molecular Dynamics Algorithm* (RHMC) [69, 26], which allows to simulate staggered fermions for an arbitrary number of flavors due to a *rational approximation* of the power $n_q \equiv N_\mathrm{q}/4$ of the fermion determinant:

$$(\det M_q)^{n_q} = \int [d\boldsymbol{\phi_e}^\dagger][d\boldsymbol{\phi_e}] e^{-\boldsymbol{\phi_e}^\dagger (M_q^\dagger M_q)^{-n_q} \boldsymbol{\phi_e}} \simeq \int [d\boldsymbol{\phi_e}^\dagger][d\boldsymbol{\phi_e}] e^{-\boldsymbol{\phi_e}^\dagger R^{(n_q)}(M_q^\dagger M_q) \boldsymbol{\phi_e}}, \tag{2.3.1}$$

$$R^{(n_q)}(M_q^\dagger M_q) = \bar{c}_0 \prod_i \frac{M_q^\dagger M_q - \bar{\gamma}_i}{M_q^\dagger M_q - \bar{\beta}_i} = \bar{c}_0 + \sum_{i=1}^{d} \frac{\bar{\alpha}_i}{M_q^\dagger M_q - \bar{\beta}_i}. \tag{2.3.2}$$

The rational approximation is obtained from the Remez algorithm and is optimized for the spectrum of the fermion matrix M, which is bounded from below by the lowest eigenvalue $\lambda \sim \hat{m}_q^2$. The partial fraction decomposition allows to make use of a *multishift solver* in the matrix inversions [71, 47], which evaluates the inversion for all shifts at the cost of the smallest shift. Nevertheless, since the conjugate gradient used for the inversion converges slower with decreasing quark mass the computational costs for the simulation of dynamical fermions increase correspondingly and become infinite in the chiral limit. Hence it is impossible to reach the chiral limit.

The RHMC algorithm consists of the molecular dynamics (MD) evolution and the Metropolis acceptance test. We will briefly discuss both parts.

2.3.1 Monte Carlo Methods

In order to evaluate the high-dimensional integral of the partition function Eq. (2.1.8), we make use of Monte Carlo methods, i.e. we evaluate it stochastically. In particular, we use *importance sampling* to improve on efficiency, i.e. configurations are generated with a probability according to their Boltzmann weight e^{-S_E}. The configurations are sequentially produced in a chain called the Markov process. The algorithm has to be designed such that the Markov chain $C_0 \to C_1 \to C_2 \to \ldots C_i \to \ldots$ is ergodic, i.e. it can move through the full configuration space. In particular it satisfies the following properties [104]:

1. the Markov property: the probability distribution of future states only depends upon the present state, the Markov chain has no memory: $P_{i,i+1} \equiv P(C_i \to C_{i+1})$
2. irreducibility: starting from an arbitrary initial configuration, the probability to reach any other configuration in a finite number of Markov steps is nonzero,
3. aperiodicity: the probability to return after a finite number of Markov steps to the initial configuration is nonzero, independent of the number of Markov steps,
4. positivity: the mean recurrence time of any configuration is finite (i.e. $\sum_{n=1}^{\infty} n p_{ii}^{(n)} = \tau_i < \infty$ with $p_{ii}^{(n)}$ the recurrence probability after n Markov steps).

In virtue of these properties, each equilibrium configuration in a Markov chain is assigned a definite probability $P(C_j)$, which is characterized by

$$P(C_j) = \sum_i P_{i,j} P(C_i) \qquad \text{and} \qquad P(C_j) = \lim_{N\to\infty} \sum_{\{i_k\}} P_{i,i_1} \ldots P_{i_{N-1},j}. \tag{2.3.3}$$

$P(C_j)$ gives the probability to find C_j in equilibrium. The information about any initial state will get lost after a large number of steps. The probabilities $P(C_j)$ are known from the lattice action. In order to recover the above properties, the algorithm producing C_j has to satisfy *detailed balance*, i.e. for all C_i, C_j:

$$P(C_i) P_{i,j} = P(C_j) P_{j,i}. \tag{2.3.4}$$

The RHMC algorithm will satisfy this property. The average of an observable O is then computed by the "time" average

$$\bar{O} = \frac{1}{N} \sum_{n=0}^{N} O\{C_n\}, \tag{2.3.5}$$

which is an approximation to the ensemble average

$$\langle O \rangle = \int [d\boldsymbol{\phi}][d\boldsymbol{\phi}^\dagger][dU] O\{\boldsymbol{\phi}, \boldsymbol{\phi}^\dagger, U\} e^{-S_E[\boldsymbol{\phi},\boldsymbol{\phi}^\dagger,U]}, \qquad \langle O \rangle = \bar{O} + \mathcal{O}\left(\frac{1}{\sqrt{N}}\right) \qquad (N \to \infty), \tag{2.3.6}$$

ensured by a theorem which is based on irreducibility and positivity.

2.3.2 Hybrid Monte Carlo

The *hybrid Monte Carlo* (HMC) algorithm [33] is a combination of a deterministic molecular dynamics (MD) evolution and a stochastic Metropolis acceptance test. From the lattice action, one obtains a fictious Hamiltonian H by introducing for conjugate momenta the gauge fields given by $\pi_{i,\mu} = \pi_{i,\mu}^a t^a$, with i a position index, which allows to reexpress the partition function as

$$\mathcal{Z} = \int [d\pi][d\boldsymbol{\phi_e}][dU] e^{-H[\pi,\boldsymbol{\phi_e},U]}, \qquad H[\pi, \boldsymbol{\phi_e}, U] = \frac{1}{2} \sum_{i,\mu} \operatorname{tr} \pi_{i,\mu}^2 + S[\boldsymbol{\phi_e}, U]. \tag{2.3.7}$$

This is equivalent to the partition function Eq. (2.1.8) up to a normalization factor from integrating out the Gaussian integral over the momenta.

The HMC consists of three steps to generate a new configuration:

1. Momentum and pseudofermion update according to a Gaussian noise.
2. Evolution of the molecular dynamics trajectory in $\tau/\delta\tau$ steps.
3. Metropolis acceptance test to the end of the trajectory which stochastically corrects the stepsize errors.

We will shortly review these steps in turn.

Gaussian Noise

The momenta in Eq. (2.3.7) are Gaussian distributed, hence the initial momenta will be determined by a statistic noise according to a Gaussian noise before MD evolution will take place:

$$P(\pi) \sim \exp\left(-\frac{1}{2}\sum_i \pi_{i,\mu}^2\right). \tag{2.3.8}$$

Likewise, for the pseudo-fermion update one generates a field η and defines the pseudofermion field

$$P(\eta) \sim \exp\left(-\frac{1}{2}\sum_i \eta_i^2\right), \qquad \boldsymbol{\phi_e} = R^{(n_q)}(M^\dagger M)\eta_e, \tag{2.3.9}$$

to obtain the correct weight according to Eq. (2.3.1).

Molecular Dynamics

The evolution of the classical system according to the Hamilton equations for the gauge fields and the momenta is given by:

$$\dot{U}_\mu(n) = i\pi_\mu(n)U_\mu(n), \tag{2.3.10}$$

$$\sum_{n,\mu} \operatorname{tr} \pi_\mu \dot{\pi}_\mu = -\dot{S}_G - \boldsymbol{\phi_e}^\dagger \frac{d(M_q^\dagger M_q)^{-n_q}}{d\tau}\boldsymbol{\phi_e} \tag{2.3.11}$$

with the dot denoting the derivative w.r.t. τ. These EoM are integrated along the time direction τ. The configuration trajectory is characterized by the conservation of energy. The integration proceeds according to the leapfrog scheme, where the gauge field equations (2.3.10) and those for the momenta (2.3.11) are integrated alternating. This leads to small step size errors $\mathcal{O}\left(\delta\tau^2\right)$, which results in a difference δH. Since the contribution of the gauge force, implicitly defined by the rhs of Eq. (2.3.11), is larger and at the same time the cost of the evaluation is smaller as compared to the fermion force, it is reasonable to integrate the gauge force on a finer MD time scale. This is achieved by making use of the *Sexton-Weingarten scheme* [109]: The Hamiltonian is split into a kinetic term and the gauge and fermion part of the action

$$H = T[\pi] + S_G[U] + S_F[U] \tag{2.3.12}$$

and one obtains a composite integrator via

$$U_{FGF}(\delta\tau) = \hat{U}_F\left(\frac{\delta\tau}{2}\right)\left[\hat{U}_G\left(\frac{\delta\tau}{\hat{n}}\right)\right]^{\hat{n}}\hat{U}_F\left(\frac{\delta\tau}{2}\right), \tag{2.3.13}$$

$$\hat{U}_G(\delta\tau) = e^{\frac{\delta\tau}{2}P_G}e^{\delta\tau Q}e^{\frac{\delta\tau}{2}P_G}, \qquad \hat{U}_F(\delta\tau) = e^{\delta\tau P_F}, \tag{2.3.14}$$

where the operators P_G and P_F represent the force terms arising from the gauge and the fermion part of the action and operator Q represents the update of the gauge field. The composite integrator has two time scales δ_τ and $\delta_\tau/\hat{n}$, $\hat{n} \in \mathbb{N}$. In practice we apply 10 gauge field updates per fermion field update. The step size has to be decreased when the quark mass is decreased.[6]

Metropolis Acceptance

In contrast to the R algorithm [59], RHMC is *stochastically exact*, i.e. it is free from step size errors. To correct for step size errors present due to the leapfrog integrator, the configuration C_f generated from C_i along the trajectory is only accepted with a probability

$$P = \min(1, e^{-\delta H}), \qquad \delta H = H_f - H_i. \tag{2.3.15}$$

If the final configuration C_f is rejected, the initial configuration C_i will be stored as the new configuration. Clearly, the acceptance rate should be not too small and not too large to move the Markov chain fast enough through configuration space. This accept/reject step is valid if the MD integrator is reversible, which is satisfied by the leapfrog scheme. Since the energy is extensive in the volume, the acceptance rate will decrease as the volume grows, which requires to adjust the step size in order to maintain a constant acceptance rate. The step size also has to be increased when the quark mass is decreased, because the fermionic part will contribute more to the MD force. This will lead to *critical slowing down*: the computational cost will increase drastically.

The rational approximation used for the Metropolis test is of higher accuracy than for the MD evolution.

2.4 Non-zero Density

2.4.1 Taylor Expansion Method

In our analysis, we will determine the slope of the pseudocritical line w.r.t. the chemical potential μ, hence also LQCD at non-zero density will be shortly addressed in this section. Monte Carlo simulations for nonzero chemical potential μ cannot be directly performed due to the *sign problem*, as the fermion determinant in the partition function

$$Z = \int DU \prod_f \det M_q(\mu) e^{-S_G[U]} \tag{2.4.1}$$

is complex-valued. Different techniques on dealing with the sign problem have been developed. We make use of the *Taylor expansion method* [2, 3] by expanding an observable around $\mu = 0$:

$$\langle \mathcal{O} \rangle = \sum_{n=0}^{\infty} c_{2n} (\mu/T)^{2n}. \tag{2.4.2}$$

CP symmetry of the QCD partition function restricts the expansions to even powers in μ. The Taylor coefficients are obtained from computing ensemble averages of the following type:

$$\frac{\partial}{\partial \mu}\langle \mathcal{O} \rangle = \left\langle \frac{\partial \mathcal{O}}{\partial \mu} \right\rangle + \frac{N_f}{4} \left(\left\langle \mathcal{O} \frac{\partial (\log \det M)}{\partial \mu} \right\rangle - \langle \mathcal{O} \rangle \left\langle \frac{\partial (\log \det M)}{\partial \mu} \right\rangle \right) \tag{2.4.3}$$

For the observables considered in this thesis, all necessary coefficients c_{2n} of the Taylor expansion can then be expressed by the derivatives

$$\mathcal{C}_n = \frac{N_f}{4} \frac{\partial^{n+1} \log \det M}{\partial \mu^n \partial m}, \qquad \mathcal{D}_n = \frac{N_f}{4} \frac{\partial^n \log det M}{\partial \mu^n}. \tag{2.4.4}$$

[6] Another improvement on efficiency is obtained by preconditioning of the fermion matrix. We make use of the Hasenbusch method [65] applied to the ratio of light- and strange quark determinant.

2.4.2 Chiral Condensate at Non-zero Density

We will particularly be interested in the expansion of the chiral condensate w.r.t. the quark chemical potential μ_q:

$$\frac{\langle\bar{\psi}\psi\rangle_q}{T^3} = \left(\frac{N_\tau}{N_\sigma}\right)^3 \frac{\partial \log \mathcal{Z}}{\partial m_q/T} = \sum_{n=0}^{\infty} c_{2n}^{\bar{\psi}\psi} \left(\frac{\mu_q}{T}\right)^{2n}, \qquad c_n^{\bar{\psi}\psi} \equiv \frac{1}{n!} \frac{\partial^n \langle\bar{\psi}\psi\rangle_q / T^3}{\partial(\mu_q/T)^n}\bigg|_{\mu_q=0}. \tag{2.4.5}$$

With the abbreviations (for details see [3])

$$\mathcal{F}_0 = \langle \mathcal{C}_0 \rangle, \qquad \mathcal{F}_2 = \langle \mathcal{C}_2 \rangle + 2\langle \mathcal{C}_1 \mathcal{D}_1 \rangle + \langle \mathcal{C}_0 \mathcal{D}_2 \rangle + \langle \mathcal{C}_0 \mathcal{D}_1^2 \rangle, \tag{2.4.6}$$

$$\mathcal{A}_2 = \langle \mathcal{D}_2 \rangle + \langle \mathcal{D}_1^2 \rangle, \tag{2.4.7}$$

we can identify the lowest Taylor coefficients as:

$$c_0^{\bar{\psi}\psi} = \frac{\langle\bar{\psi}\psi\rangle_q}{T^3}\bigg|_{\mu_q=0} = \frac{N_\tau^2}{N_\sigma^3}\mathcal{F}_0, \tag{2.4.8}$$

$$c_2^{\bar{\psi}\psi} = \frac{1}{2}\frac{\partial^2 \langle\bar{\psi}\psi\rangle_q / T^3}{\partial(\mu_q/T)^2}\bigg|_{\mu_q=0} = \frac{1}{2}\frac{1}{N_\sigma^3}\left(\mathcal{F}_2 - \mathcal{F}_0\mathcal{A}_2\right). \tag{2.4.9}$$

Chapter 3

Critical Phenomena

3.1 Phase Transitions

A thermodynamic system in equilibrium is characterized by a finite set of state variables $y_1, \dots y_n$, such as temperature T and pressure p, $\boldsymbol{y} = (T, p)$, or $\boldsymbol{y} = (T, H)$ in the context of magnetic systems with H the external magnetic field. At a phase transition, the thermodynamic variables of a macroscopic system, such as the susceptibility or the specific heat, undergo a drastic change as a function of $\boldsymbol{y}$. The different phases of the system can be distinguished by macroscopic observables such as the density (for fluids), or the magnetization (for magnetic systems). If the macroscopic observable vanishes at the transition temperature T_t and remains zero in one of the phases,

$$\Phi \begin{cases} = 0 & \text{in phase I} \\ \neq 0 & \text{in phase II} \end{cases}, \tag{3.1.1}$$

then it is called an *order parameter*. Its choice is not always unique, and in some cases there might be known only approximate order parameters.[1] In magnetic systems, the magnetization M is a true order parameter for vanishing H, where a spontaneous magnetization takes place in the ordered phase, as sketched on the right of Fig. 3.1.

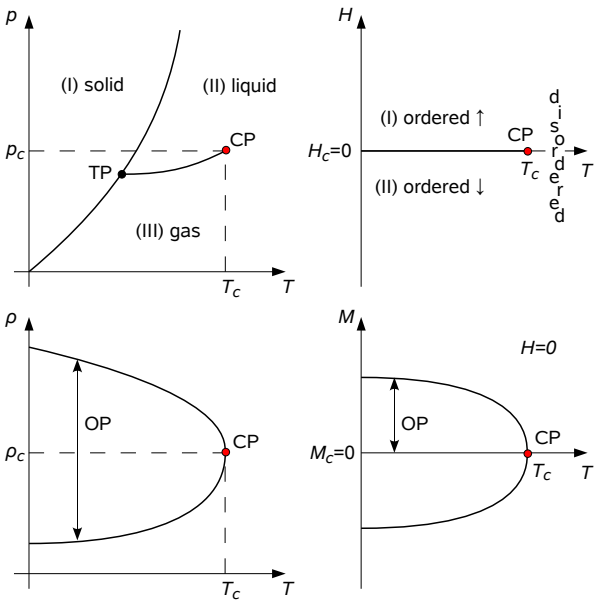

Figure 3.1: Sketch of the phase diagrams (top) and of the order parameter (OP) (bottom) for a fluid (left) and a ferromagnet (right). The solid lines denote a first order transition, the critical point (CP) is characterized by a second order phase transition. The phase diagram of the fluid also features a triple point (TP).

One arrives at a description of critical phenomena by departing from the mircosopic description, given by a Hamiltonian $\mathcal{H}$.[2] From the Hamiltonian, e.g. for the Ising model with $\mathcal{N}$ degrees of freedom on a d-dimensional hypercubic lattice and nearest neighbor interaction between pairs $\langle i, j \rangle$

[1] It depends on the order parameter whether it vanishes (approximately) in the phase above T_t (such as the chiral condensate in QCD), or in the phase below T_t (such as the Polyakov loop).

[2] For fluids, a possible Hamiltonian is $\mathcal{H} = \sum_i \frac{\boldsymbol{p_i}^2}{2m} + \sum_{i<j} V(|\boldsymbol{r_i} - \boldsymbol{r_j}|)$ where the pair interaction is e.g. given by the Lenard Jones Potential $V(r) = 4\epsilon \left((\sigma/r)^{12} - (\sigma/r)^6\right)$. The O(N) spin models are described in detail below.

separated by the lattice spacing a

$$\mathcal{H} = -J \sum_{\langle i,j \rangle} s_i s_j - \tilde{H} \sum_i s_i, \qquad s_i = \pm 1 \tag{3.1.2}$$

with the physical field $\tilde{H}$ and physical nearest neighbor coupling J, one obtains the partition function

$$\mathcal{Z}(T, H, V) = \sum_{\{s_i\}} \exp\left(-\beta \mathcal{H}\right), \qquad \beta = \frac{1}{k_B T}, \quad k_B \equiv 1, \tag{3.1.3}$$

$$\beta\mathcal{H} = -K \sum_{\langle i,j \rangle} s_i s_j - H \sum_i s_i, \qquad K = \beta J, \quad H = \beta \tilde{H}, \tag{3.1.4}$$

now in terms of the dimensionless external field H and the dimensionless coupling K. The free energy density in the finite volume $V = \mathcal{N} a^d$

$$f(T, H, V) = -\frac{1}{V} \log Z(T, H, V) \tag{3.1.5}$$

contains the complete information of the thermal system. Macroscopic observables are characterized as thermal averages via

$$\langle \mathcal{O} \rangle = \sum_{\{s_i\}} \mathcal{O}(\{s_i\}) P(\{s_i\}), \qquad P(\{s_i\}) = \frac{\exp\left(-\beta\mathcal{H}\right)}{\sum_{\{s_i\}} \exp\left(-\beta\mathcal{H}\right)}. \tag{3.1.6}$$

Here, P is a probability distribution which is essentially the normalized Boltzmann factor. Eq. (3.1.6) allows to study macroscopic observables such as the magnetization

$$M \equiv \langle \mathcal{M} \rangle = -\frac{\partial f(T, H, V)}{\partial H}, \qquad \mathcal{M} = \frac{1}{V} \sum_i s_i, \tag{3.1.7}$$

which is also given by the derivative of the free energy w.r.t. the external field. In a finite volume, the free energy is an analytic function. In the *thermodynamic limit* $V \to \infty$ ($\mathcal{N} \to \infty$, a fixed), the free energy remains analytic if the system is governed solely by short range interactions. However, if the interaction range becomes infinite for certain values of $\boldsymbol{y}$, the free energy might develop a non-analyticity in the thermodynamic limit. This non-analyticity, which is signaled by a discontinuity in one of the derivatives of f, characterizes a true phase transition.

3.1.1 Classification of Phase Transitions

Each phase is described by its own chemical potential $\mu_I(\boldsymbol{y})$, $\mu_{II}(\boldsymbol{y})$, ..., which is given by the derivative of the internal energy w.r.t. the particle number[3] in the phase, at fixed entropy S, fixed volume V and fixed number of particles $\mathcal{N}_j$ in all other phases:

$$\mu_i(\boldsymbol{y}) = \left(\frac{\partial U}{\partial \mathcal{N}_i}\right)_{S,V,\mathcal{N}_{j\neq i}}, \qquad i = I, II, \ldots \tag{3.1.8}$$

Here we will restrict to thermally driven phase transitions, where the order parameter vanishes at the *transition temperature* T_t. We have two separate phases, one below T_t (denoted by "-") and one above T_t (denoted by "+"). A phase transition occurs because at T_t, the two phases compete with each other and interchange particles in order to minimize the chemical potential. It is characterized by the equilibrium of the chemical potentials: $\mu_+(\boldsymbol{y_t}) = \mu_-(\boldsymbol{y_t})$. In general, for two state variables

[3] More generally, we may speak of degrees of freedom.

y_1, y_2 and order parameter Φ, the Clausius-Clapeyron equation implies for the transitions in the phase diagram spanned by y_1, y_2:

$$T_t \Delta\Phi \frac{dy_2(y_1)}{dy_1} = T_t(s^+ - s^-) = \epsilon^+ - \epsilon^- = q \tag{3.1.9}$$

The quantity q is called *latent heat* and gives the amount of energy released or absorbed at the transition, the derivative of $y_2(y_1)$ characterizes the slope of the coexistence line in the phase diagram, $s^\pm$ is the entropy density and $\epsilon^\pm = f + T_t s^\pm$ the energy density at the phase boundary above and below the transition temperature T_t, and $\Delta\Phi = \Phi^+ - \Phi^-$ the gap in the order parameter.

Eq. (3.1.9) motivates the following classification: If the order parameter Φ is discontinuous at T_t ($\Delta\Phi > 0$), the transition is of *first order*. If Φ is continuous at the transition ($\Delta\Phi = 0$), but some higher derivative of Φ is discontinuous, it is of *second order*, the transition temperature is then called *critical temperature* T_c. It is located at a specific value $\boldsymbol{y_c} = (y_{1,c}, y_{2,c})$ called the *critical point* sitting at the end of a first order line, at which the latent heat vanishes. If none of the derivatives are discontinuous, then f is an analytic function. Also in the absence of any criticality, there might still be rapid change of thermodynamic variables as the system evolves from one phase to another: such transitions are called *crossover transitions*, and the transition temperature is called *pseudocritical temperature* T_pc, which is however not well defined but depends on the choice of the approximate order parameter (which now does not vanish exactly at T_pc).

3.1.2 Second order Transitions and Landau Theory

From now on we will restrict to second order transitions. They are of special interest because the thermal system behaves in a characteristic way independent of the details of the microscopic interactions. In systems which are governed by more than two state variables y_i, critical points may extend to critical lines, or even critical (hyper-)surfaces. The free energy density can be decomposed into a regular part and a singular part:

$$f(\boldsymbol{y}) = f_\mathrm{reg}(\boldsymbol{y}) + f_\mathrm{s}(\boldsymbol{u}), \tag{3.1.10}$$

where $\boldsymbol{u}$ are reduced state variables known as *scaling variables*. In the context of magnetic systems, we introduce the reduced variables for the temperature and the external field:

$$t \equiv \frac{T - T_\mathrm{c}}{T_\mathrm{c}}, \qquad h \equiv \frac{\tilde{H} - \tilde{H}_c}{k_B T_\mathrm{c}}. \tag{3.1.11}$$

In most magnetic systems, one has $\tilde{H}_c = 0$ and hence $h = \beta_c \tilde{H}$.

Critical Exponents

Consider the spontaneous magnetization[4] of a magnetic system, e.g. a ferromagnet as shown in Fig. 3.1. On the *coexistence line* ($h = 0$) below the critical temperature and on the *pseudo-critical line* ($t = 0$), the magnetization can be well approximated by a power law, parametrized by so-called *critical exponents*:

$$M \sim \begin{cases} |t|^\beta & \text{for} \quad h = 0,\ t < 0 \\ |h|^{1/\delta} & \text{for} \quad t = 0 \end{cases}. \tag{3.1.12}$$

Also the correlation function[5]

$$G(\boldsymbol{r}, \boldsymbol{r'}) = \left\langle \phi(\boldsymbol{r})\phi(\boldsymbol{r'}) \right\rangle - \left\langle \phi(\boldsymbol{r}) \right\rangle \left\langle \phi(\boldsymbol{r'}) \right\rangle \tag{3.1.13}$$

[4] See section Sec. 3.2.2 for the discussion of spontaneous magnetization.

[5] For the correlation function, we already make use of the continuum formulation introduced below. For finite degrees of freedom: $G_{ij} = \langle s_i s_j \rangle - \langle s_i \rangle \langle s_j \rangle$.

signals the order of the transition: For $T > T_c$ the asymptotic behavior for large distances is given by

$$G(\boldsymbol{r}, \boldsymbol{r'}) \sim \frac{\exp\left(-|\boldsymbol{r} - \boldsymbol{r'}|/\xi(t)\right)}{|\boldsymbol{r} - \boldsymbol{r'}|}, \tag{3.1.14}$$

which is known as *Ornstein-Zernike behavior*. At T_c, the correlation length ξ behaves characteristically: it is finite for a first order phase transition (because the two phases can coexist), and infinite for a second order phase transition. In particular, the correlation function then falls off with a power of $\boldsymbol{r}$, which conventionally is written as

$$G(\boldsymbol{r}, \boldsymbol{r'}) \sim |\boldsymbol{r} - \boldsymbol{r'}|^{-(d-2+\eta)}. \tag{3.1.15}$$

Here, d is the dimension of the system and η is a critical exponent called *anomalous dimension*, which indicates the deviation from Ornstein-Zernike behavior. For large distances, another critical exponent is obtained for the correlation length on the coexistence line:

$$\xi \sim \begin{cases} |t|^{-\nu} & \text{for} \quad h = 0,\, t > 0 \\ |t|^{-\nu'} & \text{for} \quad h = 0,\, t < 0 \end{cases}. \tag{3.1.16}$$

An important observable is the *susceptibility*, which characterizes the fluctuation of the order parameter:

$$\chi \equiv \frac{\partial M}{\partial H} = \frac{\beta}{V} \int d^d r d^d r' G(\boldsymbol{r}, \boldsymbol{r'}) = \beta \int d^d r G(\boldsymbol{r}), \qquad G(\boldsymbol{r} - \boldsymbol{r'}) \equiv G(\boldsymbol{r}, \boldsymbol{r'}), \tag{3.1.17}$$

where the second identity shows that the susceptibility is also obtained from the integrated correlation function, due to the *fluctuation-dissipation theorem*, and the last identity holds if translation invariance is imposed. Near T_c it behaves as

$$\chi \sim \begin{cases} |t|^{-\gamma} & \text{for} \quad h = 0,\, t > 0 \\ |t|^{-\gamma'} & \text{for} \quad h = 0,\, t < 0 \end{cases}. \tag{3.1.18}$$

Another important quantity, obtained from the energy density ϵ, is the specific heat:

$$C_H = \left(\frac{\partial \epsilon}{\partial T}\right)_H \tag{3.1.19}$$

On the coexistence line, its critical exponents are defined as follows:

$$C_H \sim \begin{cases} |t|^{-\alpha} & \text{for} \quad h = 0,\, t > 0 \\ |t|^{-\alpha'} & \text{for} \quad h = 0,\, t < 0 \end{cases} \tag{3.1.20}$$

Usually, but not always, the critical exponents for $t < 0$ and $t > 0$ do agree, $\gamma = \gamma'$ etc., but sometimes not all of the exponents are defined (e.g. in the O(N) models for $N > 1$ discussed below, γ' does not exist). In general, the critical exponent κ of a physical quantity $a(t)$ on the coexistence line is given by

$$\kappa = \lim_{|t| \to 0} \frac{\log |a(t)|}{\log |t|}. \tag{3.1.21}$$

If $\kappa = 0$, the observable has a jump singularity. Subdominant corrections to scaling are also expressed via critical exponents:

$$a(t) = A|t|^{\kappa} \left(1 + B|t|^{\omega} + \ldots\right). \tag{3.1.22}$$

Scaling Laws and Scaling Hypothesis

The critical exponents are not independent of each other, but are related via inequalities that can be obtained from thermodynamics:

$$\begin{aligned} &\text{Rushbrooke-Inequality:} && \alpha' + 2\beta + \gamma' \geq 2, && (3.1.23)\\ &\text{Griffiths-Inequality:} && \alpha' + \beta(1+\delta) \geq 2, && (3.1.24)\\ &\text{Widom-Inequality:} && \gamma' \geq \beta(\delta - 1). && (3.1.25) \end{aligned}$$

However, they also can be naturally derived as strict identities by imposing an assumption on the singular part of the free energy called the *scaling hypothesis*:

$$b^{-d} f_{\mathrm{s}}(b^{da_t} t, b^{da_h} h, \ldots) = f_{\mathrm{s}}(t, h, \ldots) \qquad \forall b \in \mathbb{R}. \tag{3.1.26}$$

It is based on the assumption that the correlation length ξ is the only length scale of the thermodynamic system at T_{c}, and it solely determines the singular part of the free energy. Hence, f_{s} has to be a homogeneous function of an arbitrary length scale b. The critical exponents are related to the homogeneity coefficients a_t and a_h as follows:

$$\begin{aligned} &\beta = \frac{1-a_h}{a_t}, && \delta = \frac{a_h}{1-a_h}, && \gamma = \frac{2a_h - 1}{a_t} = \beta(\delta - 1),\\ &\nu = \frac{1}{a_t d} = \frac{\beta(\delta+1)}{d}, && \alpha = 2 - \frac{1}{a_t} = 2 - \beta(\delta+1). && (3.1.27) \end{aligned}$$

Hence there are only two independent critical exponents. For the Ising model and the O(2), O(4) models which we will consider below, they are given in Tab. 3.2.

Universality Hypothesis

We now turn to the question what determines the precise values of the critical exponents. Experimental results have shown that critical exponents agree in many different thermodynamic systems. This observation led to the formulation of the *universality hypothesis*, which is the statement that the critical exponents only depend on

(1) the dimension d of the system,

(2) the range of the interaction and

(3) the dimension N of the order parameter.[6]

At the critical point, thermodynamic systems which agree in these criteria are indistinguishable w.r.t their macroscopic critical behavior, they fall into the same universality class: When the correlation length diverges at T_{c}, the system is dominated by large scale fluctuations which determine the critical behavior, whereas the particular microscopic interactions do not play a crucial role.[7]

[6] For example, the order parameter is N-dimensional in the O(N) model; see below.

[7] There are however exotic models where critical exponents vary with the parameters of the partition function — see e.g. the book of Baxter [10], Chap. 11.

The Landau-Ginzburg-Wilson Hamiltonian

A first attempt to understand second-order phase transitions was the Landau Theory: It postulates that every thermodynamic system, for which the transition is characterized by an order parameter M, there exists a so-called Landau function $F(t, h, M)$ (usually the free energy), such that

(1) the thermodynamics of the system is determined by the minimum of F w.r.t. M,

(2) F is consistent with the microscopic symmetries of the system and

(3) F is analytic.

First, consider the order parameter M to be constant over space. The Landau function can then be expanded in M near the critical point [123]:

$$F(t, h, M) = F_0(t, h) + V\left\{-hM + \frac{1}{2}a(t, h)M^2 + \frac{1}{4}b(t, h)M^4 + \mathcal{O}\left(M^6\right)\right\}. \tag{3.1.28}$$

This expansion is well defined since M is small near the critical point. Note that in order the global minimum to be defined, $b(t, h)$ has to be positive.

We have implicitly assumed that the Hamiltonian is invariant under parity at $h = 0$, which requires the expansion of $F(t, h, M)$ to have even powers of M only. The value of the order parameter at thermal equilibrium is given by the minimalization condition

$$\frac{\partial F(t, h, M)}{\partial M} = 0, \qquad \frac{\partial^2 F(t, h, M)}{\partial M^2} > 0. \tag{3.1.29}$$

The typical behavior of the Landau function as a function of the order parameter M below and above the critical temperature is given in Fig. 3.2. For $h = 0$ and $a(t) > 0$, $b(t) > 0$, the system is in the non-ordered phase, the trivial solution is $M = 0$. For $h = 0$ and $a(t) < 0$, $b(t) > 0$, the system is in the ordered phase, the solution for $t < 0$ is $M = \sqrt{-a(t)/b(t)}$. Based on the approximation $a(t) \approx \alpha t$, $b(t) \approx b$, we obtain

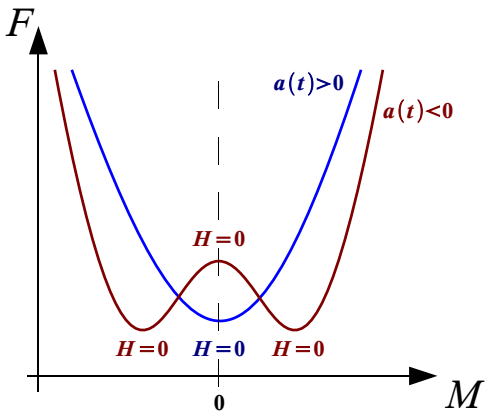

Figure 3.2: Sketch of the behavior of the Landau function below T_c ($a(t) < 0$) and above T_c ($a(t) > 0$).

$$M = \begin{cases} \pm\sqrt{-\alpha t/b} & t < 0 \\ 0 & t > 0 \end{cases} \tag{3.1.30}$$

and read off the mean field critical exponent $\beta = \frac{1}{2}$. Now, consider the order parameter to vary over space: $M = \langle\phi(\boldsymbol{r})\rangle$, which requires to translate the lattice formulation to the continuum formulation.[8] This can be achieved by making use of Gaussian integrals, and one obtains the *Landau-Ginzburg-Wilson Hamiltonian*

$$\mathcal{H}_{\mathrm{LGW}}[t, h, \phi] = \int d^d r \left\{\frac{1}{2}|\nabla\phi(\boldsymbol{r})|^2 + \frac{r_0(t)}{2}\phi^2(\boldsymbol{r}) + \frac{u_0(t)}{4!}\phi^4(\boldsymbol{r}) - H(\boldsymbol{r})\phi(\boldsymbol{r})\right\}, \tag{3.1.31}$$

where $r_0(t)$ corresponds to a mass squared in the Euclidean field theory which is negative below T_c, and $u_0(t)$ is a quartic coupling. The corresponding partition function now takes the form of an

[8] The microscopic degrees of freedom are effectively smeared out, which leads to the replacements $s_i \to K^{-1/2}\phi(\boldsymbol{r})$, $H \to HK^{1/2}$, with $K = \beta J$ the coupling constant of the discrete system. The relation to $\mathcal{H}_{\mathrm{LGW}}$ introduced below is given by $r_0 = (2 - 4d)/K - 2d$, and $u_0(t) = 4!\lambda/K^2$ corresponds to a quartic coupling of spins not considered above.

Euclidean path integral:

$$\mathcal{Z}[t,h] = \int [d\phi]\, e^{-\mathcal{H}_{\mathrm{LGW}}[t,h,\phi]}. \tag{3.1.32}$$

This Hamiltonian is the starting point of Landau theory, which demands that the thermodynamics of the system is characterized by the minimum of $\mathcal{H}_{\mathrm{LGW}}$ w.r.t. ϕ. This condition is known as *Landau Approximation* (also called *Mean Field Approximation*):[9]

$$\frac{\delta \mathcal{H}_{\mathrm{LGW}}[t,h,\phi]}{\delta \phi} = 0. \tag{3.1.33}$$

Instead of evaluating the partition function Eq. (3.1.32), one makes use of the Euler-Lagrange equations to obtain the equilibrium solution ϕ_{eq}. The free energy is then given by $\mathcal{H}_{\mathrm{LGW}}[t,h,\phi_{\mathrm{eq}}]$. This approach gives a good description of the low temperature physics. At the critical point however, where the fluctuations of ϕ are large, this approximation breaks down.[10]

Classical magnetic systems	Euclidean field theory
Spin variables	Fields
Magnetic field	Source
Hamiltonian	Euclidean action
Sum over spin configurations	Functional integral
Magnetization	Field vacuum expectation value
Magnetic susceptibility	Zero momentum two-point function
Inverse correlation length	Physical mass
Critical theory	Massless theory
Partition function	Generating functional

Table 3.1: Correspondences between classical magnetic systems and the corresponding Euclidean field theory. Taken from [126].

3.1.3 Renormalization Group

The renormalization group approach was invented to give a realistic account of critical phenomena for dimensions $d < 4$, where Landau theory is known to break down. The idea, which goes back to Kadanoff, is to integrate out the degrees of freedom at distances $r \ll \xi$ in position space (which corresponds to a cut-off Λ in momentum space). The original idea, known as *Kadanoff Blockspin Transformation* [72], which is applicable to lattice formulations, was to group the degrees of freedom (d.o.f.'s, here: spins) in blocks, e.g. hypercubes of size 2^d, and assign to each hypercube one d.o.f. determined by the underlying d.o.f.'s within the hypercube, as depicted in Fig. 3.3. In the Ising model, usually a majority rule is applied.

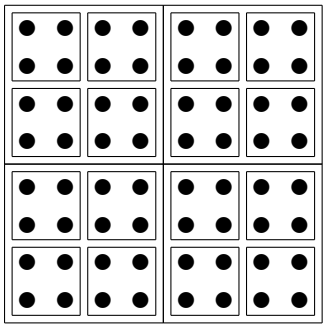

Figure 3.3: Kadanoff blockspins on a planar lattice

[9] In this context, $\mathcal{H}_{\mathrm{LGW}}[\phi]$ is also called the *Ginzburg-Landau Functional*.

[10] Landau theory does not always break down at the critical point: the *Ginzburg criterion* states that it is valid if

$$\int_V d^d r G(\boldsymbol{r}) \ll \int_V d^d r \phi_{\mathrm{eq}}^2 \qquad \Longrightarrow \qquad c|t|^{(d-4)/2} \ll 1.$$

Hence, in the limit $t \to 0$, Landau theory breaks down for dimensions $d < 4$, but remains valid for $d > 4$. In particular, for $d > 4$ the mean field critical exponents are exact.

This procedure is justified by the assumption that the spins are strongly correlated and very likely point in the same direction. However, the coupling between the block spins $K = \beta J$ has to be adjusted accordingly. This is described by a function f, which defines a so-called *renormalization group equation* (RG-eq.): $K_1 = f(K)$.[11] At the same time the correlation length is reduced by a factor of 2, $\xi(f(K)) = \frac{1}{2}\xi(K)$. At $K_c = J/T_c$, the correlation length has to diverge, which implies that K_c is a fixpoint of the RG transformation:

$$\xi(K_c) = \infty, \qquad \xi(f(K_c)) = \infty \qquad \Longrightarrow \qquad f(K_c) = K_c. \tag{3.1.34}$$

At the critical point, the system is *scale invariant*, even though the Hamiltonian does not have this feature. The absence of a characteristic length scale at the critical point is the motivation for the scaling hypothesis, Eq. (3.1.26), and hence is responsible for the appearance of power laws: Close to K_c, the RG-equation can be linearized:

$$f(K) - K_c = \lambda(K - K_c), \qquad \lambda = \frac{df(K)}{dK}. \tag{3.1.35}$$

This allows to determine critical exponents, e.g. ν:[12]

$$\frac{\xi(f(K))}{\xi(K)} = \left(\frac{f(K) - K_c}{K - K_c}\right)^{-\nu} \qquad \Longrightarrow \qquad \nu = \log 2/\log\lambda. \tag{3.1.36}$$

The RG approach has been extended by Wilson [119, 120] to arbitrary (also continuous) systems described by a set of couplings $\boldsymbol{K} = (K_1, K_2, \ldots)$ which enter the Hamiltonian $\mathcal{H}$. He proposed RG transformations (RGT) $\mathcal{R}$ in the space of Hamiltonians consistent with certain symmetry requirements, and which are characterized by the variation with the continuous scale factor l:

$$\frac{\partial\mathcal{H}(l)}{\partial l} = \mathcal{R}\{\mathcal{H}(l)\}, \qquad \frac{\partial\boldsymbol{K}(l)}{\partial l} = \boldsymbol{R}\{\boldsymbol{K}(l)\}. \tag{3.1.37}$$

The *fixed points* are defined by

$$\mathcal{R}(\mathcal{H}^*) = \mathcal{H}^*, \qquad \boldsymbol{R}(\boldsymbol{K}^*) = \boldsymbol{K}^*. \tag{3.1.38}$$

In the RG approach, a *universality class* is defined as the set of all models which flow into the same critical fixed point under RG-transformations. In the vicinity of the fixed points, the RG-equations can be linearized:

$$\mathcal{H}(l) = \mathcal{H}^* + \Delta\mathcal{H}(l) = \mathcal{H}^* + \sum_i u_i(l)\mathcal{O}_i, \tag{3.1.39}$$

$$\boldsymbol{R}(\boldsymbol{K}) = \boldsymbol{K}^* + \Delta\boldsymbol{R}(\boldsymbol{K}) = \boldsymbol{K}^* + Q(\boldsymbol{K} - \boldsymbol{K}^*), \qquad Q_{ij} = \left.\frac{\partial R_i}{\partial K_j}\right|_{\boldsymbol{K}^*}, \qquad Q\boldsymbol{e_i} = e^{\delta l y_i}\boldsymbol{e_i}. \tag{3.1.40}$$

In the RGT of the Hamiltonian, $u_i(l)$ are called the *scaling fields* and $\mathcal{O}_i$ the conjugate *scaling operators*. The RGT of the set of couplings $\boldsymbol{K}$ involves the matrix Q whose eigenvectors $\boldsymbol{e_i}$ form an orthogonal basis: $\boldsymbol{e_i}\cdot\boldsymbol{e_j} = \delta_{ij}$. The eigenvectors are defined in terms of the exponents y_i, with $\delta l = l' - l$. The deviation from the critical coupling $\Delta\boldsymbol{K} = \boldsymbol{K} - \boldsymbol{K}^*$ is expressed in the eigenvector basis:

$$\Delta\boldsymbol{K} = \sum_i u_i(l)\boldsymbol{e_i} \qquad \Longrightarrow \qquad \Delta\boldsymbol{R}(\boldsymbol{K}) = Q\sum_i u_i(l)\boldsymbol{e_i} = \sum_i u_i(l)e^{\delta l y_i}\boldsymbol{e_i}. \tag{3.1.41}$$

[11] The naive prescription, $f(K) = 2K$, based on the observation that there are two spin-spin interactions from the original interaction which couple two neighboring block spins, gives a wrong result because it is not strictly true that the spins within the block have equal spin.

[12] In the Gaussian model, where the spins s_n of the O(N) models are distributed Gaussian about zero, would recover the mean field value $\nu = 1/2$.

We observe that the RGT is multiplicative near the fixed point: $u_i(l') = e^{\delta l y_i} u_i(l)$. The scaling fields are hence characterized by

$$\frac{\partial}{\partial l} u_i(l) = y_i u_i(l) \qquad \Longrightarrow \qquad u_i(l) = u_i e^{l y_i} = u_i b^{y_i}, \qquad l = \log b \tag{3.1.42}$$

with u_i the scaling variables (e.g. $u_t \sim t$, $u_h \sim h$). Depending on the value of y_i, one distinguishes between

(1) $y_i > 0$: *relevant scaling variables*, the scaling variable increases under iterations of the RGTs,
(2) $y_i < 0$: *irrelevant scaling variables*, the scaling variable decreases under iterations of the RGTs,
(3) $y_i = 0$: *marginal scaling variable*, the scaling variable remains constant under the RGT in the linear approximation.

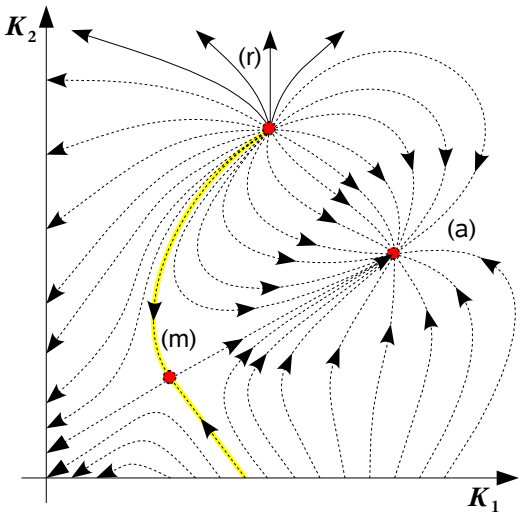

Figure 3.4: Visualization of the RG-flow induced by the RG-equation in parameter space. Classification of fixed points (FP):
(a) attractive FP (only irrelevant EV),
(r) repulsive FP (only relevant EV),
(m) mixed FP (both relevant and irrelevant EV).
The irrelevant EV of the mixed FP span the critical surface (yellow) which defines the universality class.

The relevant scaling variables correspond to those vectors which drive the system away from criticality under RG-transformations (compare Fig. 3.4). The RG-equation implies for the volume of a system of dimension d:

$$V(l) = e^{-dl} V(0) \qquad \Longrightarrow \qquad u_V(l) = e^{dl} u_V(0), \tag{3.1.43}$$

hence $u_V(l)V(l) = u_V(0)V(0)$ is constant and does not contribute to the critical behavior of the system. This implies for the RG transformation of the free energy density:

$$f(l) = e^{dl} f(0) \qquad \Longrightarrow \qquad f(t, h, u_i) = u_V + e^{-dl} f_{\mathrm{s}} \left(u_t e^{y_t l}, u_h e^{y_h l}, u_i e^{y_i l} \right), \tag{3.1.44}$$

which proves the scaling hypothesis, Eq. (3.1.26) by identifying $l = \log b$. The homogeneity coefficients are given by $a_i = y_i / d$.

3.2 O(N) Symmetric Spin Models

The physics of QCD with two flavors at low energies may be described effectively by O(N) symmetric spin models. For two light flavors, the spin components correspond to the sigma meson and pion fields $(\sigma, \boldsymbol{\pi})$, which are assumed to form an O(4) rotation invariant vector. In the magnetic language of QCD, the explicit symmetry breaking external field H corresponds to the quark mass m_q and the magnetization $\Sigma = \langle \sigma \rangle$ corresponds to the chiral condensate. We expect that the O(N) model may describe some low-energy properties of QCD in the symmetry broken phase, as will be explained in the next chapter. Here, we will review the main features of the O(N) models.

3.2.1 General Properties of O(N) Models

We will restrict the discussion in this section to the O(N) symmetric spin models in the more specific case of the O(N)-invariant *nonlinear σ models*, although also the linear O(N) invariant ϕ^4 theories are of great interest [116]. In contrast to the linear ϕ^4 theories, the longitudinal σ mode is static: it is freezed out due to an infinitely large mass. The model is defined by the Hamiltonian

$$\mathcal{H} = -J \sum_{\langle i,j \rangle} \boldsymbol{S_i} \cdot \boldsymbol{S_j} - \boldsymbol{H} \sum_i \boldsymbol{S_i}, \tag{3.2.1}$$

where $\langle i, j \rangle$ denotes a pair of nearest neighbor sites and the sum goes over a d-dimensional hypercubic lattice with $\mathcal{N}$ degrees of freedom, the volume is $V = \mathcal{N} a^d$. $\boldsymbol{S_i}$ is an N-component unit vector at site i, $|\boldsymbol{S_i}| = 1$ and $\boldsymbol{H}$ is an external magnetic field with strength $H = |\boldsymbol{H}|$. The coupling $K = \beta J$ can be interpreted as the inverse temperature. Special cases are the Ising model ($N = 1$), the XY-model ($N = 2$) and the Heisenberg model ($N = 3$). In one dimension, the Ising model has no phase transition at $T \neq 0$ because the growth of domains with equal spin costs no further energy. The Ising model in two dimensions has been solved analytically by Onsager in 1944 [97], the transition temperature is $T_c = 2J/\log\left(1 + \sqrt{2}\right)$ with critical exponents $\beta = 1/8$, $\gamma = 7/4$.[13]

For $N > 1$, the internal symmetry is continuous, allowing for rotational excitations. With the special choice $\boldsymbol{H} = (H, 0, \ldots, 0)$ the unit vectors $\boldsymbol{S_i}$ can be rewritten as

$$\boldsymbol{S_i} = (\sigma_i, \boldsymbol{\pi_i}), \qquad \sigma_i = (1 - \boldsymbol{\pi_i} \cdot \boldsymbol{\pi_i})^{1/2} \tag{3.2.2}$$

with σ_i the longitudinal mode and $\boldsymbol{\pi_i}$ the $N - 1$ transverse modes which are orthogonal to $\boldsymbol{H}$. The magnetization

$$M \equiv \left\langle \frac{1}{\mathcal{N}} \sum_i \boldsymbol{S_i} \right\rangle = \left\langle \frac{1}{\mathcal{N}} \sum_i \sigma_i \right\rangle \tag{3.2.3}$$

coincides with the expectation value of the parallel component σ_i since the transverse components are symmetric under parity in Eq. (3.2.1) and hence average to zero. The product of neighboring spins can be expanded in terms of the transverse components:

$$\boldsymbol{S_i} \cdot \boldsymbol{S_j} = 1 - \frac{1}{2}(\boldsymbol{\pi_i} + \boldsymbol{\pi_j})^2 + \boldsymbol{\pi_i} \cdot \boldsymbol{\pi_j} + \mathcal{O}\left(\boldsymbol{\pi}^4\right) = 1 - \frac{1}{2}(\boldsymbol{\pi_i} - \boldsymbol{\pi_j})^2 + \mathcal{O}\left(\boldsymbol{\pi}^4\right) \tag{3.2.4}$$

The Hamiltonian can then be rewritten as

$$\mathcal{H} = \mathcal{H}_0 + \frac{1}{2} J \sum_{\langle i,j \rangle} (\boldsymbol{\pi_i} - \boldsymbol{\pi_j})^2 - H \sum_i \sigma_i + \mathcal{O}\left(\boldsymbol{\pi}^4\right) \tag{3.2.5}$$

with $\mathcal{H}_0 = -J\mathcal{N}d$. In the continuum limit $\mathcal{N} \to \infty$ at fixed volume V, and after having dropped the irrelevant constant $\mathcal{H}_0$, we find:[14]

$$\beta\mathcal{H} = \int d^d r \left\{ \frac{1}{2} F_0^2 (\nabla \boldsymbol{\pi}(\boldsymbol{r}))^2 - \Sigma_0 H \sigma(\boldsymbol{r}) + \mathcal{O}\left(\boldsymbol{\pi}^4\right) \right\}. \tag{3.2.6}$$

The couplings are renamed into F_0, Σ_0 the meaning of which will be explained in the next section. Note that the $\boldsymbol{\pi}$ and σ mode are still restricted by the condition $\boldsymbol{\pi}^2 + \sigma^2 = 1$, which requires a corresponding delta function in the measure of the partition function.[15]

[13] The critical temperature was already determined in 1941 by Kramers and Wannier [81] by considering a duality between the high-temperature and low-temperature expansion of the Ising partition function. This method relies on the self-duality of the square lattice and is not applicable to O(N) models — e.g. the XY model is dual to a so-called "solid on solid" model which has discrete degrees of freedom.

[14] In contrast to the derivation of the Landau Ginzburg Wilson Hamiltonian Eq. (3.1.31), the continuum limit taken here does not involve Gaussian integrals. The continuum limit is straight forward and does not induce ϕ^4 terms, nevertheless it induces non-trivial temperature dependences into the new parameters, which can be described via the RG equations.

[15] In the continuum formulation, for weak external field, quasi-zero modes arise, i.e. collective spin waves which

3.2.2 Goldstone Modes in O(N) Models

The O(N) model in three and four dimensions have been studied extensively by Gasser and Hasenfratz [50, 66]. For vanishing external field H, there is no preferred direction within the magnetic system. The fact that the magnetization still acquires a nonzero expectation value is known as *spontaneous symmetry breaking*.[16] Its zero temperature expectation value obtained from Eq. (3.2.6) in the limit $H \to 0$ is dictated by the parameter Σ_0:

$$-\frac{1}{V}\frac{\partial}{\partial H}\log \mathcal{Z} = \frac{1}{V}\left\langle \int d^d r \Sigma_0 \sigma(\boldsymbol{r}) \right\rangle = \Sigma_0. \tag{3.2.7}$$

The symmetry is restored at T_c, where the magnetization vanishes in the disordered phase. Based on Eq. (3.2.3) the order parameter is identified as $\Sigma(t) = \Sigma_0 M(t)$. In practice, one needs to replace the order parameter for $H = 0$ by the approximate order parameter $\tilde{\Sigma}(t) = \Sigma_0 \tilde{M}(t)$ with $\tilde{M}(t) = \langle |\boldsymbol{S}| \rangle$ because averaging over a statistical ensemble would yield $\Sigma = 0$ even in the ordered phase.

The *Goldstone modes* are the long range transverse modes which lead to the strong correlation of the spins in the ordered phase. The mass of these excitations called the Goldstone bosons vanish for vanishing external field, and receive the following correction as can be determined from Eq. (3.2.6) by substituting the σ by the $\boldsymbol{\pi}$ mode:

$$M_H^2 = \frac{H\Sigma_0}{F_0^2} + \mathcal{O}\left(H^2\right). \tag{3.2.8}$$

F_0 is the *Goldstone boson decay constant* and is related to the so-called *helicity modulus* $\Upsilon = F_0^2$ which characterizes the stiffness of the spins w.r.t. the collective twist of the spins at some distant boundary surface: Υ determines how fast the spins within the boundary reach the new equilibrium. This process does not cost any energy above T_c, but it does at low temperatures. In particular, the decay constant, which is of mass dimension $(d-2)/2$, is zero above T_c and scales on the coexistence line as

$$F_0 \sim |t|^{\nu(d-2)/2} \qquad \text{for} \quad h = 0,\, t < 0. \tag{3.2.9}$$

For non-vanishing external field H, the magnetization receives a correction which is called the *Goldstone effect*:

$$\Sigma(H) = \Sigma_0 \left(1 - \frac{1}{2}\left\langle \boldsymbol{\pi}(\boldsymbol{0}) \cdot \boldsymbol{\pi}(\boldsymbol{0}) \right\rangle\right). \tag{3.2.10}$$

The correction stems from the correlation function of the Goldstone modes obtained from Eq. (3.2.6):

$$G_\pi(\boldsymbol{r}) \equiv \left\langle \boldsymbol{\pi}(\boldsymbol{r}) \cdot \boldsymbol{\pi}(\boldsymbol{0}) \right\rangle = \frac{N-1}{F_0^2} \int^{1/a} \frac{d^d k}{(2\pi)^d} \frac{e^{i\boldsymbol{k}\cdot\boldsymbol{r}}}{k^2 + M_H^2}. \tag{3.2.11}$$

The correlator coincides with the definition in Eq. (3.1.15) because $\langle \boldsymbol{\pi}(\boldsymbol{r}) \rangle = 0$. The lattice spacing a provides a momentum cutoff. At zero distance and vanishing external field, the correlator is

$$\left\langle \boldsymbol{\pi}(\boldsymbol{0}) \cdot \boldsymbol{\pi}(\boldsymbol{0}) \right\rangle = \frac{N-1}{F_0^2} \int^{1/a} \frac{d^d k}{(2\pi)^d} \frac{1}{k^2} = \frac{N-1}{F_0^2} \frac{\Omega_{d-1}}{(2\pi)^d} \int^{1/a} dk k^{d-3}. \tag{3.2.12}$$

rotate the overall orientation with respect to H. These modes can be treated as a collective variable for which the corresponding measure is calculated with the Faddeev-Popov technique.

[16] In the next chapter we will give a short review of spontaneous symmetry breaking in the context of chiral symmetry breaking in QCD.

From this equation, the famous *Mermin-Wagner theorem* can be derived [17], which states that for the O(N) models with dimension $d \leq 2$ and $N > 1$ (and in fact, for all models with continuous symmetry and short-range interaction) no second order phase transitions can occur at any temperature $T > 0$. In the ordered phase, the Goldstone modes diverge logarithmically in the infrared for $d = 2$. As a consequence, the order parameter is not defined. In contrast to this finding, the magnetization Σ is well behaved for $d > 2$: In three dimensions resp. four dimensions one finds (see calculation in App. B.1.1):

$$\Sigma^{(3\mathrm{D})}(H) = \Sigma_0 \left(1 + \frac{N-1}{8\pi}\frac{(\Sigma_0 H)^{1/2}}{F_0^3} + \mathcal{O}\left(H\right)\right), \tag{3.2.13}$$

$$\Sigma^{(4\mathrm{D})}(H) = \Sigma_0 \left(1 - \frac{N-1}{(4\pi)^2}\frac{\Sigma_0 H}{F_0^4}\ln\left(\frac{(\Sigma_0 H)^{1/2}}{F_0\Lambda_\Sigma}\right) + \mathcal{O}\left(H^2\right)\right). \tag{3.2.14}$$

This implies that the longitudinal susceptibility

$$\chi_L(H) \equiv \frac{\partial\Sigma(H)}{\partial H} = V\left(\langle\sigma^2\rangle - \Sigma^2\right) = V\left\langle(\delta\sigma)^2\right\rangle \tag{3.2.15}$$

is infrared divergent on the coexistence line, $T < T_\mathrm{c}$:

$$\chi_L^{(3\mathrm{D})}(H) = \frac{N-1}{16\pi}\frac{(\Sigma_0)^{3/2}}{F_0^3 H^{1/2}} + \mathcal{O}\left(H^0\right), \tag{3.2.16}$$

$$\chi_L^{(4\mathrm{D})}(H) = -\frac{N-1}{(4\pi)^2}\left(\frac{1}{2}\frac{\Sigma_0^{3/2}\Lambda_\Sigma}{F_0^3} + \frac{\Sigma_0^2}{F_0^4}\ln\left(\frac{(\Sigma_0 H)^{1/2}}{F_0\Lambda_\Sigma}\right)\right) + \mathcal{O}\left(H\right). \tag{3.2.17}$$

Based on the decomposition of the full susceptibility, we also introduce the transverse susceptibility:

$$\chi_F \equiv V\left(\left\langle \boldsymbol{S}^2\right\rangle - \left\langle \boldsymbol{S}\right\rangle^2\right) = \chi_L + (N-1)\chi_T, \tag{3.2.18}$$

$$\chi_T(H) \equiv \frac{V}{N-1}\left\langle \boldsymbol{\pi}\cdot\boldsymbol{\pi}\right\rangle = \frac{\Sigma(H)}{H}. \tag{3.2.19}$$

The second kinematic identity is exact and relies on a so-called *chiral Ward identity*:

$$\Sigma(H) = H\frac{1}{N-1}\int d^d r G_\pi(\boldsymbol{r}). \tag{3.2.20}$$

3.3 O(N) Scaling Functions

We will now turn to critical scaling and investigate its consistency with Goldstone scaling:

$$\Sigma(H, T < T_\mathrm{c}) = \Sigma_0(T) + b(T)H^{1/2}, \qquad \Sigma(H, T = T_\mathrm{c}) = cH^{1/\delta}, \tag{3.3.1}$$

$$\chi_L(H, T < T_\mathrm{c}) = \frac{b(T)}{2}H^{-1/2}, \qquad \chi_L(H, T = T_\mathrm{c}) = \frac{c}{\delta}H^{1/\delta - 1}. \tag{3.3.2}$$

We will restrict the discussion to three dimensions, because when applied later to QCD, we have reason to believe that the system close to the critical temperature is already effectively three dimensional. The critical exponents for $d = 3$ O(N) models are given in Tab. 3.2.

[17] Note that the Mermin-Wagner theorem does not prevent every kind of phase transition, e.g. the XY-model exhibits the so-called Kosterlitz-Thouless transition, where the low-temperature phase is quasi-long-ranged ordered and the correlation function shows an algebraic decay.

Model	β	δ	γ	ν
Mean Field	1/2	3	1	2/3
Ising	0.3258	4.8048	1.2396	0.6304
O(2)	0.349	4.7798	1.3192	0.6724
O(4)	0.380	4.86	1.4668	0.7423

Table 3.2: The critical exponents [35, 36] for various three-dimensional O(N)-symmetric models, also compared to mean field exponents, which satisfy the scaling relations for $d = 4$.

3.3.1 Magnetic Equation of State

The singular part of the free energy density

$$f_{\mathrm{s}}(u_t, u_h) = b^{-d} f_{\mathrm{s}}(b^{y_t} u_t, b^{y_h} u_h), \qquad y_t = d a_t, y_h = d a_h \tag{3.3.3}$$

with the scaling variables $u_t = c_t t + \mathcal{O}\left(t^2, H^2\right)$, $u_h = c_h H + \mathcal{O}\left(tH\right)$,[18] allows to determine the magnetization also in the vicinity of the critical point. To this purpose, we introduce a normalization of the reduced scaling variables different from Eq. (3.1.11)

$$u_t \;\mapsto\; t = \frac{1}{t_0}\frac{T - T_{\mathrm{c}}}{T_{\mathrm{c}}}, \qquad u_h \;\mapsto\; h = \frac{H}{h_0}, \tag{3.3.4}$$

which corresponds to $c_t = t_0^{-1}$, $c_h = h_0^{-1}$ and the omission of higher order terms in u_t, u_h. Hence we can write:

$$b^{y_h} h = 1 \qquad \Longrightarrow \qquad f_{\mathrm{s}}(t, h) = h^{1/a_h} f_{\mathrm{s}}(z, 1) = h^{1+1/\delta} f_{\mathrm{s}}(z, 1), \qquad z \equiv t/h^{1/\beta\delta}. \tag{3.3.5}$$

Note that the variable z is invariant under rescaling with b, whereas t and h are not. Hence also the normalization constant

$$z_0 = h_0^{1/\beta\delta}/t_0 \tag{3.3.6}$$

is invariant under rescaling, although it is not a universal quantity and will depend on the underlying microscopic theory (e.g. on next to nearest neighbor couplings). After taking the derivative w.r.t. H we obain the *magnetic equation of state* (MEoS):[19]

$$M = -\frac{\partial f_{\mathrm{s}}(t, h)}{\partial H} = h^{1/\delta} f_G(z), \qquad f_G(z) = -h_0^{-1}\left\{\left(1 + \frac{1}{\delta}\right) f_{\mathrm{s}}(z, 1) - \frac{z}{\beta\delta}\frac{\partial}{\partial z} f_{\mathrm{s}}(z, 1)\right\} \tag{3.3.7}$$

The function $f_G(z)$ is the scaling function for the magnetization. A perturbative expression for the MEoS is obtained by making use of the *Widom-Griffiths form of the equation of state* [61]:

$$y = f(x), \qquad y \equiv h/M^{\delta}, \qquad x \equiv t/M^{1/\beta}, \tag{3.3.8}$$

which is a universal function as well and which is related to f_G:

$$x = z f_G(z)^{-1/\beta}, \qquad y = f_G(z)^{-\delta}, \qquad z = x/y^{1/\beta\delta}. \tag{3.3.9}$$

The normalization constants t_0, h_0 are chosen such that the following condition holds:

$$f(0) = 1, \quad f(-1) = 0 \qquad \Longleftrightarrow \qquad f_G(0) = 1, \quad \lim_{z\to-\infty} \frac{f_G(z)}{(-z)^{\beta}} = 1. \tag{3.3.10}$$

[18] The higher order corrections are based on the fact that u_t corresponds to an even coupling and u_h corresponds to an odd coupling w.r.t. the spins.

[19] In this chapter, we will denote the magnetization with M as customary in the literature, and there should be no confusion with the mass M_H.

The perturbative form of $f(x)$ has been calculated in the low temperature region $x < 0$ via ϵ-expansion up to $\mathcal{O}\left(\epsilon^2\right)$ by Brezin et al. [20] and thereafter has been considered in the limit $x \to -1$, i.e. close to the coexistence line, by Wallace and Zia [117]:

$$x + 1 = \tilde{c}_1 y + \tilde{c}_2 y^{d/2-1} + \tilde{d}_1 y^2 + \tilde{d}_2 y^{d/2} + \tilde{d}_3 y^{d-2} + \dots \tag{3.3.11}$$

The coefficients $\tilde{c}_i$, $\tilde{d}_i$ are obtained from the calculation of the transverse susceptibility, Eq. (3.2.19). The behavior of $f(x)$ in the high temperature region $x > 0$ is given by Griffiths' analytic condition [61]:

$$f(x) = \sum_{n=1}^{\infty} a_n x^{\gamma - 2(n-1)\beta}. \tag{3.3.12}$$

Interpolation Ansatz

In three dimensions, the series in $\epsilon = 4 - d$ for the coefficients does not converge. Instead, the scaling function $f_G(z)$ has been measured via Monte Carlo simulations by Engels et al. [35]. For this purpose, the analytic condition was inverted and the following parameterization was used to fit the scaling function to the Monte Carlo data:

$$x_s(y) = -1 + \tilde{c}_2 y^{1/2} + (\tilde{c}_1 + \tilde{d}_3) y + \tilde{d}_2 y^{3/2}, \tag{3.3.13}$$

$$x_l(y) = a y^{1/\gamma} + b y^{(1-2\beta)/\gamma}, \tag{3.3.14}$$

$$x(y) = x_s(y) \frac{y_0^p}{y_0^p + y^p} + x_l(y) \frac{y^p}{y_0^p + y^p} \tag{3.3.15}$$

with $x_s(y)$ the expansion for small x, $x_l(y)$ the expansion for large x and y_0, p free parameters that are adjusted to give good agreement of the interpolation with the data. The results for the coefficients are given in Tab. 3.3. The value of $\tilde{d}_2$ was not determined in [35] but set to $\tilde{d}_2 = 1 - (\tilde{c}_1 + \tilde{d}_3) - \tilde{c}_2$ according to the normalization condition in Eq. (3.3.10). However, for small values of y_0, the normalization condition is spoiled. Hence we have used

$$\tilde{d}_2 = 1 - \frac{a + b}{y_0^p} - \tilde{c}_2 - (\tilde{c}_1 + \tilde{d}_3) \tag{3.3.16}$$

instead. In particular, this choice improves the interpolation for the derivatives of f_G discussed below. The resulting scaling functions are shown in Fig. 3.5.

Model	$\tilde{c}_1 + \tilde{d}_3$	$\tilde{c}_2$	a	b	y_0	p
O(2)	0.352(30)	0.592(10)	1.260(3)	-1.163(20)	0.9	2.2
O(4)	0.345(12)	0.674(08)	1.084(6)	-0.994(100)	0.4	1.8

Table 3.3: Parameters of the low- and high temperature expansions $x_s(y)$, $x_l(y)$ and interpolation parameters y_0, p between these branches for $x(y)$.

Identification of the Goldstone contribution

To see that Goldstone scaling is encoded within the O(N) scaling function $f_G(z)$, we expand the MEoS in the low temperature region:

$$f_G^-(z) = \lim_{z \to =-\infty} f_G(z) = |z|^\beta \left\{ 1 + \beta \tilde{c}_2 |z|^{-\beta\delta/2} + \left(\beta(\tilde{c}_1 + \tilde{d}_3) - \frac{\beta(\beta+1) + \beta^2\delta}{2} \tilde{c}_2^2 \right) |z|^{-\beta\delta} \right\}. \tag{3.3.17}$$

The asymptotic scaling function $f_G^-(z)$ implies for the magnetization below T_c:

$$M(h, t < 0) \simeq |t|^\beta \left\{ 1 + \beta \tilde{c}_2 |t|^{-\beta\delta/2} h^{1/2} + \left(\beta(\tilde{c}_1 + \tilde{d}_3) - \frac{\beta(\beta+1) + \beta^2\delta}{2} \tilde{c}_2^2 \right) |t|^{-\beta\delta} h \right\}. \quad (3.3.18)$$

Note that the prefactor of the Goldstone term $b(T)$ from Eq. (3.3.1) is proportional to $\tilde{c}_2$:

$$b(T) = |t|^{\beta(1-\delta/2)} \beta \tilde{c}_2 h_0^{-1/2}. \quad (3.3.19)$$

The precise value of the Goldstone coefficient $\tilde{c}_2$ is however not known. We emphasize that $\tilde{c}_2$ in Eq. (3.3.13) only serves to parameterize the scaling function, but as higer orders in Eq. (3.3.13) are dropped, it can not pin down its value. The values of $\tilde{c}_i$, $\tilde{d}_i$ as measured in [35] and given in Tab. 3.3 can only be regarded as rough estimates. The critical exponents and the coefficients $\tilde{c}_i$, $\tilde{d}_i$ have also been calculated via ϵ-expansion [121, 122, 20, 117], however,

$$\tilde{c}_2 = \frac{N-1}{N+8} \left(1 + \frac{9(N+8)\log 3 + 22N + 116}{2(N+8)^2} \epsilon \right) + \mathcal{O}\left(\epsilon^2\right) \quad (3.3.20)$$

is only known to first order in ϵ, which yields $\tilde{c}_2 = 0.1 + 0.129\epsilon + \mathcal{O}\left(\epsilon^2\right)$ for $N = 2$. The large first order coefficient indicates that the convergence is slow, and higher order corrections may be substantial in three dimensions, $\epsilon = 1$.

The consistency of Goldstone scaling and critical scaling has been numerically well established for O(N) models, in particular for O(2) and O(4) [35, 36]. These scaling functions measured by Engels and collaborators will form the basis of our scaling analysis of lattice QCD data for 2+1 flavors of staggered fermions.

Thermal Version of Magnetic Equation of State

A thermal version of the MEoS is obtained by demanding $b^{y_t} t = 1$ instead of Eq. (3.3.5)

$$f_s(t, h) = |t|^{d\nu} f_s(t|t|^{-1}t, h|t|^{-\beta\delta}) \equiv |t|^{d\nu} f_s^\pm(\pm 1, w), \qquad w = h|t|^{-\beta\delta}, \quad (3.3.21)$$

and after taking again the derivative w.r.t. H:

$$M = \frac{\partial}{\partial h} f_s^\pm(\pm 1, w) = |t| \frac{\partial}{\partial w} f_s^\pm(\pm 1, w) \frac{\partial w}{\partial h} = |t|^\beta f_T^\pm(w), \qquad f_T^\pm(w) = \frac{\partial}{\partial w} f_s^\pm(\pm 1, w) \quad (3.3.22)$$

where $f_T^+(w)$ describes the high temperature region and $f_T^-(w)$ the low temperature region. With this we can write:

$$M|t|^{-\beta} = f_T^\pm(w), \quad (3.3.23)$$

which is plotted in Fig. 3.6. $f_T^\pm(w)$ is related to $f_G(z)$ by

$$w = y|x|^{-\beta\delta} = |z|^{-\beta\delta} \quad \Longleftrightarrow \quad z^\pm(w) = \pm w^{-1/\beta\delta}, \quad (3.3.24)$$

$$f_T^\pm(w) = |t|^\beta h^{1/\delta} f_G(z^\pm(w)) = w^{1/\delta} f_G(\pm w^{-1/\beta\delta}). \quad (3.3.25)$$

The limit $w \to 0$ corresponds to the limit $z^+(w) \to \infty$, or $z^-(w) \to -\infty$. With the asymptotic form $f_G^\pm(t)$, one obtains:

$$\lim_{w\to 0} f_T^+ = 0, \qquad \lim_{w\to 0} f_T^- = 1. \quad (3.3.26)$$

This alternative representation of the scaling function will be useful when we attempt to identity the contribution of the Goldstone modes to the scaling function.

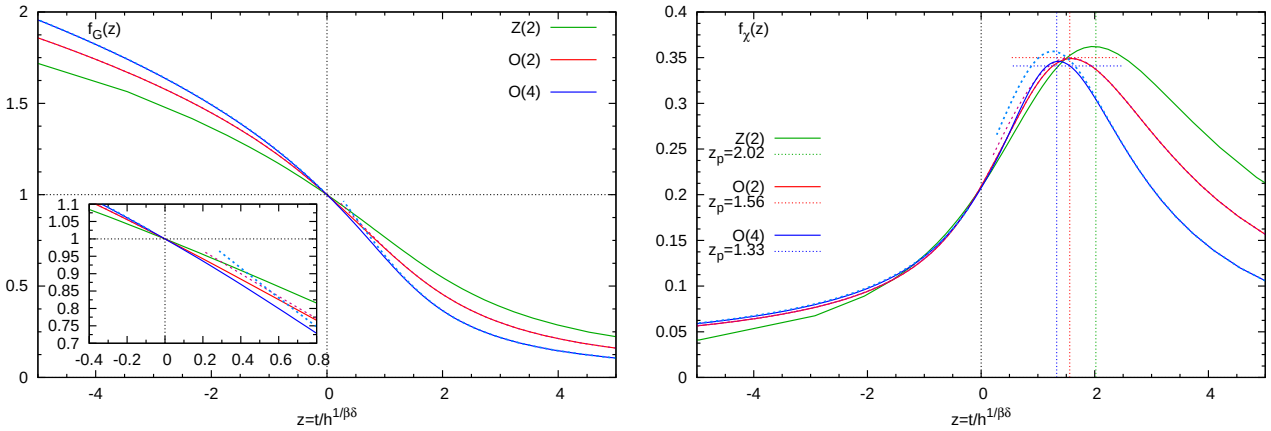

Figure 3.5: Scaling functions $f_G(z)$, $f_\chi(z)$ for the magnetization (left) and for the magnetic susceptibility (right) for the universality classes Z(2), O(2) and O(4). Also shown are the low- and high temperature branches based on $x_s(y)$ and $x_l(y)$.

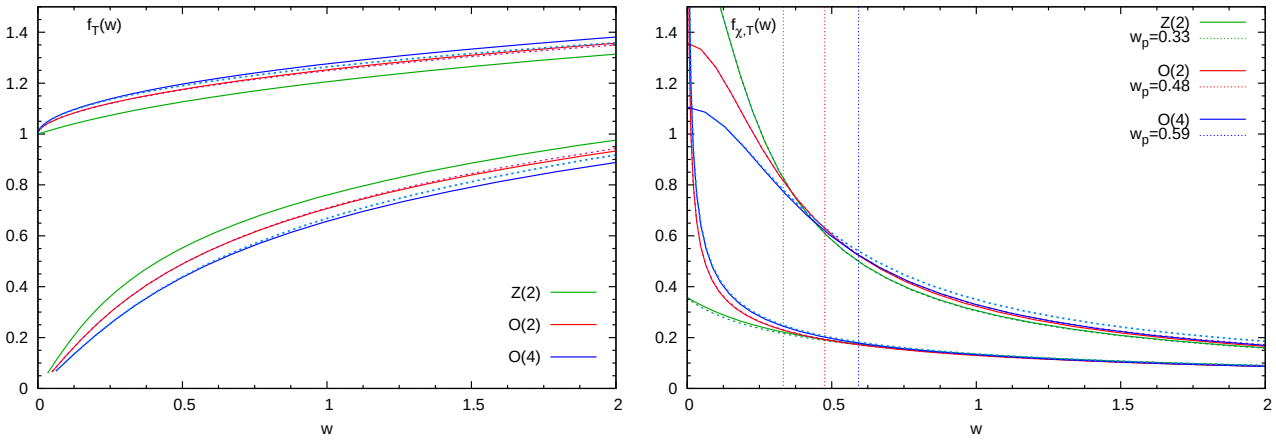

Figure 3.6: Thermal version of MEoS: scaling function $f_T(w)$, $f_{\chi,T}(w)$ for magnetization and susceptibility.

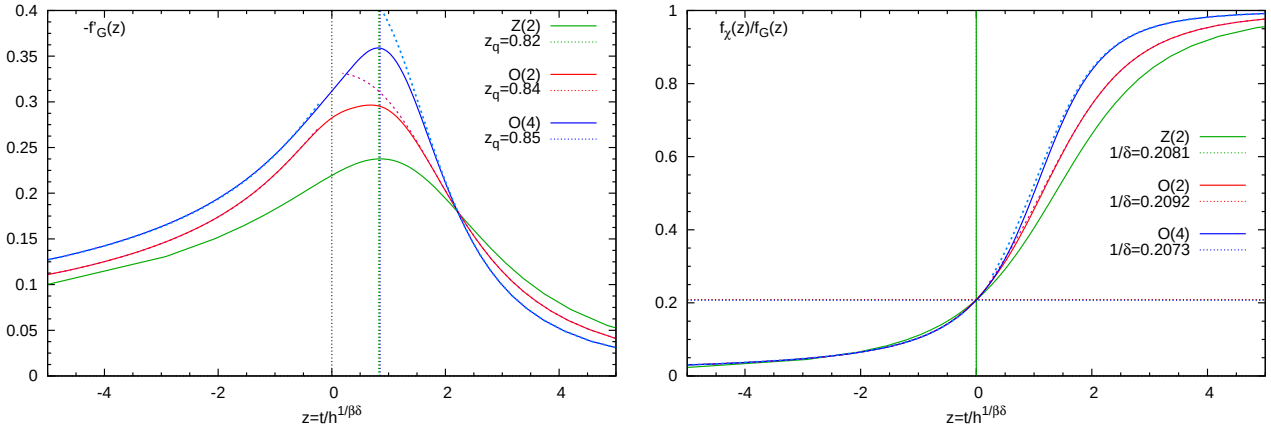

Figure 3.7: Scaling function of the derivative of $f_G(z)$ w.r.t. the temperature $f'_G(z)$ (left), which describes the scaling of the thermal susceptibility χ_t, and the ratio $f_\chi(z)/f_G(z)$ (right), which describes the scaling of the cumulant Δ.

3.3.2 Scaling Function for the Susceptibilities and the Cumulant

From the MEoS a scaling function for the susceptibility is obtained by taking the derivative of Eq. (3.3.7) w.r.t. H:

$$\chi(h,t) = \frac{1}{h_0} h^{1/\delta - 1} f_\chi(z), \qquad f_\chi(z) = \frac{1}{\delta}\left(f_G(z) - \frac{z}{\beta} f_G'(z)\right) \tag{3.3.27}$$

Note that $f_\chi(0) = 1/\delta$. This scaling function is characterized by the position of its peak maximum at z_p, which takes different values depending on the universality class. From the low temperature expansion (3.3.18) we obtain an expansion for the susceptibility as well:

$$\chi(h, t<0) \simeq \frac{1}{h_0}|t|^\beta \left\{ \frac{\beta}{2}\tilde{c}_2 |t|^{-\beta\delta/2} h^{-1/2} + \left(\beta(\tilde{c}_1 + \tilde{d}_3) + \frac{\beta(\beta+1) - \beta^2\delta}{2}\tilde{c}_2^2\right)|t|^{-\beta\delta} \right\}. \tag{3.3.28}$$

Note that it is important not to drop the higher order term $\mathcal{O}\left(h^0\right)$: in the limit $t \to 0$ this constant diverges faster than the Goldstone term. It is the main contribution to the scaling function at $h \approx 0$ and $\lim t \to 0$. *If* the Goldstone term were *not* present, the critical amplitude for the susceptibility and the critical exponent γ' would be defined as

$$\chi(h=0, t \lesssim 0) \simeq \text{ GS-Div. } + \frac{\beta}{h_0}\left(\tilde{c}_1 + \tilde{d}_3 + \frac{1-\gamma}{2}\tilde{c}_2^2\right)|t|^{-\gamma'} \tag{3.3.29}$$

and in fact one finds $\gamma' = \beta(\delta - 1) = \gamma$.

We will also consider a cumulant obtained from the ratio of longitudinal and transversal susceptibility, which can as well be described by the scaling functions close to the critical point:

$$\Delta(H,T) \equiv \frac{\chi_L(H,T)}{\chi_T(H,T)} = \frac{H\chi_L(H,T)}{M(H,T)}, \qquad \Delta(z) = \frac{f_\chi(z)}{f_G(z)} = \begin{cases} 0 & z \to -\infty \\ 1/\delta & z = 0 \\ 1 & z \to +\infty \end{cases}. \tag{3.3.30}$$

$\Delta(z)$ is a montonously increasing function, as shown in Fig. 3.7. Remarkably, as Δ is not rescaled with h_0 or t_0, it is in principle possible to determine z_0 directly. However, as it involves the susceptibility which is usually very noisy, it is only of limited use.

The thermal susceptibilty is the response function of the order parameter w.r.t. variation of the temperature. In the vicinity of T_c, it is well described by the derivative of the scaling function f_G:

$$\chi_t \equiv \frac{\partial M}{\partial T} = \frac{1}{t_0 T_\mathrm{c}} = \frac{1}{t_0 T_\mathrm{c}} h^{(\beta-1)/\beta\delta} f_G'(z). \tag{3.3.31}$$

3.3.3 Finite Size Scaling and Binder Cumulant

Finite Size Scaling

In a finite volume $V = L^d$, the correlation length cannot diverge and the critical point $\boldsymbol{y}_c$ in the space of the state variables is replaced by a pseudo-critical point $\boldsymbol{y}_{c,L}$. The susceptibility has its maximum at a pseudo-critical temperature $T_{c,L}$. The scaling hypothesis can be extended into the form

$$b^{-d} f_\mathrm{s}(b^{y_t} t, b^{y_h} h, b^d V, \ldots) = f_\mathrm{s}(t, h, V \ldots) \qquad \forall b \in \mathbb{R}. \tag{3.3.32}$$

The maximum of the susceptibility at a second order transition[20] is located at $\chi_{c,L} \sim L^{\gamma/\nu}$. After taking the derivative w.r.t. the reduced temperature t and demanding that it has to vanish at the pseudocritical temperature $t_{c,L}$

$$\frac{\partial \chi(t, h, V^{-1})}{\partial t} \sim L^{(\gamma+1)/\nu}\, \tilde{\chi}(L^{1/\nu} t, 0, 1)\Big|_{t=t_{c,L}} = 0 \tag{3.3.33}$$

[20] For a first order transition, the susceptibility scales with the volume, $\chi_{c,L} \sim L^d$, whereas in the crossover region, the susceptibility is independent of the volume to a first approximation.

one obtains the central relation for *finite size scaling* (FSS):

$$T_{c,L} = T_{\mathrm{c}} \left(1 + \tilde{t} L^{-1/\nu}\right), \qquad \tilde{t} = L^{1/\nu} t_{c,L}, \tag{3.3.34}$$

where $\tilde{t}$ is the root of $\tilde{\chi}(\tilde{t}, 0, 1)$ and can be determined from a set of measurements for different volumes.

Binder Cumulant

Another method which allows to extract the critical temperature from data for a set of finite volumes is the calculation of cumulants. The cumulants of an observable $\mathcal{O}$ are linear combinations of the central momenta

$$\mu_i = \left\langle \delta\mathcal{O}^i \right\rangle, \qquad \delta\mathcal{O} = \mathcal{O} - \langle \mathcal{O} \rangle, \tag{3.3.35}$$

which are generated from a characteristic function (here the partition function with the external field as a source term):

$$\kappa_n = (-1)^n \frac{\partial^n}{\partial H^n} \log Z(H)|_{H=0}, \qquad \mathcal{Z}(H) = \left\langle e^{-H\mathcal{O}} \right\rangle. \tag{3.3.36}$$

They characterize the geometric shape of the distribution of the observable $\mathcal{O}$. By taking ratios of cumulants, the so-called reduced cumulants, one obtains useful quantities which allow to study the critical region in Monte Carlo simulations. They are defined as:

$$B_{2k} \equiv \frac{\mu_{2k}}{\mu_k^2}, \qquad B_4 = \frac{\mu_4}{\mu_2^2} = 3\left(1 + \frac{\kappa_4}{3\kappa_2^2}\right) \tag{3.3.37}$$

with B_4 the the specific ratio for $k = 2$ called the *Binder cumulant* introduced by K. Binder[21] [15, 16]. Close to the critical point, the reduced cumulants can be described via the derivatives of $f_h(h) \equiv f_{\mathrm{s}}(t = 0, h, L^{-d})$ w.r.t. the reduced external field h:

$$B_{2k}(\tilde{h}) = \frac{f_h^{(2k)}(\tilde{h})}{(f_h^{(k)}(\tilde{h}))^2}, \qquad \tilde{h} = L^{da_h} h. \tag{3.3.38}$$

At a second order transition, B_{2k} will approach a renormalization group invariant value which is unique to the universality class. Moreover, the cumulants are independent of the volume within the scaling region.

The Gaussian distribution is characterized by $\kappa_1 = \langle \mathcal{O} \rangle$, $\kappa_2 = \sigma$ with σ the standard deviation, and $\kappa_n = 0$ for $n > 2$, which implies $B_4 = 3$. This is the expected value in the crossover region, where $\mathcal{O}$ are Gaussian distributed. For first oder transitions, the distribution will be strongly double-peaked, and the value $B_4 = 1$ is expected. These values for a crossover and first-order transition are only attained in the infinite volume limit. At the critical point, the distribution of $\delta\mathcal{O}$ is universal, which results in the characteristic values of B_4 given in Tab. 3.4. Hence the Binder cumulant allows the determination of the universality class even in finite volumes.

Model	B_4	B_4^r
Ising	1.604(2)	1.604(2)
O(2)	1.242(2)	1.863(3)
O(4)	1.092(3)	2.184(2)

Table 3.4: The universal values the of the Binder cumulant B_4, B_4^r [68] for various three-dimensional O(N)-symmetric models.

[21] Binder introduced the following quantity: $U_L = -\frac{\kappa_4}{3\kappa_2^2} = 1 - \frac{\mu_4}{3\mu_2^2}$ which is related to the definition used nowadays by $B_4 = 3(1 - U_L)$.

If the critical point is located at $h = 0$, it is crucial for the analysis of Monte Carlo data to take into account whether the simulations were performed directly at $h = 0$ or at several values $h_i > 0$ and extrapolated to $h = 0$. In the second case, the spin direction parallel to the external field is always defined.[22] The Binder cumulant then needs to be multiplied by a factor obtained from an angular integrations [107]:

$$B_4^r = \frac{\langle \sigma^4 \rangle}{\langle \sigma^2 \rangle^2} = \frac{\langle |\boldsymbol{S}|^4 \rangle \int_{-1}^{1} dx x^4 f_N(x)}{\langle |\boldsymbol{S}|^2 \rangle^2 \left(\int_{-1}^{1} dx x^2 f_N(x) \right)^2} = B_4 \times \begin{cases} 1 & \text{for} \quad N = 1 \\ \frac{3}{2} & \text{for} \quad N = 2 \\ 2 & \text{for} \quad N = 4 \end{cases}, \tag{3.3.39}$$

$$f_N(x) = c_N \int_0^\pi d\theta_{N-2} \sin^{N-2} \theta_{N-2} \delta(x - \cos \theta_{N-2}), \tag{3.3.40}$$

resulting in a refined universal value of the Binder B_4^r cumulant given in Tab. 3.4. The functions $f_N(x)$ are probability densities which reflect the geometric distribution of the spin component $x = \cos \theta_{N-2}$ which is taken to be aligned parallel to the external field h. They are calculated in the App. A.1.

At a tricritical point, mean field exponents are expected, and the Binder cumulant takes a universal value which depends on the dimension N of the order parameter, e.g. $B_4 = 2$ for a 1-component order parameter and $B_4 = \Gamma(1/3)\Gamma(2/3)^2 \simeq 1.4610$ for a 2-component order parameter [79].

3.4 Finite Size Effects in the O(N) Model below T_c

Since the correlation length of the Goldstone modes diverges on the coexistence line, they are also very sensitive to finite size effects in large volumes. In particular, if both the Goldstone boson mass (defined at infinite volume) and the inverse length $1/L = V^{-1/d}$ are much smaller than any other mass scale of the physical system, the Goldstone modes will be strongly influenced by the finite size effects. Hasenfratz and Leutwyler [66] have calculated the leading and subleading finite size corrections for the nonlinear sigma model via chiral perturbation theory.

3.4.1 Higher Order Effective Lagrangian at Infinite Volume

Starting point is the effective Lagrangian

$$\mathcal{L}_{\text{eff}} = \frac{1}{2} F_0^2 (\nabla \boldsymbol{S})^2 - \Sigma_0 (\boldsymbol{H} \cdot \boldsymbol{S}) \tag{3.4.1}$$

$$+ k_1 \frac{\Sigma_0}{F_0^2} (\boldsymbol{H} \cdot \boldsymbol{S})(\partial_\mu \boldsymbol{S} \partial_\mu \boldsymbol{S}) - k_2 \frac{\Sigma_0^2}{F_0^4} (\boldsymbol{H} \cdot \boldsymbol{S})^2 - k_3 \frac{\Sigma_0^2}{F_0^4} (\boldsymbol{H} \cdot \boldsymbol{H})^2 + \ldots \tag{3.4.2}$$

which extends the Lagrangian Eq. (3.2.6) discussed above to higher order in a well defined (unique) way and introduces the new coupling constants k_1, k_2, k_3 which are not universal, but dictated by the underlying theory which is modeled.[23]

3.4.2 Expansion Schemes in Chiral Perturbation Theory

Remarkably, it is possible to determine these constants in a finite volume, even if L is smaller than the Compton wave length of the Goldstone boson. However, it is required that L is large compared to the inverse mass of the longitudinal sigma mode. This gives rise to a large volume expansion, with the constraint that

$$u_0 \equiv \Sigma_0 H V \approx M_H^2 F_0^2 V \tag{3.4.3}$$

[22] In QCD, we face the second case since it is not possible to do simulations with vanishing quark mass.

[23] These coupling constants can be identified with coupling constants of the O(4) nonlinear sigma model considered in [50], where the O(4) fields are given by real O(4) matrices U fulfilling $U^T U = \mathbb{1}$: $k_1 = l_4$, $k_2 = l_3 + l_4$, $k_3 = h_1 - l_4$.

is fixed: Only for large u_0 the external field is able to align the magnetization. The Goldstone modes feel the boundary conditions strongly: $M_H^2 L^2 \ll 1$. In fact, this large volume expansion corresponds to the ϵ-regime power scheme in chiral perturbation theory.

In contrast, in the limit of small u_0 one reaches the regime of p-expansion, which is performed at fixed

$$v \equiv \Sigma_0 H L^2 / F_0^2 \approx M_H^2 L^2, \tag{3.4.4}$$

see Fig. 3.8. Here, the Goldstone modes are not sensitive to the boundary conditions. This is the regime for chiral perturbation theory at infinite volume and low temperature, which we will discuss in detail in the next chapter applied to QCD. The ϵ-regime is of interest because it allows to predict how the magnetization in the ordered phase vanishes in the chiral limit, as there is no true phase transition in a finite volume.

The momentum of a non-zero mode is of order L^{-1}. Based on the counting scheme for the large volume expansion (ϵ-regime):

$$\boldsymbol{\pi} \sim L^{1-d/2}, \quad \nabla \sim L^{-1}, \quad H \sim L^{-d} \tag{3.4.5}$$

for $d = 3$ and expansion up to order L^{-2}, the Lagrangian is needed to order L^{-5}. The large volume expansion of the partition function is then fully determined by F_0 and Σ_0. For $d = 4$ and expansion up to order L^{-4}, the Lagrangian is needed to order L^{-8} and the large volume expansion is now also determined by the parameters k_1, k_2, k_3.

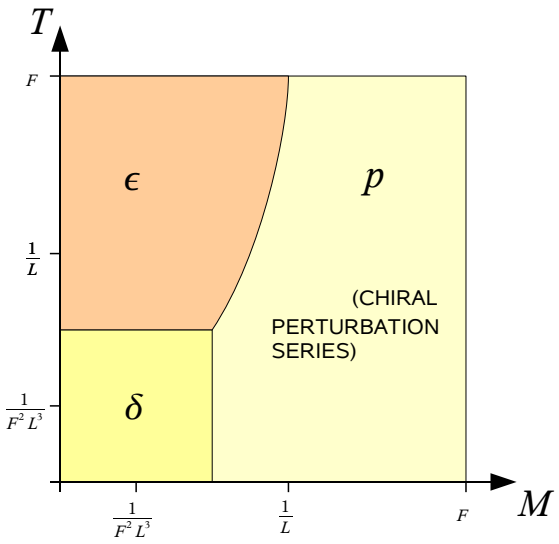

Figure 3.8: Sketch of the domains (reproduced from [87]) in which the three low energy expansions for chirap perturbation theory are valid, applied to the 3+1 dim. volume $V = L^3/T$. All expansions are power series in $1/F^2L^2$.
p-regime: $M \sim T \sim L^{-1}$, ML and LT fixed,
ϵ-regime: $M \ll T \sim L^{-1}$, LT and $F^2M^2L^3/T$ fixed,
δ-regime: $M \sim T \ll L^{-1}$, M/T and $F^2M^2L^3/T$ fixed.

In the four-dimensional infinite volume, these parameters are fixed by the cut-offs Λ_Σ, Λ_F and Λ_M, which appear in the chiral logarithms

$$\Sigma(H) = \Sigma_0 \left\{ 1 + \frac{N-1}{16\pi^2} \frac{M_H^2}{F_0^2} \ln \frac{\Lambda_\Sigma}{M_H} + \mathcal{O}\left(H^2\right) \right\}, \tag{3.4.6}$$

$$F(H) = F_0 \left\{ 1 + \frac{N-2}{16\pi^2} \frac{M_H^2}{F_0^2} \ln \frac{\Lambda_F}{M_H} + \mathcal{O}\left(H^2\right) \right\}, \tag{3.4.7}$$

$$M_H^2(H) = M_H^2 \left\{ 1 + \frac{N-3}{16\pi^2} \frac{M_H^2}{F_0^2} \ln \frac{\Lambda_M}{M_H} + \mathcal{O}\left(H^2\right) \right\} \tag{3.4.8}$$

via the relations

$$\frac{N-1}{8\pi^2} \ln \Lambda_\Sigma = 4(k_2 + k_3) - \frac{N-1}{8\pi^2} c_1, \tag{3.4.9}$$

$$\frac{N-2}{8\pi^2} \ln \Lambda_F = 2k_1 - \frac{N-2}{8\pi^2} c_1, \tag{3.4.10}$$

$$\frac{N-3}{8\pi^2} \ln \Lambda_M = 4(k_1 - k_2) - \frac{N-3}{8\pi^2} c_1 \tag{3.4.11}$$

with $c_1 \sim 1/(d-4)$ a constant absorbed in the renormalization of the coupling constants k_i. In a finite volume in $V = L^d$, one obtains for the partition function:

$$\mathcal{Z} = NY_N(\rho_1 u_0) \exp\left(\frac{\rho_2 u_0^2}{(F^2 L^{d-2})^2}\right), \qquad Y_N(u) = \sum_{k=0}^{\infty} \frac{1}{k!\Gamma(k+N/2)} \left(\frac{u}{2}\right)^{2k}, \tag{3.4.12}$$

$$\rho_1 = 1 + \frac{N-1}{2F^2 L}\beta_1 - \frac{(N-1)(N-3)}{8F^4 L^2}\left\{\beta_1^2 - 2\beta^2 + \delta(d-4)\frac{1}{4\pi^2}\log(\Lambda_\Sigma L)\right\}, \tag{3.4.13}$$

$$\rho_2 = \frac{N-1}{4}\left\{\beta_2 + \delta(d-4)\frac{1}{8\pi^2}\log(\Lambda_\Sigma L)\right\}, \tag{3.4.14}$$

where β_1, β_2 are shape coefficients depending on the dimension d, and the functions ρ_1, ρ_2 are valid for $d = 3$ and $d = 4$, where the chiral logarithms only enter for $d = 4$. This implies for the order parameter:

$$\Sigma(H, L) = \Sigma_0 \left\{\rho_1 \frac{Y_N'(\rho_1 u_0)}{Y_N(\rho_1 u_0)} + 2\rho_2 u_0 \left(\frac{1}{F^2 L^{d-2}}\right)^2\right\}, \tag{3.4.15}$$

$$\frac{Y_N'(u)}{Y_N(u)} = \frac{1}{N}u - \frac{1}{N^2(N+2)}u^3 + \mathcal{O}\left(u^5\right).$$

As can be clearly seen from the expansion, $\Sigma(H, L)$ vanishes in the chiral limit $u_0 \to 0$ at fixed volume V. Note that in four dimensions Eq. (3.4.15) allows in principle to determine Λ_Σ and Λ_M in a finite volume.

Chapter 4

Spontaneous Chiral Symmetry Breaking and the Chiral Transition

The chiral phase transition of QCD is characterized by the restoration of chiral symmetry at the (pseudo-)critical temperature $T_{\rm ch}$. Below $T_{\rm ch}$ the chiral symmetry of the QCD Lagrangian is *spontaneously broken* ("spontaneous chiral symmetry breaking", abbreviated SχSB) according to the pattern:

$$\mathrm{SU}(N_{\rm f})_{\rm L} \times \mathrm{SU}(N_{\rm f})_{\rm R} \to \mathrm{SU}(N_{\rm f})_{\rm V}. \tag{4.0.1}$$

In the chiral limit of the quark masses, $m_q \to 0$, the chiral condensate is a true order parameter of this transition:

$$\langle\bar\psi\psi\rangle = -\frac{T}{V}\frac{\partial}{\partial m_q}\log\mathcal{Z}, \qquad \langle\bar\psi\psi\rangle \begin{cases} \neq 0 & \text{for} \quad T < T_{\rm ch} \\ = 0 & \text{for} \quad T \geq T_{\rm ch} \end{cases} . \tag{4.0.2}$$

Finite quark masses m_q break the chiral symmetry explicitly, but SχSB still provides a good approximation to low energy QCD where pions are conceived as pseudo-Goldstone bosons.

As was already discussed in the introduction, the order of the transition crucially depends on the quark masses, and in particular on the number of light quarks. First- and second order transitions may even occur within a range of finite quark masses. Hence it is very important to understand the quark mass dependence of chiral observables for temperatures below $T_{\rm ch}$. This is achieved via chiral perturbation theory (χPT), which is the effective theory of hadrons. This effective approach allows us to study the low energy properties of QCD, in particular the consequences of spontaneous symmetry breaking. In this chapter we will focus on mesonic chiral perturbation theory, where the relevant degrees of freedom are the pseudo-Goldstone bosons. It is based on the assumption that there are light mesonic degrees of freedom — the pseudo-Goldstone bosons — and enables to calculate the consequences in terms of a perturbative series in the small but finite quark masses.

Before I will discuss the χPT calculations for chiral observables relevant for the analysis of the lattice data, in particular the Goldstone effect already mentioned for O(N) models, I want to give a short overview on spontaneous symmetry breaking and χPT.

4.1 Chiral Symmetry and its Spontaneous Breaking

4.1.1 QCD Lagrangian in the Chiral Limit

In the limit of vanishing quark masses, the QCD Lagrangian

$$\mathcal{L}_{\rm QCD}^{\mathcal{M}=0} = \sum_{f=1}^{N_{\rm f}} \bar\psi_f i\not{D}\psi_f - \frac{1}{4}G^a_{\mu\nu}G^{a\,\mu\nu} = \sum_{f=1}^{N_{\rm f}} \left(\bar\psi_{{\rm R},f} i\not{D}\psi_{{\rm R},f} + \bar\psi_{{\rm L},f} i\not{D}\psi_{{\rm L},f}\right) - \frac{1}{4}G^a_{\mu\nu}G^{a\,\mu\nu} \tag{4.1.1}$$

exhibits chiral symmetry, i.e. left-handed and right-handed components of the quark fields can be transformed independently. The second equality is due to the decomposition of the quark fields into left-handed and right-handed components via the projectors

$$\psi_{\rm R} = P_{\rm R}\psi, \qquad \psi_{\rm L} = P_{\rm L}\psi \qquad \text{with} \qquad P_{\rm R} = \frac{1}{2}\left(\mathbb{1}+\gamma_5\right), \quad P_{\rm L} = \frac{1}{2}\left(\mathbb{1}-\gamma_5\right), \tag{4.1.2}$$

which obey the properties $P_{\rm R}+P_{\rm L}=\mathbb{1}$, $P_{\rm R}^2=P_{\rm R}$, $P_{\rm L}^2=P_{\rm L}$, $P_{\rm R}P_{\rm L}=0$.[1] Note that due to ${\gamma^5}^\dagger=\gamma^5$ the projections in Eq. (4.1.2) imply

$$\bar\psi_{\rm R} \equiv (P_{\rm R}\psi)^\dagger\gamma_0 = \psi^\dagger\gamma_0 P_{\rm L} = \bar\psi P_{\rm L}, \qquad \bar\psi_{\rm L} \equiv (P_{\rm L}\psi)^\dagger\gamma_0 = \psi^\dagger\gamma_0 P_{\rm R} = \bar\psi P_{\rm R}. \tag{4.1.3}$$

Hence, for quark bilinears one finds

$$\bar\psi\Gamma_i\psi = \begin{cases} \bar\psi_{\rm R}\Gamma_1\psi_{\rm R} + \bar\psi_{\rm L}\Gamma_1\psi_{\rm L} & \text{for} \quad \Gamma_1 \in \{\gamma^\mu, \gamma^\mu\gamma_5\} \\ \bar\psi_{\rm R}\Gamma_2\psi_{\rm L} + \bar\psi_{\rm L}\Gamma_2\psi_{\rm R} & \text{for} \quad \Gamma_2 \in \{\mathbb{1}, \gamma_5, \gamma^{\mu\nu}\} \end{cases}, \tag{4.1.4}$$

because $\{\Gamma_1,\gamma_5\}=0$ and $[\Gamma_2,\gamma_5]=0$. The Lagrangian (4.1.1) is invariant under the chiral transformations

$$\psi_{\rm R} \mapsto U_{\rm R}\psi_{\rm R}, \qquad \psi_{\rm L} \mapsto U_{\rm L}\psi_{\rm R}, \qquad U_{\rm R/L} = \exp\left(-i\sum_{a=1}^{N_{\rm f}^2-1}\theta_{\rm R/L}^a t^a\right)\exp\left(-i\theta_{\rm R/L}\right)., \tag{4.1.5}$$

where t^a are the generators of $\mathrm{SU}(N_{\rm f})$. From these global symmetries, the following $2N_{\rm f}^2$ currents are obtained via the Noether theorem:[2]

$$\begin{array}{llll} j_{\rm R}^{\mu,a} & = \bar\psi_{\rm R}\gamma^\mu t^a\psi_{\rm R}, & j_{\rm L}^{\mu,a} & = \bar\psi_{\rm L}\gamma^\mu t^a\psi_{\rm L}, \\ j_{\rm V}^{\mu} & = \bar\psi\gamma^\mu\psi, & j_{\rm A}^{\mu} & = \bar\psi\gamma^\mu\gamma_5\psi, \end{array} \tag{4.1.6}$$

from which all but the axial current (due to the axial anomaly $\mathrm{U_A}(1)$) is conserved:

$$\partial_\mu j_{\rm R}^{\mu,a} = 0, \qquad \partial_\mu j_{\rm L}^{\mu,a} = 0, \qquad \partial_\mu j_{\rm V}^{\mu} = 0, \qquad \partial_\mu j_{\rm A}^{\mu} = \mathcal{A}, \qquad \mathcal{A} = N_{\rm f}\frac{g^2}{32\pi^2}\epsilon_{\mu\nu\rho\sigma}G_{\mu\nu}^a G^{a\,\rho\sigma}. \tag{4.1.7}$$

The chiral charges

$$Q_{\rm L}^a = \int d^3x j_{\rm L}^{0,a}(\boldsymbol{x},t), \qquad Q_{\rm R}^a = \int d^3x j_{\rm R}^{0,a}(\boldsymbol{x},t), \qquad Q_{\rm V} = \int d^3x j_{\rm V}^{0}(\boldsymbol{x},t) \tag{4.1.8}$$

form the so-called *chiral algebra*

$$\begin{array}{lll} [Q_{\rm L}^a, Q_{\rm L}^a] = if_{abc}Q_{\rm L}^c, & [Q_{\rm R}^a, Q_{\rm R}^a] = if_{abc}Q_{\rm R}^c, & \\ [Q_{\rm L}^a, Q_{\rm V}] = 0, & [Q_{\rm R}^a, Q_{\rm V}] = 0, & [Q_{\rm L}^a, Q_{\rm R}^a] = 0, \end{array} \tag{4.1.9}$$

with f_{abc} the structure constants of $\mathrm{SU}(N_{\rm f})$. The symmetry group of the QCD chiral Lagrangian can be directly read off from the chiral algebra, i.e. the symmetry group factorizes:

$$\mathrm{SU}(N_{\rm f})_{\rm L} \times \mathrm{SU}(N_{\rm f})_{\rm R} \times \mathrm{U_V}(1). \tag{4.1.10}$$

From $\mathrm{U_V}(1)$ one obtains the baryon number conservation,

$$B \equiv Q_{\rm V} = Q_{\rm L} + Q_{\rm R} = \int d^3x\psi^\dagger(\boldsymbol{x},t)\psi(\boldsymbol{x},t). \tag{4.1.11}$$

In contrast, the axial charge $Q_{\rm A} = Q_{\rm L} - Q_{\rm R}$ is not conserved due to the anomaly. The non-singlet chiral charges $Q_{\rm L}^a$ and $Q_{\rm R}^a$ are not conserved separately if chiral symmetry is broken, as will be explained in the next section.

[1] In general, $\psi_{R/L}$ are not helicity eigenstates, but chirality eigenstates: $\gamma_5\psi_{R/L} = \pm\psi_{R/L}$, which agree only in the chiral limit. We will make use of the chiral representation of the Dirac matrices throughout this work.

[2] Eq. (4.1.6) can also be written in the form

$$j_{\rm V}^{\mu,a} = \bar\psi\gamma^\mu t^a\psi, \qquad j_{\rm A}^{\mu,a} = \bar\psi\gamma^\mu\gamma_5 t^a\psi$$

with the identification $\theta_{\rm V}^a = \theta_{\rm R}^a + \theta_{\rm L}^a$, $\theta_{\rm A}^a = \theta_{\rm R}^a - \theta_{\rm L}^a$ in the corresponding transformations $U_{\rm V/A}$ in Eq. (4.1.5).

4.1.2 Spontaneous Chiral Symmetry Breaking and Goldstone Theorem

It is still not fully understood nowadays why SχSB occurs in QCD. Some insight has been achieved by effective models such as the NJL-models [94], which draw an analogy with symmetry breaking due to the forming of cooper pairs in a superconductor. Nevertheless, it is strongly believed *that* SχSB occurs, because one can show that it would solve the puzzles one is confronted with in the mass spectrum of hadrons.

The usual arguments will be summarized in this section. The $\mathrm{U_V}(1)$ symmetry allows to classify all hadrons into two classes with $B = 0$ (the mesons) and $B = 1$ (the baryons). Note that Q^a_{V} forms a closed algebra, whereas Q^a_{A} does not,

$$[Q^a_{\mathrm{V}}, Q^b_{\mathrm{V}}] = i f_{abc} Q^c_{\mathrm{V}}, \qquad [Q^a_{\mathrm{A}}, Q^b_{\mathrm{A}}] = i f_{abc} Q^c_{\mathrm{V}}. \tag{4.1.12}$$

For $N_{\mathrm{f}} = 3$ flavors, based on the quantum numbers isospin I and strangeness S, one obtains the well-known classification in terms of the octet+singlet structure for mesons, and decouplet+2×octet+singlet structure for baryons:[3]

$$3 \otimes \bar{3} = 8 \oplus 1, \qquad 3 \otimes 3 \otimes 3 = 10 \oplus 8 \oplus 8 \oplus 1. \tag{4.1.13}$$

For each set of the quantum numbers angular momentum J, parity P and charge conjugation C one obtains one such nonet in the meson sector, characterized by J^{PC} (with $J = S_1 + S_2 + L$), as illustrated in Fig. 4.1.

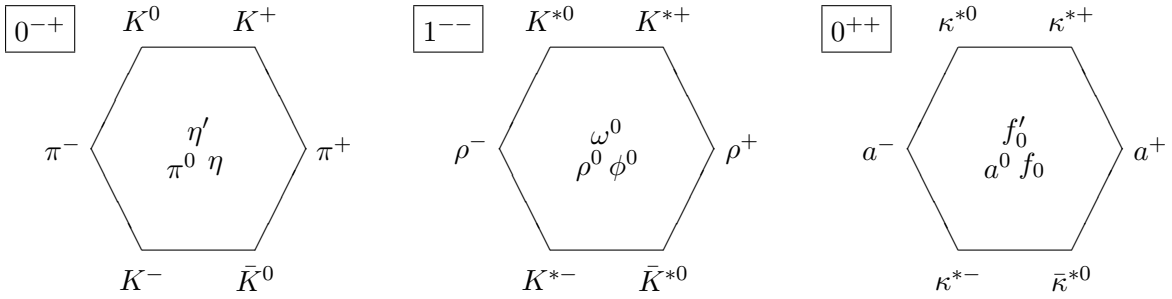

Figure 4.1: The meson nonets for the pseudoscalar mesons (0^{-+}), the vector mesons (1^{--}) and the scalar mesons (0^{++}). The f_0 and a_0, which are particularly involved and have not been identified unambiguously in experiments, are also sometimes called the σ and δ. We will talk of the σ and δ meson only in the context of $N_{\mathrm{f}} = 2$ flavors.

If chiral symmetry was not broken, there would have to exist a *parity doubler* for each state, i.e. a state with opposite parity but same mass. This can be seen by noting that chiral charges commute with the QCD Hamiltonian H^0_{QCD} obtained from the Lagrangian in Eq. (4.1.1),

$$[Q^a_{\mathrm{V}}, H^0_{\mathrm{QCD}}] = 0, \qquad [Q^a_{\mathrm{A}}, H^0_{\mathrm{QCD}}] = 0. \tag{4.1.14}$$

Taking an eigenstate of H^0_{QCD} with positive parity, i.e

$$H^0_{\mathrm{QCD}}|i,+\rangle = E_i|i,+\rangle, \qquad P|i,+\rangle = +|i,+\rangle, \tag{4.1.15}$$

one could define a parity doubler in this way:

$$|\phi\rangle \equiv Q^a_{\mathrm{A}}|i,+\rangle \qquad \Longrightarrow \qquad H^0_{\mathrm{QCD}}|\phi\rangle = E_i|\phi\rangle, \qquad P|\phi\rangle = \underbrace{P Q^a_{\mathrm{A}} P^{-1}}_{-Q^a_{\mathrm{A}}}.P|i,+\rangle = -|\phi\rangle \tag{4.1.16}$$

[3] Note that the SU(3) flavor structure (the *Eightfold Way*), reflected by the Gell-Mann matrices, relies on the assumption $m_u, m_d, m_s \ll \Lambda_{\mathrm{QCD}}$, which is well fulfilled.

The question arises whether such a state can exist; if so, it should be possible to expand it in terms of members of the multiplets with negative parity,

$$|\phi\rangle = -\sum_j t^a_{ij}|j,-\rangle, \qquad \text{with} \qquad [Q^a_{\mathrm{A}}, a^\dagger_i] = -t^a_{ij} b^\dagger_j, \tag{4.1.17}$$

where the constants t_{ij} are determined by the relation between the creation operators $a^\dagger_i$, $b^\dagger_i$ for positive/negative parity states of energy E_i. However, this reasoning assumes that the chiral charges Q^a_{A} annihilate the ground state [105]:

$$Q^a_{\mathrm{A}}|i,+\rangle = Q^a_{\mathrm{A}} a^\dagger_i|0\rangle = \left([Q^a_{\mathrm{A}}, a^\dagger_i] + a^\dagger_i Q^a_{\mathrm{A}}\right)|0\rangle \stackrel{?}{=} -\sum_j t^a_{ij}|j,-\rangle. \tag{4.1.18}$$

The empirical evidence suggests that this is *not the case*: We do not find parity doublers in nature. The ρ meson for example has a mass of 770 MeV, whereas its parity partner, the a_1 meson, has a mass of 1250 MeV. This implies that axial transformations do not leave the vacuum invariant: the axial symmetry is broken spontaneously. In contrast, Q^a_{V} does annihilate the ground state, which means that the vacuum is invariant under vector transformations.

SχSB provides an explanation why pseudoscalar mesons are very light via the famous *Goldstone theorem*, which states that for each generator of a spontaneously broken symmetry, there exists a massless Goldstone boson ϕ with spin 0, and with symmetry properties that are related to those of the symmetry transformation [58]. In particular, the Goldstone bosons of SχSB are just the pseudoscalar mesons, because Q^a_{A} is odd under parity and the Goldstone bosons have to form an octet under Q^a_{V}:

$$[Q^a_{\mathrm{V}}, Q^b_{\mathrm{A}}] = i f_{abc} Q^c_{\mathrm{A}} \qquad \Longrightarrow \qquad [Q^a_{\mathrm{V}}, \phi^b] = i f_{abc}\phi^c. \tag{4.1.19}$$

The Chiral Condensate

We have already noted that the chiral condensate acquires a non-vanishing expectation value if chiral symmetry is broken. This is however a sufficient but not a necessary condition, the chiral symmetry could in principle be broken for other reasons than a non-vanishing chiral condensate:[4]

$$\langle 0|\bar\psi\psi|0\rangle \neq 0 \quad \Longrightarrow \quad \text{S}\chi\text{SB}. \tag{4.1.20}$$

To see this, we introduce the scalar and pseudoscalar densities

$$S(x) = \bar\psi(x)\psi(x), \qquad S^a(x) = \bar\psi(x) t^a \psi(x), \tag{4.1.21}$$

$$P(x) = i\bar\psi(x)\gamma_5\psi(x), \qquad P^a(x) = \bar\psi(x)\gamma_5 t^a\psi(x), \qquad a = 1,\dots N_{\mathrm{f}}^2 - 1 \tag{4.1.22}$$

and calculate the commutator of the vector charges Q^a_{V} with the scalar densities:

$$[Q^a_{\mathrm{V}}, S(x)] = 0, \qquad [Q^a_{\mathrm{V}}, S^b(x)] = i\sum_{c=1}^{N_{\mathrm{f}}^2-1} f_{abc} S^c(x). \tag{4.1.23}$$

The non-vanishing commutator can be inverted for the non-singlet densities by making use of the quadratic Casimir operator of the adjoint representation:

$$\sum_{a,b=1}^{N_{\mathrm{f}}^2-1} f_{abc} f_{abd} = N_{\mathrm{f}}\delta_{cd} \qquad \Longrightarrow \qquad S^a(x) = -\frac{i}{N_{\mathrm{f}}}\sum_{b,c=1}^{N_{\mathrm{f}}^2-1} f_{abc}[Q^b_{\mathrm{V}}, S^c(x)], \tag{4.1.24}$$

[4] Already from this implication it follows that $\langle 0|\bar\psi\psi|0\rangle$ is an order parameter for chiral symmetry restoration.

which for $N_\mathrm{f} = 3$ gives rise to the relations[5]

$$\langle 0|\bar{u}u|0\rangle - \langle 0|\bar{d}d|0\rangle = 0, \qquad \langle 0|\bar{u}u|0\rangle + \langle 0|\bar{d}d|0\rangle - 2\langle 0|\bar{s}s|0\rangle = 0. \tag{4.1.25}$$

No such inversion is possible for the singlet density. Hence it is conceptually possible that the chiral condensate does not vanish, although it is not clear at that stage why this should be due to SχSB. From the relation

$$\langle 0|i[Q_a^A, P^a(x)]|0\rangle = \frac{2}{N_\mathrm{f}}\langle 0|S(x)|0\rangle, \qquad a = 1, \dots N_\mathrm{f}^2 - 1 \tag{4.1.26}$$

one can see immediately that a non-vanishing chiral condensate implies that Q_a^A does not annihilate the vacuum. In reverse, once chiral symmetry is restored, the chiral condensate vanishes.[6] Hence, the chiral condensate turns out to be an order parameter of the chiral phase transition.

In the case of $N_\mathrm{f} = 2$ massless flavors and at zero temperature[7] one can apply the group theoretical isomorphism

$$\mathrm{SU}(2)_\mathrm{L} \times \mathrm{SU}(2)_\mathrm{R} \simeq \mathrm{O}(4) \to \mathrm{O}(3) \simeq \mathrm{SU}(2)_\mathrm{V} \tag{4.1.27}$$

to the Lagrangian in Eq. (4.1.1). Hence QCD with two light flavors has the same global symmetry as the O(4) spin model, which is therefore often studied as a model for SχSB. Moreover, the chiral condensate — the order parameter of the chiral transition — indicates this symmetry pattern as well. This suggests that the chiral transition in the chiral limit lies in the universality class of O(4). However, this might only be true in the limit of an infinite strange quark mass, and even in this case there is no strict proof.

The Pion Decay Constant

From Eq. (4.1.26) one can also obtain a *necessary and sufficient condition* for SχSB. Due to Lorentz invariance one can write for the corresponding axial current:

$$\langle 0|j_\mathrm{A}^{\mu,a}(0)|\phi^b(p)\rangle = ip^\mu F_0 \delta^{ab}. \tag{4.1.28}$$

From this equation we can see that Q_A^a has a non-vanishing matrix element between the vacuum and the massless one particle states $|\phi^b\rangle$, parameterized by F_0, if and only if Q_A^a does not annihilate the vacuum:

$$F_0 \neq 0 \quad \Longleftrightarrow \quad \mathrm{S}\chi\mathrm{SB}. \tag{4.1.29}$$

4.1.3 Explicit Chiral Symmetry Breaking

If we add to the Lagrangian in Eq. (4.1.1) the mass term

$$\mathcal{L}_\mathcal{M} = -\sum_{f=1}^{N_\mathrm{f}} \bar{\psi}_f \mathcal{M} \psi_f = -\sum_{f=1}^{N_\mathrm{f}} \left(\bar{\psi}_{\mathrm{R},f}\mathcal{M}\psi_{\mathrm{L},f} + \bar{\psi}_{\mathrm{L},f}\mathcal{M}\psi_{\mathrm{R},f}\right), \qquad \mathcal{M} = \mathrm{diag}\,(m_u, m_d, m_s, \dots) \tag{4.1.30}$$

[5] These relations are only valid in the chiral limit of all quark masses, we will however keep the strange quark mass finite, which spoils this relation.

[6] In principle, the chiral condensate might vanish at some temperature although the chiral symmetry is still spontaneously broken. But see next section.

[7] At non-zero temperature, the axial symmetry might be effectively restored, leading to a different symmetry group. See Sec. 4.3 for details.

with $\mathcal{M}$ the quark matrix[8], chiral symmetry is explicitly broken due to the mixing of left- and right-handed components induced by the quark masses. Hence, the divergence of the chiral currents is non-vanishing:

$$\left.\begin{aligned}\partial_\mu j_L^\mu &= -i\left(\bar\psi_{\mathrm{L}}\mathcal{M}\psi_{\mathrm{R}} - \bar\psi_{\mathrm{R}}\mathcal{M}\psi_{\mathrm{L}}\right)\\ \partial_\mu j_R^\mu &= -i\left(\bar\psi_{\mathrm{R}}\mathcal{M}\psi_{\mathrm{L}} - \bar\psi_{\mathrm{L}}\mathcal{M}\psi_{\mathrm{R}}\right)\end{aligned}\right\} \implies \left\{\begin{aligned}\partial_\mu j_V^\mu &= 0\\ \partial_\mu j_A^\mu &= 2i\bar\psi\mathcal{M}\gamma_5\psi + \mathcal{A}\end{aligned}\right., \tag{4.1.31}$$

$$\left.\begin{aligned}\partial_\mu j_L^{\mu,a} &= -i\left(\bar\psi_{\mathrm{L}}t^a\mathcal{M}\psi_{\mathrm{R}} - \bar\psi_{\mathrm{R}}\mathcal{M}t^a\psi_{\mathrm{L}}\right)\\ \partial_\mu j_R^{\mu,a} &= -i\left(\bar\psi_{\mathrm{R}}t^a\mathcal{M}\psi_{\mathrm{L}} - \bar\psi_{\mathrm{L}}\mathcal{M}t^a\psi_{\mathrm{R}}\right)\end{aligned}\right\} \implies \left\{\begin{aligned}\partial_\mu j_V^{\mu,a} &= i\bar\psi[\mathcal{M}, t^a]\psi\\ \partial_\mu j_A^{\mu,a} &= i\bar\psi\{\mathcal{M}, t^a\}\gamma_5\psi\end{aligned}\right.. \tag{4.1.32}$$

Note however that in the degenerate case $\mathcal{M} = m\mathbb{1}_{N_{\mathrm{f}}\times N_{\mathrm{f}}}$ also $\partial_\mu j_V^{\mu,a} = 0$.[9] If the quark masses are small, chiral symmetry and its spontaneous breakdown are still approximately valid. The corrections induced by the finite quark masses can then be effectively described via chiral perturbation theory.

4.2 Chiral Perturbation Theory for 2+1 Flavors

4.2.1 Chiral Perturbation Theory at Zero Temperature

Chiral perturbation theory (χPT) proved to be a very important method for the determination of some low energy observables in QCD, such as the masses of pseudoscalar mesons, their decay constants and chiral observables. A sophisticated version has been developed for three non-degenerate flavors [51], which we will discuss in this section for the special case $N_{\mathrm{f}} = 2 + 1$, i.e.

$$m_l \equiv m_u = m_d, \qquad m_l \neq m_s \qquad \Longrightarrow \qquad \tan(2\epsilon) \equiv \sqrt{3}\frac{m_d - m_u}{2m_s - m_d - m_u} = 0, \tag{4.2.1}$$

where the vanishing of the mixing angle ϵ implies that there is no $\pi^0-\eta$ mixing, and the quark content of these particles is simply given by the Gell-Mann matrices λ_3, λ_8. However, we will sometimes also compare with the three flavor case $m_s = m_l$, the two flavor case $m_s \to \infty$, or more general the case of N_{f} degenerated flavors.

The starting point of χPT is the effective Lagrangian for low energy physics, in which the pseudoscalar mesons are the relevant degrees of freedom. It can be written as a power series in the momenta $\mathcal{O}\left(p^{(2n)}\right)$ and contains all possible terms consistent with chiral symmetry:

$$\mathcal{L}_{\mathrm{eff}} = \mathcal{L}^{(2)} + \mathcal{L}^{(4)} + \ldots \tag{4.2.2}$$

The χPT for zero temperature discussed here relies on the p-expansion scheme (compare Fig. 3.8) which is based on a twofold expansion, in the momenta and in the quark masses, provided that

$$\frac{p}{\Lambda_\chi} < 1, \qquad \frac{M_P}{\Lambda_\chi} < 1, \qquad \Lambda_\chi = 4\pi F_0 \tag{4.2.3}$$

with M_P the mass of the pseudoscalar meson considered and Λ_χ the chiral scale.[10] At lowest order it is the Lagrangian of the non-linear sigma model, which is very similar to the spin models we have already encountered in Sec. 3.2:

$$\mathcal{L}^{(2)} = \frac{1}{4}F_0^2\left\{\mathrm{Tr}\left(\partial_\mu U^\dagger \partial_\mu U\right) - 2B_0\,\mathrm{Tr}\left(\mathcal{M}^\dagger U + \mathcal{M}U^\dagger\right)\right\}. \tag{4.2.4}$$

[8] In the following, we will either consider three non-degenerate flavors $N_{\mathrm{f}} = 2 + 1$ or we restrict to the degenerate cases $\mathcal{M} = m\mathbb{1}_{N_{\mathrm{f}}\times N_{\mathrm{f}}}$, $N_{\mathrm{f}} = 2, 3$. The charm quark is too heavy to be subject to chiral perturbation theory.

[9] Also note that $\partial_\mu A^{\mu,a}$ is proportional to pseudoscalar quadratic forms, which gives rise to the well-known PCAC relations.

[10] This power scheme implies that the quark masses are of $\mathcal{O}\left(p^2\right)$ in the chiral expansion, due to the GMOR relation (4.2.9) discussed below.

The unitary matrix U is composed of the meson fields:

$$U = \exp(i\Phi/F_0), \qquad \Phi = \sum_{a=1}^{N_\mathrm{f}^2-1} \phi^a \lambda^a, \qquad \lambda^a = 2t^a. \tag{4.2.5}$$

For $N_\mathrm{f} = 2+1$ flavors the explicit fields are:[11]

$$\Phi = \sum_{a=1}^{8} \phi^a \lambda^a = \sum_{P=1}^{8} \phi_P \lambda_P = \begin{pmatrix} \pi^0 + \frac{1}{\sqrt{3}}\eta & \sqrt{2}\pi^+ & \sqrt{2}K^+ \\ \sqrt{2}\pi^- & -\pi^0 + \frac{1}{\sqrt{3}}\eta & \sqrt{2}K^0 \\ \sqrt{2}K^- & \sqrt{2}\bar{K}^0 & -\frac{2}{3}\eta \end{pmatrix}, \tag{4.2.6}$$

$$\begin{aligned} \lambda_{\pi^\pm} &= \mp\frac{1}{\sqrt{2}}(\lambda^1 \pm i\lambda^2), \quad \lambda_{K^\pm} = \mp\frac{1}{\sqrt{2}}(\lambda^4 \pm i\lambda^5), \quad \lambda_{\pi^0} = \lambda^3, \\ \lambda_{K^0} &= -\frac{1}{\sqrt{2}}(\lambda^6 + i\lambda^7), \quad \lambda_{\bar{K}^0} = -\frac{1}{\sqrt{2}}(\lambda^6 - i\lambda^7), \quad \lambda_\eta = \lambda^8, \end{aligned} \tag{4.2.7}$$

where the sum over P denotes the pseudoscalar mesons, $P \in \{\pi^+, \pi^-, \pi^0, K^+, K^-, K^0, \bar{K}^0, \eta\}$. The normalization is chosen such that the standard kinetic term is reproduced when expanding $U(x)$:

$$\mathcal{L}^{(2)} = \frac{1}{2}\partial_\mu\phi_P\partial_\mu\phi_P + \frac{1}{2}\mathring{M}_P^2\phi_P^2 + \mathcal{L}_\mathrm{int}^{(2)}, \qquad \mathring{M}_P^2 = B_0 \operatorname{tr}\left(\mathcal{M}\lambda_P\lambda_P^\dagger\right). \tag{4.2.8}$$

and the interaction term $\mathcal{L}_\mathrm{int}^{(2)}$ contains higher powers of the pseudoscalar fields. The mass term in Eq. (4.2.4) is constructed such that it is invariant under chiral transformations, which is achieved by forcing $\mathcal{M}$ to transform in the same way as $U(x)$. The Lagrangian is parameterized by the low energy constants F_0 and B_0: the pion decay constant with $F_0 \simeq 93$ MeV[12], and the constant

$$B_0 = -\lim_{m_f \to 0} \frac{\langle 0|\bar{\psi}\psi|0\rangle}{N_\mathrm{f} F_0^2}, \tag{4.2.9}$$

which defines the vacuum expectation value of the chiral condensate in the chiral limit, $B_0 \simeq 1.4$ GeV. The tree-level masses $\mathring{M}_P$ of the pseudoscalar mesons P, valid in the vicinity of the chiral limit, can be read off Eq. (4.2.8) after having identified the quark content from the Gell-Mann matrices (see App. B.2.3):

$$\mathring{M}_{\pi^0}^2 = \mathring{M}_{\pi^+}^2 = \mathring{M}_{\pi^-}^2 = B_0(m_u + m_d) \simeq 2B_0 m_l, \tag{4.2.10}$$

$$\mathring{M}_{K^+}^2 = \mathring{M}_{K^-}^2 = B_0(m_u + m_s) \simeq B_0(m_l + m_s), \tag{4.2.11}$$

$$\mathring{M}_{K^0}^2 = \mathring{M}_{\bar{K}^0}^2 = B_0(m_d + m_s) \simeq B_0(m_l + m_s), \tag{4.2.12}$$

$$\mathring{M}_\eta^2 = \frac{1}{3}B_0(m_u + m_d + 4m_s) \simeq \frac{2}{3}B_0(m_l + 2m_s), \tag{4.2.13}$$

where the circle indicates that this result holds only to lowest order. These formulae together with Eq. (4.2.9) are known as Gell-Mann/Oakes/Renner (GMOR) relation [56]. By plugging in the experimental values for the meson masses, they allow to estimate the value of the quark masses: from the ratio M_K^2/M_π^2 one obtains $m_s/m_l = 25.9$, from M_η^2/M_π^2 one obtains $m_s/m_l = 24.3$.
At lowest order, the effective Lagrangian $\mathcal{L}^{(2)}$ reproduces the necessary and sufficient condition for SχSB, i.e. SχSBis broken if and only if $F_0 > 0$:

$$\begin{aligned} J_A^{\mu,a} = -i\frac{1}{4}F_0^2 \operatorname{Tr}\left(\lambda_a\{U(x), \partial^\mu U^\dagger(x)\}\right) &= -F_0\partial^\mu\phi_a + \dots \\ \implies \qquad \langle 0|J_A^{\mu,a}|\phi^b(p)\rangle &= -F_0 p_\mu \exp\left(-ip\cdot x\right)\delta^{ab}. \end{aligned} \tag{4.2.14}$$

[11] We will restrict to $m_l \equiv m_u = m_d$ and neglect mixing, which corresponds to set $\epsilon = 0$ in reference [51]. However, it is instructive to keep light flavors distinct.

[12] Note that this value is the experimental value for physical quark masses, which will later be denoted by F_π. In the chiral limit, F_0 takes slightly smaller values, depending also on the number of flavors. For three flavors, Gasser and Leutwyler give the value $F_0 = 87$ MeV [51].

For higher order corrections of the meson masses, but also for the leading order contribution to the chiral condensate, one has to perform a one-loop calculation. This makes it mandatory to include terms from the effective Lagrangian $\mathcal{L}^{(4)}$ of order $\mathcal{O}\left(p^4\right)$, which in the case of $N_\mathrm{f} = 3$ is:[13]

$$\mathcal{L}^{(4)} = \sum_{i=1}^{8} L_i P_i + H_2 Q_2 \tag{4.2.15}$$

$$\begin{aligned}
P_1 &= \mathrm{Tr}\left(\partial_\mu U^\dagger \partial_\mu U\right)^2 & P_6 &= 4B_0^2\,\mathrm{Tr}\left(\mathcal{M}^\dagger U + \mathcal{M} U^\dagger\right)^2 \\
P_2 &= \mathrm{Tr}\left(\partial_\mu U^\dagger \partial_\nu U\right)\mathrm{Tr}\left(\partial_\mu U^\dagger \partial_\nu U\right) & P_7 &= 4B_0^2\,\mathrm{Tr}\left(\mathcal{M}^\dagger U - \mathcal{M} U^\dagger\right)^2 \\
P_3 &= \mathrm{Tr}\left(\partial_\mu U^\dagger \partial_\mu U \partial_\nu U^\dagger \partial_\nu U\right) & P_8 &= 4B_0^2\,\mathrm{Tr}\left(\mathcal{M}^\dagger U \mathcal{M}^\dagger U + \mathcal{M} U^\dagger \mathcal{M} U^\dagger\right) \\
P_4 &= 2B_0\,\mathrm{Tr}\left(\partial_\mu U^\dagger \partial_\mu U\right)\mathrm{Tr}\left(\mathcal{M}^\dagger U + \mathcal{M} U^\dagger\right) & & \\
P_5 &= 2B_0\,\mathrm{Tr}\left(\partial_\mu U^\dagger \partial_\mu U \left(\mathcal{M}^\dagger U + \mathcal{M} U^\dagger\right)\right) & Q_2 &= \mathrm{Tr}\left(\mathcal{M}^\dagger \mathcal{M}\right),
\end{aligned}$$

where the L_i are further low energy constants and H_2 is a contact term which only contributes to the vacuum energy.[14] At this order, also quark mass differences will enter into chiral observables. The calculation of the corrections to chiral observables employs dimensional regularization. To this purpose, we introduce the parameter Λ which defines the scale at which the low/high-energy constants are renormalized:

$$L_i = L_i^r + \Gamma_i \lambda, \quad i = 1, \ldots 8; \qquad H_2 = H_2^r + \tilde{\Gamma}_2 \lambda, \tag{4.2.16}$$

$$\lambda = \frac{\Lambda^{d-4}}{(4\pi)^2}\left\{\frac{1}{d-4} - \frac{1}{2}\left(\log(4\pi) - \gamma_E + 1\right)\right\}. \tag{4.2.17}$$

Note that the Feynman propagator of the pseudoscalar particle P

$$\Delta_P(x) \equiv \int \frac{d^d p}{(2\pi)^d} \frac{e^{ipx}}{\mathring{M}_P^2 + p^2} \tag{4.2.18}$$

develops a pole in four dimensions, which also shows up in λ. Hence the following integrated scalar propagators are evaluated in $d = 4 - \epsilon$ dimensions, which allows expansion in $\epsilon > 0$:

$$I_P \equiv -i\Lambda^\epsilon \Delta_P(0) = 2\mathring{M}_P^2 \lambda + \frac{1}{(4\pi)^2}\mathring{M}_P^2 \log\frac{\mathring{M}_P}{\Lambda} + \mathcal{O}(\epsilon), \tag{4.2.19}$$

$$\begin{aligned}
J_{PQ} &\equiv -i\Lambda^\epsilon \int d^d x \Delta_P(-x)\Delta_Q(x) \\
&= 2\lambda + \frac{1}{(4\pi)^2}\frac{1}{\mathring{M}_P^2 - \mathring{M}_Q^2}\left(\mathring{M}_P^2 \log\frac{\mathring{M}_P}{\Lambda} - \mathring{M}_Q^2 \log\frac{\mathring{M}_Q}{\Lambda}\right) + \mathcal{O}(\epsilon),
\end{aligned} \tag{4.2.20}$$

where I_P is the one-loop integral for the particle P and J_{PQ} is an integrated correlation function, i.e. an one-loop integral with two vertices separated by some distance (so-called "bubble term") and the two scalar propagators may belong to different particles P, Q. Based on these integrals and a

[13] Note that for $N_\mathrm{f} = 2$ the Lagrangian $\mathcal{L}^{(4)}$ is differently parameterized, because the symmetries are different. The mapping of terms between the $N_\mathrm{f} = 3$ and $N_\mathrm{f} = 2$ Lagrangians is rather tedious and not straightforward: One needs to perform the chiral limit in the light quark masses for fixed strange quark mass, but the resulting mapping involves non-trivial relations between the renormalization constant.

[14] This is Eq. (6.16) in Ref. [50] for the special case that no external vector field v_μ and axial vector field a_μ are present, resulting in $\nabla^\mu = \nabla_\mu = \partial_\mu$ and $F_{\mu\nu}^{\mathrm{L/R}} = 0$. With this, $\chi(x)$ reduces to $\chi(x) = 2B_0\mathcal{M}$. For this choice of $\chi(x)$, the terms proportional to L_9, L_{10} and H_1 vanish.

set of renormalized parameters Λ_i which deviate from Λ due to the counterterms from $\mathcal{L}^{(4)}$ — the Λ_i involve the low/high-energy constants depending on the observable[15] — we define the following symbols:

$$\mu_{P,i} \equiv \frac{1}{(4\pi F_0)^2} \mathring{M}_P^2 \log \frac{\mathring{M}_P}{\Lambda_i}, \tag{4.2.21}$$

$$\mu_{PQ,i} \equiv \frac{1}{(4\pi F_0)^2} \frac{1}{\mathring{M}_P^2 - \mathring{M}_Q^2} \left(\mathring{M}_P^2 \log \frac{\mathring{M}_P}{\Lambda_i} - \mathring{M}_Q^2 \log \frac{\mathring{M}_Q}{\Lambda_i} \right) = \frac{\mu_{P,i} - \mu_{Q,i}}{\mathring{M}_P^2 - \mathring{M}_Q^2} = \mu_{QP,i}, \tag{4.2.22}$$

$$\mu_{PP,i} \equiv \frac{1}{(4\pi F_0)^2} \log \left(\frac{\mathring{M}_P}{\Lambda_i} + 1 \right) = \frac{\partial}{\partial \mathring{M}_P^2} \mu_{P,i}, \tag{4.2.23}$$

$$\sigma_{PQ} \equiv \frac{1}{4} B_0 \operatorname{tr} \left(\{\lambda_P, \lambda_Q^\dagger\} \mathcal{M} (U + U^\dagger) \right) - \delta_{PQ} \mathring{M}_P^2. \tag{4.2.24}$$

With these definitions, the energy density of the vacuum obtained from the one-loop generating functional [51] is expressed as follows:[16]

$$\begin{aligned} \epsilon_0 =& c_0 + \frac{i}{2} \sum_{P=1}^{N_\mathrm{f}^2-1} \Delta_P(0) \sigma_{PP} - \frac{i}{4} \sum_{P,Q=1}^{N_\mathrm{f}^2-1} \int dx \Delta_P(-x) \Delta_Q(x) \sigma_{PQ} \sigma_{QP} + \mathcal{O}\left(\phi^6\right) && (4.2.25) \\ =& c_0 + F_0^2 \sum_{P=1}^{N_\mathrm{f}^2-1} \mathring{M}_P^2 \left(-\frac{N_\mathrm{f}}{2(N_\mathrm{f}^2-1)} + \mu_{P,3} \right) - \mathcal{L}_\mathrm{ren}^{(4)} \\ & + F_0^2 \sum_{P,Q=1}^{N_\mathrm{f}^2-1} \sigma_{PQ} \sigma_{QP} \mu_{PQ,1} + \mathcal{O}\left(\mathring{M}_P^6 \right), && (4.2.26) \end{aligned}$$

where c_0 specifies the energy density of the ground state in the chiral limit and $\mathcal{L}_\mathrm{ren}^{(4)}$ denotes the contributions of $\mathcal{L}^{(4)}$ with L_i and H_2 replaced by the renormalized constants L_i and H_2 (see App. B.1.2). The remaining terms are one-loop contributions from $\mathcal{L}^{(2)}$: The sum over P denotes the tadpole contribution, whereas the sum over P, Q stems from one loop graphs with two vertices ("bubble graphs"). This second term is difficult to calculate in the non-degenerate case, it will contribute to the chiral susceptibility. We will postpone its calculation to Sec. 4.4.5 in the context of staggered chiral perturbation theory.[17]

[15] We will assume without giving a proof here that at each order of the effective Lagrangian, the divergent parameter λ can be absorbed in the renormalized parameters Λ_i. Hence we will drop contributions from λ in the integrals I_P, J_{PQ}, because they are implicitly accounted for in the new defined symbols $\mu_{P,i}$, $\mu_{PQ,i}$.

[16] The calculation of the degenerated case for $N_\mathrm{f}^2 - 1$ pions is given in the appendix B.2, the vacuum energy is:

$$\epsilon_0 = c_0 - F_0^2 \mathring{M}_\pi^2 \left\{ \tfrac{1}{2} N_\mathrm{f} + \tfrac{1}{2}(N_\mathrm{f}^2 - 1) \mu_{\pi,3} + \frac{N_\mathrm{f}^2 - 1}{N_\mathrm{f}} (\mu_{\pi,1})^2 \right\} + c_1 \mathring{M}_\pi^6 + \mathcal{O}\left(\mathring{M}_\pi^8 \right).$$

[17] The reason for this difficulty is that one can not simultaneously keep track of quark-line connected and disconnected contributions, and express the computation in the physical propagators introduced above. Therefore we will compute the connected and disconnected parts by making use of mesonic mass eigenstates $\mathring{M}_U$, $\mathring{M}_D$ $\mathring{M}_S$. The connected and disconnected parts will have contributions in these unphysical states, which will finally cancel in the sum of both terms. See also Tab. 4.3.

The Chiral Condensate from χPT

The chiral condensate is obtained by making use of the derivatives

$$\frac{\partial \mu_{P,i}}{\partial \mathring{M}_P} = \frac{2}{\mathring{M}_P}\mu_{P,i} + \frac{\mathring{M}_P}{(4\pi F_0)^2}, \tag{4.2.27}$$

$$\frac{\partial \epsilon_0}{\partial \mathring{M}_P} = F_0^2 \mathring{M}_P \left(-\frac{N_\mathrm{f}}{(N_\mathrm{f}^2-1)} + \mathring{M}_P \frac{\partial \mu_{P,3}}{\partial \mathring{M}_P} \right) + F_0^2 \sum_{Q=1}^{N_\mathrm{f}^2-1} \frac{\partial}{\partial \mathring{M}_P} \{\sigma_{PQ}\sigma_{QP}\mu_{PQ,1}\} + \mathcal{O}\left(\mathring{M}_P^5\right) \tag{4.2.28}$$

The quark condensates for $N_\mathrm{f} = 2+1$ are determined by the quark mass derivatives:

$$\begin{aligned}
\langle 0|\bar{u}u|0\rangle &= \frac{\partial \epsilon_0}{\partial m_u} = \frac{3}{2}\frac{B_0}{\mathring{M}_\pi}\frac{\partial \epsilon_0}{\partial \mathring{M}_\pi} + \frac{B_0}{\mathring{M}_{K^\pm}}\frac{\partial \epsilon_0}{\partial \mathring{M}_{K^\pm}} + \frac{1}{6}\frac{B_0}{\mathring{M}_\eta}\frac{\partial \epsilon_0}{\partial \mathring{M}_\eta} \\
&= -B_0F_0^2\left(1 - 3\mu_\pi - 2\mu_{K^\pm} - \tfrac{1}{3}\mu_\eta + m_u K_1 + (m_u+m_d+m_s)K_2\right), \qquad (4.2.29) \\
\langle 0|\bar{d}d|0\rangle &= \frac{\partial \epsilon_0}{\partial m_d} = \frac{3}{2}\frac{B_0}{\mathring{M}_\pi}\frac{\partial \epsilon_0}{\partial \mathring{M}_\pi} + \frac{B_0}{\mathring{M}_{K^0}}\frac{\partial \epsilon_0}{\partial \mathring{M}_{K^0}} + \frac{1}{6}\frac{B_0}{\mathring{M}_\eta}\frac{\partial \epsilon_0}{\partial \mathring{M}_\eta} \\
&= -B_0F_0^2\left(1 - 3\mu_\pi - 2\mu_{K^0} - \tfrac{1}{3}\mu_\eta + m_d K_1 + (m_u+m_d+m_s)K_2\right), \qquad (4.2.30) \\
\langle 0|\bar{s}s|0\rangle &= \frac{\partial \epsilon_0}{\partial m_s} = \frac{B_0}{\mathring{M}_{K^\pm}}\frac{\partial \epsilon_0}{\partial \mathring{M}_{K^\pm}} + \frac{B_0}{\mathring{M}_{K^0}}\frac{\partial \epsilon_0}{\partial \mathring{M}_{K^0}} + \frac{2}{3}\frac{B_0}{\mathring{M}_\eta}\frac{\partial \epsilon_0}{\partial \mathring{M}_\eta} \\
&= -B_0F_0^2\left(1 - 2\mu_{K^\pm} - 2\mu_{K^0} - \tfrac{4}{3}\mu_\eta + m_s K_1 + (m_u+m_d+m_s)K_2\right), \qquad (4.2.31) \\
K_1 &= \frac{8B_0}{F_0^2}(2L_8^r + H_2^r), \qquad K_2 = \frac{32B_0}{F_0^2}L_6^r, \qquad (4.2.32)
\end{aligned}$$

where we have dropped higher orders in the quark masses. The linear terms, determined by the constants K_1, K_2, stem from $\mathcal{L}^{(4)}$. The scale dependence of the chiral logarithms μ_P cancel the scale dependence of the low and high energy constants L_6^r, L_8^r and H_2^r, the vacuum expectation values are independent of the chiral scale set by Λ_i, hence we suppressed the index i in $\mu_{P,i}$. Note that only K_1 may be divergent due to the high energy constant H_2. For completeness, we also give the chiral condensate, the pion mass M_π and the pion decay constant F_π to one loop order for N_f degenerate flavors [50]:[18]

$$\langle 0|\bar{\psi}\psi|0\rangle = -B_0F_0^2\left\{1 - 2\frac{N_\mathrm{f}^2-1}{N_\mathrm{f}}\mu_{\pi,3} + \mathcal{O}\left(M_0^4\right)\right\}, \tag{4.2.33}$$

$$M_\pi = M_0\left\{1 + \frac{1}{N_\mathrm{f}}\mu_{\pi,2} + \mathcal{O}\left(M_0^4\right)\right\}, \tag{4.2.34}$$

$$F_\pi = F_0\left\{1 - N_\mathrm{f}\mu_{\pi,1} + \mathcal{O}\left(M_0^4\right)\right\}. \tag{4.2.35}$$

One finds that the tree-level GMOR formula $2m_q\langle 0|\bar{\psi}\psi|0\rangle = M_0^2F_0^2$ also holds to next to leading order:

$$2m_l\langle 0|\bar{\psi}\psi|0\rangle = M_\pi^2F_\pi^2 + \mathcal{O}\left(M_0^4\right), \qquad \text{if} \qquad \log\Lambda_3 = \frac{N_\mathrm{f}^2\log\Lambda_2 - \log\Lambda_1}{N_\mathrm{f}^2-1}. \tag{4.2.36}$$

However, this nontrivial relation between the cut-offs Λ_i is not granted.

[18] These equations can be readily compared to the O(N) results, Eq. (3.4.6 - 3.4.8). The matching works for $N_\mathrm{f} = 2 \leftrightarrow N = 4$ only! One finds $N_\mathrm{f}^2 - 1 = 3 = N - 1$, $N_\mathrm{f} = 2 = N - 2$ and $1/N_\mathrm{f} = 1/2 = (N-3)/2$, the last identity is due to the fact that in the O(N) model the *square* of the Goldstone boson mass was expanded in the external field. Note also that the number of all modes for each $\langle 0|\bar{q}q|0\rangle$ ($q = u, d, s$) is $2(N_\mathrm{f}^2-1)/N_\mathrm{f} = 16/3$ for $N_\mathrm{f} = 3$, which agrees with the degenerate case $\langle 0|\bar{\psi}\psi|0\rangle$.

The Disconnected and Connected Susceptibility from χPT

The chiral susceptibility is the quark mass derivative of the chiral condensate. In contrast to the magnetic susceptibility in O(N) spin models, Eq. (3.2.15), also quark-line connected diagrams contribute to the full susceptibility, due to an additional Wick contraction:

$$\chi^{\text{full}} = \frac{\partial}{\partial m_q}\langle 0|\bar{\psi}\psi|0\rangle \equiv \chi^{\text{dis}} + \chi^{\text{con}}, \qquad \chi^{\text{dis}} = N_{\text{f}}^2\left(\langle 0|(\bar{\psi}\psi)^2|0\rangle - \langle 0|\bar{\psi}\psi|0\rangle^2\right),$$
$$\chi^{\text{con}} = N_{\text{f}}\langle 0|\bar{\psi}(x)\overbrace{\psi(x)\bar{\psi}(0)}\psi(0)|0\rangle. \tag{4.2.37}$$

The full susceptibilities are obtained from Eqs. (4.2.30 - 4.2.32) by taking the quark mass derivatives, and by also taking into account additional terms from the second line of Eq. (4.2.26):

$$\chi_{uu}^{\text{full}} = \frac{\partial}{\partial m_u}\langle 0|\bar{u}u|0\rangle = B_0^2F_0^2\left(\tfrac{3}{2}\mu_{\pi\pi} + \mu_{K^+K^-} + \tfrac{1}{3}\mu_{\pi\eta} + \tfrac{1}{18}\mu_{\eta\eta} + K_1 + K_2\right), \tag{4.2.38}$$

$$\chi_{dd}^{\text{full}} = \frac{\partial}{\partial m_d}\langle 0|\bar{d}d|0\rangle = B_0^2F_0^2\left(\tfrac{3}{2}\mu_{\pi\pi} + \mu_{K^0\bar{K}^0} + \tfrac{1}{3}\mu_{\pi\eta} + \tfrac{1}{18}\mu_{\eta\eta} + K_1 + K_2\right), \tag{4.2.39}$$

$$\chi_{ss}^{\text{full}} = \frac{\partial}{\partial m_s}\langle 0|\bar{s}s|0\rangle = B_0^2F_0^2\left(\mu_{K^0\bar{K}^0} + \mu_{K^+K^-} + \tfrac{8}{9}\mu_{\eta\eta} + K_1 + K_2\right), \tag{4.2.40}$$

$$\chi_{ud}^{\text{full}} = \frac{\partial}{\partial m_u}\langle 0|\bar{d}d|0\rangle = B_0^2F_0^2\left(\tfrac{3}{2}\mu_{\pi\pi} - \tfrac{1}{3}\mu_{\pi\eta} + \tfrac{1}{18}\mu_{\eta\eta} + K_2\right) = \chi_{du}^{\text{full}}, \tag{4.2.41}$$

$$\chi_{su}^{\text{full}} = \frac{\partial}{\partial m_u}\langle 0|\bar{s}s|0\rangle = B_0^2F_0^2\left(\mu_{K^+K^-} + \tfrac{2}{9}\mu_{\eta\eta} + K_2\right) = \chi_{us}^{\text{full}}, \tag{4.2.42}$$

$$\chi_{sd}^{\text{full}} = \frac{\partial}{\partial m_d}\langle 0|\bar{s}s|0\rangle = B_0^2F_0^2\left(\mu_{K^0\bar{K}^0} + \tfrac{2}{9}\mu_{\eta\eta} + K_2\right) = \chi_{ds}^{\text{full}}, \tag{4.2.43}$$

$$\tag{4.2.44}$$

where μ_{PQ} are the UV- and IR-divergent logarithms defined in Eqs. (4.2.22-4.2.24), and higher order terms are dropped. In the susceptibilities χ_{qq}^{full}, both connected and disconnected contributions enter, whereas $\chi_{qq'}^{\text{full}}$ consists only of the disconnected term for $q \neq q'$. In this framework (in the basis of the physical states) it is not possible to identify the connected and disconnected parts for the non-degenerate case. We will identify them in Sec. 4.4.5 after having adopted a basis in terms of the mass eigenstates. Adding together all contributions, one obtains:

$$\chi^{\text{full}} = B_0^2F_0^2\left(6\mu_{\pi\pi} + 4\mu_{K^+K^-} + 4\mu_{K^0\bar{K}^0} + 2\mu_{\eta\eta} + 3K_1 + 9K_2\right). \tag{4.2.45}$$

In the degenerated case, the full susceptibility is given by

$$\chi^{\text{full}} = 2B_0^2\frac{N_{\text{f}}^2-1}{(4\pi)^2}\log\frac{\Lambda^2}{\mathring{M}_\pi^2} + N_{\text{f}}K_1 + N_{\text{f}}^2K_2. \tag{4.2.46}$$

The connected susceptibility can also be calculated within chiral perturbation theory [110], for details on the calculation, see App. (B.2):

$$\chi^{\text{con}} = B_0^2\frac{N_{\text{f}}^2-4}{(4\pi)^2}\log\frac{\Lambda^2}{M_\pi^2} + N_{\text{f}}K_1. \tag{4.2.47}$$

The remarkable feature of this expression is that the infrared divergent part vanishes for $N_{\text{f}} = 2$. Hence, no Goldstone Effect is expected for the connected susceptibility! Note also that the UV-divergent constant K_1 only appears in the connected part. By subtracting the connected susceptibility from the full susceptibility, one also obtains the disconnected susceptibility:

$$\chi^{\text{dis}} = B_0^2\frac{N_{\text{f}}^2+2}{(4\pi)^2}\log\frac{\Lambda^2}{M_\pi^2} + N_{\text{f}}^2K_2, \tag{4.2.48}$$

which has always a non-vanishing infrared-divergent part.

4.2.2 Chiral Perturbation Theory at Finite Temperature

The finite temperature free energy density of a gas consisting of pseudoscalar mesons can be decomposed into a zero temperature contribution ϵ_0 which contains ultraviolet and infrared divergent contributions, and the pressure $P(T)$, which does not contain additional divergences:

$$f(T) = \epsilon_0 - P(T) \tag{4.2.49}$$

$$= -\lim_{V\to\infty} \frac{T}{V} \log\left[\int \mathcal{D}U \exp\left(-\int_T d\tau d^3x \mathcal{L}_{\text{eff}}\right)\right]. \tag{4.2.50}$$

Here, $\mathcal{L}_{\text{eff}}$ will be the chiral Lagrangian considered above. In order to calculate the finite temperature contribution, it is customary to rewrite the Feynman propagator for the pseudoscalar particle P in the integral representation [57]:

$$\Delta_P(x) \equiv \int \frac{d^dp}{(2\pi)^d} \frac{e^{ipx}}{\mathring{M}_P^2 + p^2} = \int_0^\infty \frac{d\lambda}{(4\pi\lambda)^{d/2}} \exp\left(-\lambda \mathring{M}_P^2 - x^2/4\lambda\right). \tag{4.2.51}$$

The free energy density of a pion gas (the degenerated case) at low temperatures has been computed [50] via chiral perturbation theory to one loop by considering the scalar propagator at finite temperature. In time direction, a periodicity conditions is imposed on the scalar fields, which implies the replacement of the Feynman propagator by

$$G_{P,T}(x) = \sum_{n_4=-\infty}^{\infty} \Delta_P(\boldsymbol{x}, x_4 + n_4/T), \tag{4.2.52}$$

where $\Delta_P(x)$ is the scalar propagator at zero temperature. This thermal propagator in position space for $x = 0$ is related via Fourier transformation to the Matsubara sum over momentum propagators

$$g_1(M_P, T) = T \sum_n \int \frac{d^dp}{(2\pi)^d} \frac{1}{\mathring{M}_P^2 + p^2 + \omega_n^2}, \qquad \omega_n = 2\pi T n, \qquad n \in \mathbb{Z}. \tag{4.2.53}$$

Hence, the free energy of the pseudoscalar meson gas is calculated via integrals related to the d-dimensional non-interacting Bose gas $g_0(M_P, T)$ and its derivatives, from which the interactions are derived:

$$g_r(M_P, T) = 2\int_0^\infty \frac{d\lambda}{(4\pi\lambda)^{d/2}} \lambda^{r-1} \exp\left(-\lambda M_P^2\right) \sum_{n_4=1}^{\infty} \exp\left(-n_4^2/4\lambda T^2\right), \tag{4.2.54}$$

$$g_{r+1}(M_P, T) = -\frac{\partial}{\partial M_P^2} g_r(M_P, T). \tag{4.2.55}$$

In $d = 3 + 1$ dimensions, we obtain:

$$g_0(M_P, T) = \frac{2T}{(2\pi)^3} \int d^3p \log\left(\frac{1}{1 - e^{-E/T}}\right)$$

$$= \frac{\pi^2 T^4}{45} - \frac{T^2 M_P^2}{12} + \frac{T M_P^3}{6\pi} + \frac{M_P^4}{(4\pi)^2}\left[\log\left(\frac{M_P}{4\pi T}\right) + \gamma_E - 3/4\right] + \mathcal{O}\left(M_P^6/T^2\right), \tag{4.2.56}$$

$$g_1(M_P, T) = \frac{1}{(2\pi)^3} \int \frac{d^3p}{E} \frac{1}{e^{-E/T} - 1}$$

$$= \frac{T^2}{12} - \frac{T M_P}{4\pi} - \frac{2M_P^2}{(4\pi)^2}\left(\log\left(\frac{M_P}{4\pi T}\right) + \gamma_E - 1/2\right) + \mathcal{O}\left(M_P^4/T^2\right), \tag{4.2.57}$$

$$E = (M_P^2 + \boldsymbol{p}^2)^{1/2}, \tag{4.2.58}$$

where the expansion of g_0 was calculated by Haber and Weldon [63], and the integral g_1 was introduced by Gasser and Leutwyler [52, 57] and is indeed another representation of Eq. (4.2.53). The expansions above are known as high-temperture expansion in thermal field theory [84] because the series converges only for $T \gg M_P$. Oftentimes, one does not make use of the expansions (because it breaks down for low temperatures) but calculate the defining integrals numerical. Calculations at finite temperature have been performed both in the p-regime and in the ϵ-regime[19] (compare Sec. 3.4.2). We will restrict here to the p-regime and take the pion correlation length always smaller than the volume. Moreover, in this section we will only consider the degenerate case of $N_\mathrm{f}^2 - 1$ pions: $M_P = M_\pi$. This simplifies the calculations considerably. The pressure can be derived from the effective Lagrangian [52, 57], and one obtains a similar expression as for the energy density, Eq. (4.2.26), but with the zero temperature Feynman propagators replaced by the thermal integrals $g_i(M_P, T)$:[20]

$$\begin{aligned} P(T) &= \frac{N_\mathrm{f}^2-1}{2} g_0(M_P,T) - \frac{N_\mathrm{f}^2-1}{4N_\mathrm{f}} \frac{M_P^2}{F_0^2} [g_1(M_P,T)]^2 + \mathcal{O}\left(p^8\right) \\ &= (N_\mathrm{f}^2-1)\left[\frac{\pi^2}{90}T^4 - \left(\frac{T^2}{24} + \frac{T^4}{576 N_\mathrm{f} F_0^2}\right) M_P^2 + \left(\frac{1}{12\pi} + \frac{T^2}{96\pi N_\mathrm{f} F_0^2}\right) T M_P^3 \right. \\ &\left. - \frac{M_P^4}{128\pi^2} + \left(\frac{1}{32\pi^2} - \frac{T^2}{192\pi^2 N_\mathrm{f} F_0^2}\right) M_P^4 \left(\log\left(\frac{M_P}{4\pi T}\right) + \gamma_E - 1/2\right)\right] + \mathcal{O}\left(M_P^6/T^2\right). \end{aligned} \tag{4.2.59}$$

Note that the temperature independent terms can be disregarded by definition of the pressure, because $P(T=0) = 0$. They are artifacts of the expansion which is only valid for high temperatures. These terms can be shuffled into the energy density and absorbed in renormalization constants. No such finite terms remain if the integrals g_0, g_1 are evaluated numerically.

Chiral Condensate at Finite Temperature

To calculate the chiral condensate at finite temperature, we make use of the GMOR relation and the derivatives

$$\frac{\partial M_P}{\partial \mathring{M}_P} = 1 + \frac{1}{16\pi^2 N_\mathrm{f}} \frac{\mathring{M}_P^2}{F_0^2} \left(1 + 3\log\left(\mathring{M}_P/\Lambda_1\right)\right) + \mathcal{O}\left(\mathring{M}_P^3\right), \tag{4.2.60}$$

$$\begin{aligned} \frac{\partial P}{\partial M_P^2} &= (N_\mathrm{f}^2-1)\left[-\left(\frac{T^2}{24} + \frac{T^4}{576 N_\mathrm{f} F_0^2}\right) + \left(\frac{1}{8\pi} + \frac{T^2}{64\pi N_\mathrm{f} F_0^2}\right) T M_P \right. \\ &\left. - \frac{M_P^2}{64\pi^2} + \left(\frac{1}{4\pi^2} - \frac{T^2}{24\pi^2 N_\mathrm{f} F_0^2}\right) M_P^2 \left(\log\left(\frac{M_P}{4\pi T}\right) + \gamma - 1/4\right) + \mathcal{O}\left(M_P^4/T^2\right)\right] \end{aligned} \tag{4.2.61}$$

[19] In a finite volume, chiral symmetry will not break down spontaneously; the vanishing of the condensate can then be treated via ϵ-expansion [87], where the integral takes the form

$$g_r(M_\pi, T, L) = 2\int_0^\infty \frac{d\lambda}{(4\pi\lambda)^{d/2}} \lambda^{r-1} \exp\left(-\lambda M_\pi^2\right) \sum_{n \in (\mathbb{Z}\smallsetminus 0)^4} \exp\left(-n^2/4\lambda\right).$$

[20] The pion mass which enters in the calculation of ϵ_0 is the tree level mass $\mathring{M}_\pi = (2m_l B_0)^{1/2}$, because this mass appears in the Feynman propagator Eq. (4.2.18); corrections are then calculated via zero temperature chiral perturbation theory. In contrast, the pressure P has as its input parameter the *physical pion mass* M_π, characterized as the lowest lying one particle state contributing to the pressure [57]:

$$\lim_{T\to 0} P = e^{-M_\pi T} \quad \Longrightarrow \quad M_\pi = -\lim_{T\to 0} T \log P$$

which is up to the next order in m_l related to $\mathring{M}_P$ via the zero-temperature expansion given in Eq. (4.2.35). We assume that for all pseudoscalar mesons the masses M_P instead of $\mathring{M}_P$ enter into the calculation of the pressure.

and by inserting this back into the free energy, one can derive the quark mass dependence of the chiral condensate [63]:

$$\begin{aligned}\langle\bar{\psi}\psi\rangle &= \frac{\partial f}{\partial m_q} = \frac{\partial f}{\partial \mathring{M}_P}\frac{\partial \mathring{M}_P}{\partial m_q} = \frac{B_0}{\mathring{M}_P}\left(\frac{\partial \epsilon_0}{\partial \mathring{M}_P} - \frac{\partial P}{\partial \mathring{M}_P}\right) = \frac{B_0}{\mathring{M}_P}\frac{\partial \epsilon_0}{\partial \mathring{M}_P}\left(1 + \frac{C}{F_0^2}\frac{\partial P}{\partial M_P^2}\right) \\ &= \frac{B_0}{\mathring{M}_P}\frac{\partial \epsilon_0}{\partial \mathring{M}_P}\left\{1 + \frac{C}{F_0^2}(N_\mathrm{f}^2-1)\left[-\left(\frac{T^2}{24} + \frac{T^4}{576 N_\mathrm{f} F_0^2}\right) + \left(\frac{1}{8\pi} + \frac{T^2}{64\pi N_\mathrm{f} F_0^2}\right) T M_P \right.\right. \\ &\quad \left.\left. - \frac{M_P^2}{64\pi^2} + \left(\frac{1}{16\pi^2} - \frac{T^2}{96\pi^2 N_\mathrm{f} F_0^2}\right) M_P^2 \left(\log\left(\frac{M_P}{4\pi T}\right) + \gamma - 1/4\right) + \mathcal{O}\left(M_P^4/T^2\right)\right]\right\}, \qquad (4.2.62)\end{aligned}$$

$$C = -F_0^2\left(\frac{\partial \epsilon_0}{\partial \mathring{M}_P}\right)^{-1}\frac{\partial M_P^2}{\partial \mathring{M}_P} = \frac{2}{N_\mathrm{f}}\left(1 - \mathcal{O}\left(\mathring{M}_P^2\right)\right), \qquad (4.2.63)$$

where C is a temperature independent constant [57]. At $T = 0$, we obtain due to the defining property $P(0) = 0$:

$$\langle 0|\bar{\psi}\psi|0\rangle = \frac{B_0}{\mathring{M}_P}\frac{\partial \epsilon_0}{\partial \mathring{M}_P}. \qquad (4.2.64)$$

Close to the chiral limit, where $M_P \approx \mathring{M}_P$ and $C = 2/N_\mathrm{f}$, we obtain for non-zero temperature:

$$\begin{aligned}\langle\bar{\psi}\psi\rangle = \langle 0|\bar{\psi}\psi|0\rangle &\left\{1 + \frac{N_\mathrm{f}^2-1}{N_\mathrm{f}}\left[-\left(\frac{(T/F_0)^2}{12} + \frac{(T/F_0)^4}{288 N_\mathrm{f}}\right) + \left(\frac{1}{4\pi} + \frac{(T/F_0)^2}{32\pi N_\mathrm{f}}\right)\frac{T\mathring{M}_P}{F_0^2}\right.\right. \\ &\left.\left. - \frac{\mathring{M}_P^2}{32\pi^2} + \left(\frac{1}{8\pi^2} - \frac{(T/F_0)^2}{48\pi^2 N_\mathrm{f}}\right)\left(\frac{\mathring{M}_P}{F_0}\right)^2\left(\log\left(\frac{\mathring{M}_P}{4\pi T}\right) + \gamma - 1/4\right) + \mathcal{O}\left(\mathring{M}_P^4/T^2\right)\right]\right\}. \qquad (4.2.65)\end{aligned}$$

We are now able to identify the Goldstone term, which is the term in the temperature expansion linear in $\mathring{M}_P$ in the regime $0 \ll \mathring{M}_P \ll T$. In fact, after neglecting terms of $\mathcal{O}\left((T/F_0)^2\right)$, the correction is of the same form as in the three-dimensional O(N) spin model Eq. (3.2.13):

$$\begin{aligned}\langle\bar{\psi}\psi\rangle &= \langle 0|\bar{\psi}\psi|0\rangle\left\{1 + \frac{N_\mathrm{f}^2-1}{N_\mathrm{f}}\left(\frac{1}{4\pi}\frac{T\mathring{M}_P}{F_0^2}\right) + \mathcal{O}\left(\mathring{M}_P^2, (T/F_0)^2\right)\right\} \qquad (4.2.66) \\ &\equiv \langle 0|\bar{\psi}\psi|0\rangle\left\{1 + \frac{N_\mathrm{f}^2-1}{4\pi N_\mathrm{f}}\frac{\mathring{M}_P}{\tilde{F_0}^2} + \mathcal{O}\left(\mathring{M}_P^2, (T/F_0)^2\right)\right\},\end{aligned}$$

where $\tilde{F}_0 \equiv F_0/(T)^{1/2}$ can be identified with the pion decay constant in three dimensions. Again, the prefactors match only for $N_\mathrm{f} = 2$. The Goldstone term stems from $g_0(M_\pi, T)$ and can be identified as the mode which does not pick up an extra factor of T within the integral. In fact, it stems from the zero mode in the matsubara sum in Eq. (4.2.53), hence it is essentially three-dimensional. However, a satisfying comparison of the $d = 3+1$ system with a $d = 3$ cannot be achieved because the temperature expansion becomes invalid for large temperatures. To see this, consider the chiral limit, where $\mathring{M}_P = 0$. The chiral condensate can then be computed up to order $\mathcal{O}\left(T^8\right)$ [90]:

$$\begin{aligned}\langle\bar{\psi}\psi\rangle_T &= \langle 0|\bar{\psi}\psi|0\rangle\left[1 - c_1\left(\frac{T^2}{8F_0^2}\right) - c_2\left(\frac{T^2}{8F_0^2}\right)^2 - c_3\left(\frac{T^2}{8F_0^2}\right)^3\log\left(\frac{\Lambda_q}{T}\right) + \mathcal{O}\left(T^8\right)\right], \qquad (4.2.67) \\ c_1 &= \frac{2}{3}\frac{N_\mathrm{f}^2-1}{N_\mathrm{f}}, \qquad c_2 = \frac{2}{9}\frac{N_\mathrm{f}^2-1}{N_\mathrm{f}^2}, \qquad c_3 = \frac{8}{27}(N_\mathrm{f}^2+1)N_\mathrm{f}, \qquad \Lambda_q = 470 \pm 110\,\mathrm{MeV}.\end{aligned}$$

This result holds to three loops, and it gives large corrections for temperatures above $T \approx 150$ MeV. Hence, this expansion cannot be trusted, in particular it is not possible to determine the chiral transition temperature.[21]

[21] The three-loop result indicates for the temperature where the condensate vanishes $T_\mathrm{ch} = 190$ MeV, but it is believed that the expansion is not convergent in that temperature region, mainly because the computations are obtained in the

Disconnected and Connected Susceptibility at Finite Temperature

The chiral susceptibility at finite temperature is a measure for the fluctuations of the order parameter, the transition temperature can be determined from its peak position. In Sec. 4.2.1 we have already identified the connected and disconnected contributions at zero temperature, moreover we have argued that at finite temperature, the Goldstone term in the condensate is proportional to temperature T. Taking another quark mass derivative, we obtain for $N_{\rm f}$ degenerated flavors [51]:

$$\chi^{\rm full,IR}(T) = TB_0^2 \frac{N_{\rm f}^2-1}{4\pi^2}\frac{1}{\mathring{M}}. \tag{4.2.68}$$

Smilga and Verbaarschot [111] have shown in close analogy to the zero temperature finding Eq. (4.2.47) that in the temperature region $M_\pi \ll T \ll T_{\rm ch}$, the connected susceptibility is given by

$$\chi^{\rm con,IR}(T) = TB_0^2 \frac{N_{\rm f}^2-4}{8\pi^2}\frac{1}{\mathring{M}}. \tag{4.2.69}$$

This implies for the disconnected part:

$$\chi^{\rm dis,IR}(T) = TB_0^2 \frac{N_{\rm f}^2+2}{8\pi^2}\frac{1}{\mathring{M}}. \tag{4.2.70}$$

Let us assume for the moment that the chiral transition is of second order, $T_{\rm ch} = T_{\rm c}$. In Sec. 3.3.1 we have argued that Goldstone modes are an intrinsic part of the scaling function, the nonanalyticities induced by them are present on the whole coexistence line $T < T_{\rm c}$. In the present case of $d = 3+1$ dimensions, even though the temperature expansion breaks down significantly below $T_{\rm c}$, we will nevertheless assume that the infrared divergences coming from the Goldstone modes are described by the above expressions. Only the temperature dependence may be more complicated in the vicinity of $T_{\rm c}$.

4.3 The QCD Phase Diagram Revisited: The Rôle of the Chiral Anomaly

Now that we have extensively discussed both chiral symmetry and χPT, let us reconsider the QCD phase diagram. From chiral perturbation theory, based on the non-linear σ model, we expect that critical behavior only arises in the chiral limit. However, the value of the strange quark mass turns out to be crucial for the order of the transition. Furthermore, the axial anomaly also may have a strong influence on the nature of the transition. This influence was studied by Pisarski and Wilczek [100] for a linear σ model, which we will introduce first

4.3.1 Linear σ Model

In this chapter we have restricted the discussion to the non-linear σ model because it is conceptually and computationally simpler. However, at least in principle the *linear σ model* introduced by Gell-Mann and Levy [86] gives a more realistic account of the chiral symmetry restoration at $T_{\rm c}$ because the σ mode is treated as an independent degree of freedom. The most general renormalizable Lagrangian consistent with $\mathrm{SU}(N_{\rm f})_{\rm L} \times \mathrm{SU}(N_{\rm f})_{\rm R}$ is

$$\mathcal{L}_{\rm eff}^{\rm lin} = \frac{1}{2}\,\mathrm{tr}(\partial_\mu \Phi^\dagger)(\partial_\mu \Phi) - \frac{1}{2}m^2\,\mathrm{tr}\,\Phi^\dagger\Phi - \frac{\pi^2}{3}g_1(\mathrm{tr}\,\Phi^\dagger\Phi)^2 - \frac{\pi^2}{3}g_2\,\mathrm{tr}(\Phi^\dagger\Phi)^2 \tag{4.3.1}$$

non-linear sigma model, which does not account for a truly dynamical sigma mode.

with $g_2 > 0$, $g_1 + g_2/N_\mathrm{f} > 0$ such that the potential is bounded from below. In contrast to the non-linear sigma model, the longitudinal mode given by the scalar isosinglet σ meson is included and also all the other scalar and pseudo-scalar fields are modeled as linear fields:[22]

$$\Phi = \left(\phi_\sigma \mathbb{1} + i \sum_{P=1}^{N_\mathrm{f}^2-1} \phi_P \lambda_P \right). \tag{4.3.3}$$

At zero temperature, a non-zero vacuum expectation value $\langle \Phi \rangle = \phi_\sigma$ is obtained if $m^2 < 0$

4.3.2 Order of the Chiral Phase Transition

Pisarski and Wilczek have argued based on ϵ expansion that the axial anomaly has a decisive influence on the order of the chiral transition. They add to the Lagrangian Eq. (4.3.1) a term which mimics the 't Hooft vertex [115]:[23]

$$\mathcal{L}_{\mathrm{U_A}(1)} = c \left(\det \Phi + \det \Phi^\dagger \right). \tag{4.3.4}$$

For $c \neq 0$, this term leads to the $\eta - \eta'$ splitting. In the massless limit,[24] the anomaly does not break down $\mathrm{U_A}(1)$ completely, but there is a residual discrete axial symmetry $\mathbb{Z}_A(N_\mathrm{f})$. Following [100], we denote the symmetry groups for the unbroken and broken case by:

$$G_f = \mathrm{U_A}(1) \times \mathrm{SU}(N_\mathrm{f})_\mathrm{L} \times \mathrm{SU}(N_\mathrm{f})_\mathrm{R}, \qquad G'_f = Z_A(N_\mathrm{f}) \times \mathrm{SU}(N_\mathrm{f})_\mathrm{L} \times \mathrm{SU}(N_\mathrm{f})_\mathrm{R}. \tag{4.3.5}$$

In the mean field analysis of $\mathcal{L}_\mathrm{eff}^\mathrm{lin}$, m^2 and σ_0 vanish at T_ch (see also the LGW-Hamiltonian Sec. 3.1.31). The authors assume the system to be effectively three-dimensional at the transition temperature, which allows to study the Lagrangian via ϵ-expansion in $d = 4 - \epsilon = 3$ dimensions. To leading order in $\epsilon = 1$ and in the chiral limit, they find:

(G_f) In the large N_c limit with $c = 0$ there is no infrared-stable fixed point if $N_\mathrm{f} > 3$. Moreover, there is an IR-stable FP with $g_{2*} = 0$ for $\sqrt{2} > N_\mathrm{f} \geq 0$. In particular, for $N_\mathrm{f} = 1$ the transition is of second order with $G_f = O(2)$ critical exponents, and for $N_\mathrm{f} \geq 2$ it is of first order, induced by fluctuations which destroy the IR-stable FP.

(G'_f) For a small number of colors, c is of the same order as g_1, g_2. Again, the transition is of first order if $N_\mathrm{f} \geq 3$, but this is now driven by $\mathcal{L}_{\mathrm{U_A}(1)}$. Only for $N_\mathrm{f} > 4$ the anomaly term $\mathcal{L}_{\mathrm{U_A}(1)}$ becomes an irrelevant operator and does not affect the critical behavior. There is no phase transition for $N_\mathrm{f} = 1$. The situation is not so clear for $N_\mathrm{f} = 2$: if the η' remains massive at T_ch, the transition is of second order with $G'_f = O(4)$ critical exponents, however, the temperature dependence of $c \equiv c(T)$ may lead to a different result: assuming that the 't Hooft vertex is proportional to the instanton density, $c(T) \sim d_I(T)$, which drops to zero in the limit $T \to \infty$, one expects the effective restoration of the $\mathrm{U_A}(1)$ symmetry. If $c(T_\mathrm{ch})$ is sufficiently small, the chiral transition for $N_\mathrm{f} = 2$ may be also of first order with $G_f = O(2) \times O(4)$.

[22] The non-linear sigma model fields are related to the linear fields by expanding the exponential to lowest order

$$\Phi = \sum_{a=0}^{N_\mathrm{f}^2-1} (\sigma_a + i\pi_a). \tag{4.3.2}$$

In the non-linear σ model, the σ mode is constrained by the unitarity condition; for $N_\mathrm{f} = 2$, where the symmetric structure constants d_{ijk} vanish, this constraint is given by $\phi_\sigma = \left(F_0^2 - \sum_{P=1}^{N_\mathrm{f}^2-1} \phi_P^2 \right)^{1/2}$. This condition is now abandoned, and in effect, the Lagrangian Eq. (4.2.2) is transformed in a ϕ^4 theory.

[23] Instantons generate a vertex a $2N_\mathrm{f}$-point interaction between massless fermions of the form $\det \Phi$ and anti-instantons generate a vertex $\det \Phi^\dagger$.

[24] The strength of the anomaly depends both on the number of flavors and the number of colors, it vanishes in the quenched limit $N_\mathrm{f} = 0$, and in the large N_c limit.

The finite quark masses are expected to weaken the first order transitions, but not to wash them out completely. Gocksch, Gavai and Pisarski [55] have investigated the effect of a symmetry breaking background field added to the Lagrangian Eq. (4.3.1):

$$\mathcal{L}_H = -\operatorname{tr}\left(\Phi + \Phi^\dagger\right), \qquad H = h_0 t_0 - \sqrt{2} h_8 t_8, \tag{4.3.6}$$

which are related to the quark masses in the following way:

$$m_u = m_d = h_0 - h_8, \qquad m_s = h_0 + 2h_8. \tag{4.3.7}$$

Based on mean field arguments, the authors have come to the conclusion that the first order behavior of $N_\mathrm{f} = 3$ flavors ends at a critical endpoint, characterized by a critical mass m_u^c. It is expected to lie in the Ising universality class, as the order parameter field is one-component, which is the sigma meson (f_0). The current status of our knowledge on the order of the transition obtained via RG-flow methods is summarized in Tab. 4.1. We are specifically interested in the $N_\mathrm{f} = 2+1$ case with m_s physical. However, the model calculations do not allow for the determination of the second order critical line $m_s^{\mathrm{2nd}}(m_l)$ — this question has to be addressed by lattice QCD calculations. In particular, the location of the tricritical point $m_s^{\mathrm{tric}} = m_s^{\mathrm{2nd}}(0)$ is an open issue and will be addressed in the analysis of our lattice data in Sec. 5.4.

	$\mathrm{U_A(1)}$ anomaly $\mathrm{SU}(N_\mathrm{f})_\mathrm{L} \times \mathrm{SU}(N_\mathrm{f})_\mathrm{R} \to \mathrm{SU}(N_\mathrm{f})_\mathrm{V}$	suppressed anomaly at T_c $\mathrm{U}(N_\mathrm{f})_\mathrm{L} \times \mathrm{U}(N_\mathrm{f})_\mathrm{R} \to \mathrm{U}(N_\mathrm{f})_\mathrm{V}$
$N_\mathrm{f} = 1$	crossover or first order	O(2) or first order
$N_\mathrm{f} = 2$	O(4) or first order	$\mathrm{U}(2)_L \times \mathrm{U}(2)_R/\mathrm{U}(2)_V$ or first order
$N_\mathrm{f} \geq 3$	first order	first order

Table 4.1: Dependence of the order of the chiral transition on number of flavors (for vanishing quark mass) and the strength of the axial anomaly, from RG predictions, see [116].

4.3.3 Chiral Susceptibilities and the Anomaly

In the light of the linear sigma model, we also want to shortly review the chiral susceptibilities and discuss their relation to the meson masses. Following Rajagopal and Wilzek [103] we may define for $N_\mathrm{f} = 2$ QCD (up to a normalization factor):

$$\chi_\sigma \equiv \chi_l^{\mathrm{full}} = \frac{1}{M_\sigma^2}, \qquad \chi_\delta \equiv \chi_l^{\mathrm{con}} = \frac{1}{M_\delta^2}, \qquad \chi_\pi \equiv \frac{\langle \bar{\psi}\psi \rangle_l}{m_l} = \frac{1}{M_\pi^2}. \tag{4.3.8}$$

For $N_\mathrm{f} = 2+1$ flavors, the σ corresponds to the scalar isosinglet f_0, and the δ corresponds to the scalar isovector a_0, see Fig. 4.1. These relations are also sketched in Fig. 4.2. Via the fluctuation-dissipation theorem, the susceptibilities can be identified with integrated Euclidean two-point functions of the mesonic fields in momentum space:

$$\begin{aligned}\chi_\phi = \int d^4 r \, \langle \phi(r)\phi(0) \rangle = \int \frac{d^4 r d^4 p}{(2\pi)^4} \frac{e^{ipr}}{p^2 + M_\phi^2} &= \langle \phi(0)\phi(0) \rangle + \int \frac{d^4 r d^4 p}{(2\pi)^4} \frac{(2\pi)^4 \delta(p^2)}{p^2 + M_\phi^2} \\ &= \langle \phi(0)\phi(0) \rangle + \frac{1}{M_\phi^2}\end{aligned} \tag{4.3.9}$$

with $\langle \phi(0)\phi(0) \rangle$ the "bubble terms" contribution, i.e. the Goldstone term discussed in the previous sections. We note that the isovector propagator is quark-line connected and hence corresponds to the

connected susceptibility, whereas the isosinglet propagator has quark-line disconnected contribution which gives rise to the geometric series:

$$\langle \bar{u}u(-p);\bar{u}u(p)\rangle = \frac{1}{p^2+M_\delta^2}\sum_{n=0}^{\infty}\left(\frac{m_0^2}{p^2+M_\delta^2}\right)^n = \frac{1}{p^2+M_\delta^2-m_0^2}, \qquad M_\sigma^2 = M_\delta^2 - m_0^2.$$

This relation defines the sigma mass in terms of the coupling constant m_0 from the t'Hooft vertex and which gives the η' a large mass. From this, also the disconnected susceptibility can be attributed a mass:

$$\chi_l^{\rm dis} = \frac{1}{M_\sigma^2} - \frac{1}{M_\delta^2}. \tag{4.3.10}$$

From these relations, we will expect that the full susceptibility will strongly peak when the sigma mass becomes mass degenerated with the pion, which defines the chiral phase transition, whereas the connected susceptibility will most likely not diverge as the delta becomes mass degenerated with the pion only when $\mathrm{U_A}(1)$ is effectively restored, which is expected to happen above $T_{\rm ch}$. In fact, we can construct order parameters of the chiral transition and the axial transition from these susceptibilities separately [89]:

$$\chi_{SU(2)\times SU(2)} \equiv \chi_\sigma - \chi_\pi, \qquad \chi_{\mathrm{U_A}(1)} \equiv \chi_\delta - \chi_\pi. \tag{4.3.11}$$

These are expected to be non-zero below and zero above the transition temperatures $T_{\rm ch}$ resp. $T_{\mathrm{U_A}(1)}$. In fact, we will consider them in a slightly different form:

$$\chi_{SU(2)\times SU(2)} = -\frac{1}{m_l}\left(\langle\bar{\psi}\psi\rangle_l - m_l\chi_l^{\rm full}\right), \tag{4.3.12}$$

$$\chi_{\mathrm{U_A}(1)} = -\frac{1}{m_l}\left(\langle\bar{\psi}\psi\rangle_l - m_l\chi_l^{\rm con}\right). \tag{4.3.13}$$

We will soon see that both $M_f \equiv -m_l m_s \chi_{SU(2)\times SU(2)}/T^4$ and $M_c \equiv -m_l m_s \chi_{\mathrm{U_A}(1)}/T^4$ define subtracted order parameters which may help to improve on the chiral limit.

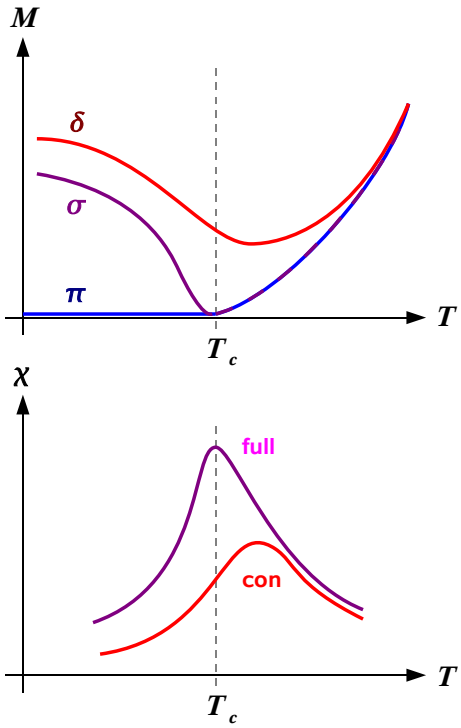

Figure 4.2: The correspondence between full susceptibility with the sigma mode, and the connected susceptibility with the delta mode.

Finally, we also want to mention that the mixed susceptibility $\chi_{l,s}^{dis}$, obtained from the propagator

$$\langle \bar{u}u(-p);\bar{s}s(p)\rangle = \frac{1}{p^2+M_{s,\rm con}^2}\sum_{n=1}^{\infty}\left(\frac{m_0^2}{p^2+M_\delta^2}\right)^n = \frac{1}{p^2+M_{s,\rm con}^2}\frac{m_0^2}{p^2+M_\sigma^2}, \tag{4.3.14}$$

at zero momentum might also peak at $\mathrm{T_{ch}}$ if $\mathrm{U_A}(1)$ is not effectively restored there:

$$\chi_{l,s}^{\rm dis} = \frac{1}{M_{s,\rm con}}\left(\frac{M_\delta^2}{M_\sigma^2}-1\right) \simeq \chi_l^{\rm dis}\times\chi_s^{\rm con}/\chi_l^{\rm con}, \tag{4.3.15}$$

with $M_{s,\rm con}^2 = 1/\chi_s^{\rm con}$ the mass corresponding to the pole mass of the connected scalar meson propagator, which is expected to be almost constant in the chiral limit of the light quark masses. The second equality is only approximate because the susceptibilities will gain loop corrections known as bubble terms which differ for each of them. We will however see in the next section that $\chi_{l,s}^{dis}$ does not receive Goldstone mode contributions in its bubble term below $T_{\rm ch}$.

4.4 Staggered Chiral Perturbation Theory

4.4.1 Staggered Fermions and Taste Breaking

The lattice discretization scheme for staggered fermions leads to lattice artifacts known as taste breaking, which amounts to an unphysical mixing of the multiple flavors known as tastes, see Sec. 2.1.3. As a result, the taste symmetries are only approximate. This has also an effect on the meson masses measured on the lattice, in particular on the pion mass, which for non-zero lattice spacing will remain non-zero even in the chiral limit when averaging over the tastes.

In this section we give a short introduction to staggered chiral perturbation theory (SχPT) and explain why one finds an unphysical Goldstone effect for the connected susceptibility, in contrast to the finding in the continuum, Eq. (4.2.69).

4.4.2 Elements of Staggered Chiral Perturbation Theory

In order to parameterize the effect of taste violations on pseudoscalar meson masses and chiral observables, we make use of the so-called Lee-Sharpe Lagrangian [85]

$$\mathcal{L}_{\text{eff}}^{\text{stag}} = \frac{1}{4}F_0^2\left\{\text{Tr}(\partial_\mu U^\dagger \partial^\mu U) - 2B_0\,\text{Tr}(\mathcal{M}U^\dagger + \mathcal{M}^\dagger U)\right\} + \frac{m_0^2}{2}\phi_{0,I}^2 + a^2\mathcal{V}(U), \tag{4.4.1}$$

which is a straightforward extension of the effective chiral Lagrangian Eq. (4.2.4) to the staggered fermions. There are three modifications: First, the the unitary matrix U contains pseudoscalar fields in the mass eigenbasis for each taste channel t:

$$\begin{aligned} U &= \exp(i\Phi/F_0), \qquad \Phi = \sum_{t=1}^{16} T_t\phi_t, \qquad T_t = \{1, \xi_5, i\xi_\mu, i\xi_5\xi_\mu\, i\xi_\nu\xi_\mu\}, \\ \mathcal{M} &= \begin{pmatrix} m_u & 0 & 0 \\ 0 & m_d & 0 \\ 0 & 0 & m_s \end{pmatrix} \otimes \mathbb{1}_{n_\text{r}\times n_\text{r}}, \qquad \phi_t = \begin{pmatrix} U_t & \pi_t^+ & K_t^+ \\ \pi_t^- & D_t & K_t^0 \\ K_t^- & \bar{K}_t^0 & S_t \end{pmatrix}, \end{aligned} \tag{4.4.2}$$

where T_t are the Euclidean gamma matrices. Second, the coupling m_0 provides an additional mass term for the η', which is a heuristic ansatz for the 't Hooft vertex. Third, a taste-breaking term is introduced as a sum over all possible taste-breaking operators:

$$-\mathcal{V}(U) = \sum_{k\in\{1,3,4,6\}} C_k\mathcal{O}_k + \sum_{k'\in\{2V,2A,5V,5A\}} C_{k'}\mathcal{O}_{k'}, \tag{4.4.3}$$

where the first sum is over single-trace operators:[25]

$$\begin{aligned} \mathcal{O}_1 &= \text{Tr}\left(\hat{\xi}_5 U \hat{\xi}_5 U^\dagger\right), & \mathcal{O}_3 &= \frac{1}{2}\sum_\nu \text{Tr}\left(\hat{\xi}_5 U \hat{\xi}_5 U + \text{H.c}\right), \\ \mathcal{O}_4 &= \frac{1}{2}\sum_\nu \text{Tr}\left(\hat{\xi}_{\nu 5} U \hat{\xi}_{\nu 5} U + \text{H.c}\right), & \mathcal{O}_6 &= \sum_{\mu<\nu} \text{Tr}\left(\hat{\xi}_{\mu\nu} U \hat{\xi}_{\mu\nu} U^\dagger\right) \end{aligned} \tag{4.4.4}$$

and the second sum is over double-trace operators

$$\begin{aligned} \mathcal{O}_{2V} &= \frac{1}{4}\sum_\nu \left[\text{Tr}\left(\hat{\xi}_\nu U\right)\text{Tr}\left(\hat{\xi}_\nu U\right) + \text{H.c.}\right], & \mathcal{O}_{5V} &= \frac{1}{2}\sum_\nu \left[\text{Tr}\left(\hat{\xi}_\nu U\right)\text{Tr}\left(\hat{\xi}_\nu U^\dagger\right)\right], \\ \mathcal{O}_{2A} &= \frac{1}{4}\sum_\nu \left[\text{Tr}\left(\hat{\xi}_{\nu 5} U\right)\text{Tr}\left(\hat{\xi}_{\nu 5} U\right) + \text{H.c.}\right], & \mathcal{O}_{5A} &= \frac{1}{2}\sum_\nu \left[\text{Tr}\left(\hat{\xi}_{\nu 5} U\right)\text{Tr}\left(\hat{\xi}_{\nu 5} U^\dagger\right)\right]. \end{aligned} \tag{4.4.5}$$

[25] The following operators contain generalizations of the Euclidean gamma matrices to $4N_\text{f}\times 4N_\text{f}$ dimensions, with $\hat{\xi}_t = \text{diag}\,(\xi_t, .., \xi_t)$.

The operators in $\mathcal{V}(U)$ are the leading order terms $\mathcal{O}(m_q, a^2)$ of a joint Taylor expansion in the quark mass m_q and the lattice spacing a. For details on how to derive these operators see App. (B.3). In short, they are matched with four-fermion operators in staggered fermion action. In order to incorporate different flavors, the fields ϕ_t are $N_{\rm f}n_{\rm r} \times N_{\rm f}n_{\rm r}$ matrices, with $n_{\rm r}$ an arbitrary number of taste replicas which at the end of the calculations will be set to $n_{\rm r} = \frac{1}{4}$ in order to implement rooting. Due to taste-breaking, the tree-level pseudoscalar meson masses with quark flavor content f, f' are shifted by taste splitting terms $a^2\Delta_t$

$$m^2_{f,f',t} = B_0(m_f + m_{f'}) + a^2\Delta_t. \tag{4.4.6}$$

In the continuum limit, the GMOR relation Eq. (4.2.9) is recovered, hence we will denote Eq. (4.4.6) as StaggGMOR relation. The splittings Δ_t can be computed from the effective Lagrangian [6]:

$$\begin{aligned}
\Delta_I &= \frac{16}{F_0^2}(4C_3 + 4C_4), & \Delta_5 &= 0,\\
\Delta_\mu &= \frac{16}{F_0^2}(C_1 + C_3 + 3C_4 + 3C_6), & \Delta_{\mu 5} &= \frac{16}{F_0^2}(C_1 + 3C_3 + C_4 + 3C_6),\\
\Delta_{\mu\nu} &= \frac{16}{F_0^2}(2C_3 + 2C_4 + 4C_6),
\end{aligned} \tag{4.4.7}$$

The important observation is that for the pseudo taste channel, taste violations are not present. This is due to the fact that the taste nonsinglet $U_A(1)$ symmetry

$$U \to e^{i\theta\xi_5} U e^{i\theta\xi_5} \tag{4.4.8}$$

is unbroken by the lattice. Hence, π_5 is the only true Goldstone boson. Note that only the single-trace operators enter into the meson masses, whereas the double-trace operators give rise to two-point mixing vertices among vector tastes and axial tastes. In this formalism, these mixing vertices have in fact the same structure as the effective anomaly vertex in the taste isosinglet channel. These two-point vertices need to be considered in the calculation of chiral observables.

Term in $\mathcal{L}_{\rm eff}$	[Taste]$\times$ Rotation symmetry
$\mathcal{L}^{(2)}_{\mathcal{M}=0}$	$[\mathrm{U}(1)_{\rm VEC} \times \mathrm{SU}(4n_r)_L \times \mathrm{SU}(4n_r)_R] \times \mathrm{SO}(4)$
$\mathcal{L}^{(2)}_{\mathcal{M}\neq 0}$	$[(\mathrm{U}(1)_{\rm vec} \times \mathrm{SU}(4)_{\rm vec})^{n_{\rm r}}] \times \mathrm{SO}(4)$
$\mathcal{L}^{(3)}_{\rm glue}$	$[\mathrm{U}(1)_{\rm VEC} \times \mathrm{SU}(4n_r)_L \times \mathrm{SU}(4n_r)_R] \times \mathrm{SW}_4$
$\mathcal{L}^{(3)}_{\rm bilin}(m=0)$	$[\mathrm{U}(1)_{\rm VEC} \times \mathrm{SU}(4n_r)_L \times \mathrm{SU}(4n_r)_R] \times \mathrm{SW}_4$
$\mathcal{L}^{(3)}_{\rm bilin}(m\neq 0)$	$[(\mathrm{U}(1)_{\rm vec} \times \mathrm{SU}(4)_{\rm vec})^{n_r}] \times \mathrm{SW}_4$
$\mathcal{L}^{(3)}_{\rm FF(A)}$	$[\mathrm{U}(n_r)_{\rm l} \times \mathrm{U}(n_r)_{\rm r} \times (\Gamma_4 \rtimes \mathrm{SO}(4))] \times \mathrm{SO}(4)$
$\mathcal{L}^{(3)}_{\rm FF(B)}$	$\mathrm{U}(n_r)_{\rm l} \times \mathrm{U}(n_r)_{\rm r} \times (\Gamma_4 \rtimes \mathrm{SW}_{4,\rm diag})$
$\mathcal{L}^{(3)}(m=0)$	$\mathrm{U}(n_r)_{\rm l} \times \mathrm{U}(n_r)_{\rm r} \times (\Gamma_4 \rtimes \mathrm{SW}_{4,\rm diag})$
$\mathcal{L}^{(3)}(m\neq 0)$	$(\mathrm{U}(1)_{\rm vec})^{n_r} \times \Gamma_4 \rtimes \mathrm{SW}_{4,\rm diag}$

Table 4.2: Taste- and rotation symmetries respected by the terms of the staggered effective Lagrangian defined in App. (B.3) In $\mathcal{L}^{(3)}_{\rm glue}$ The symmetry group $\mathrm{U}(1)_{\rm VEC}$ includes overall fermion numbers, $\mathrm{U}(1)_{\rm vec}$ applies to individual flavors. For the definition of the residual chiral group $\mathrm{U}(n_r)_{\rm l} \times \mathrm{U}(n_r)_{\rm r}$ see [6], where this table was taken from. The matching with the Lee-Sharpe Lagrangian to the order $\mathcal{O}\left(a^2, m\right)$, Eq. (4.4.1), involves terms from $\mathcal{L}^{(3)}_{\rm FF(A)}$, but not from $\mathcal{L}^{(3)}_{\rm FF(B)}$.

4.4.3 Scalar Propagators

In order to calculate chiral observables, we need an expression for the meson propagators. The quark-line connected propagators are a straightforward modification of the continuum scalar propagator:

$$\left\langle \phi^t_{gs,fr}(-k)\phi^t_{f'r',g's'}(k)\right\rangle_{\rm con} = \frac{\delta_{rr'}\delta_{ff'}\delta_{gg'}\delta_{ss'}}{k^2+m^2_{fg,t}}, \tag{4.4.9}$$

where $f,g,f',g' \in u,d,s$ denote the flavors whereas the replica indices $r,r',s,s' \in \{1,..n_r\}$ are specifying a taste in replica space. However, there are also quark-line disconnected propagators in the I, V and A taste channels, due to the double trace terms in the effective potential. They give rise to so-called hairpin diagrams. To obtain an expression for them, consider the full inverse propagator

$$G_t^{-1} = G_{0,t}^{-1} + \delta_t, \qquad (G^{-1}_{0,t})_{XY} = (q^2+m^2_{M,t})\delta_{XY}, \qquad \delta_t = \begin{cases} \frac{m_0^2}{3n_r} & \text{for } t=I \\ \delta'_V a^2 & \text{for } t=V \\ \delta'_V a^2 & \text{for } t=A \end{cases}. \tag{4.4.10}$$

The flavor indices for the valence quarks $X,Y \in \{U,D,S\}$ refer to flavor neutral mesons in the basis of the unmixed masses $m_{X,t}$, $m_{Y,t}$. The result for G_t can then be expressed in terms of the unmixed flavor-neutral states $L \in \{U,D,S\}$ and the physical mixed flavor-neutral states $F \in \{\pi,\eta,\eta'\}$

$$G_t = G_{0,t} + \mathcal{D}^t_{XY}, \qquad \mathcal{D}^t_{XY} = -\delta_t \frac{\prod_L (q^2+m^2_{L,t})}{(q^2+m^2_{X,t})(q^2+m^2_{Y,t})\prod_F (q^2+m^2_{F,t})} \tag{4.4.11}$$

which provide the pole masses [6]. For $N_{\rm f} = 2+1$, one obtains:

$$\mathcal{D}^t_{UU} = \mathcal{D}^t_{DD} = \mathcal{D}^t_{UD} = \mathcal{D}^t_{DU} = -\delta_t \frac{(k^2+m^2_{S,t})}{(k^2+m^2_{\pi,t})(k^2+m^2_{\eta,t})(k^2+m^2_{\eta',t})}, \tag{4.4.12}$$

$$\mathcal{D}^t_{US} = \mathcal{D}^t_{DS} = \mathcal{D}^t_{SU} = \mathcal{D}^t_{SD} = -\delta_t \frac{(k^2+m^2_{\pi,t})}{(k^2+m^2_{S,t})(k^2+m^2_{\eta,t})(k^2+m^2_{\eta',t})}, \tag{4.4.13}$$

$$\mathcal{D}^t_{SS} = -\delta_t \frac{1}{(k^2+m^2_{\eta,t})(k^2+m^2_{\eta',t})}. \tag{4.4.14}$$

With these matrix elements, the disconnected propagator is given by

$$\left\langle \phi^t_{gs,fr}(-k)\phi^t_{f'r',g's'}(k)\right\rangle_{\rm dis} = \delta_{rs}\delta_{r's'}\delta_{fg}\delta_{f'g'}\mathcal{D}^t_{XY}, \qquad X=(fg),\, Y=(f'g'). \tag{4.4.15}$$

The masses of the π, η and η' in the taste channels I, V and A differ from the StaggGMOR relation Eq. (4.4.6) due to the disconnected meson propagator. One can obtain these masses by studying the meson self energy diagrams on the quark level, taking hairpin diagrams into account [6]. This amounts to diagonalizing the full mass matrix of the effective Lagrangian after adding the flavor-neutral mixing terms in $\mathcal{L}$:

$$\begin{pmatrix} m^2_{U,t}+\delta_t n_{\rm r} & \delta_t n_{\rm r} & \delta_t n_{\rm r} \\ \delta_t n_{\rm r} & m^2_{D,t}+\delta_t n_{\rm r} & \delta_t n_{\rm r} \\ \delta_t n_{\rm r} & \delta_t n_{\rm r} & m^2_{S,t}+\delta_t n_{\rm r} \end{pmatrix} \quad \xrightarrow{\text{diag.}} \quad \begin{pmatrix} m^2_{\pi,t} & 0 & 0 \\ 0 & m^2_{\eta,t} & 0 \\ 0 & 0 & m^2_{\eta',t} \end{pmatrix}. \tag{4.4.16}$$

With $m_u = m_d$ ($m_{U,t} = m_{D,t}$), the masses of the flavor-neutral mesons are:

$$m^2_{\pi,t} = m^2_{U,t} = m^2_{D,t}, \tag{4.4.17}$$

$$m^2_{\eta,t} = \frac{1}{2}\left(m^2_{U,t} + m^2_{S,t} + 3n_{\rm r}\delta_t - Z_t\right). \tag{4.4.18}$$

$$m^2_{\eta',t} = \frac{1}{2}\left(m^2_{U,t} + m^2_{S,t} + 3n_{\rm r}\delta_t + Z_t\right), \tag{4.4.19}$$

$$Z_t = \left(\left(m^2_{S,t}-m^2_{U,t}\right)^2 - 2n_{\rm r}\delta_t\left(m^2_{S,t}-m^2_{U,t}\right) + (3n_{\rm r}\delta_t)^2\right)^{1/2}. \tag{4.4.20}$$

For the isosinglet taste channel we will be interested both in the limit $m_0 \to \infty$ and $m_0 \to 0$, since we also want to study how effective restoration of $\mathrm{U_A}(1)$ symmetry effects the connected susceptibility. In the limit $m_0 \to \infty$, one obtains the usual result known from continuum perturbation theory:

$$m^2_{\eta,I} = \frac{1}{3}\left(m^2_{U,I} + 2m^2_{S,I}\right) + \mathcal{O}\left(1/m_0^2\right), \tag{4.4.21}$$

$$m^2_{\eta',I} = m_0^2 + \frac{1}{3}\left(2m^2_{U,I} + m^2_{S,I}\right) + \mathcal{O}\left(1/m_0^2\right). \tag{4.4.22}$$

In the limit of vanishing m_0 we find:

$$m^2_{\eta,I} = m^2_{U,I}, \qquad m^2_{\eta',I} = m^2_{S,I}. \tag{4.4.23}$$

It is advisable to perform a partial fraction expansion of the disconnected propagator in order to obtain a sum of propagators of the physical flavor-neutral states:

$$\left\langle \phi^t_{gs,fr}(-k)\phi^t_{f'r',g's'}(k)\right\rangle_{\mathrm{dis}} = -\delta_{rs}\delta_{r's'}\delta_{fg}\delta_{f'g'}\delta_t\left(\frac{g^t_\pi}{k^2+m_{\pi,t}} + \frac{g^t_\eta}{k^2+m_{\eta,t}} + \frac{g^t_{\eta'}}{k^2+m_{\eta',t}}\right). \tag{4.4.24}$$

The residues g^t_π, g^t_η are given in App. (B.3).

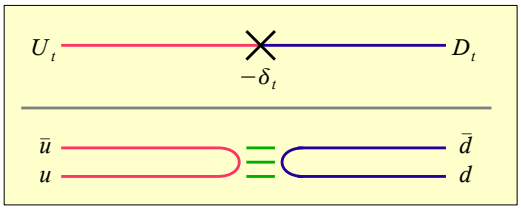

Figure 4.3: The disconnected meson propagator, which induces flavor mixing in the taste channels I,V,A. On the mesonic level (top), it shows up as two-point vertex, on the quark level it is depicted as a four-fermion interaction known as "hairpin diagram".

4.4.4 Chiral Condensate from SχPT

The one-loop corrections of the chiral condensate, already discussed in Sec. 4.2.1 can be reproduced via SχPT, one simply has to evaluate the expression

$$\begin{aligned}
C_{ff,I} &= \mathcal{N}\sum_k \sum_{g=u,d,s}\sum_{r,s=1}^{n_r}\sum_{t=1}^{16}\left\langle \phi^t_{fr,gs}(-k)\phi^t_{gs,fr}(k)\right\rangle \\
&= \mathcal{N}\sum_k \sum_{g=u,d,s}\sum_{r,s=1}^{n_r}\left[\sum_{t=1}^{16}\frac{\delta_{ff}\delta_{rr}\delta_{gg}\delta_{ss}}{k^2+m^2_{fg,t}}\right. \\
&\quad \left. - \sum_{t=I,4V,4A}\delta_{fg}\delta_{rs}\delta_t\left(\frac{g_{\pi/S}}{k^2+m^2_{\pi/S,t}} + \frac{g_\eta}{k^2+m^2_{\eta,t}} + \frac{g'_\eta}{k^2+m^2_{\eta',t}}\right)\right] \\
&= \mathcal{N}\sum_k\left[\sum_{t=1}^{16}\sum_{g=u,d,s}\frac{n_r^2}{k^2+m^2_{fg,t}} - \sum_{t=I,4V,4A} n_r\delta_t\left(\frac{g_{\pi/S}}{k^2+m^2_{\pi/S,t}} + \frac{g_\eta}{k^2+m^2_{\eta,t}} + \frac{g_{\eta'}}{k^2+m^2_{\eta',t}}\right)\right]
\end{aligned} \tag{4.4.25}$$

By setting $f = u, d, s$ and explicitly writing the taste isosinglet, one obtains:

$$C_{uu,I} = \mathcal{N} \sum_k \left[\sum_{t=1}^{16} \left(\frac{2n_r^2}{k^2 + m_{\pi,t}^2} + \frac{n_r^2}{k^2 + m_{K,t}^2} \right) - \frac{1/2}{k^2 + m_{\pi,I}^2} - \frac{m_0^2}{3} \left(\frac{g_\eta}{k^2 + m_{\eta,t}^2} + \frac{g'_\eta}{k^2 + m_{\eta',t}^2} \right) \right.$$
$$\left. -4 \sum_{t=V,A} n_r \delta_t \left(\frac{g_\pi}{k^2 + m_{\pi,t}^2} + \frac{g_\eta}{k^2 + m_{\eta,t}^2} + \frac{g_{\eta'}}{k^2 + m_{\eta',t}^2} \right) \right] = C_{dd,I}, \tag{4.4.26}$$

$$C_{ss,I} = \mathcal{N} \sum_k \left[\sum_{t=1}^{16} \left(\frac{2n_r^2}{k^2 + m_{K,t}^2} + \frac{n_r^2}{k^2 + m_{S,t}^2} \right) - \frac{1}{k^2 + m_{S,I}^2} - \frac{m_0^2}{3} \left(\frac{g_\eta}{k^2 + m_{\eta,t}^2} + \frac{g'_\eta}{k^2 + m_{\eta',t}^2} \right) \right.$$
$$\left. -4 \sum_{t=V,A} n_r \delta_t \left(\frac{g_S}{k^2 + m_{S,t}^2} + \frac{g_\eta}{k^2 + m_{\eta,t}^2} + \frac{g_{\eta'}}{k^2 + m_{\eta',t}^2} \right) \right]. \tag{4.4.27}$$

In the continuum limit, and in the limit $m_0 \to \infty$ we recover the continuum result Eq. (4.2.1):

$$C_{uu,I} = \mathcal{N} \sum_k \left[\left(\frac{3/2}{k^2 + m_\pi^2} + \frac{1}{k^2 + m_K^2} \right) + \frac{1/6}{k^2 + m_\eta^2} + \frac{1/3}{k^2 + m_{\eta'}^2} \right], \tag{4.4.28}$$

$$C_{ss,I} = \mathcal{N} \sum_k \left[\frac{2}{k^2 + m_K^2} + \frac{2/3}{k^2 + m_\eta^2} + \frac{1/3}{k^2 + m_{\eta'}^2} \right]. \tag{4.4.29}$$

After replacing the sum by a four-dimensional integral, we obtain the chiral logarithms discussed by Leutwyler and Gasser, with the additional piece from the η' contribution. This contribution will be of interest at higher temperatures, when m_0 (and m'_η) may become small.

4.4.5 Chiral Susceptibilities from Scalar Correlators

The effect of taste violations and the anomaly on the Goldstone effect in the susceptibilities can be calculated via so-called bubble terms for the scalar mesons $B_{ff;ee}(p)$, which are integrated correlation functions. The relation between IR-divergent contributions of the bubble terms and chiral susceptibility for low temperatures is: [26]

$$\chi_l^{\mathrm{IR}} = \chi_l^{\mathrm{IR,con}} + \chi_l^{\mathrm{IR,dis}}, \tag{4.4.30}$$

$$\chi_l^{\mathrm{IR,con}} = B_{uu;uu}^{\mathrm{con,IR}}(0) + B_{dd;dd}^{\mathrm{con,IR}}(0), \tag{4.4.31}$$

$$\chi_l^{\mathrm{IR,dis}} = B_{uu;uu}^{\mathrm{dis,IR}}(0) + B_{dd;dd}^{\mathrm{dis,IR}}(0) + B_{uu;dd}^{\mathrm{dis,IR}}(0) + B_{dd;uu}^{\mathrm{dis,IR}}(0). \tag{4.4.32}$$

Apart from these IR-divergent contributions from the bubble terms, there is also the contribution from the scalar propagator itself, as discussed in Sec. 4.3.3. For staggered fermions, the expression of such a bubble term for valence quark flavors f,f' and e,e' in the isosinglet taste channel I is given by [14]:

$$B_{ff',ee',I}(\boldsymbol{p}, ta) = \mathcal{N} \sum_k \sum_{g,s,r,t} \sum_{g',s',r',t'} \left[\left\langle \phi_{fr,gs}^t(-k) \phi_{er',g's'}^{t'}(k) \right\rangle \left\langle \phi_{gs,f'r}^t(k-p) \phi_{g's',e'r}^{t'}(p-k) \right\rangle \right.$$
$$\left. + \left\langle \phi_{fr,gs}^t(-k) \phi_{g's',e'r'}^{t'}(k) \right\rangle \left\langle \phi_{gs,f'r}^t(k-p) \phi_{er',g's'}^{t'}(p-k) \right\rangle \right], \tag{4.4.33}$$

[26] The quark-line connected bubble terms are related to the scalar correlation function of the scalar meson a_0, f_0: $B_{a_0}(p) = \frac{1}{2}\left(B_{ud;du}(p) + B_{du;ud}(p)\right)$, because $B_{ud;du} = B_{du;ud} = B_{uu;uu}^{\mathrm{con}}$. Likewise, $B_{f_0}(p) = \frac{1}{2}\left(B_{uu;uu}(p) + B_{dd;dd}(p) + B_{uu;dd}(p) + B_{dd;uu}(p)\right)$ with the equalities $B_{uu;uu} = B_{uu;uu}^{\mathrm{con}} + B_{uu;uu}^{\mathrm{dis}}$ and $B_{uu;dd}(0) = B_{dd;uu} = B_{uu;uu}^{\mathrm{dis}}$.

where g,g' are the quark flavors of the sea quarks, r,r',s,s' are replica indices and t, t' are taste indices. The normalization constant is $\mathcal{N} = B_0^2/N_\sigma^3 N_\tau 4a^2$. After performing the Wick contractions, which are shown in Fig. 4.4, the bubble term for valence flavors f, f' and e, e' in $N_\mathrm{f} = 2+1$ becomes

$$\begin{aligned}
B_{ff';ee'}(p) = \mathcal{N}\sum_k \Bigg[& n_\mathrm{r}^2 \delta_{ff'}\delta_{ee'} \sum_{t=1}^{16} \frac{1}{k^2+m_{fe,t}^2}\frac{1}{(k+p)^2+m_{ef',t}^2} \\
& -2n_\mathrm{r}\delta_{fe'}\delta_{ef'} \sum_{t=I,4A,4V} \frac{1}{k^2+m_{fe,t}^2}\delta_t \left(\frac{g_{\pi/S}^t}{(k+p)^2+m_{\pi/S,t}} + \frac{g_\eta^t}{(k+p)^2+m_{\eta,t}} + \frac{g_{\eta'}^t}{(k+p)^2+m_{\eta',t}} \right) \\
& -2n_\mathrm{r}\delta_{fe'}\delta_{ef'} \sum_{t=I,4A,4V} \frac{1}{(k+p)^2+m_{fe,t}^2}\delta_t \left(\frac{g_{\pi/S}^t}{k^2+m_{\pi/S,t}} + \frac{g_\eta^t}{k^2+m_{\eta,t}} + \frac{g_{\eta'}^t}{k^2+m_{\eta',t}} \right) \\
& +2n_\mathrm{r}^2\delta_{ff'}\delta_{ee'} \sum_{t=I,4V,4A} \delta_t^2 \left(\frac{g_{\pi/S}^t}{k^2+m_{\pi/S,t}} + \frac{g_\eta^t}{k^2+m_{\eta,t}} + \frac{g_{\eta'}^t}{k^2+m_{\eta',t}} \right) \\
& \qquad \left(\frac{g_{\pi/S}^t}{(k+p)^2+m_{\pi/S,t}} + \frac{g_\eta^t}{(k+p)^2+m_{\eta,t}} + \frac{g_{\eta'}^t}{(k+p)^2+m_{\eta',t}} \right) \\
& +n_\mathrm{r}^2 \sum_{g=u,d,s} \delta_{fe'}\delta_{ef'} \sum_{t=1}^{16} \frac{1}{k^2+m_{fg,t}^2}\frac{1}{(k+p)^2+m_{ge,t}^2} \Bigg],
\end{aligned} \tag{4.4.34}$$

where $\sum_{t=I,4V,4A}$ indicates the sum over one taste-singlet, 4 taste-vector and 4 taste-axialvector channels. This expression simplifies at zero momentum $p = 0$, and after identifying the quark-line connected and disconnected parts one obtains:

$$\begin{aligned}
B_{ff';ee'}^{\mathrm{con}}(0) = \mathcal{N}\sum_k \Bigg[& -4n_\mathrm{r}\delta_{fe'}\delta_{ef'} \sum_{t=I,A,V} \frac{1}{k^2+m_{fe,t}^2}\delta_t \left(\frac{g_{\pi/S}^t}{k^2+m_{\pi/S,t}} + \frac{g_\eta^t}{k^2+m_{\eta,t}} + \frac{g_{\eta'}^t}{k^2+m_{\eta',t}} \right) \\
& +n_\mathrm{r}^2 \sum_{g=u,d,s} \delta_{fe'}\delta_{ef'} \sum_{t=1}^{16} \frac{1}{k^2+m_{fg,t}^2}\frac{1}{k^2+m_{ge,t}^2} \Bigg],
\end{aligned} \tag{4.4.35}$$

$$\begin{aligned}
B_{ff';ee'}^{\mathrm{dis}}(0) = \mathcal{N}\sum_k \Bigg[& n_\mathrm{r}^2\delta_{ff'}\delta_{ee'} \sum_{t=1}^{16} \frac{1}{\left(k^2+m_{fe,t}^2\right)^2} \\
& +2n_\mathrm{r}^2\delta_{ff'}\delta_{ee'} \sum_{t=I,4V,4A} \delta_t^2 \left(\frac{g_{\pi/S}^t}{k^2+m_{\pi/S,t}^2} + \frac{g_\eta^t}{k^2+m_{\eta,t}^2} + \frac{g_{\eta'}^t}{k^2+m_{\eta',t}^2} \right)^2 \Bigg].
\end{aligned} \tag{4.4.36}$$

The bubble terms for the light quark flavors are:

$$\begin{aligned}
B_{uu;uu}^{\mathrm{con}}(0) = \mathcal{N}\sum_k \Bigg[& n_\mathrm{r}^2 \sum_{g=u,d,s} \sum_{t=1}^{16} \left(\frac{2}{(k^2+m_{\pi,t}^2)^2} + \frac{2}{(k^2+m_{K,t}^2)^2} \right) \\
& -4n_\mathrm{r} \sum_{t=I,4V,4A} \frac{1}{k^2+m_{\pi,t}^2}\delta_t \left(\frac{g_\pi^t}{k^2+m_{\pi,t}^2} + \frac{g_\eta^t}{k^2+m_{\eta,t}^2} + \frac{g_{\eta'}^t}{k^2+m_{\eta',t}^2} \right) \Bigg] = B_{dd;dd}^{\mathrm{con}}(0),
\end{aligned} \tag{4.4.37}$$

$$B^{\text{dis}}_{uu;uu}(0) = \mathcal{N}\sum_k \left[n_{\text{r}}^2 \sum_{t=1}^{16} \frac{1}{\left(k^2+m^2_{\pi,t}\right)^2} \right.$$
$$\left. +2n_{\text{r}}^2 \sum_{t=I,4V,4A} \delta_t^2 \left(\frac{g^t_\pi}{k^2+m^2_{\pi,t}} + \frac{g^t_\eta}{k^2+m^2_{\eta,t}} + \frac{g^t_{\eta'}}{k^2+m^2_{\eta',t}} \right)^2 \right] = B^{\text{dis}}_{dd;dd}(0). \tag{4.4.38}$$

In analogy to the symbols defined in Eq. (4.2.22), we introduce the short-hand notation

$$\hat{\mu}_{PQ,t} = \sum_k \frac{1}{(k^2+m^2_{P,t})(k^2+m^2_{Q,t})}, \qquad P,Q \in \{\pi, K, \eta, \eta'\}. \tag{4.4.39}$$

where the hat denotes that it is a lattice loop integral over discrete momenta. Plugging in the vertices δ_t and coefficients $g^t_\pi = 1/2n_r\delta_t$ one obtains

$$B^{\text{con}}_{uu;uu}(0) = \mathcal{N}\left[n_{\text{r}}^2 \sum_{t=1}^{16} (2\hat{\mu}_{\pi\pi,t} + \hat{\mu}_{KK,t}) - 2\hat{\mu}_{\pi\pi,I} - \frac{4m_0^2}{3}\left(g^I_\eta \hat{\mu}_{\pi\eta,I} + g^I_{\eta'}\hat{\mu}_{\pi\eta',I}\right) \right.$$
$$\left. -4\sum_{t=V,A}\left(2\hat{\mu}_{\pi\pi,t} + 4n_{\text{r}}\delta_t\left(g^t_\eta\hat{\mu}_{\pi\eta,t} + g^t_{\eta'}\hat{\mu}_{\pi\eta,t}\right)\right)\right], \tag{4.4.40}$$

$$B^{\text{dis}}_{uu;uu}(0) = \mathcal{N}\left[n_{\text{r}}^2 \sum_{t=1}^{16} \hat{\mu}_{\pi\pi,t} + \frac{1}{2}\hat{\mu}_{\pi\pi,I} + \frac{2m_0^2}{3}\left(g^I_\eta\hat{\mu}_{\pi\eta,I} + g^I_{\eta'}\hat{\mu}_{\pi\eta',I}\right) \right.$$
$$+ \frac{2m_0^4}{9}\left((g^I_\eta)^2\hat{\mu}_{\eta\eta,I} + (g^I_{\eta'})^2\hat{\mu}_{\eta'\eta',I} + 2g^I_\eta g^I_{\eta'}\hat{\mu}_{\eta\eta',I}\right)$$
$$+ 2\sum_{t=V,A}\left(\hat{\mu}_{\pi\pi,t} + 4n_{\text{r}}\delta_t\left(g^t_\eta\hat{\mu}_{\pi\eta,t} + g^t_{\eta'}\hat{\mu}_{\pi\eta',t}\right)\right.$$
$$\left. \left. +4n_{\text{r}}^2\delta_t^2\left((g^t_\eta)^2\hat{\mu}_{\eta\eta,t} + (g^t_{\eta'})^2\hat{\mu}_{\eta'\eta',t} + 2g^t_\eta g^t_{\eta'}\hat{\mu}_{\eta\eta',t}\right)\right)\right]. \tag{4.4.41}$$

In the continuum limit, where $\delta_{V/A} \to 0$, all hairpin diagrams in the taste channels V, A cancel (and also in I for vanishing anomaly, $m_0 \to 0$). If we furthermore neglect taste violations in the meson masses, $\Delta_t = 0\ \forall t$, $\hat{\mu}_{PQ,t} \to \hat{\mu}_{PQ}$, we obtain the continuum result:

$$B^{\text{con}}_{uu;uu}(0) = \mathcal{N}\left[32n_{\text{r}}^2\hat{\mu}_{\pi\pi} + 16n_{\text{r}}^2\hat{\mu}_{KK} - 2\hat{\mu}_{\pi\pi} - \frac{4m_0^2}{3}\left(g_\eta\hat{\mu}_{\pi\eta} + g_{\eta'}\hat{\mu}_{\pi\eta'}\right)\right], \tag{4.4.42}$$

$$B^{\text{dis}}_{uu;uu}(0) = \mathcal{N}\left[16n_{\text{r}}^2\hat{\mu}_{\pi\pi} + \frac{1}{2}\hat{\mu}_{\pi\pi} + \frac{2m_0^2}{3}\left(g_\eta\hat{\mu}_{\pi\eta} + g_{\eta'}\hat{\mu}_{\pi\eta'}\right)\right.$$
$$\left. + \frac{2m_0^4}{9}\left((g_\eta)^2\hat{\mu}_{\eta\eta} + (g_{\eta'})^2\hat{\mu}_{\eta'\eta'} + 2g_\eta g_{\eta'}\hat{\mu}_{\eta\eta'}\right)\right]. \tag{4.4.43}$$

In the limit $m_0 \to \infty$ we neglect the contribution of the $\pi - \eta'$ channel, in the limit $m_0 \to 0$ however all isosinglet channels cancel, and after setting $n_{\text{r}} = 1/4$ we obtain:

$$\lim_{m_0\to\infty} B^{\text{con}}_{uu;uu}(0) = \mathcal{N}\left[\hat{\mu}_{KK} + \tfrac{2}{3}\hat{\mu}_{\pi\eta} + \tfrac{4}{3}\hat{\mu}_{\pi\eta'}\right], \tag{4.4.44}$$

$$\lim_{m_0\to 0} B^{\text{con}}_{uu;uu}(0) = \mathcal{N}\left[2\hat{\mu}_{\pi\pi} + \hat{\mu}_{KK}\right], \tag{4.4.45}$$

$$\lim_{m_0\to\infty} B^{\text{dis}}_{uu;uu}(0) = \mathcal{N}\left[\tfrac{3}{2}\hat{\mu}_{\pi\pi} + \tfrac{1}{18}\hat{\mu}_{\eta\eta} + \tfrac{2}{9}\hat{\mu}_{\eta'\eta'} - \tfrac{1}{3}\hat{\mu}_{\pi\eta} - \tfrac{2}{3}\hat{\mu}_{\pi\eta'} + \tfrac{2}{9}\hat{\mu}_{\eta\eta'}\right], \tag{4.4.46}$$

$$\lim_{m_0\to 0} B^{\text{dis}}_{uu;uu}(0) = \mathcal{N}\hat{\mu}_{\pi\pi}. \tag{4.4.47}$$

For $m_0 \to \infty$, this result is due to a cancellation of the two-pion-states in the connected susceptibility, as expected in the continuum for two light flavors. The surviving modes are $K\bar{K}$ and $\pi\eta$ (and $\pi\eta'$ if m_0 is large but still finite). For $m_0 \to 0$, however we are left with 2 pions, here the η and η' prevent the pions to be "eaten".

If we assume taste violations to be large, one obtains Goldstone modes in the a_0 bubble term only in the pseudo-taste channel, where $\Delta_P = 0$:

$$B^{\mathrm{con,IR}}_{uu;uu}(0) + B^{\mathrm{con,IR}}_{dd;dd}(0) = \mathcal{N}\frac{1}{4}\hat{\mu}_{\pi\pi,P}, \tag{4.4.48}$$

$$B^{\mathrm{disIR}}_{uu;uu}(0) + B^{\mathrm{disIR}}_{dd;dd}(0) + B^{\mathrm{disIR}}_{uu;dd}(0) + B^{\mathrm{disIR}}_{dd;uu}(0) = \mathcal{N}\frac{1}{4}\hat{\mu}_{\pi\pi,P}. \tag{4.4.49}$$

In the IR part, the T, V, A and I channels were disregarded since the mesons in these channels have strong taste violations ($\mathrm{U_A(1)}$ violations resp.). Only the P channel is of interest here. Also the $\hat{\mu}_{KK,P}$ channel was disregarded as it remains heavy in the chiral limit for the light flavors.

We have argued that we expect the Goldstone contributions at finite temperature QCD to appear from the Matsubara zero modes in the thermal propagator which enters the pressure, i.e. they are proportional to temperature and are effectively three-dimensional. Hence, the bubble terms can be integrated in three dimensions (we replace the sum over $\boldsymbol{k}$ by an integral, see App. B.1.1). The taste violations then induce the following IR divergences ($N_{\mathrm{f}} = 2+1$):

$$\chi^{\mathrm{con,IR}}_{\mathrm{S}\chi\mathrm{PT}} = \mathcal{N}\frac{1}{4\pi}\frac{1/8}{M_{\pi,5}}, \tag{4.4.50}$$

$$\chi^{\mathrm{dis,IR}}_{\mathrm{S}\chi\mathrm{PT}} = \mathcal{N}\frac{1}{4\pi}\frac{1/8}{M_{\pi,5}}, \tag{4.4.51}$$

$$\chi^{\mathrm{full,IR}}_{\mathrm{S}\chi\mathrm{PT}} = \mathcal{N}\frac{1}{4\pi}\frac{1/4}{M_{\pi,5}}, \tag{4.4.52}$$

as compared to the result of IR divergences in the continuum limit:

$$\chi^{\mathrm{con,IR}}_{\mathrm{cont}} = 0, \tag{4.4.53}$$

$$\chi^{\mathrm{dis,IR}}_{\mathrm{cont}} = \mathcal{N}\frac{1}{4\pi}\frac{3}{M_\pi} = \chi^{\mathrm{full,IR}}_{\mathrm{cont}}. \tag{4.4.54}$$

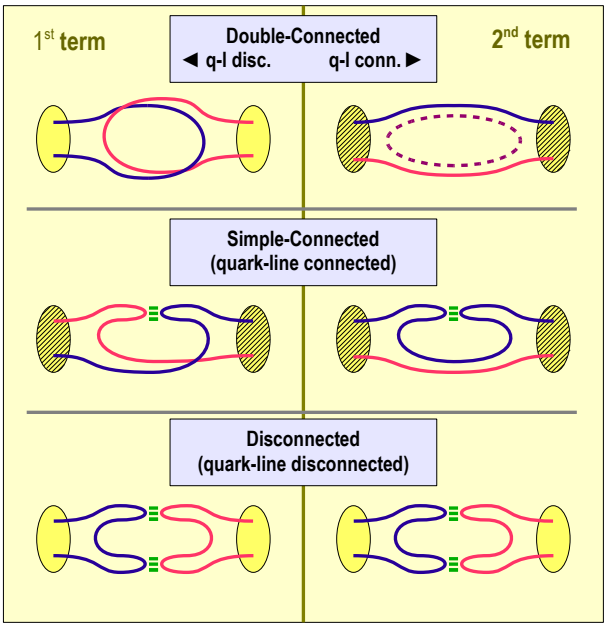

Figure 4.4: Distinction between quark-line connected and quark-line disconnected diagrams in the f_0 bubble term. The connected diagrams can be identified with the a_0 bubble term.

Hence we expect to find a 24 times larger prefactor for the physical Goldstone term than for the pseudo-Goldstone term from the P-taste channel in the disconnected part, and a 12 times larger prefactor for the full susceptibility.

Likewise we have computed the strange quark susceptibilities with strange valence quarks, see Appendix (B.3). We summarize the results for 2+1 flavors in Tab. 4.3. However, with a strange quark as a valence quark involved, no additional IR divergences arise, as pion loops are impossible. Note that the unphysical $\hat{\mu}_{SS}$, $\hat{\mu}_{S\eta}$ and $\hat{\mu}_{S\eta'}$ drop out in the full susceptibility, but not in the connected and disconnected part. In the continuum limit, the expressions for the full susceptibilities agree with those obtained in Sec. 4.2.1 when replacing $\hat{\mu}_{PQ,t}$ by the chiral logarithms μ_{PQ}.

	$m_0 = 0$	$m_0 > 0$	$m_\eta < \infty$	#
flavors	$\langle uu, uu\rangle + \langle dd, dd\rangle + \langle uu, dd\rangle + \langle dd, uu\rangle$			$N_l = 2$
$\frac{1}{N_l}\chi^{\text{con}}$	$\boldsymbol{2\pi\pi} + 1KK$	$\boldsymbol{-2\pi\pi} + \frac{2}{3}\pi\eta$	$+\frac{4}{3}\pi\eta'$	$N_\text{f} - 4/N_\text{f} + 4/N_\text{f}$ $\boldsymbol{N_l - 4/N_l = 0}$
$\frac{1}{N_l^2}\chi^{\text{dis}}$	$\boldsymbol{1\pi\pi}$	$+\boldsymbol{\frac{1}{2}\pi\pi} - \frac{1}{3}\pi\eta + \frac{1}{18}\eta\eta$	$+\frac{2}{9}\eta'\eta' - \frac{2}{3}\pi\eta' + \frac{2}{9}\eta\eta'$	$1 + 2/N_\text{f}^2 - 2/N_\text{f}^2$ $\boldsymbol{1 + 2/N_l^2 = 3/2}$
χ^{full}	$\boldsymbol{8\pi\pi} + 2KK$	$\boldsymbol{-2\pi\pi} + \frac{2}{9}\eta\eta$	$+\frac{8}{9}\eta'\eta' + \frac{8}{9}\eta\eta'$	$10 - 20/9 + 20/9$ $\boldsymbol{2(N_l^2 - 1)}$
flavors	$\langle ss, ss\rangle$			$N_s = 1$
χ^{con}	$2KK + 1SS$	$-4SS + \frac{8}{3}S\eta$	$+\frac{4}{3}S\eta'$	$N_\text{f} - 4/N_\text{f} + 4/N_\text{f}$ $\boldsymbol{0}$
χ^{dis}	$1SS$	$+2SS - \frac{8}{3}S\eta + \frac{8}{9}\eta\eta$	$+\frac{2}{9}\eta'\eta' + \frac{8}{9}\eta\eta' - \frac{4}{3}S\eta'$	$1 + 2/N_\text{f}^2 - 2/N_\text{f}^2$ $\boldsymbol{0}$
χ^{full}	$2KK + 2SS$	$-2SS + \frac{8}{9}\eta\eta$	$+\frac{2}{9}\eta'\eta' + \frac{8}{9}\eta\eta'$	$4 - 10/9 + 10/9$ $\boldsymbol{0}$
flavors	$\langle uu, ss\rangle + \langle dd, ss\rangle + \langle ss, uu\rangle + \langle ss, dd\rangle$			$N_l = 2, N_s = 1$
χ^{con}	—			0 $\boldsymbol{0}$
$\frac{1}{2N_l}\chi^{\text{dis}}$	$1KK$	$+\frac{2}{9}\eta\eta$	$+\frac{2}{9}\eta'\eta' - \frac{4}{9}\eta\eta'$	$1 + 2/N_\text{f}^2 - 2/N_\text{f}^2$ $\boldsymbol{0}$
χ^{full}	$4KK$	$+\frac{8}{9}\eta\eta$	$+\frac{8}{9}\eta'\eta'$	$4 + 8/9 - 8/9$ $\boldsymbol{0}$
flavors	$\sum_{f=u,d,s}\sum_{e=u,d,s}\langle ff, ee\rangle$			$N_\text{f} = N_l + N_s = 3$
χ^{con}	$\boldsymbol{4\pi\pi} + 4KK$	$\boldsymbol{-4\pi\pi} + \frac{4}{3}\pi\eta - 4SS + \frac{8}{3}S\eta$	$+\frac{8}{3}\pi\eta' + \frac{4}{3}S\eta'$	$N_\text{f}^2 - 4 + 4$ $\boldsymbol{N_l^2 - 4 = 0}$
χ^{dis}	$\boldsymbol{4\pi\pi} + 4KK + SS$	$\boldsymbol{+2\pi\pi} - \frac{4}{3}\pi\eta + 2\eta\eta + 2SS - \frac{8}{3}S\eta$	$+2\eta'\eta' - \frac{8}{3}\pi\eta' - \frac{4}{3}S\eta'$	$N_\text{f}^2 + 2 - 2$ $\boldsymbol{N_l^2 + 2 = 6}$
χ^{full}	$\boldsymbol{8\pi\pi} + 8KK + 2SS$	$\boldsymbol{-2\pi\pi} - 2SS + 2\eta\eta$	$+2\eta'\eta'$	$2(N_\text{f}^2 - 1 + 1)$ $\boldsymbol{2(N_l^2 - 1) = 6}$

Table 4.3: Multiplicities of the modes $\hat{\mu}_{PQ,t}$ (abbreviated to PQ) contributing to the chiral susceptibilities. Multiplicities of the Goldstone modes $\mu_{\pi\pi}$ are highlighted in bold font. The first column $m_0 = 0$ corresponds to the multiplicities for the pseudoscalar sector including the η' as a Goldstone boson (in this limit, $\eta = \pi$, $\eta' = S$), the second column $m_0 > 0$ gives the corrections if the flavor singlet η' decouples from the octet, due to the disconnected meson propagator. The third column $m_0 < \infty$ gives the modes involving the η' if its mass is not too large to be disregarded. The fourth column gives the multiplicities for the different contributions.

Chapter 5

Analysis of 2+1 Flavor Lattice Data

5.1 Methods

5.1.1 Random Noise Estimator

The position space traces of operators containing the inverse fermion matrices, in particular for the chiral condensate and the connected susceptibility

$$\operatorname{tr} M^{-1} = \frac{1}{N_\sigma^3 N_\tau} \sum_n M^{-1}_{nn}, \qquad \operatorname{tr} M^{-2} = \frac{1}{N_\sigma^3 N_\tau} \sum_{n,n'} M^{-1}_{nn'} M^{-1}_{n'n}, \tag{5.1.1}$$

can not be computed directly because the fermion matrix is of very large dimension and its inversion is too expensive. Instead we make use of so-called *random noise vectors* (RNVs), which enable to estimate the inverse of a matrix statistically. We choose the RNVs $\boldsymbol{R}$ to take values from Z(2), i.e.

$$\boldsymbol{R}: \quad n \mapsto R_n = (\pm 1, 0, 0), \qquad n \in \Gamma_{N_\sigma, N_\tau}, \tag{5.1.2}$$

where only the first color component is occupied, and the final result will be multiplied with N_c. In the limit of a large number N of RNVs, the orthogonality relation

$$\lim_{N\to\infty} \sum_{a=1}^{N} R^a_n R^a_{n'} = \delta^{(4)}(n - n') \tag{5.1.3}$$

is fulfilled, i.e. they give an estimate of the identity matrix in position space. The traces of the inverse fermion matrix and its powers are then estimated as

$$\operatorname{tr} M^{-1} \simeq \frac{1}{N} \sum_{a=1}^{N} (\boldsymbol{R}^a)^T M^{-1} \boldsymbol{R}^a = \frac{1}{N} \sum_{a=1}^{N} (\boldsymbol{R}^a)^T \boldsymbol{X}^a, \tag{5.1.4}$$

$$\operatorname{tr} M^{-2} \simeq \frac{1}{N} \sum_{a=1}^{N} (\boldsymbol{R}^a)^T M^{-1} M^{-1} \boldsymbol{R}^a = \frac{1}{N} \sum_{a=1}^{N} (\boldsymbol{R}^a)^T M^{-1} \boldsymbol{X}^a = \frac{1}{N} \sum_{a=1}^{N} (\boldsymbol{R}^a)^T \boldsymbol{Y}^a. \tag{5.1.5}$$

The linear equation for the solution vector $\boldsymbol{X}^a = M^{-1}\boldsymbol{R}^a$ can be computed via the conjugate gradient method. For higher powers, the linear equations are solved recursively. For the disconnected susceptibility, also the product of two traces has to be considered. By computing this product, one needs to take care of the correlations between the RNVs. In particular, the diagonal contributions have to be neglected to avoid autocorrelation:

$$\operatorname{tr} M^{-1} \operatorname{tr} M^{-1} \simeq \frac{1}{N(N-1)} \sum_{a\neq b} (\boldsymbol{R}^a)^T M^{-1} \boldsymbol{R}^a (\boldsymbol{R}^b)^T M^{-1} \boldsymbol{R}^b. \tag{5.1.6}$$

5.1.2 Error Estimation

In practice we are confronted with the problem that the configurations generated in a Markov chain might be strongly correlated. In particular, we find "critical slowing down" of the updating process if the parameters are chosen close to the critical values signaling a phase transition. This needs to be taken into account when estimating reliable errors. The standard error systematically underestimates the statistical uncertainties in observables. This problem can be avoided by making use of the *Jackknife method*, which gives a better error estimate on correlated data sets. Moreover, this method has the advantage that uncertainties for the secondary quantities $f(\{O_i\})$ need not to be calculated via Gaussian error propagation from primary quantities $\{O_i\}$, $i = 1 \dots N$. The Jackknife is a resampling method: the original data are reordered or combined to new samples which are then further evaluated. In our case, we form N/n bins, where n is the so-called bin length, and each bin contains n samples in successive order according to their production. From these bins, N/n resampled primary quantities P_s are calculated by omitting one of the bins via

$$P_s = \frac{1}{N/n - 1} \sum_{r \neq s} \sum_{i \in \text{bin } r} O_i, \qquad s = 1, \dots N/n \tag{5.1.7}$$

and from these the secondary quantities $S_s^j = f^j(P_s)$ are calculated. The mean value $\bar{S}^j$ and the error σ^j of these secondary quantities is then given by

$$\bar{S}^j = \frac{n}{N} \sum_{s=1}^{N/n} \left(S_s^j\right), \qquad \sigma^j = \left(\frac{N/n - 1}{N/n} \sum_{s=1}^{N/n} \left(S_s^j - \bar{S}^j\right)^2 \right)^{\frac{1}{2}}. \tag{5.1.8}$$

The estimate for the standard deviation σ^j depends on the bin length n. For $n = 1$ and $f^j(P_s) = P_s$ one can easily check that σ^j coincides with the conventional standard deviation. Increasing the bin size n, will also increase σ^j, until it saturates to a stable error σ^j_{sat} as the bins become uncorrelated. The corresponding binsize n_s is a measure for the correlation of the configurations for the observables in question. We have applied the Jackknife method to estimate the errors of all chiral observables. We found $n_s \gtrsim 20$ for the configurations considered (measured on every 10^{th} RHMC trajectory, see Sec. 5.2.1), which implies that only every 200^{th} trajectory gives a statistically independent measurement. Note that our measurements have entirely and solely been performed in the transition region.

5.1.3 Ferrenberg-Swendsen Reweighting

The aim of the *Ferrenberg-Swendsen Method* (FSM) described in [43] is to increase the amount of information obtained from a simulation. The lattice data obtained from a Monte Carlo simulation are averages of thermodynamic quantities at a single point in parameter space (β,$\hat{m}_l$,$\hat{m}_s$), but the configurations also contain information of the neighborhood to this point, as long as the probability that some configurations could have been produced by those other points is not negligibly small. In principle, for an infinite Markov chain, the data from a single simulation may suffice to study the entire scaling region near a phase transition. In practice it is required that the action distribution of the given parameters has an overlap with the expected distribution of the new parameters. The FSM is especially useful when the thermodynamic system displays sharp peaks in an observable, such as for first- or second- order phase transitions, and allows to determine uniquely the peak position and its height.

Multiple Histogram Method

Often it is not sufficient to rely on only one single point in parameter space. The *multiple histogram method* introduced in [44] allows to extract information from several points in parameter space. It

can be applied over a wide range of parameters. We will shortly describe this extended FSM for O(N)-type Hamiltonians, which can be decomposed in an energy- and magnetization part:

$$\mathcal{H}_l = J_l E + H_l M, \tag{5.1.9}$$

where the index $l = 1, \dots L$ labels the parameter sets on which the histograms are based. The number of measurements of E and M for a given l is denoted by N_l. The histogram is then characterized by the distribution

$$\mathcal{N}_l(E, M) \qquad \text{with} \qquad \sum_{E,M} \mathcal{N}_l(E, M) = N_l. \tag{5.1.10}$$

The density of states is then expressed in terms of the normalized histogram, the partition function and a Boltzmann factor:

$$W_l(E, M) = \frac{\mathcal{N}_l(E, M)}{N_l(E, M)} Z(J_l, H_l) e^{\beta(J_l E + H_l M)} = \frac{\mathcal{N}_l(E, M)}{N_l(E, M)} e^{\beta(-F(J_l, H_l) + J_l E + H_l M)}, \tag{5.1.11}$$

$$W(E, M) = \sum_{l=1}^{L} p_l(E, M) W_l(E, M), \qquad \sum_{l=1}^{L} p_l(E, M) = 1. \tag{5.1.12}$$

The weighting factors p_l can be chosen arbitrarily. In practice they are chosen such that the errors of $W(E, M)$ are minimized, based on the variance of $\mathcal{N}_l$:

$$\delta^2 \mathcal{N}_l(E, M) = g_l \overline{\mathcal{N}_l(E, M)}, \qquad g_l = 1 + 2\tau_l, \tag{5.1.13}$$

where the bar denotes the expectation value w.r.t. all Monte Carlo simulations of length N_l and τ_l is the correlation time of the Markov chain. The weighting factors are then given by

$$p_l(E, M) = \frac{g_l^{-1} N_l e^{-\beta(-F(J_l, H_l) + J_l E + H_l M)}}{\sum_{k=1}^{L} g_k^{-1} N_{J_k, H_k} e^{-\beta(-F(J_k, H_k) + J_k E + H_k M)}}. \tag{5.1.14}$$

Here, $F(J_l, H_l)$ is the free energy of data set l. Plugging the weighting factors and the Boltzmann factor into the density of states yields:

$$W(E, M) = \frac{\sum_{l=1}^{L} g_l^{-1} \mathcal{N}_l(E, M)}{\sum_{k=1}^{L} g_k^{-1} N_{J_k, H_k} e^{-\beta(F(J_k, H_k) + J_k E + H_k M)}}. \tag{5.1.15}$$

With this result, the partition function for the new couplings J', H' is given by:

$$Z(J', H') = \sum_{E,M} W(E, M) e^{-\beta(J' E + H' M)}. \tag{5.1.16}$$

With the last two equations, the free energies $F(J_l, H_l)$ can be calculated iteratively, by setting $F(J_1, H_1) = 0$ (as the free energy is only determined up to an additive constant). By this one obtains a self-consistent value. Finally, the expectation values of an observable $O(\{\sigma\})$ in the new couplings is given by a weighted sum: the probability distribution for the new couplings $P_{J', H'}(E, M)$ is obtained from the partition function $Z(J', H')$ and the iteratively determined free energy, and $\langle O \rangle_{J', H'}$ is the mean value of the observable based on all configurations $\{\sigma_i\}$ which happened to have precisely the energy E and magnetization M considered in the sum:

$$\langle O \rangle_{J', H'} = \sum_{E,M} O(E, M) P_{J', H'}(E, M), \tag{5.1.17}$$

$$O(E, M) = \frac{\sum_{\{\sigma_i\}} \sum_{l=1}^{L} O(\{\sigma_i\}) g_l^{-1} \delta(E - E(\{\sigma_i\})) \delta(M - M(\{\sigma_i\}))}{\sum_{\{\sigma_i\}} \sum_{k=1}^{L} g_k^{-1} \delta(E - E(\{\sigma_i\})) \delta(M - M(\{\sigma_i\}))}. \tag{5.1.18}$$

Application to QCD

Reweighting from a set of QCD parameters $w = \{\beta, m_l, m_s\}$ to the new set $w' = \{\beta', m_l', m_s'\}$ for an observable O is obtained by

$$\langle O \rangle_{w'} = \frac{\langle OR(w', w) \rangle_w}{\langle R(w', w) \rangle_w}, \tag{5.1.19}$$

where the *reweighting factor* $R(w', w)$ is defined in terms of the determinant of the full fermion matrix and the gauge action S_G:

$$R(w', w) = \frac{(\det M_l(w'))^2 \det M_s(w')}{(\det M_l(w))^2 \det M_s(w)} e^{S_G(w') - S_G(w)}. \tag{5.1.20}$$

The identifications with the previous section are straight forward (here, $L = 1$): the energy E corresponds to the gauge action S_G and J corresponds to the gauge coupling β. The magnetization M is given by the chiral condensate $\langle \bar{\psi}\psi \rangle_q$ and the external field H by the quark mass m_q.

We will make use of FSM in two respects: First, we perform reweighting in the gauge coupling β in order to estimate the peak locations of the chiral susceptibility; here we use the multi-histogram method, because reweighting in β can be done exactly as the coupling enters linear in the gauge action. Second, we perform reweighting in the quark masses, which is needed in order to enable the scaling analysis for the $N_\tau = 8$ data. It also allows to investgate the dependence of a scaling constant on the strange quark mass. We will only apply ordinary reweighting w.r.t. the quark masses, i.e. we do not use the multi-histogram method. Reweighting in the quark mass can not be done exactly but requires an approximation based on the Taylor expansion of the fermion determinant.

We performed reweighting both in the light and strange quark masses by requiring that the ratio m_l/m_s is kept fixed:

$$m_{l,0} \to m_{l,r}, \qquad m_{s,0} \to m_{s,r}, \qquad m_{l,r}/m_{s,r} = m_{l,0}/m_{s,0} = H. \tag{5.1.21}$$

The reweighting factor for 2+1 staggered flavors

$$R = \exp\left(\frac{1}{2} \log\left(\frac{\det M_{l,r}}{\det M_{l,0}} \right) + \frac{1}{4} \log\left(\frac{\det M_{s,r}}{\det M_{s,0}} \right) \right) \tag{5.1.22}$$

is calculated by the following approximation:

$$\frac{N_q}{4} \log\left(\frac{\det M_{q,r}}{\det M_{q,0}} \right) = \frac{N_q}{4} \sum_{n=1}^{\infty} \frac{(m_{q,r} - m_{q,0})^n}{n!} \frac{\partial^n}{\partial m_{q,0}^n} \operatorname{tr} \log M_{q,0} \qquad q = l, s \tag{5.1.23}$$

$$= \frac{N_q}{4} \left(\operatorname{tr} M_{q,0}^{-1}(m_{l,r} - m_{q,0}) - \frac{1}{2} \operatorname{tr} M_{q,0}^{-2}(m_{q,r} - m_{q,0})^2 \right) + \mathcal{O}\left((m_{q,r} - m_{q,0})^3 \right). \tag{5.1.24}$$

Also the chiral observables, chiral condensate and connected susceptibility, have to be expanded:

$$\operatorname{tr} M_{q,r}^{-1} = \operatorname{tr} M_{q,0}^{-1} - \operatorname{tr} M_{q,0}^{-2}(m_{q,r} - m_{q,0}) + \operatorname{tr} M_{q,0}^{-3}(m_{q,r} - m_{q,0})^2 + \mathcal{O}\left((m_{q,r} - m_{q,0})^3 \right), \tag{5.1.25}$$

$$\operatorname{tr} M_{q,r}^{-2} = \operatorname{tr} M_{q,0}^{-2} - 2 \operatorname{tr} M_{q,0}^{-3}(m_{q,r} - m_{q,0}) + 3 \operatorname{tr} M_{q,0}^{-4}(m_{q,r} - m_{q,0})^2 + \mathcal{O}\left((m_{q,r} - m_{q,0})^3 \right). \tag{5.1.26}$$

The reweighted chiral condensate is shown in Fig. 5.1, the operators which enter in Eq. (5.1.26) are shown in Fig. 5.2. Due to the poor statistics it is pointless to reweight the disconnected susceptibility as well. However, we have reason to believe that reweighting would only have a small effect on the disconnected part for the quark mass differences $m_{q,r} - m_{q_0}$ considered here, and would not shift the mean value beyond the error bars.

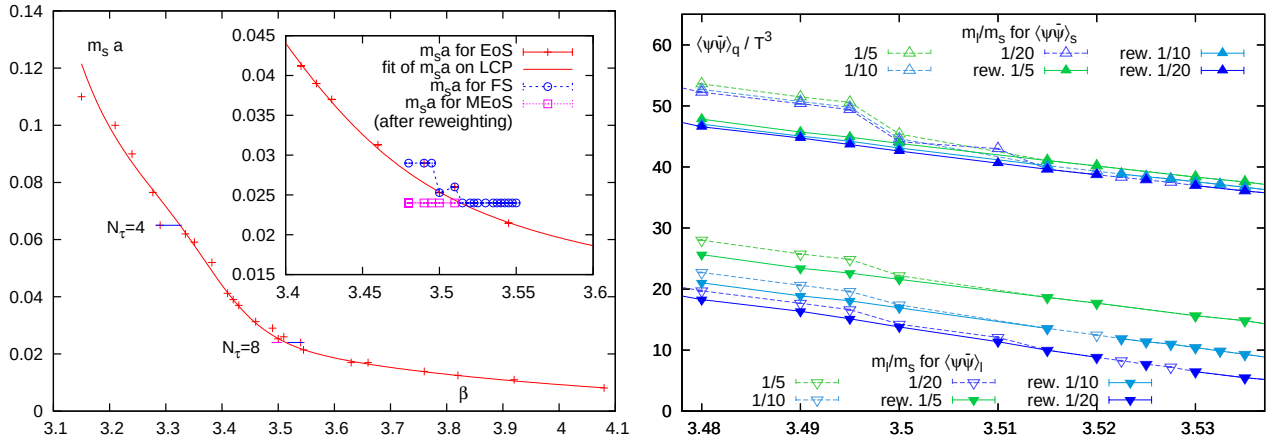

Figure 5.1: Left: Relation between quark mass $\hat{m}_s$ and the gauge coupling β on the LCP. Parts for $N_\tau = 8$ have been reweighted to the constant value $\hat{m}_s = 0.024$ (blue to magenta) which allows better comparison with the $N_\tau = 4$ data. Right: Comparison of raw data and reweighted data for light and strange quark condensate ($N_\tau = 8$) in the range $\beta \in [3.480, 3.515]$.

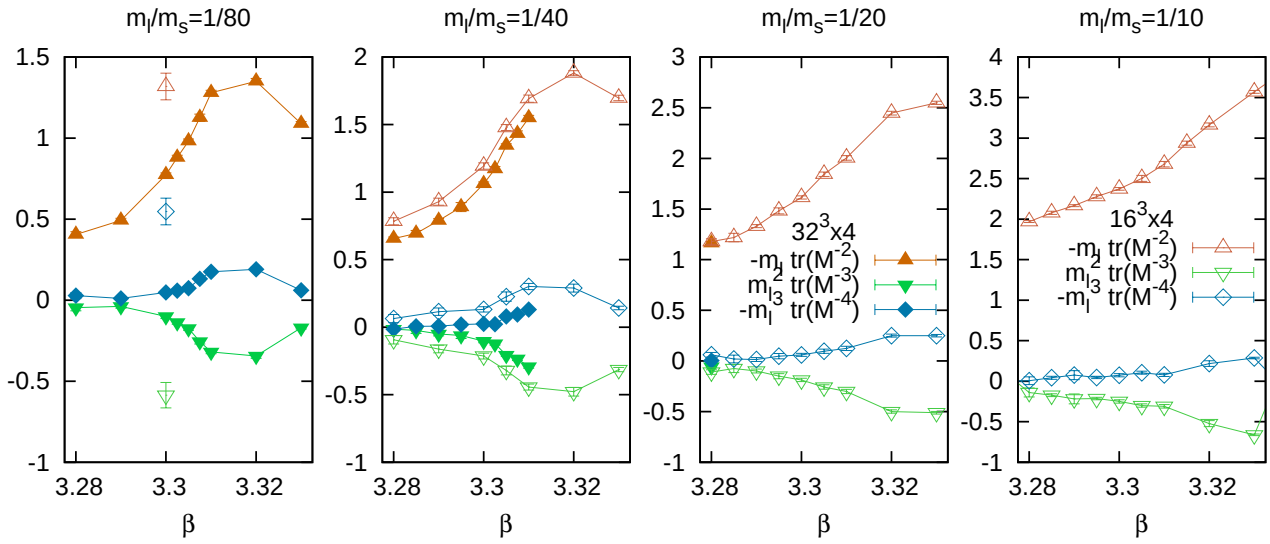

Figure 5.2: Comparison of operators $\mathrm{tr}\, M^{-n}$, which are needed for reweighting according to the approximation Eq. (5.1.26). Full symbols denote $N_\sigma = 32$, half symbols denote $N_\sigma = 16$. Finite size effects for the n-point chiral operators grow with n.

5.2 Preliminaries

5.2.1 Setup of Lattice Calculations

In our lattice calculations we used the Symanzik tree-level improved gauge action and the p4fat3 fermion action. The condensates and susceptibilities were measured with up to 15 random vectors on every 10th trajectory generated by RHMC evolution.

The strange quark mass was fixed in the peak region to $\hat{m}_s = 0.065$ for $N_\tau = 4$ and $\hat{m}_s = 0.024$ for $N_\tau = 8$, which corresponds to a physical pseudoscalar meson mass $M_S = 669$ MeV. This scale setting, explained in detail in the next section, is based on the analysis of zero temperature measurements of the RBC-Bielefeld collaboration [24, 25]. The ratio $m_l/m_s = 1/20$ corresponds to the physical pion mass (see Tab. 5.1). All configurations are separated by 10 trajectories.

m_l/m_s	$M_{\pi,5}$ [MeV]
1/80	75
1/40	105
1/20	150
1/10	210

Table 5.1: Pion masses $M_{\pi,5}$ for various ratios of m_l/m_s.

The Tab. 5.2 below shows an overview of the gathered data. Most lattice data have been generated on the parallel supercomputers NewYork Blue and QCDOC at BNL, in a common effort of the RBC-Bielefeld collaboration. Some data of the $32^3 \times 8$ lattices belong to the HotQCD collaboration. Some of these data for $m_l/m_s = 1/5$ have been generated at the Lawrence Livermore National Laboratory (LLNL). Detailed information on the statistics and the expectation values can be found in App. C.

lattice dim.	m_l/m_s	statistics	lattice dim.	m_l/m_s	statistics
$32^3 \times 4$	1/80	$\mathcal{O}(20000)$			
$32^3 \times 4$	1/40	$\mathcal{O}(20000)$			
$16^3 \times 4$	1/40	$\mathcal{O}(30000)$	$32^3 \times 8$	1/40	$\mathcal{O}(5000)$
$16^3 \times 4$	1/20	$\mathcal{O}(40000)$	$32^3 \times 8$	1/20	$\mathcal{O}(20000)$
$16^3 \times 4$	1/10	$\mathcal{O}(40000)$	$32^3 \times 8$	1/10	$\mathcal{O}(30000)$
$16^3 \times 4$	1/5	$\mathcal{O}(40000)$	$32^3 \times 8$	1/5	$\mathcal{O}(30000)$
$16^3 \times 4$	2/5	$\mathcal{O}(40000)$			

Table 5.2: List of lattices on which the scaling analysis is based. On the $N_\tau = 4$ lattice, 12 different β values between 3.28 and 3.33 were generated, on the $N_\tau = 8$ lattice 16 different β values between 3.48 and 3.545. The approximate order of the statistics for each β value is given in the number of trajectories. For details see App. C.

5.2.2 Setting the Scale

Lattice simulations are characterized by the geometrical parameters N_σ and N_τ, the dimensionless parameters bare gauge coupling g_0 (or equivalently $\beta = 2N_c/g_0^2$) and the bare quark masses $\hat{m}_l$ and $\hat{m}_s$. In order to obtain physical quantities, the lattice spacing has to be determined as a function of β. In this section we will review the procedure used by the RBC-Bi collaboration [24, 25] in particular for the scale setting for the equation of state. This will be of importance to convert the coupling β to the temperature $T = 1/N_\tau a(\beta)$.

The Beta Function

In the weak coupling limit and with massless quarks, the lattice spacing is determined by the gauge coupling only. The relation between β and a is obtained by the requirement that in the continuum limit $a \to 0$, $\beta \to \beta^{\mathrm{cr}}$ all lattice quantities given in lattice units, such as correlation lengths, have to

diverge such that their physical counterparts remain finite [104]: $\hat{\xi} = a^{-1}\xi \to \infty$. More general, we expect that for any observable Θ of mass dimension d_Θ, the physical quantity scales as

$$\Theta(\beta(a), a) = a^{-d_\Theta}\hat{\Theta}(\beta(a)), \tag{5.2.1}$$

if the continuum limit exists and β is tuned such that $\beta(a)$ approaches the critical point β^{cr}. The crucial point is that the scale dependence of all observables is determined by the same function $\beta(a)$. This function can be determined by the RG equation, e.g. for the static quark potential (see next section), now expressed in terms of $g_0 \equiv g_0(a)$:

$$V_{qq}(R, g_0, a) = \frac{1}{a}\hat{V}_{qq}(\hat{R}, g_0), \tag{5.2.2}$$

where $R = \hat{R}a$ gives the separation distance of the quark pair. For fixed R, the potential should become independent of a in the continuum limit:

$$a\frac{d}{da}V_{qq}(R, g_0, a) = a\left(\frac{\partial}{\partial a} + \frac{\partial g_0}{\partial a}\frac{\partial}{\partial g_0}\right)V_{qq}(R, g_0, a) = 0. \tag{5.2.3}$$

With this we obtain the RG-equation

$$\left(a\frac{\partial}{\partial a} - \bar{\beta}(g_0)\frac{\partial}{\partial g_0}\right)V_{qq}(R, g_0, a) = 0, \tag{5.2.4}$$

where the well-known *Callan-Symanzik beta-function* for SU(N_c) gauge is given by

$$\begin{aligned}\bar{\beta}(g_0) \equiv -a\frac{\partial g_0}{\partial a} = b_0 g_0^3 + b_1 g_0^5 + \mathcal{O}(g_0^7), \qquad b_0 &= \frac{1}{(4\pi)^2}\left(\frac{11}{3}N_\mathrm{c} - \frac{2}{3}N_\mathrm{f}\right), \\ b_1 &= \frac{1}{(4\pi)^4}\left(\frac{34}{3}N_\mathrm{c}^2 - \frac{10}{3}N_\mathrm{c}N_\mathrm{f} - \frac{N_\mathrm{c}^2-1}{N_\mathrm{c}}N_\mathrm{f}\right),\end{aligned} \tag{5.2.5}$$

and the expansion of the beta function in the weak coupling limit[1] has been calculated via perturbative QCD [62, 101, 22], which proved asymptotic freedom for QCD ($N_\mathrm{c} = 3$).[2] Equation (5.2.5) can be integrated to obtain the function $a(\beta)$:

$$\begin{aligned}\ln(\Lambda_L a) &= -\frac{1}{2b_0 g_0^2} - \frac{b_1 \ln(g_0)}{b_0^2} + \frac{b_1 \ln(b_0 + b_1 g_0^2)}{2b_0^2} \\ a(\beta) &= \frac{1}{\Lambda_L}\left(\frac{2N_\mathrm{c}b_0}{\beta}\right)^{-b_1/2b_0^2}\exp\left(-\frac{\beta}{4N_\mathrm{c}b_0}\right)\left(1 + \mathcal{O}(\beta^{-1})\right).\end{aligned} \tag{5.2.6}$$

This equation is only valid for N_f massless quarks in the continuum. On the lattice, the function $a(\beta)$ is expected to deviate from Eq. (5.2.6) because (a) we are not in the perturbative region,(b) the quark masses are finite, and (c) cut-off and finite size effects are present. Hence $a(\beta)$ has to be

[1] Only the first two coefficients are independent of the renormalization scheme, compare [29].

[2] The first coefficient b_0, calculated by Politzer, Gross, Wilzek in 1973 [62, 101], was sufficient to show that QCD is asymptotically free, provided that $N_\mathrm{f} \leq 16$:

$$\alpha_s(Q^2) \equiv \frac{g_0^2(Q^2)}{4\pi} \simeq \frac{1}{4\pi b_0} = \frac{12\pi}{(33 - 2N_\mathrm{f})\log(Q^2/\Lambda_L^2)}.$$

According to asymptotic freedom, in the limit $a \to 0$ (or equivalently $Q^2 \to \infty$), β^{cr} is expected to diverge. This standard view has been disputed by Seiler [108], who claims that the critical point β^{cr} might as well be finite, but there is no numerical evidence for this scenario.

determined via zero temperature lattice simulations. However, we will use the above expression for the special case $N_\mathrm{f} = 3$ massless quarks as a starting point:

$$R_2(\beta) \equiv \left(\frac{8\pi^2}{26}\beta\right)^{\frac{32}{81}} \exp\left(-\frac{4\pi^2}{27}\beta\right) = \Lambda_L a(\beta)\left(1 + \mathcal{O}(\beta^{-1})\right). \tag{5.2.7}$$

The function $R_2(\beta)$ is denoted as the 2-loop β function. The value of Λ_L is experimentally not well known, which is another reason why $a(\beta)$ has to be determined via zero temperature lattice simulations.

Scale Setting Inspired by the Line of Constant Physics

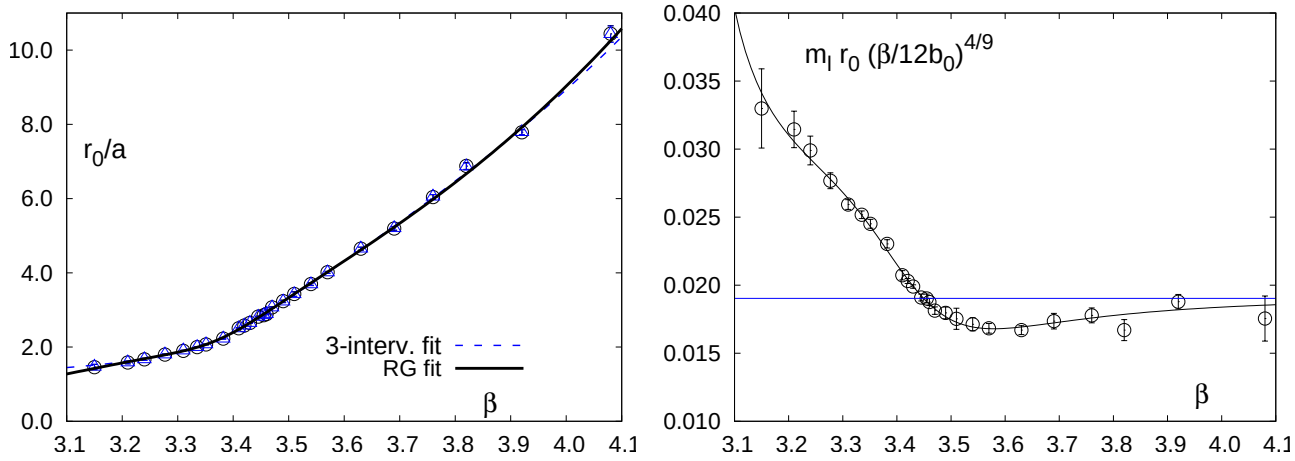

Figure 5.3: The functions $r_0/a(\beta)$ (left) and $m^{\mathrm{RGI}} r_0 P(\beta)$ (right) which allow to determine the lattice parameters $\hat{m}_l$ and $\hat{m}_s$ on the LCP. Taken from [24].

With the lattice spacing, also the physical bare quark masses $m_l = \hat{m}_l/a$ and $m_s = \hat{m}_s/a$ depend on the gauge coupling in a non-trivial way if we require the bare quark masses to produce constant physical results when approaching the continuum limit. The line in the space of lattice bare quark masses $(\hat{m}_l, \hat{m}_s)$ parameterized by the gauge coupling, which corresponds to identical physical situations, is called a *line of constant physics* (LCP). Despite the fact that we investigate the chiral limit and hence do not fix the physical conditions, we are nevertheless justified to make use of the scale setting used for the LCP of the RBC-Bielefeld collaboration:[3] Although M_K will take values different from the physical mass as we vary the quark mass ratio

$$H \equiv \frac{m_l}{m_s} = \frac{\hat{m}_l}{\hat{m}_s}, \tag{5.2.8}$$

at fixed $\hat{m}_s$ the dependence of M_K on $\hat{m}_l$ is rather weak. We also take the value of the lattice spacing from the LCP in order to determine the reduced temperature, which also depends only weak on m_l. We will shorty review the functions $r_0/a(\beta)$ and $r_0 m_s(\beta)$, which specify the LCP.

[3] The specific LCP considered by RBC-Bi is defined by two conditions: (1) The mass of the (hypothetical) pseudoscalar meson composed of the $\bar{s}s$ pair M_S, expressed in units of the Sommer scale r_0, is constant. (2) The ratio of the pseudoscalar mesons M_S/M_K is constant.

The Sommer scale is defined in terms of the slope of the static quark potential [112]:

$$r^2 \frac{d}{dr} V_{\bar{q}q}(r)\Big|_{r_0} = 1.65, \tag{5.2.9}$$

which is usually given in the Cornell parameterization[4]

$$V_{\bar{q}q}(r) = -\frac{\alpha_{\text{eff}}}{r} + \sigma r + c. \tag{5.2.10}$$

The specific value of the slope at r_0 is chosen by convention, but with the intention that r_0 is an intermediate distance. The Sommer scale has been measured on the lattice by a combined analysis of the static quark potential together with level splittings in bottomium spectra [8, 60]. The recent numerical value is $r_0 = 0.469(7)$ fm.

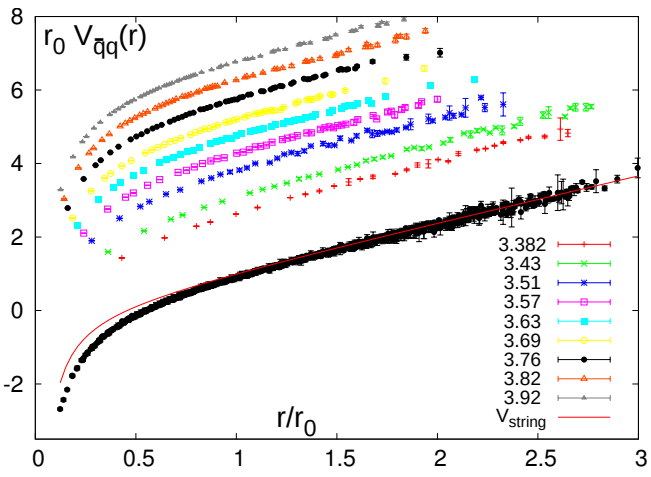

Figure 5.4: The static quark potential in units of r_0 versus the distance r/r_0. The lowest curve combines the potentials for all gauge couplings by $\beta \in [3.15, 4.08]$ and matches them to the string potential $V_{\text{string}} = -\pi/12r + \sigma r$ which is predicted from string models. Taken from [24].

The RBC-Bi collaboration has calculated the static quark potential from smeared Wilson loops [24], shown in Fig. 5.4, to determine the dimensionless scale parameter $\hat{r}_0 \equiv r_0/a$ as a function of the gauge coupling. The fit ansatz is as follows:

$$\hat{r}_0(\beta) = \frac{1 + e_r \hat{a}^2(\beta) + f_r \hat{a}^4(\beta)}{a_r R_2(\beta)(1 + b_r \hat{a}^2(\beta) + c_r \hat{a}^4(\beta) + d_r \hat{a}^6(\beta))}, \qquad \hat{a}(\beta) = \frac{R_2(\beta)}{R_2(3.4)}, \tag{5.2.11}$$

i.e. the deviation from the 2-loop β function in a gauge coupling region about $\beta = 3.4$ is captured via a rational function. We will make use of the parameterization in order to convert the gauge coupling into the (reduced) temperature.

Even though we have not applied the LCP condition to fix M_S in physical units and fixed $\hat{m}_s$ in lattice units, we will shortly review the relation between the lattice quark masses and the gauge coupling as it allows to relate the quark masses used on different lattice spacings, e.g. those for $N_\tau = 4$ and $Nt = 8$. In order to impose the physical value

$$M_S = \sqrt{2M_K^2 - M_\pi^2} \simeq 669\text{MeV}, \tag{5.2.12}$$

we require $M_S r_0 = 1.59$. The corresponding value of the strange quark mass $\hat{m}_s$ has to be determined via zero temperature measurements.

$m_l/m_s = 1/10$	
$a_r = 13.25(36)$	$b_m = -2.15(12)$
$b_r = -1.20(09)$	$c_m = 1.68(18)$
$c_r = 0.05(20)$	$d_m = -0.37(14)$
$d_r = 0.40(11)$	$e_m = -2.29(16)$
$e_r = -1.68(10)$	$f_m = 1.83(43)$
$f_r = 0.82(08)$	$g_m = -0.36(34)$

Table 5.3: Parameters of the polynomial ansätze Eqs. (5.2.11, 5.2.14) which establish the LCP.

Since it is linked to the light quark mass $\hat{m}_l$, they both depend on the same function $H\hat{m}_s\hat{r}_0(\beta) = \hat{m}_l\hat{r}_0(\beta)$. After adjusting the lattice quark masses such that the calculation of pseudoscalar meson masses $M_\pi r_0$, $M_K r_0$ and $M_\eta r_0$ gives the physical results expected for $H = 1/10$, the such determined

[4] The Sommer scale is related to the string tension σ, as is evident from the Cornell parameterization Eq. (5.2.10), $r_0 = \sqrt{(1.65 - \alpha_{\text{eff}})/\sigma}$. The string tension is not the best choice for setting the scale because at large distances the large fluctuations of the gauge field gives large statistical errors.

quark masses were fitted [24]. The fit ansatz is based on the tree-level analysis of the anomalous scaling dimension for the quark mass[5] [49]

$$\hat{m}_l \hat{r}_0(\beta) = m^{\mathrm{RGI}} r_0 \left(\frac{12 b_0}{\beta}\right)^{4/9} P(\beta) \tag{5.2.13}$$

and $m_{\mathrm{RGI}} = 8.0(4)$ MeV is an RG-invariant mass, which yields $m_{RGI} r_0 = 0.0190(9)$. The rational function

$$P(\beta) = \frac{1 + b_m \hat{a}^2(\beta) + c_m \hat{a}^4(\beta) + d_m \hat{a}^6(\beta)}{1 + e_m \hat{a}^2(\beta) + f_m \hat{a}^4(\beta) + g_m \hat{a}^6(\beta)} \tag{5.2.14}$$

describes the deviation on the lattice from the above scaling. The parameterizations of $r_0/a(\beta)$ and $\hat{m}_l \hat{r}_0(\beta)$ are shown in Fig. 5.3.

5.2.3 Chiral Observables on the Lattice

UV-Divergent Contributions to Chiral Observables

The LQCD partition function Eq. (2.1.8) is a function of the quark masses, $\mathcal{Z} = \mathcal{Z}(m_l, m_s)$, and can be expanded in even powers of m_l, m_s. Already a leading order tree-level calculation of the chiral condensate at finite temperature shows that it contains a UV-divergent contribution on the lattice which is linear in the quark mass m_q. From the partition function for a gas of free fermions in an infinite volume, one obtains for the free energy

$$\frac{T}{V} \log \mathcal{Z} \simeq T \int_0^{\pi/a} \frac{d^3p}{(2\pi)^3} \log\left(1 + e^{-E(\boldsymbol{p})/T}\right) + \int_0^{1/a} \frac{d^3p}{(2\pi)^3} \frac{E(\boldsymbol{p})}{2}, \qquad E(\boldsymbol{p}) = \sqrt{p^2 + m_q^2}, \tag{5.2.15}$$

where the momentum cut-off is provided by the inverse lattice spacing. The first term gives the finite temperature part which yields the pressure of the ideal fermion gas, whereas the second term yields the vacuum energy and is divergent in the continuum limit. This also implies a UV-divergent term in the chiral condensate which is linear in the quark mass, provided $a \ll m_q^{-1}$:

$$\begin{aligned} \left\langle \bar{\psi}\psi \right\rangle_{q,\mathrm{UV-div}} &= \nu_f \frac{\partial}{\partial m_q} \int_0^{\pi/a} \frac{dp^3}{(2\pi)^3} \frac{E(\boldsymbol{p})}{2} = \frac{\nu_f \Omega_2}{(2\pi)^3} \frac{m_q}{2} \int_0^{\pi/a} \frac{p^2 dp}{\sqrt{p^2 + m_q^2}} \\ &= m_q \frac{\nu_f}{(2\pi)^2} \left[p\sqrt{p^2 + m_q^2} - m_q^2 \log\left(2\left(p + \sqrt{p^2 + m_q^2}\right)\right)\right]_0^{\pi/a} \end{aligned} \tag{5.2.16}$$

$$\Longrightarrow \qquad \lim_{m_q a \ll 1} \left\langle \bar{\psi}\psi \right\rangle_{q,\mathrm{UV-div}} = \frac{\nu_f}{4} \frac{m_q}{(2\pi)^2} + \frac{\nu_f}{4a^2} m_q^3 \log a/(4\pi) \tag{5.2.17}$$

where $\nu_f = 2 N_{\mathrm{c}} N_{\mathrm{f}}$ is the number of degrees of freedom. The logarithmic divergence, which gives rise to a cubic term, is of course much weaker, hence we concentrate on the quadratic divergence.[6] Note that it is the valence quark mass $m_q = m_q^{\mathrm{val}}$ which enters here. The prefactor of the UV-divergent constant $c_{\mathcal{UV}} = 3N_{\mathrm{f}}/2$ is temperature independent.[7] The expected behavior of the chiral condensate

[5] From the RG-equation for the anomalous dimension γ one obtains

$$\gamma(g_0) \equiv \frac{a}{m_q} \frac{\partial m_q}{\partial a} = \gamma_0 g^2 + \gamma_1 g^4 + \mathcal{O}\left(g_0^6\right), \quad \gamma_0 = 2/(2\pi)^2, \qquad \gamma_1 = \frac{1}{(2\pi)^4}\left(\frac{101}{12} - \frac{5}{18} N_{\mathrm{f}}\right).$$

Hence, the quark mass renormalization at leading order is $m_l^0 = m^{\mathrm{RGI}} \left(\frac{12 b_0}{\beta}\right)^{-2\gamma_0/b_0}$.

[6] There might be additional UV-divergent terms at $\mathcal{O}\left(m_q^3\right)$.

[7] The UV-divergence does not depend on the temporal extent of the lattice, Eq. (5.2.15) is also valid at zero temperature.

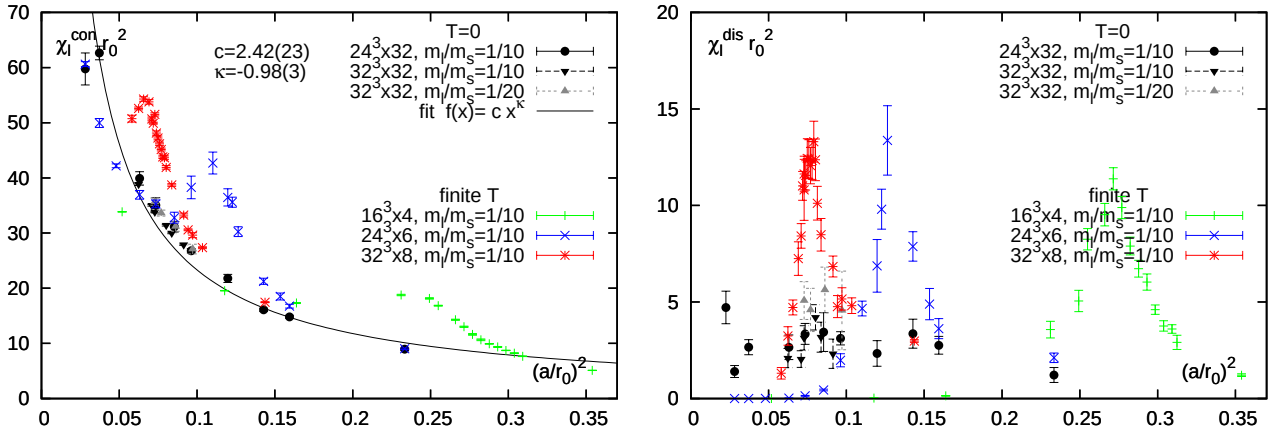

Figure 5.5: Comparison of zero temperature and finite temperature measurements of connected (left) and disconnected (right) chiral susceptibility. It can be clearly seen that the connected part contains a UV-divergent constant which is compatible with the predicted behavior $\sim a^{-2}$ ($\kappa \simeq -1$), whereas there is no indication for such a constant in the disconnected part. The fit is based on the $24^3 \times 32$ lattice.

at finite temperature for the quark flavors $q = l, s$ is then:

$$\left\langle \bar{\psi}\psi \right\rangle_q (T) = \left\langle \bar{\psi}\psi \right\rangle_0 (T) + c_2(T) m_q + \frac{c_{\mathcal{UV}}}{a^2} m_q + \mathcal{O}\left(m_q^3\right) + \delta_{ql} \begin{cases} c_1(T) m_q^{1/2} & T < T_c \\ c_1(T) m_q^{1/\delta} & T = T_c \\ 0 & T > T_c \end{cases} \tag{5.2.18}$$

where the last term containing Goldstone and critical scaling is only present for the light quark condensate. Beside the constant $c_{\mathcal{UV}}$ there is also a finite but temperature dependent constant $c_2(T)$, which in practice is difficult to discriminate from $c_{\mathcal{UV}}$.

Based on the chiral Ward identity (see Sec. 3.2.20)

$$\left\langle \bar{\psi}\psi \right\rangle_q = m_q \int d^4 r G_\pi(\boldsymbol{r}) \tag{5.2.19}$$

the UV-divergent constant $c_{\mathcal{UV}}/a^2$ can be identified with a contact term of the $G_\pi(\boldsymbol{r})$ correlation function. The chiral susceptibility then also has an UV-divergent constant

$$\chi_q(T) = c_2(T) + \frac{c_{\mathcal{UV}}}{a^2} + \mathcal{O}\left(m_q^2\right) + \delta_{ql} \begin{cases} \frac{c_1(T)}{2} m_q^{-1/2} & T < T_c \\ \frac{c_1(T)}{\delta} m_q^{1/\delta - 1} & T = T_c \\ 0 & T > T_c \end{cases}, \tag{5.2.20}$$

which shows up mainly in the connected part, as is also conjectured from CPT, see Sec. 4.2.1. This conjecture can be tested with zero temperature lattice data. In Fig. 5.5 we show by a fit of data on the (1-flavor) connected susceptibility, that we indeed find the expected behavior: Based on the simple fit ansatz (without a constant term)

$$\chi_l^{\text{con}}(T=0) r_0^2 = c_{\text{meas}}^{con} (a/r_0)^{2\kappa} \tag{5.2.21}$$

applied to the lattice data on the LCP with $H = 1/10$ ($24^3 \times 32$), we obtain $c_{\text{meas}}^{\text{con}} = 2.4(2)$ and an exponent $\kappa = -0.98(3)$ consistent with the expectation $\kappa = -1$. The disconnected part shows no such divergence. The zero temperature measurements of χ_l^{con} and χ_l^{dis} have a logarithmic quark mass dependence, which interferes with the value of $c_{\text{meas}}^{\text{con}}$. Also higher order corrections might

explain the deviation of $c^{\rm con}_{\rm meas}$ from the predicted value $c_{\mathcal{UV}} = 1.5$. We will however see that this value is close to the value expected from the chiral extrapolation of the finite temperature connected susceptibilities.

In order to compare chiral observables obtained for different lattice spacings, multiplicative renormalization has to be applied as well. This is achieved by multiplying with the appropriate power of the quark mass, which eliminates the wave function renormalization factors:

$$m_q^n \frac{\partial^n}{\partial m_q^n} \frac{T}{V} \log \mathcal{Z}. \tag{5.2.22}$$

As the light and strange quark masses are related by the fixed ratio H, we may as well multiply with the strange quark mass when taking the light quark mass derivative:

$$\frac{\partial^n}{\partial H^n} \frac{T}{V} \log \mathcal{Z} = m_s^n \frac{\partial^n}{\partial m_l^n} \frac{T}{V} \log \mathcal{Z}. \tag{5.2.23}$$

We introduce the 1-flavor light quark condensate[8] which we call the *Bare Order Parameter:*

$$M_0 \equiv \frac{m_s}{T^4} \left\langle \bar{\psi}\psi \right\rangle_l = \hat{m}_s N_\tau^4 \frac{1}{4} \left\langle \operatorname{tr} M_l^{-1} \right\rangle, \tag{5.2.24}$$

where the temperature prefactor is introduced to obtain a dimensionless quantity. This is viable as T does not vary much in the critical region around $T_{\rm c}$ and can be regarded as being constant to first approximation in the scaling analysis. The full, connected and disconnected susceptibilities of M_0 are given by

$$\chi^{\rm full}_{M_0} \equiv m_s \frac{\partial}{\partial m_l} M_0 = \chi^{\rm con}_{M_0} + \chi^{\rm dis}_{M_0}, \tag{5.2.25}$$

$$\chi^{\rm con}_{M_0} = \frac{1}{2} \frac{m_s^2}{T^4} \chi_l^{\rm con} = \hat{m}_s^2 N_\tau^4 \frac{1}{4} \left\langle - \operatorname{tr} M_l^{-2} \right\rangle, \tag{5.2.26}$$

$$\chi^{\rm dis}_{M_0} = \frac{1}{2} \frac{m_s^2}{T^4} \chi_l^{\rm dis} = \hat{m}_s^2 N_\tau^4 \frac{1}{8} \left(\left\langle (\operatorname{tr} M_l^{-1})^2 \right\rangle - \left\langle \operatorname{tr} M_l^{-1} \right\rangle^2 \right), \tag{5.2.27}$$

where additional factors $\frac{1}{2}$ have been provided to account for the single flavor. In the scaling analysis, we will also consider the cumulants

$$\Delta_{M_0} \equiv \frac{H \chi^{\rm full}_{M_0}}{M_0} = \frac{m_l (\chi_l^{\rm con} + \chi_l^{\rm dis})}{\left\langle \bar{\psi}\psi \right\rangle_l}, \qquad \Delta^{\rm dis}_{M_0} \equiv \frac{H \chi^{\rm dis}_{M_0}}{M_0} = \frac{m_l \chi_l^{\rm dis}}{\left\langle \bar{\psi}\psi \right\rangle_l}. \tag{5.2.28}$$

In order to remove the leading order additive UV divergence, we do not rely on the constant $c_{\mathcal{UV}}$ but introduce the following subtracted order parameters, involving the strange quark condensate or the connected susceptibility. First we define the *Strange Condensate Subtraction:*

$$M_s \equiv \frac{m_s}{T^4} \left(\left\langle \bar{\psi}\psi \right\rangle_l - \frac{m_l}{m_s} \left\langle \bar{\psi}\psi \right\rangle_s \right) = \hat{m}_s^2 N_\tau^4 \frac{1}{4} \left(\left\langle \operatorname{tr} M_l^{-1} \right\rangle - \frac{m_l}{m_s} \left\langle \operatorname{tr} M_s^{-1} \right\rangle \right) \tag{5.2.29}$$

[8] The strange quark condensate subtraction considered below requires $N_l = 1$, which is introduced here already for better comparison of the different order parameters.

and corresponding susceptibilities

$$\chi^{\text{full}}_{M_s} \equiv m_s \frac{\partial}{\partial m_l} M_s = \chi^{\text{con}}_{M_s} + \chi^{\text{dis}}_{M_s}, \tag{5.2.30}$$

$$\chi^{\text{con}}_{M_s} = \frac{m_s^2}{T^4}\left(\frac{1}{2}\chi_l^{\text{con}} - \frac{1}{m_s}\left\langle\bar{\psi}\psi\right\rangle_s\right) = \hat{m}_s^2 N_\tau^4 \frac{1}{4}\left(\left\langle -\operatorname{tr} M_l^{-2}\right\rangle - \frac{1}{\hat{m}_s}\left\langle\operatorname{tr} M_s^{-1}\right\rangle\right), \tag{5.2.31}$$

$$\chi^{\text{dis}}_{M_s} = \frac{1}{2}\frac{m_s^2}{T^4}\left(\chi_l^{\text{dis}} - \frac{m_l}{m_s}\chi_{l,s}^{\text{dis}}\right) = \hat{m}_s^2 N_\tau^4 \left(\frac{1}{8}\left(\left\langle(\operatorname{tr} M_l^{-1})^2\right\rangle - \left\langle\operatorname{tr} M_l^{-1}\right\rangle^2\right)\right.$$
$$\left. -\frac{1}{16}\frac{\hat{m}_l}{\hat{m}_s}\left(\left\langle\operatorname{tr} M_l^{-1}\operatorname{tr} M_s^{-1}\right\rangle - \left\langle\operatorname{tr} M_l^{-1}\right\rangle\left\langle\operatorname{tr} M_s^{-1}\right\rangle\right)\right) \tag{5.2.32}$$

and cumulant

$$\Delta_{M_s} \equiv \frac{H\chi^{\text{full}}_{M_s}}{M_s} = \frac{m_l\left(\chi_l^{\text{con}} - \frac{1}{m_s}\left\langle\bar{\psi}\psi\right\rangle_s + \chi_l^{\text{dis}} - \frac{m_l}{m_s}\chi_{l,s}^{\text{dis}}\right)}{\left\langle\bar{\psi}\psi\right\rangle_l - \frac{m_l}{m_s}\left\langle\bar{\psi}\psi\right\rangle_s}. \tag{5.2.33}$$

This subtraction will remove both constants $c_{\mathcal{UV}}$ and $c_2(T)$, so no linear term should be present. The attribution of the strange quark condensate to the connected susceptibility is due to the fact that it is a connected diagram. It will also make the cancellation of $c_{\mathcal{UV}}$ to occur within the connected susceptibility.[9] Second, we define the *Connected Susceptibility Subtraction:*

$$M_c \equiv \frac{m_s}{T^4}\left(\left\langle\bar{\psi}\psi\right\rangle_l - \frac{1}{2}m_l\chi_l^{\text{con}}\right) = \hat{m}_s^2 N_\tau^4 \frac{1}{4}\left(\left\langle\operatorname{tr} M_l^{-1}\right\rangle - m_l\left\langle\operatorname{tr} M_l^{-2}\right\rangle\right) \tag{5.2.34}$$

and corresponding susceptibilities

$$\chi^{\text{full}}_{M_c} \equiv m_s \frac{\partial}{\partial m_l} M_c = \chi^{\text{con}}_{M_c} + \chi^{\text{dis}}_{M_c}, \tag{5.2.35}$$

$$\chi^{\text{con}}_{M_c} = \frac{m_s^2}{T^4}\left[-\frac{1}{2}\frac{\partial}{\partial m_l}\chi_l^{\text{con}}\right]_{\text{con}} = \hat{m}_s^2 N_\tau^4 \frac{1}{2}\left\langle\operatorname{tr} M_l^{-3}\right\rangle, \tag{5.2.36}$$

$$\chi^{\text{dis}}_{M_c} = \frac{m_s^2}{T^4}\left(\frac{1}{2}\chi_l^{\text{dis}} - \frac{1}{2}\left[\frac{\partial}{\partial m_l}\chi_l^{\text{con}}\right]_{\text{dis}}\right) = \hat{m}_s^2 N_\tau^4 \left(\frac{1}{8}\left(\left\langle(\operatorname{tr} M_l^{-1})^2\right\rangle - \left\langle\operatorname{tr} M_l^{-1}\right\rangle^2\right)\right.$$
$$\left. -\frac{1}{8}\left(\left\langle\operatorname{tr} M_l^{-1}\operatorname{tr} M_l^{-2}\right\rangle - \left\langle\operatorname{tr} M_l^{-1}\right\rangle\left\langle\operatorname{tr} M_l^{-2}\right\rangle\right)\right) \tag{5.2.37}$$

and cumulant

$$\Delta_{M_c} \equiv \frac{H\chi^{\text{full}}_{M_c}}{M_c} = \frac{m_l\left(\chi_l^{\text{dis}} - \frac{\partial}{\partial m_l}\chi_l^{\text{con}} - \frac{1}{m_s}\left\langle\bar{\psi}\psi\right\rangle_s\right)}{\left\langle\bar{\psi}\psi\right\rangle_l - m_l\chi_l^{\text{con}}}. \tag{5.2.38}$$

This subtraction is designed in order to remove only $c_{\mathcal{UV}}$, but not the whole linear term in M_0. It also eliminates the operator $\left\langle\operatorname{tr} M_l^{-2}\right\rangle$ completely. The connected part subtraction corresponds to a lowest order Taylor expansion of the chiral density operator towards the chiral limit:

$$\left(\bar{\psi}\psi\right)_0 = \left(\bar{\psi}\psi\right)_l - m_l\chi_l^{\text{con}} + \mathcal{O}\left(m_l^2\right). \tag{5.2.39}$$

[9] Note that the definition of the susceptibility for M_s as light quark mass derivative does not coincide with the fluctuation-definition of the susceptibility, but is symmetric w.r.t. m_l and m_s:

$$\chi^{fluc}_{M_s} \equiv \left\langle(\delta M_s)^2\right\rangle = \frac{1}{T^4}\left(m_s^2\chi_l^{\text{full}} - 2m_l m_s\chi_{q,s}^{\text{dis}} + m_l^2\chi_s^{\text{full}}\right).$$

A subtraction of the full susceptibility would correspond to a lowest order Taylor expansion of the chiral condensate itself:

$$\langle\bar{\psi}\psi\rangle_0 = \langle\bar{\psi}\psi\rangle_l - m_l\chi_l^{\text{full}} + \mathcal{O}\left(m_l^2\right) \tag{5.2.40}$$

and would also remove the linear term in m_l completely. We may denote this order parameter by M_f. However, due to the insufficient statistics of χ_l^{dis} we will not make use of it. We have noted in Sec. 4.3.3 that M_f is an order parameter for the chiral transition, but M_c is rather an order parameter for the $\mathrm{U_A}(1)$ restauration. Nevertheless, M_c is expected to drop rapidly at T_{ch} even if it does not vanish above T_{ch}. We will assume that $M_c \to M_0$ for $m_l \to 0$, i.e. we assume that χ_l^{con} does not diverge in the chiral limit with a critical exponent.

Chiral Condensate Measurements

In Fig. 5.6 we show the lattice data on the order parameters M_i, $i \in \{0, s, c\}$, as well as the normalized strange quark condensate

$$M_{0,s} \equiv \frac{m_s}{T^4}\langle\bar{\psi}\psi\rangle_s\,. \tag{5.2.41}$$

for $N_\tau = 4$. The corridors in this and the following plots were obtained with the Ferrenberg-Swendsen method. In all three order parameters we observe the characteristic decrease with the temperature, which becomes more pronounced for smaller quark masses. For the smallest quark mass $H = 1/80$, M_i is already very close to zero at $\beta = 3.33$, whereas it seems to remain finite for $\beta = 3.28$. The critical coupling in the chiral limit is hence to be expected in this interval. Note that the subtractions strongly effect the data points for large m_l, but has only a very small effect on $H = 1/80$. Nevertheless, the subtractions will be of importance for the magnetic equation of state.

In Fig. 5.7 M_0 and M_s are plotted for $N_\tau = 8$, FSM in β was applied before reweighting in the quark mass to β values with $\hat{m}_s = 0.24$ ($\beta \geq 3.515$) and $\hat{m}_s = 0.29$ ($\beta \leq 3.495$), but not in between. These observables display similar behavior, although it is more difficult to read off the critical region here because the window of β values defining the critical region is wider. Due to multiplicative and approximate additive renormalization in M_s, this observable should be comparable in magnitude for the two lattice spacings; this is indeed observed, e.g. we find that for $H = 1/40$, the value $M_s = 1.3$ is reached for $N_\tau = 4$ at $\beta = 3.30$ and for $N_\tau = 8$ at $\beta = 3.515$.

In Fig. 5.8 we show the typical distribution of light quark condensate data for various β values in the peak region. In Fig. 5.9 we show the correlation between light and strange quark condensates. One can clearly see that the correlation is large for $H = 1/10$, but much smaller for $H = 1/80$. Also, the shape of the distribution dependends more on the value of β for the smaller quark masses.

Disconnected and Connected Chiral Susceptibility Measurements

The full susceptibility provides the best signal for a phase transition by the characteristic divergence of its peak with some power of the light quark mass. For a second order transition, the peaks of χ_l^{full} for the various masses define the pseudo-critical couplings β_{pc} which characterize the transition temperature.

The lattice data on the unsubtracted 2-flavor susceptibility $2\chi_{M_0}^{\text{full}}$ and its disconnected and connected parts $2\chi_{M_0}^{\text{dis}}$, $2\chi_{M_0}^{\text{con}}$ are shown both for $N_\tau = 4$ and $N_\tau = 8$ in Fig. 5.10 and 5.11. The peak of the disconnected part is difficult to determine, the statistics may still not be sufficient for the smallest m_l, which leads to the unphysical situation that χ_l^{dis} for $H = 1/80$ peaks at a higher value of β as χ_l^{dis} for $H = 1/40$. From the expected behavior of the connected and disconnected susceptibility discussed in Sec. 4.3, it is believed that the disconnected part is sufficient to determine the transition temperature. However, the lattice data show that the connected part also has a strong quark mass dependence. The fact that the connected part is *large in magnitude* can be attributed

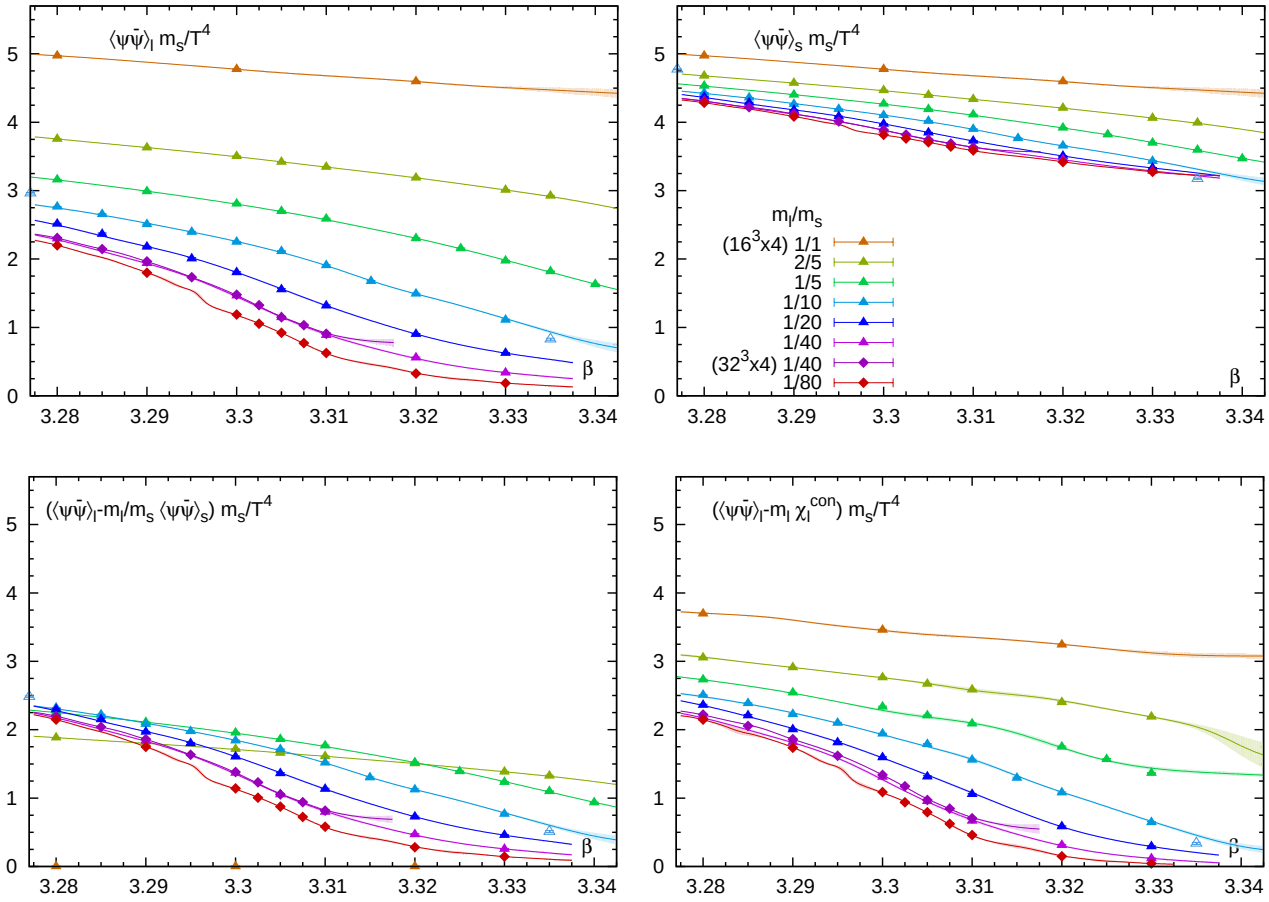

Figure 5.6: Chiral Condensates for $N_\tau = 4$ (1-flavor normalized): for the light quark (top left) and the strange quark (top right), and with subtractions corresponding to the order parameters M_s (bottom left) and M_c (bottom right) defined in Eq. (5.2.29, 5.2.34). Full symbols have $\hat{m}_s = 0.065$, empty symbols are from the LCP. The volume dependence for $H = 1/40$ on the lattices $16^3 \times 4$ and $32^3 \times 4$ is small.

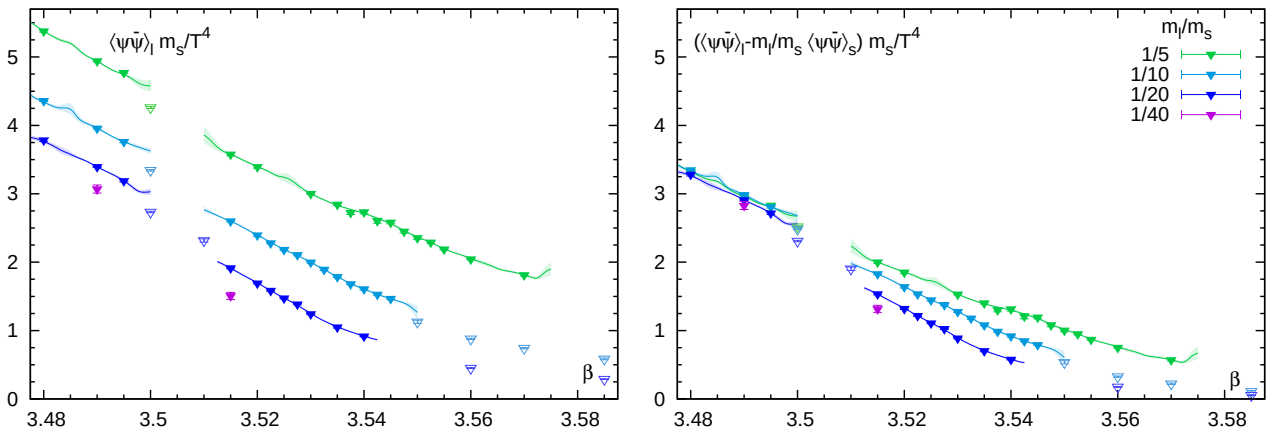

Figure 5.7: Chiral Condensates for $N_\tau = 8$ (1-flavor normalized) for the light quark, without subtraction (M_0, left) and with subtraction (M_s, right). Data in this plot are not reweighted, for reweighted data see Fig. 5.1.

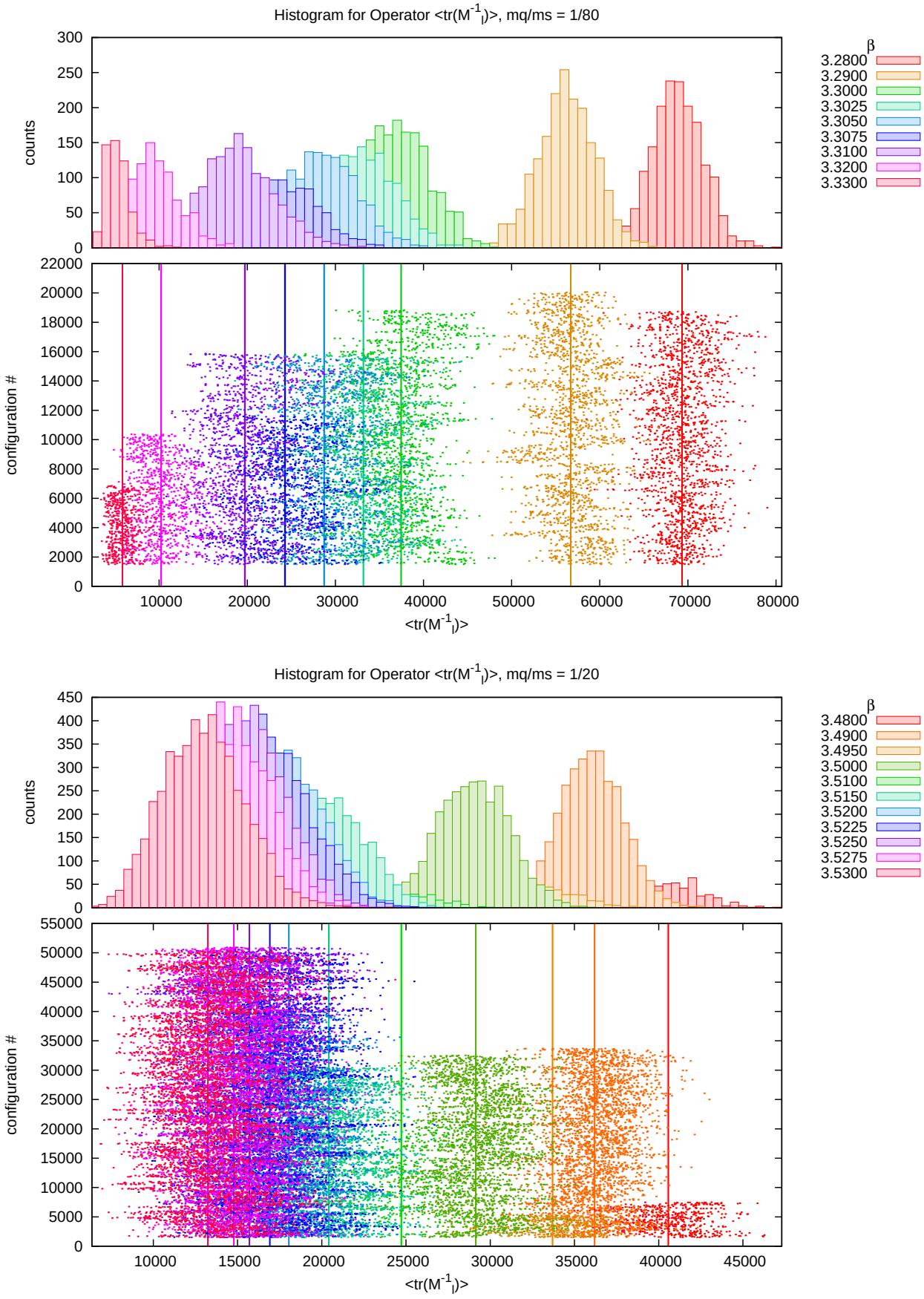

Figure 5.8: Histograms of the chiral condensate for $N_\tau = 4$ with $H = 1/80$ and for $N_\tau = 8$ with $H = 1/20$.

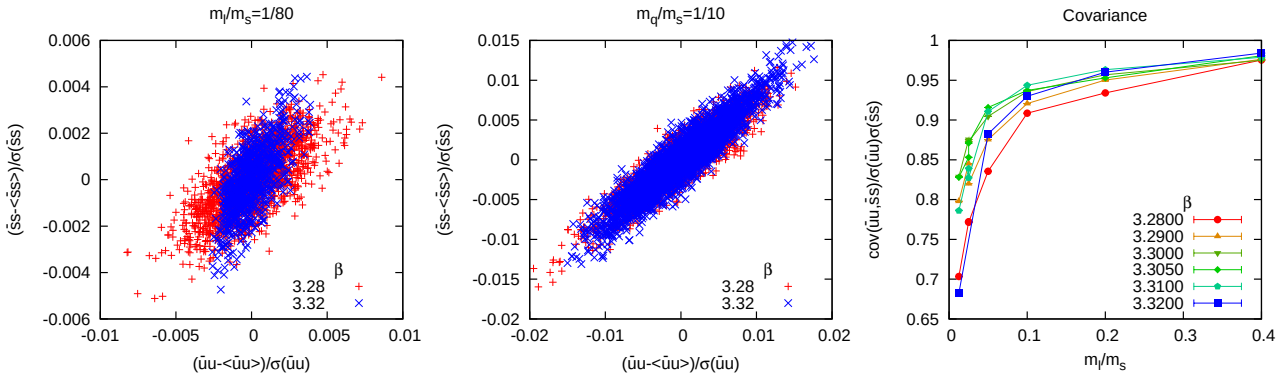

Figure 5.9: Correlation between light quark and strange quark condensate fluctuations, for $H = 1/80$ (left) and $H = 1/20$ (center) for two beta values below ($\beta = 3.28$) and above ($\beta = 3.32$) the critical temperature. The covariance (right) decreases in the chiral limit.

to the UV-divergent constant, for one flavor given by

$$\tilde{c}_{\mathcal{UV}}^{(N_\tau)} = c_{\mathcal{UV}} \hat{m}_s^2 N_\tau^4 = \begin{cases} \tilde{c}_{\mathcal{UV}}^{(4)} = 1.6224 & N_\tau = 4 \\ \tilde{c}_{\mathcal{UV}}^{(8)} = 3.5389 & N_\tau = 8 \end{cases}, \tag{5.2.42}$$

which in both cases is small enough such that after subtraction the connected susceptibilities remain positive for $H < 1$. However, for $N_\tau = 4$ and $\hat{m}_l \geq \hat{m}_s$, the 2-flavor connected part drops below the value of $2\tilde{c}_{\mathcal{UV}}^{(4)}$. This might be due to additional quark mass dependences such as a cubic term. Also, the contribution of $2\tilde{c}_{\mathcal{UV}}^{(8)}$ to the $N_\tau = 8$ connected part seems to be underestimated. Due to these uncertainties, it is not a save strategy to subtract this constant for additive renormalization of chiral observables.

The large *quark mass dependence* of χ_l^{con} is however not really understood. The standard scenario is that χ_l^{con} does not contribute to the full susceptibility in the chiral limit as $m_\delta > 0$ for all temperatures. The lattice data shown in Fig. 5.10 however do not support this picture. In order to quantify the relative divergence of χ_l^{con} and χ_l^{dis}, we have plotted the ratio

$$R_{\text{dis}}^{\text{con}} \equiv \frac{\chi_l^{\text{con}} - 2\chi_s^{\text{con}}}{\chi_l^{\text{dis}} - 4\chi_s^{\text{dis}}}, \tag{5.2.43}$$

where the subtraction shall remove the UV-divergence. Note that this ratio does not require multiplicative renormalization and can be readily compared for different lattice spacings, see Fig. 5.12. We observe that the ratio $R_{\text{dis}}^{\text{con}}$ remains finite at temperatures below the peak region and even grows above the peak region. We note that the same qualitative behavior is found if $c_{\mathcal{UV}}$ is subtracted instead the strange quark susceptibilities. The observation that $R_{\text{dis}}^{\text{con}}$ is constant below β_{c} can be attributed to the presence of Goldstone modes in the connected part, as will be discussed in Sec. 5.3.2. Unexpectedly, this behavior extends into the peak region, and we find $R_{\text{dis}}^{\text{con}}(\beta_{\text{pc}}) \simeq 0.5$ for $N_\tau = 4$ and $R_{\text{dis}}^{\text{con}}(\beta_{\text{pc}}) \simeq 1.0$ for $N_\tau = 8$. At least in the mass range considered, we have no indication that $R_{\text{dis}}^{\text{con}} \simeq m_\sigma^2/m_\delta^2$ tends to zero in the chiral limit.

One might speculate whether this finding is due to lattice artifacts or is of physical origin. It is at least conceptually possible that the strong divergence of χ_l^{con} is related to the effective restoration of the $\text{U}_\text{A}(1)$ symmetry, as explained in Sec. 4.3. One expects $m_\sigma = m_\delta$ above the $\text{U}_\text{A}(1)$ transition temperature $T_{\text{U}_\text{A}(1)}$.

The mixed susceptibility $\chi_{l,s}^{\text{dis}} \sim 1/m_\sigma^2$ is not bounded but develops a sharp peak at T_{c}, almost as strong as χ_l^{dis}. This can be understood via the corresponding scalar propagator, see Eq. (4.3.14). However, the ratio $\chi_{l,s}^{dis}/\chi_l^{\text{dis}} = M_\delta^2/M_{s,\text{con}}^2$ seems to vanish in the chiral limit, as can be seen in

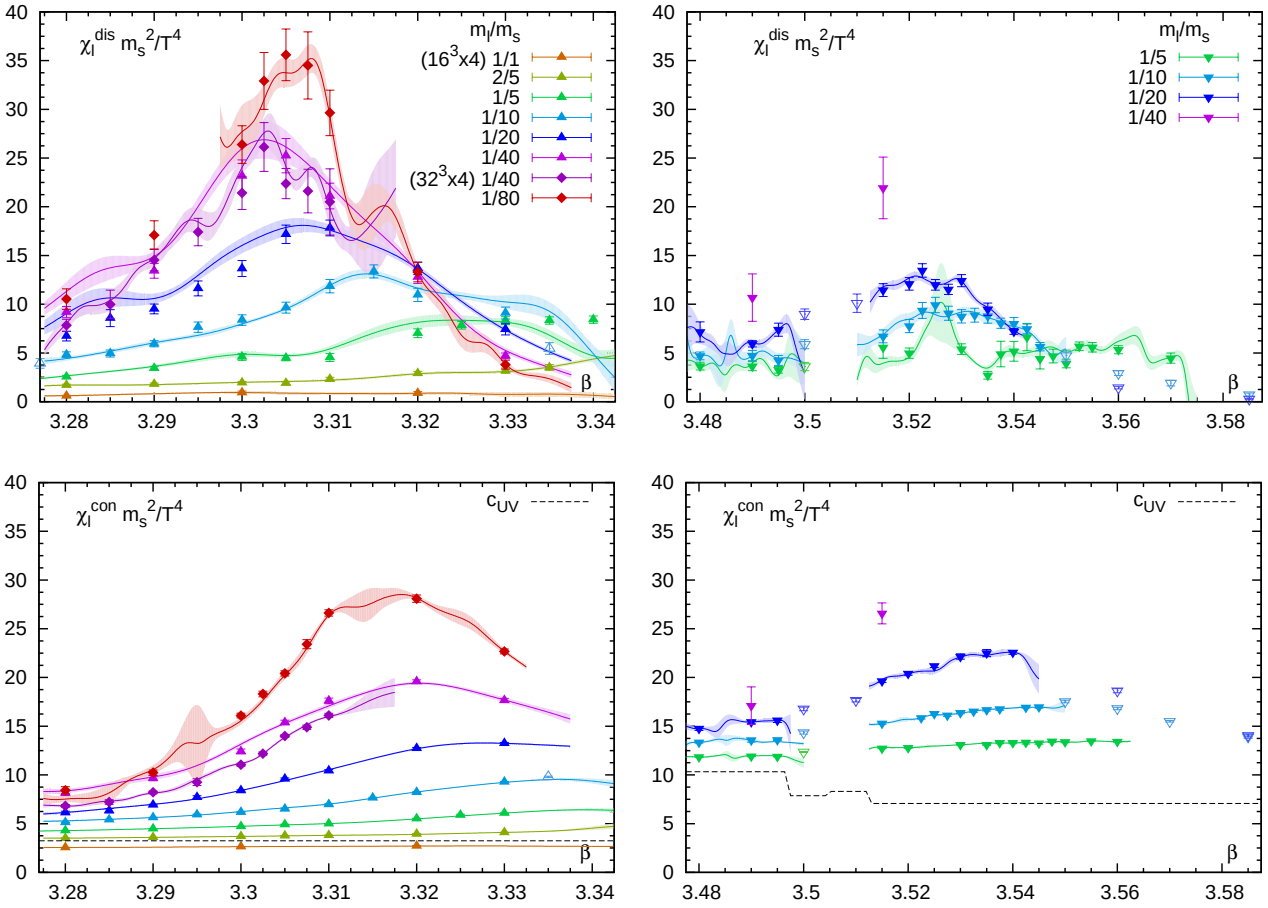

Figure 5.10: Comparison of (2-flavor normalized) chiral susceptibilities $2\chi^{\rm dis}_{M_0}$ (top) and $2\chi^{\rm con}_{M_0}$ (bottom) for $N_\tau = 4$ (left) and $N_\tau = 8$ (right): the disconnected susceptibility (top) develops a sharp peak. The connected susceptibility (bottom) develops a broader peak at a somewhat higher temperature. Nevertheless, the quark mass dependence is strong. The value of $2\hat{c}^{(N_\tau)}_{\mathcal{UV}}$ is indicated by the dotted line.

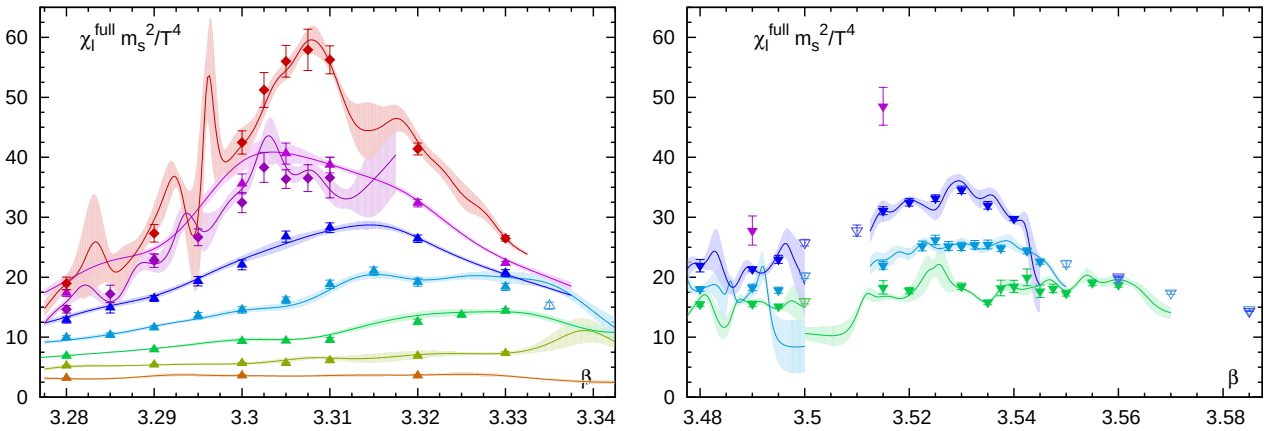

Figure 5.11: Full chiral susceptibility $2\chi_{M_0}$ (2-flavor normalized) for $N_\tau = 4$ (left) and $N_\tau = 8$ (right). Note that the peak positions are shifted slightly as compared to $\chi^{\rm dis}_l$ due to the contribution of $\chi^{\rm con}_l$.

Fig. 5.13. This could also be a signal for $U_A(1)$ restauration. But it may as well be that the ratio saturates above zero, We conclude that we have no strong indication for the scenario $T_{U_A(1)} = T_c$ in the chiral limit.

Even if $T_{U_A(1)} > T_c$ remains true in the chiral limit[10], the connected part is nevertheless indispensable for the scaling analysis based on results for finite quark masses. For example, the connected part seems to be an integral part of the definition of the cumulant Δ_{M_0}, Eq. (5.2.28). Only this definition exhibits the feature that it is monotonically increasing, from 0 at low temperatures to 1 at high temperatures, as can be derived from the scaling laws, Sec. 3.3.2. This behavior is indeed observed for Δ_{M_0}, see Fig. 5.14, but $\Delta^{\rm dis}_{M_0}$ in contrast drops down again above the critical temperature.

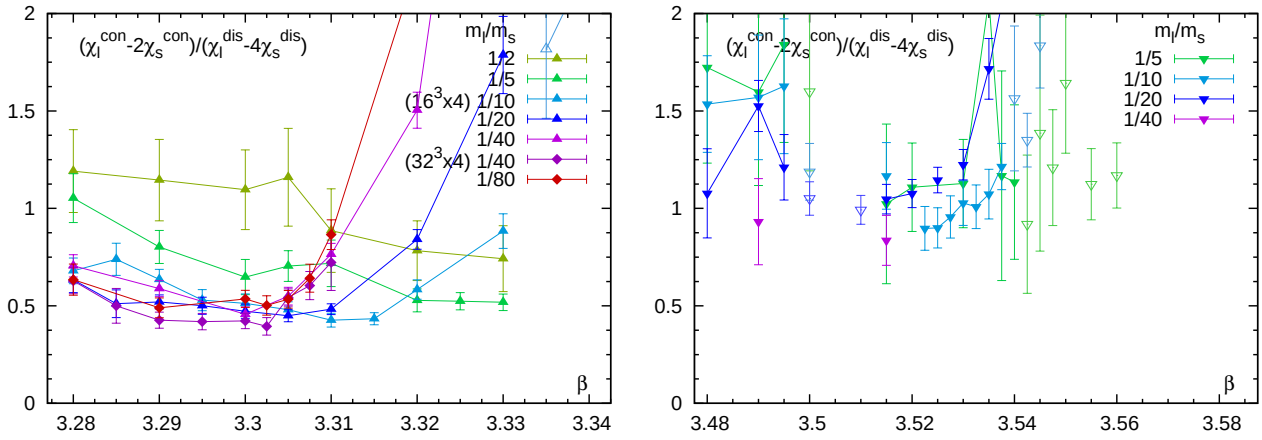

Figure 5.12: Ratio of connected and disconnected susceptibility $R^{\rm con}_{\rm dis}$ for $N_\tau = 4$ (left) and $N_\tau = 8$ (right).

Finite Size Effects and Thermodynamic Limit

Before we will persue the scaling analysis, we show evidence that for all quark masses down to $m_l/m_s = 1/80$ the chiral observables do not show strong finite size effects (FSE). The lattice volumes are chosen such that the thermodynamic limit is well under control: For the smallest quark mass, we find $M_{\pi,5}N_\sigma \simeq 3$, i.e. the pion correlation length fits well on the lattice. In Fig. 5.15 we show that the chiral condensate and the full susceptibility for $H = 1/40$ only exhibit small FSE of $\mathcal{O}\left(V^{-1}\right)$. The proportionality factors of these FSE are temperature dependent: above T_c, the thermal mass of the pion reduces the pion correlation length, reducing the $\mathcal{O}\left(V^{-1}\right)$ term. The data sets for $N_\sigma = 16$ and $N_\sigma = 32$ are almost indistinguishable. Only $\chi^{\rm con}_l$ exhibits considerable finite size effects below $\beta_{\rm pc}$ (see Fig. 5.2), which does however not drastically effect $\chi^{\rm full}_l$. We conclude that for $H \gtrsim 1/40$ the thermodynamic limit is almost reached for $N_\sigma = 16$. We also analyzed FSE for $H = 1/80$ and found that $N_\sigma = 32$ is sufficiently large to determine chiral observables.

5.2.4 Determination of β_c

Since we expect that $m^c_l = 0$, finite size scaling (FSS) according to Eq. (3.3.34) is not applicable. However, close to the chiral limit we would expect to find subleading corrections to FSS. Unfortunately we do not have enough lattice volumes to perform a detailed FSS analysis. Also, new critical exponents would enter for the subleading corrections, which would complicate the situation

[10] For physical quark masses, lattice data clearly support that $T_{U_A(1)}$ is effectively restored above the chiral transition temperature. For example, the RBC-Bi collaboration [83] observed splittings between the screening masses of the scalar and pseudoscalar channels which are substantial at least up to $T_{U_A(1)} \simeq 1.2 T_{\rm ch}$.

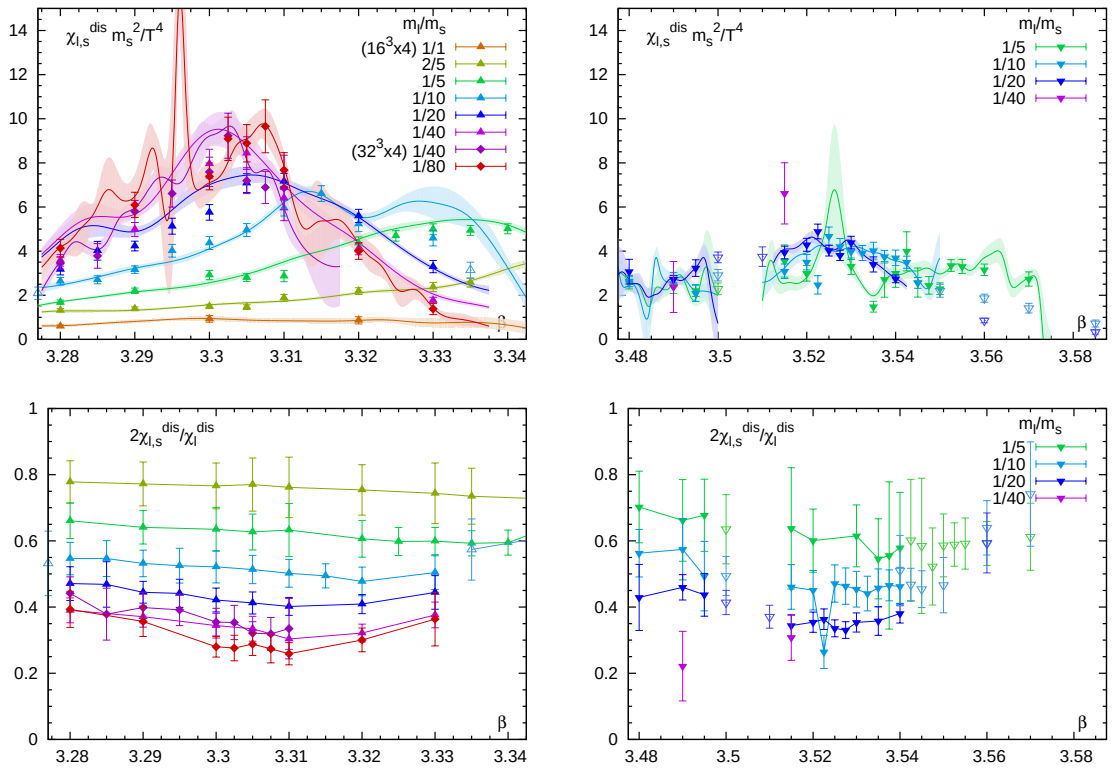

Figure 5.13: Mixed susceptibility $\chi_{l,s}^{dis}$ (top) and ratio with disconnected susceptibility χ_l^{dis} (bottom) for $N_\tau = 4$ (left) and $N_\tau = 8$ (right), which shows that $\chi_{l,s}^{dis}$ does not diverge as strong as χ_l^{dis}.

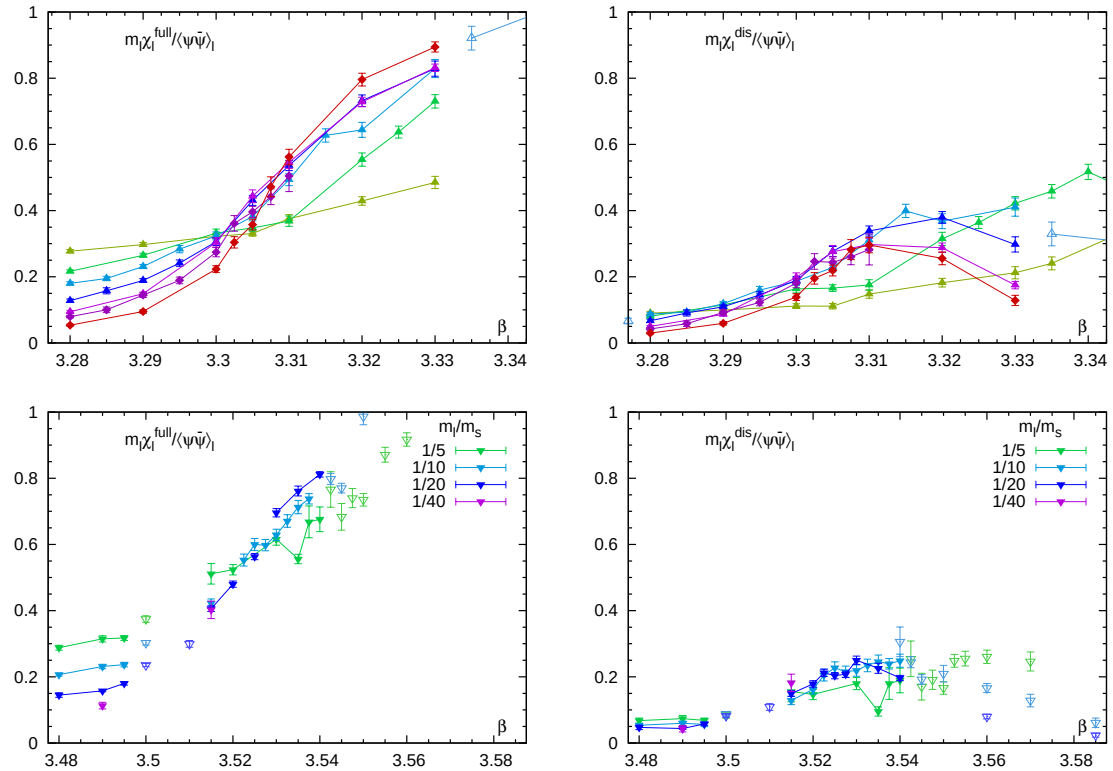

Figure 5.14: Cumulants Δ_{M_0} (top) and $\Delta_{M_0}^{\text{dis}}$ (bottom), for $N_\tau = 4$ (left) and $N_\tau = 8$ (right).

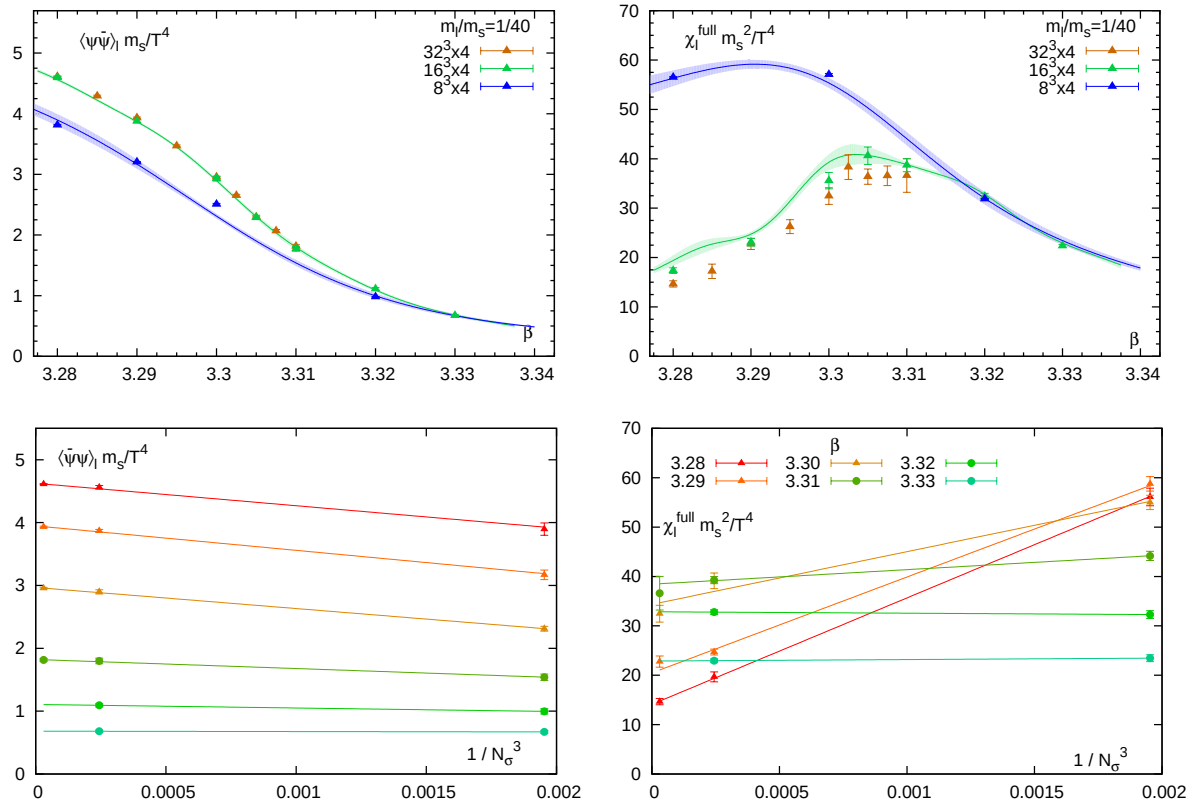

Figure 5.15: Finite size effects for $N_\tau = 4$, $m_l/m_s = 1/40$, which are of $\mathcal{O}(1/V)$. The $32^3 \times 4$ is close enough to the infinite volume limit.

greatly. Nevertheless, we have shown that our lattice volumes are large enough to determine the pseudo-critical couplings $\beta_{\rm pc}$ directly.

Susceptibility Peaks and Inflection Point

In this section, we calculate the various pseudo-critical lines from the pseudo-critical couplings of the chiral observables, as well as from the inflection point of the chiral condensate. For a second order transition at some light quark mass m_l^c, the peak locations define the pseudo-critical couplings $\beta_{\rm pc}$ which are characterized by

$$\beta_{\rm pc} - \beta_{\rm c} = c(m_l - m_l^c)^{1/\beta\delta}, \tag{5.2.44}$$

because to leading order the reduced temperature is proportional to the coupling, $t \sim \beta - \beta_{\rm c}$. This amounts to a linear approximation of the function $r_0/a(\beta)$. The above relation also characterizes the inflection point of the chiral condensate, i.e. the coupling $\beta_{\rm pc}^{\rm infl}$ at which the temperature derivative of $\langle\bar{\psi}\psi\rangle_l$ known as the thermal susceptibility χ_t peaks. In the limit $m_l \to m_l^c$, we expect $\beta_{\rm pc}^{\rm infl} \to \beta_{\rm pc}^{\rm full}$, but due to deviations from scaling, we will not expect them to agree for $m_l > m_l^c$. The peak heights of the chiral susceptibility $\chi_l^{\rm full}$ and the thermal susceptibility χ_t at $\beta_{\rm pc}$ are governed by two distinct scaling relations:

$$\chi_{l,\rm max}^{\rm full} = c_m(m_l - m_l^c)^{1/\delta - 1}, \qquad \chi_{t,\rm max} = c_t(m_l - m_l^c)^{(\beta-1)/\beta\delta} \tag{5.2.45}$$

We will eventually see that we have no evidence that $m_l^c \neq 0$, hence we expect to find O(N) rather than Z(2) critical exponents. The statistics of the QCD lattice data is however not sufficient to determine the critical exponents directly. In this section, we will assume O(2) critical exponents, $1/\beta\delta = 0.599$.

We also expect that lattice artifacts will effect the value of the pseudo-critical couplings. In order to obtain T_c in the chiral limit, the RBC-Bi collaboration made use of the fit ansatz

$$(T_{\rm pc} r_0)_{\hat{m}_l,\hat{m}_s,N_\tau} = (T_c r_0)_{0,m_s,\infty} + A(M_{\pi,5} r_0)^{2/\beta\delta} + B/N_\tau^2, \tag{5.2.46}$$

also incorporating a term B/N_τ^2 which accounts for cut-off effects of $\mathcal{O}\left(a^2\right)$. The RBC-Bi analysis of the transition temperature for physical masses, which appeared in Cheng *et. al.* (2006) [23], was based on $N_\tau = 4$ and $N_\tau = 6$ lattices. They calculated the pseudo-critical couplings for the Polyakov loop susceptibility, the light and the strange quark susceptibility. The coefficients in Eq. (5.2.46) were determined to be $A = 0.041(5)$, $B = 0.34(9)$.

Our collaboration has generated more data in the critical region since then: in particular the $N_\tau = 4$ data for the small masses $H = 1/40, 1/80$ and the $N_\tau = 8$ data. Based on these data, we consider here the couplings for the full, disconnected, connected and mixed susceptibility $\beta_{\rm pc}^{\rm full}$, $\beta_{\rm pc}^{\rm dis}$, $\beta_{\rm pc}^{\rm con}$, $\beta_{\rm pc}^{\rm mix}$ separately. We have also determined the inflection point of the chiral condensate $\beta_{\rm pc}^{\rm infl}$ by fitting the Ferrenberg-Swendson interpolated chiral condensate data in the pseudo-critical region. The fits are based on polynomials $P(\beta)$ of various degrees up to six, the inflection point is obtained by the determination of the root of the second derivative $P''(\beta_{\rm pc}^{\rm infl}) = 0$. Errors have been obtained by quantifying the variation of the result with the degree of P.

In order to compare our chiral extrapolation with the one of Cheng *et. al.* we have used a similar ansatz

$$(T_{pc} r_0)_{\hat{m}_l,\hat{m}_s,N_\tau} = (T_c r_0)_{0,m_s,\infty} + \breve{A}_{N_\tau} H^{1/\beta\delta} + B/N_\tau^2. \tag{5.2.47}$$

where $M_{\pi,5} r_0$ is replaced by H due to the lack of zero temperature measurements. For the same reason we will not attempt a continuum extrapolation although the ansatz contains a $1/N_\tau^2$ term for compatibility. The new fit parameters are related via $\breve{A}_{N_\tau} = A(M_S r_0)^{2/\beta\delta}$. We fit the $N_\tau = 4$ and $N_\tau = 8$ data separately to compare $\breve{A}_4$ with $\breve{A}_8$, because the corresponding values $m_s = \hat{m}_s a$ might differ slightly for both lattice spacings.

N_τ	$\hat{m}_s$	$\hat{m}_l$	$\beta_{pc}^{\rm dis}$	$\beta_{pc}^{\rm mix}$	$\beta_{pc}^{\rm con}$	$\beta_{pc}^{\rm full}$	$\beta_{pc}^{\rm infl}$
4	0.065	0.026	3.3375(5)	3.3375(5)	3.3775(5)	3.3377(6)	3.3410(41)
		0.013	3.3158(19)	3.3156(14)	3.3392(10)	3.3284(62)	3.3177(48)
		0.0065	3.3141(3)	3.3138(2)	3.3367(4)	3.3153(212)	3.3175(18)
		0.00325	3.3069(13)	3.3056(9)	3.3277(6)	3.3146(28)	3.3070(6)
	(16^3)	0.001625	3.3025(8)	3.3012(7)	3.3204(3)	3.3034(19)	3.3022(30)
	(32^3)	0.001625	3.3030(9)	3.3028(14)	-	3.3031(6)	3.3019(2)
		0.0008125	3.3076(6)	3.3072(8)	3.3183(8)	3.3083(4)	3.3043(53)
extrapolation $\hat{m}_l \to 0$			3.2951(24)	3.2940(35)	3.3107(27)	3.2909(28)	3.2921(12)
8	0.024	0.0048	3.5213(3)	3.5211(3)	3.5393(120)	3.5294(9)	3.5387(1)
		0.0024	3.5311(41)	3.5306(59)	3.5449(135)	3.5387(4)	3.5258(3)
		0.0012	3.5425(50)	-	3.5554(5)	3.5540(27)	3.5242(1)
extrapolation $\hat{m}_l \to 0$			3.5042(10)	3.5024(0)	3.5261(10)	3.5093(7)	3.5128(2)

Table 5.4: The pseudo-critical couplings from various susceptibilities for physical strange quark mass.

The pseudo-critical couplings are plotted in Fig. 5.16 from the values given in Tab. 5.4. They have been obtained from FSM, errors were obtained by combining Jackknife with FSM. We have not included the data for $H = 1/80$ because the statistics is not sufficient to rely on FSM. The peak positions $\beta_{\rm pc}$ for $H = 1/80$ are clearly too large as they are even larger then the peak positions for $H = 1/40$. Note that we converted the couplings $\beta_{\rm pc}$ into the pseudo-critical temperature $T_{\rm pc} r_0$ by making use of the rational function $r_0/a(\beta)$ given in Eq. (5.2.11) before the chiral extrapolation as required according to Eq. (5.2.47), because the region of couplings considered is too large to rely on

a linear approximation of the function $r_0/a(\beta)$. This is `not` to be understood as a statement about the physical temperature, as we lack a physical scale as given from pion mass measurements. The results of the chiral extrapolation are given in Tab. 5.4 and 5.5. We observe that the extrapolations of $\beta_{\rm pc}$ for $\chi_l^{\rm dis}$ and $\chi_{l,s}^{\rm dis}$ do not coincide with the extrapolation for $\chi_l^{\rm full}$, which can be attributed to the contribution of $\chi_l^{\rm con}$. The connected part peaks at larger values of β as compared to $\chi_l^{\rm dis}$ for all considered quark masses. As a consequence, $\beta_{\rm pc}^{\rm con} > \beta_{\rm pc}^{\rm dis}$ seems to remain valid even in the chiral limit. This might be an indication that $\chi_l^{\rm con}$ does not contribute to critical scaling as expected in the standard scenario. However, it is remarkable that $\beta_{\rm pc}^{\rm con}$ also scales according to O(2) critical exponents.

Based on $\beta_{\rm pc}^{\rm dis}$ and $\beta_{\rm pc}^{\rm full}$ we identify the critical region in the chiral limit for $N_\tau = 4$ around $3.29 < \beta_c = 3.30$ and for $N_\tau = 4$ around $3.50 < \beta_c = 3.51$. We also give the fit coefficients $\breve{A}_{N_\tau}$ and observe that $\breve{A}_8$ is substantially larger than $\breve{A}_4$ (for all $\beta_{\rm pc}$ apart from $\beta_{\rm pc}^{\rm con}$) which might indicate that the pseudo-critical line might become steeper on finer lattices. We expect $\breve{A}_{N_\tau}$ to be comparable to the constant $A(M_S r_0)^{2/\beta\delta} = 0.072(8)$ obtained from Cheng *et. al.*, which is in good agreement with $\breve{A}_4$, but not with $\breve{A}_8$. The ratio for the full susceptibility is $\breve{A}_8/\breve{A}_4 \simeq 1.4$ and for the disconnected susceptibility $\breve{A}_8/\breve{A}_4 \simeq 1.9$. For completeness we note that the parameter B is of the order $0.5 < B < 1.0$ which is larger than what was determined by Cheng *et. al.* from $N_\tau = 4$ and 6 lattices. In the chiral limit we then obtain the critical temperatures $(T_c r_0)_{0,\hat{m}_s,N_\tau}$ for $N_\tau = 4$ and $N_\tau = 8$ which are summarized in Tab. 5.5 and depicted in 5.17.

We have also analyzed the peak maxima of the full, disconnected, connected and mixed susceptibilities, which are expected to scale according to Eq. (5.2.45). We have obtained the maxima not by FSM, but by fitting a Breit-Wigner form in the peak region.[11] We choose the fit ansatz

$$(\chi^i_{l,\max})_{\hat{m}_l,\hat{m}_s,N_\tau} = b^i_{N_\tau} H^\kappa + c^i_{N_\tau} \tag{5.2.48}$$

with $i \in \{\text{full}, \text{dis}, \text{con}, \text{mix}\}$. We have performed two fits, the first with fixed exponent $\kappa = 1/\delta - 1$ (both for $N_\tau = 4$ and $N_\tau = 8$), the second with a free exponent as a third fit parameter (only

[11] Another method sometimes applied to obtain a peak maximum estimate is to fit inverse parabola. Note that the susceptibility peaks are not symmetric, hence this method can not be used to fit the entire shape.

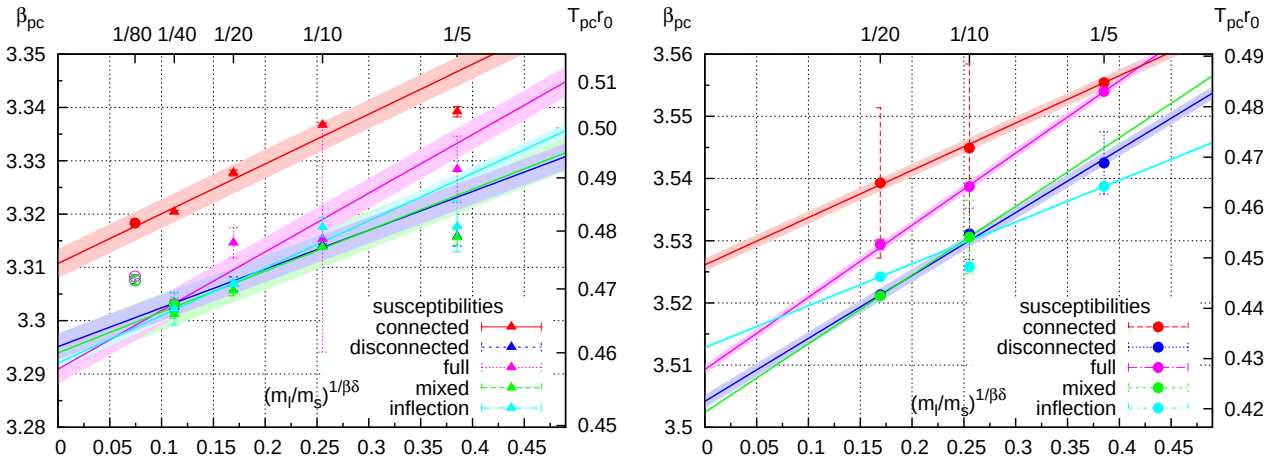

Figure 5.16: Pseudo-critical couplings and temperatures for $N_\tau = 4$ (left) and $N_\tau = 8$ (right), plotted over $(m_l/m_s)^{1/\beta\delta}$. Linear fits allow to extract β_c for the full and disconnected susceptibility. Triangles are for $N_\sigma = 16$ lattices, bullets are for $N_\sigma = 32$. Empty symbols are not fitted. The resulting β_c are listed in Tab. 5.4. The results of Tab. 5.5 were obtained by similar fits on a linear scale for Tr_0 instead the linear scale in β shown here.

for $N_\tau = 4$). We have included all masses $H \leq 1/10$ but not smaller masses because we observe scaling deviations for $H = 1/5$, as we have also seen for the pseudo-critical couplings. The fit results are shown in Tab. 5.6 and in Fig. 5.18. The connected part and the mixed susceptibility are not necessarily expected to scale with a critical exponent, but in both cases we find consistency with the O(2) exponent. In fact, the connected part shows even stronger divergence than the disconnected part in the free fit. The amplitude of the divergent term is given by the coefficient $a^i_{N_\tau}$. It is very remarkable that $a_4^{\rm con} < a_4^{\rm dis}$, but $a_8^{\rm con} > a_4^{\rm dis}$. The disconnected maximum seems to decrease, whereas the connected maximum seems to increase as one goes to finer lattices. On this basis, one should however not conclude that the connected part diverge stronger than the disconnected part as one performs the continuum limit: the situation described here might be due to lattice artifacts such as taste breaking, and might vanish as one includes even smaller masses. It will be interesting to see whether this tendency persists, as one includes more precise data on $H = 1/40$ for $N_\tau = 8$, as the estimates we have so far do not yet constrain the fits much.

We conclude that the pseudo-critical couplings show scaling behavior consistent with O(2) critical exponents, and that deviations are due to the insufficient statistics for the very light quark masses, and small deviations from scaling is apparent for $H = 1/5$. We expect that the physical point $H = 1/20$ is already close to the scaling region. Note that we have not determined the critical exponent via the scaling relation directly, hence we can not exclude other universality classes yet.

	$N_\tau = 4$		$N_\tau = 8$	
observable	$(T_c r_0)_{0,\hat{m}_s,4}$	$\breve{A}_4$	$(T_c r_0)_{0,\hat{m}_s,8}$	$\breve{A}_8$
disconnected	0.4607(19)	0.064(8)	0.4215(13)	0.125(7)
mixed	0.4595(27)	0.068(11)	0.4193	0.136
connected	0.4728(24)	0.099(14)	0.4487(12)	0.094(3)
full	0.4562(25)	0.104(21)	0.4279(9)	0.143(2)
inflection	0.4583(10)	0.076(8)	0.4322(3)	0.083(1)

Table 5.5: Fit parameters $T_c r_0$, $\breve{A}_{N_\tau}$ of the pseudo-critical line. The mixed susceptibility for $N_\tau = 8$ has no error as for $H = 1/5$ FSM could not be applied (partially LLNL data).

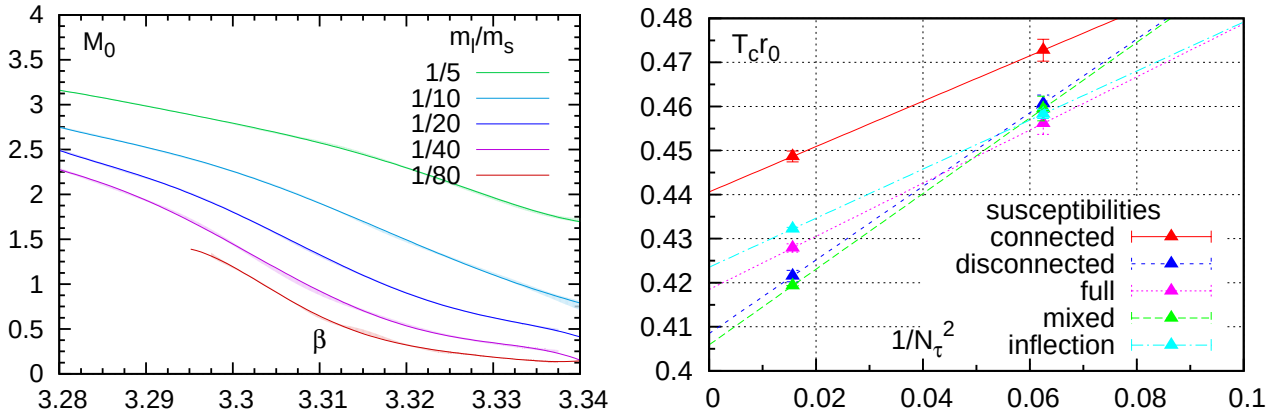

Figure 5.17: Left: Determination of the inflection point via a polynomial fit of the chiral condensate. Right: Cut-off dependence of the critical temperatures. We do not attempt a continuum extrapolation of the critical temperature here, based on only two lattice spacings.

	$N_\tau = 4$		$N_\tau = 4$ with free κ			$N_\tau = 8$	
observable	b	c	b	c	κ	b	c
connected	0.75(4)	5.22(56)	1.4(1.1)	3.2(2.9)	-0.66(15)	1.18(10)	9.59(83)
disconnected	0.93(7)	6.95(75)	2.2(2.2)	3.5(5.1)	-0.61(20)	0.78(16)	4.63(122)
full	1.54(6)	10.99(70)	4.9(3.2)	2.6(6.6)	-0.56(12)	1.97(34)	13.90(309)
mixed	0.17(2)	5.43(35)	0.7(1.6)	4.1(3.1)	-0.51(43)	0.11(6)	3.43(61)

Table 5.6: Fit parameters for the peak maxima of various chiral susceptibilities, for $N_\tau = 4$ and $N_\tau = 8$. For $N_\tau = 4$ also a fit with a free exponent κ is made, which is to be compared with $1/\delta - 1 = -0.793$ for O(2).

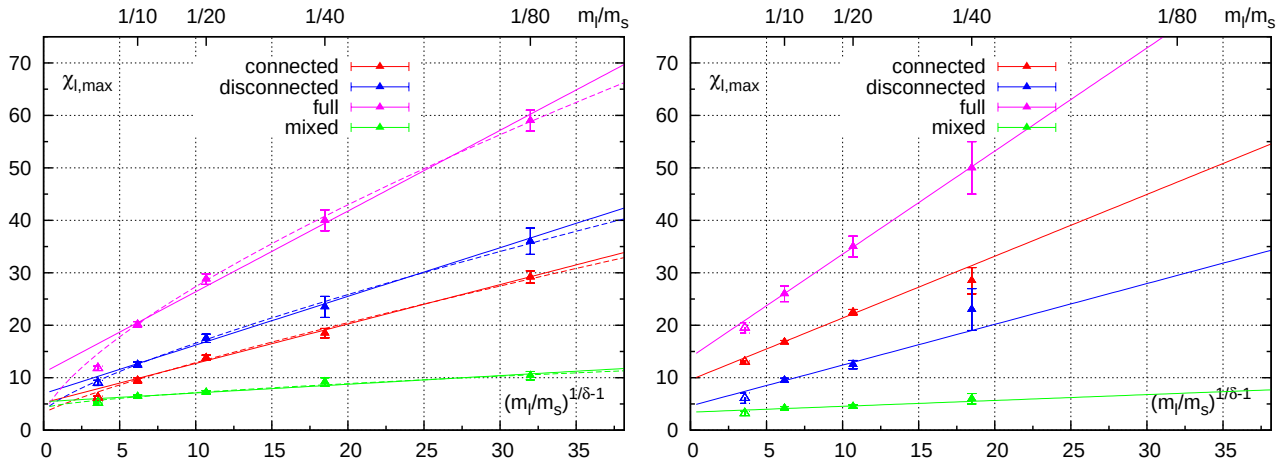

Figure 5.18: Peak Maxima of various chiral susceptibilities for $N_\tau = 4$ (left) and $N_\tau = 8$ (right). Full symbols are included in the fit, according to the ansatz Eq. (5.2.48). Full lines are fitted with O(2) critical exponents, dotted lines are fits with free exponent κ, fit results are given in Tab. 5.6.

5.3 Goldstone Modes

The next part of the scaling analysis is devoted to the Goldstone effect. After having identified the critical region in the chiral limit, we expect Goldstone scaling (GS) to appear for $\beta \lesssim 3.30$ ($N_\tau = 4$) and $\beta \lesssim 3.51$ ($N_\tau = 8$). True Goldstone scaling will hold as long as the (pseudo-taste) pion is massless, which is expected in the chiral limit below T_c. If we hit the critical line at a finite light quark mass, $m_l^c(m_s^{\mathrm{phys}}) \neq 0$ and we find Ising scaling, GS does not contribute to the Z(2) scaling function, but nevertheless will be present in the chiral limit.

We will look for GS in the chiral condensate and also in the susceptibility, where the singular behavior manifests as an IR divergence. We will investigate both the connected and disconnected part since we expect GS in both quantities due to taste violations, as explained in Sec. 4.4.5.

5.3.1 Goldstone Fits for the Chiral Condensate

For the light quark condensate, assuming that pions dominate the quark mass dependence, we choose the following simplified Goldstone fit ansatz for $\langle\bar{\psi}\psi\rangle_l$:

$$f_{\langle\bar{\psi}\psi\rangle_l}(m_l) = \bar{a} + \bar{b} m_l^{1/2} + \bar{c}_l m_l, \tag{5.3.1}$$

or equivalently for the bare order parameter M_0

$$\mathcal{F}_{M_0}(H) = a_{M_0} + b_{M_0} H^{1/2} + c_{M_0} H, \qquad H \equiv \frac{m_l}{m_s}. \tag{5.3.2}$$

The parameters $a_{M_0}, b_{M_0}, c_{M_0}$ are temperature dependent coefficients which are fitted for each β separately. All fit results are given in the tables in App. C.2. We also included a cubic term $\sim H^3$ in the above fit ansatz, but the 3-parameter fit already captures the quark mass dependence very well, and although the fits further improve by introducing a fourth parameter, the systematics is not well under control due to cancellations between the linear and the cubic coefficient, which have opposite signs and may become arbitrarily large. Hence we decided not to discuss them in this section.

In order to obtain a fit ansatz for M_s, we need an ansatz for the strange quark condensate as well. Inspired by the replacement of the pion mode by a kaon mode, we make the ansatz

$$\mathcal{F}_{M_{0,s}}(H) = a_{M_{0,s}} + b_{M_{0,s}} \sqrt{1/2 + H/2} + c_{M_{0,s}} H. \tag{5.3.3}$$

However, let us assume for the moment that there is no *light quark* mass dependence in the strange quark condensate, which results in the following expectation for $M_{0,s}$:

$$M_{0,s}(H=1) = M_0(H=1) \qquad \Longrightarrow \qquad \mathcal{F}_{M_{0,s}}(H) \simeq \mathcal{F}_{M_{0,s}}(H=1) = a_{M_0} + b_{M_0} + c_{M_0}, \tag{5.3.4}$$

i.e. the strange quark condensate is assumed to be determined by the sum of the light quark coefficients. This results in the following fit ansatz for the strange subtracted order parameters:

$$\mathcal{F}_{M_s}(H) = a_{M_s} + b_{M_s} H^{1/2} + (c_{M_s} - a_{M_s} - b_{M_s}) H, \qquad c_{M_s} \stackrel{!}{=} 0, a_{M_s} \stackrel{!}{=} a_{M_0}, b_{M_s} \stackrel{!}{=} b_{M_0}, \tag{5.3.5}$$

where the claimed identities rely on the assumption we made. The coefficient c_{M_s} is expected to vanish. Only if the prefactor of the linear terms of the light and strange quark condensate differ c_{M_s} is non-zero. Indeed it turns out that c_{M_s} is consistent with zero (see top at Fig. 5.19), hence there seems to be no genuine linear term in M_s. To ensure that the fit ansatz for M_s is a good approximation, we also fitted the strange quark condensate with the ansatz Eq. (5.3.3). We find that this ansatz describes the small light quark mass dependence of the strange condensate data very well, see center of Fig. 5.19. We expect that

$$\mathcal{F}_{M_0}(H=1) \simeq \mathcal{F}_{M_{0,s}}(H=1) \qquad \Longrightarrow \qquad a_{M_0} + b_{M_0} + c_{M_0} \simeq a_{M_{0,s}} + b_{M_{0,s}} + c_{M_{0,s}}. \tag{5.3.6}$$

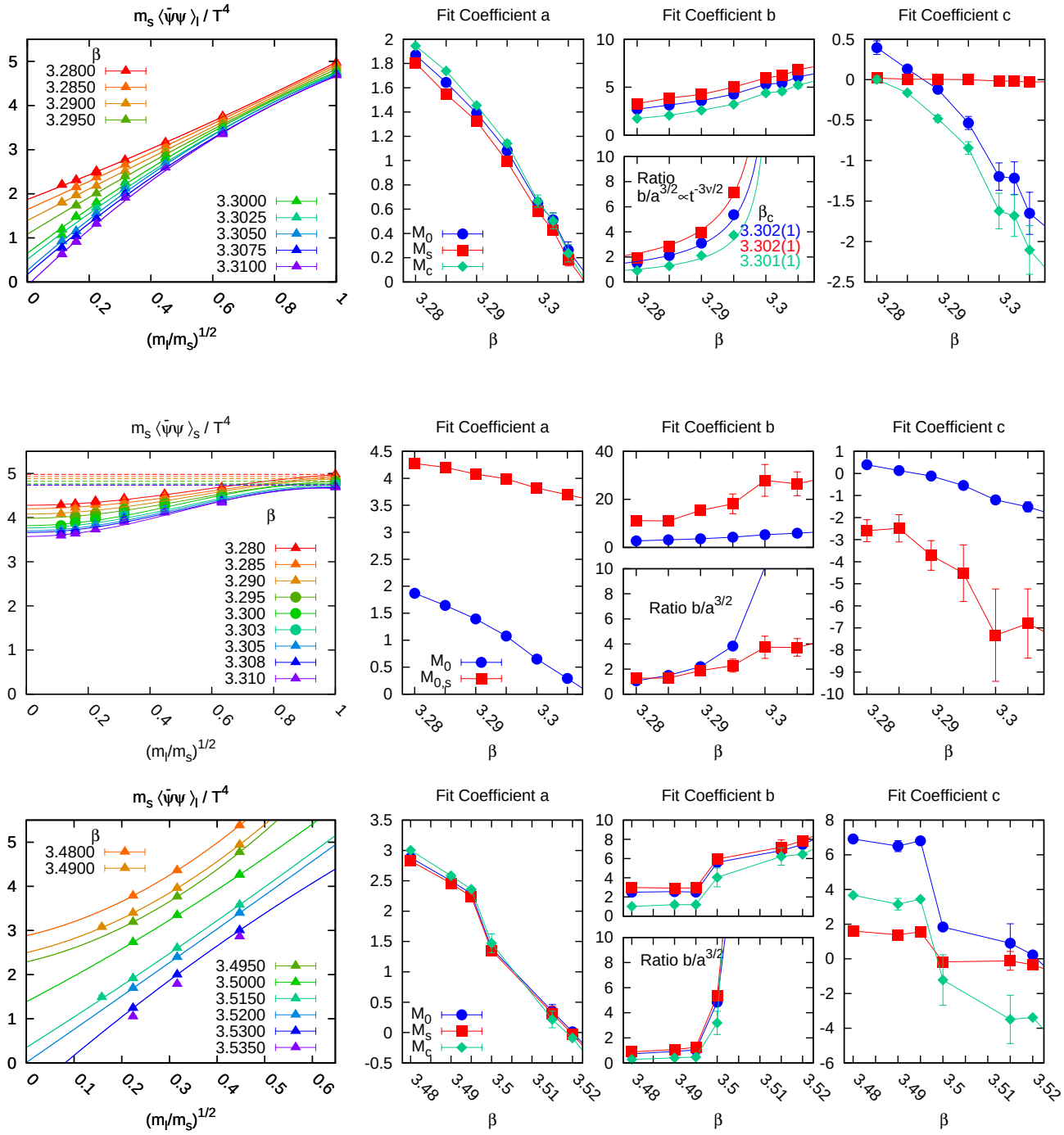

Figure 5.19: Goldstone fits of the renormalized chiral condensates M_0 (top) and $M_{0,s}$ (center) for $N_\tau = 4$, and M_0 for $N_\tau = 8$ (bottom). The fit coefficients are shown on the right and compared to the fits of M_s and M_c. The ratio $b/a^{3/2}$ is fitted for M_0 as explained in the text. For the fit ansätze see Eqs. (5.3.4),(5.3.5),(5.3.7),(5.3.3).

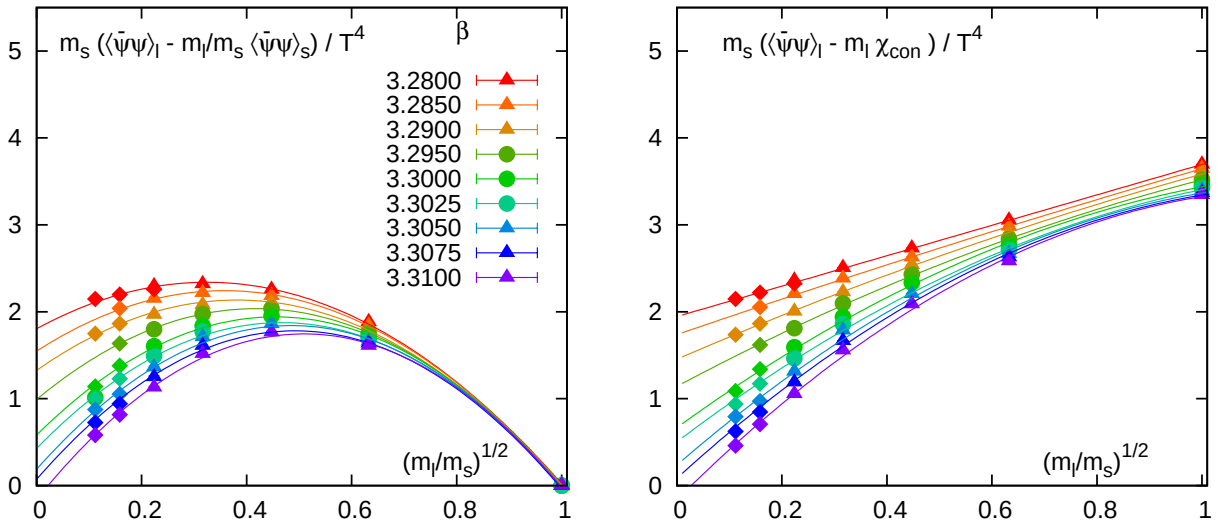

Figure 5.20: Goldstone fit of the strange subtracted order parameter M_s (left) and the connected subtracted order parameter M_c for $N_\tau = 4$. For fit coefficients see Fig. 5.19 and Tab. C.5.

This is indeed found: In Fig. 5.19 (center) the sum of the fit coefficients of M_0 given by $\mathcal{F}_{M_0}(H = 1)$ is indicated by the horizontal lines, which agrees well with the value of the strange quark condensate at $H = 1$.

It follows that the approximation in Eq. (5.3.5) is satisfactory in two limits: (1) in the chiral limit $H \to 0$, where $M_{0,s}$ deviates from the constant $\mathcal{F}_{M_0}(H = 1)$, but does not contribute to M_s, and (2) in the limit $H \to 1$, where we find $M_{0,s}$ indeed to be almost constant and M_s drops to zero. The ansatz for M_s shown on the left in Fig. 5.20 interpolates between these well-behaved limits for intermediate values of H in an acceptable way, as becomes clear when comparing the fit coefficients of M_0 and M_s. We conclude that the physical strange quark mass is in the reach of chiral perturbation theory.

The fit ansatz of the order parameter M_c with the connected part subtraction

$$\mathcal{F}_{M_c}(H) = a_{M_c} + b_{M_c} H^{1/2} + c_{M_c} H, \qquad a_{M_c} \stackrel{!}{=} a_{M_0},\ b_{M_c} \stackrel{!}{\lesssim} b_{M_0},\ c_{M_c} \stackrel{!}{=} (c_{M_0} - c_{\mathcal{U}} m_s^2/T^4) \quad (5.3.7)$$

is justified by the assumption that in the continuum limit, $b_{M_c} = b_{M_0}$, as there are no Goldstone modes present in the connected part.

We will now discuss they physical significance of the fit coefficients in detail:

(a) The fit coefficient $\bar a = \langle\bar\psi\psi\rangle_0$ gives the chiral condensate in the chiral limit, which also determines the limit of all order parameters M_i:

$$a = \lim_{H\to 0} M_0 = \lim_{H\to 0} M_s = \lim_{H\to 0} M_c = m_s \langle\bar\psi\psi\rangle_0 / T^4, \qquad a = \bar a \hat m_s N_\tau^4. \quad (5.3.8)$$

Hence we expect to recover the same fit parameter a for all order parameters, see Fig. 5.19. Above the critical coupling β_c, a becomes negative, which is not unexpected because the GS fit ansatz breaks down here.

(b) The fit coefficient b is the prefactor of the Goldstone term and becomes large at β_c. If we assume that a three-dimensional Goldstone ansatz as given in Eq. (3.2.13) is valid in the vicinity of

the chiral transition, and this term is linear in temperature, as shown in Eq. (4.2.67), we may write:

$$\begin{aligned}
\left\langle\bar{\psi}\psi\right\rangle_l(T,m_l) &= \left\langle\bar{\psi}\psi\right\rangle_0(T)\left(1+T\frac{N_\mathrm{f}^2-1}{8\pi}\frac{\left(\left\langle\bar{\psi}\psi\right\rangle_0(T)m_l\right)^{1/2}}{F_0^3(T)}\right)+\mathcal{O}(m_l),\\
M_0 &= \frac{m_s}{T^4}\left\langle\bar{\psi}\psi\right\rangle_0(T)\left(1+T\frac{N_\mathrm{f}^2-1}{8\pi}\frac{\left(\left\langle\bar{\psi}\psi\right\rangle_0(T)Hm_s\right)^{1/2}}{F_0^3(T)}\right)+\mathcal{O}(H),\\
a &= \frac{m_s}{T^4}\left\langle\bar{\psi}\psi\right\rangle_0(T), \qquad b=\frac{m_s}{T^3}\frac{N_\mathrm{f}^2-1}{8\pi}\frac{\left(\left\langle\bar{\psi}\psi\right\rangle_0(T)^3m_s\right)^{1/2}}{F_0^3(T)},\\
\Longrightarrow \qquad b/a^{3/2} &= \frac{N_\mathrm{f}^2-1}{8\pi}\frac{T^3}{F_0^3(T)},
\end{aligned} \tag{5.3.9}$$

where $\left\langle\bar{\psi}\psi\right\rangle_0(T)=\left\langle\bar{\psi}\psi\right\rangle_l(t,h=0)\sim|t|^\beta$ is the chiral condensate in the chiral limit. With $T\simeq T_\mathrm{c}$ being a proportionality constant, we expect the ratio $b/a^{3/2}\sim 1/F_0^3$ to diverge when approaching T_c, because $F_0\sim|t|^{\nu/2}$ on the coexistence line below T_c (in an effectively three dimensional system) such that F_0 vanishes in this limit. In fact, this behavior can be derived from the Goldstone prefactor of the scaling function, as given in Eq. (3.3.19). Re-expressed in the reduced scaling variables h, t which we will discuss in detail in the next section, we have

$$a=|t|^\beta, \qquad b=|t|^{\beta(1-\delta/2)}\beta\tilde{c}_2h_0^{-1/2} \tag{5.3.10}$$

$$\Longrightarrow \qquad b/a^{3/2}=|t|^{-\beta(1+\delta)/2}\beta\tilde{c}_2h_0^{-1/2}\equiv c_{F_0}|t|^{-3\nu/2}, \tag{5.3.11}$$

because $\beta(\delta+1)=d\nu$ and we consider the $d=3$ O(2) scaling function. Hence we indeed find the correct scaling of the pion decay constant and are even in the position to determine its value from the normalization constants of the scaling variables. A preliminary result of the fit for $N_\tau=4$ is given in Tab. 5.7. For $N_\tau=8$ we were not able to extract fit parameters, due to th mass gap in the critical region.

c_{F_0}	β_c
0.0354(21)	3.3023(11)
0.0491(55)	3.3023(12)
0.0210(26)	3.3015(19)

Table 5.7: Fit results for the ratio $b/a^{3/2}=c_{F_0}(\beta_c-\beta)^{3\nu/2}$.

We noted that the Goldstone prefactor of M_c should coincide with that of M_0 in the continuum limit. On coarse lattice we expect $b_{M_c}<b_{M_0}$, which is indeed found, see top of Fig. 5.19. If the prediction of SχPT is correct and the disconnected and connected part should have the same Goldstone prefactor, then we expect $b_{M_c}=3/4b_{M_0}$ (subtracting the full susceptibility would yield $b_{M_c}=1/2b_{M_0}$, an extra factor 1/2 is provided by the derivative of the square root.) We find however, that not the ratio is constant (for the two smallest β values we find $b_{M_c}/b_{M_0}\simeq 0.65$ for $N_\tau=4$ and $b_{M_c}/b_{M_0}\simeq 0.45$ for $N_\tau=8$), but the difference $b_\mathrm{con}\equiv b_{M_0}-b_{M_c}$is constant in the whole β range. We find $b_\mathrm{con}=1.04(2)$ for $N_\tau=4$ and $b_\mathrm{con}=1.20(11)$ for $N_\tau=8$. The reason for this may be that the connected Goldstone prefactor is much less temperature dependent than the disconnected part as it will not contribute to the critical behavior at T_c, and $b_\mathrm{con}/a_{M_c}^{3/2}$ is not expected to diverge with exponent $3\nu/2$ if the connected part does not contribute to the scaling function.

(c) The fit coefficient c parameterizes the sum of both the physical and unphysical (UV-divergent) linear quark mass dependence. In Fig. 5.19 one can clearly see that the subtracted order parameter M_s has a strongly reduced linear term, as expected, whereas the parameter c of M_c is only shifted w.r.t M_0 and is only zero at $\beta=3.28$. The UV divergence in M_c may be removed, but not the complete linear term. It is plotted on the right in Fig. 5.20. If the

UV-divergence is the dominant part of the linear term, then we expect that the difference of the fit coefficients $c_{M_0} \simeq (c_2(T) + c_{\mathcal{UV}})m_s^2/T^4$ and $c_{M_c} \simeq (c_2(T))m_s^2/T^4$ is approximately the value of $\tilde{c}_{\mathcal{UV}}^{(N_\tau)}$. We find that the difference is almost the same over the whole β range and we determined its value $c_{M_0} - c_{M_c} = 0.32(2)$ for $N_\tau = 4$ and and $c_{M_0} - c_{M_c} = 3.38(9)$ for $N_\tau = 8$. It is not clear what the origin of this large discrepancy is. The fact that both coefficient c_{M_0} and c_{M_c} drop rapidly with temperature is most likely a fit artifact, as the fit ansätze are not able to capture critical scaling.

The Goldstone fits for the $N_\tau = 8$ data are less satisfactory. Note that we have not reweighted the data in the Goldstone region to the bare strange mass $\hat{m}_s = 0.024$, but left it at $\hat{m}_s = 0.029$, because reweighting introduces further uncertainties. This may explain why a gap in all fit coefficients appears. In the Goldstone region, where M_0 is still large, the fit branches do not show the typical proportionality $\sim m_l^{1/2}$, but they are slightly deformed, indicating a large linear term $\sim m_l$. This is also apparent by comparing the fit parameters b_{M_0} and c_{M_0}. It is not clear whether this behavior persists if further data for smaller quark masses were available. If one corrects for the apparent defect in $N_\tau = 8$ when comparing the fit parameters of M_0 for $N_\tau = 4$ and $N_\tau = 8$, both a_{M_0} and b_{M_0} are compatible. c_{M_0} is less compatible, and it is still not possible to identify the two contributions $c(T) = c_{\text{phys}}(T) + c_{\mathcal{UV}}$.

5.3.2 Goldstone Fits for the Chiral Susceptibilities

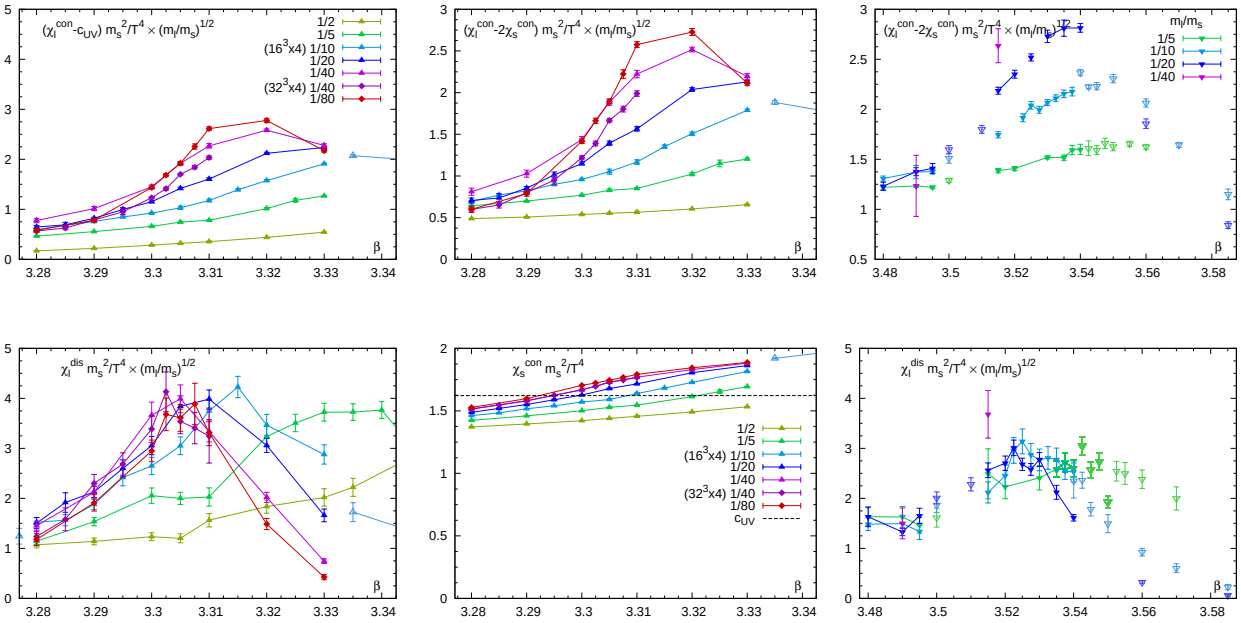

Figure 5.21: Chiral susceptibilities rescaled with a factor $(m_l/m_s)^{1/2}$ such that Goldstone scaling is apparent from the overlap of the data. Disconnected part (left bottom) and connected part, from which $\tilde{c}_{\mathcal{UV}}^{(4)}$ was subtracted before rescaling (left top), or the strange connected part (center top), which takes a very similar value as $\tilde{c}_{\mathcal{UV}}^{(4)}$ (center bottom). Goldstone scaling is also seen for the $N_\tau = 8$ disconnected and connected parts (right).

A first evidence for Goldstone scaling in both susceptibilities is obtained by multiplying χ_l^{dis} and $\chi_l^{\text{con}} - \tilde{c}_{\mathcal{UV}}^{(N_\tau)}$ with a factor $(m_l/m_s)^{1/2}$ and identify the region where the data for intermediate and small quark masses overlap. This is shown in Fig. 5.21. Indeed, the subtraction of $c_{\mathcal{UV}}$ is sufficient to establish GS in χ_l^{con}, only the connected part of the lattice $16^3 \times 4$, $H = 1/40$ is ill-behaved as it has

substantial finite size effects. We emphasize that GS in $\chi_l^{\rm con}$ is a lattice artifact and results from taste breaking. The difference $\chi_l^{\rm con} - \chi_s^{\rm con}$ is expected to be free of a UV-divergent term, multiplied with $(m_l/m_s)^{1/2}$ it also exhibits GS. The disconnected susceptibility shows GS for $\beta \lesssim \beta_c$, and remarkably it does not show critical scaling $\sim m_l^{1/\delta-1}$ along the pseudocritical line. The interference with GS might explain why it is difficult to observe critical scaling. Also, the statistics becomes poor as we approach the chiral limit, hence the data are not conclusive on this issue. We have argued that GS is part of the scaling function, but for intermediate masses GS dominates for $T \lesssim T_{\rm c}$, and only in the chiral limit one might clearly observe critical scaling.

The fits for the susceptibilities, shown in Fig. 5.22, are derived from the ansätze for the condensates. They are the derivatives and hence the fit-coefficients of the full susceptibilities χ_{M_i} should be comparable to those of the order parameters M_i:

$$\mathcal{G}_{\chi_{M_0}}(H) \equiv \frac{\partial}{\partial H}\mathcal{F}_{M_0}(H) = \frac{1}{2}b_{\chi_{M_0}}H^{-1/2} + c_{\chi_{M_0}}, \tag{5.3.12}$$

$$\mathcal{G}_{\chi_{M_s}}(H) \equiv \frac{\partial}{\partial H}\mathcal{F}_{M_s}(H) = \frac{1}{2}b_{\chi_{M_s}}H^{-1/2} - a_{\chi_{M_s}} - b_{\chi_{M_s}}, \tag{5.3.13}$$

$$\mathcal{G}_{\chi_{M_c}}(H) \equiv \frac{\partial}{\partial H}\mathcal{F}_{M_c}(H) = \frac{1}{2}b_{\chi_{M_c}}H^{-1/2} + c_{\chi_{M_c}}. \tag{5.3.14}$$

Note that the fit parameters a_{M_0} and a_{M_c} drop out, and we also remove c_{M_s}, as it is expected and found to be zero. Hence we are left with 2-parameter fits. One should not expect them to be extraordinarily good, but if we introduced an additional quadratic term (corresponding to a cubic term in M_i), at this stage we would not be in the position to compare the Goldstone prefactors with those of the condensate. The connected and disconnected parts of χ_{M_i}, $i \in \{0, s, c\}$, as defined in Eqs. (5.2.25), (5.2.30), (5.2.35), are fitted with the same ansatz as the full susceptibility. We expect to find for $i \in \{0, s, c\}$ and $j \in \{0, c\}$:

$$a_{\chi_{M_s}} \stackrel{!}{=} a_{\chi^{\rm con}_{M_s}} + a_{\chi^{\rm dis}_{M_s}} \stackrel{!}{=} a_{M_s}, \quad b_{\chi_{M_i}} \stackrel{!}{=} b_{\chi^{\rm con}_{M_i}} + b_{\chi^{\rm dis}_{M_i}} \stackrel{!}{=} b_{M_i}, \quad c_{\chi_{M_j}} \stackrel{!}{=} c_{\chi^{\rm con}_{M_j}} + c_{\chi^{\rm dis}_{M_j}} \stackrel{!}{=} c_{M_j}. \tag{5.3.15}$$

Indeed we find qualitatively similar behavior when comparing the fit coefficients. One can also see how the coefficients of the full susceptibility are composed of the sum of the coefficients of its disconnected and connected part. Note that the disconnected coefficient $c_{\chi_{M_0^{dis}}}$ has a much smaller (indeed negative) value, as compared to the connected coefficient $c_{\chi_{M_0^{con}}}$, which is somewhat lower than the expected value $\tilde{c}^{(4)}_{\mathcal{UV}} = 1.6224$.

Comparing the Goldstone fit coefficient of the disconnected and connected parts yields that $b_{M_0^{\rm dis}}$ is about twice as large as $b_{M_0^{\rm con}}$, which seems to contradict our prediction that on a coarse lattice they should be equal. However, at this stage we have not included taste violations in the fit. Both $b_{M_0^{\rm con}}$, $b_{M_0^{\rm dis}}$ might still be sensitive to pseudo-Goldstone boson in other taste-channels in the mass range considered, or the constant term is interfering. In contrast, $b_{M_s^{\rm dis}}$ and $b_{M_s^{\rm con}}$ are similar in magnitude, which may be an improvement due to elimination of all constants coming from the linear term. We also find that $b_{M_c^{\rm con}}$ does not show any GS, which is expected as it does not contain the usual connected susceptibility (see the definition Eq. (5.2.35)).

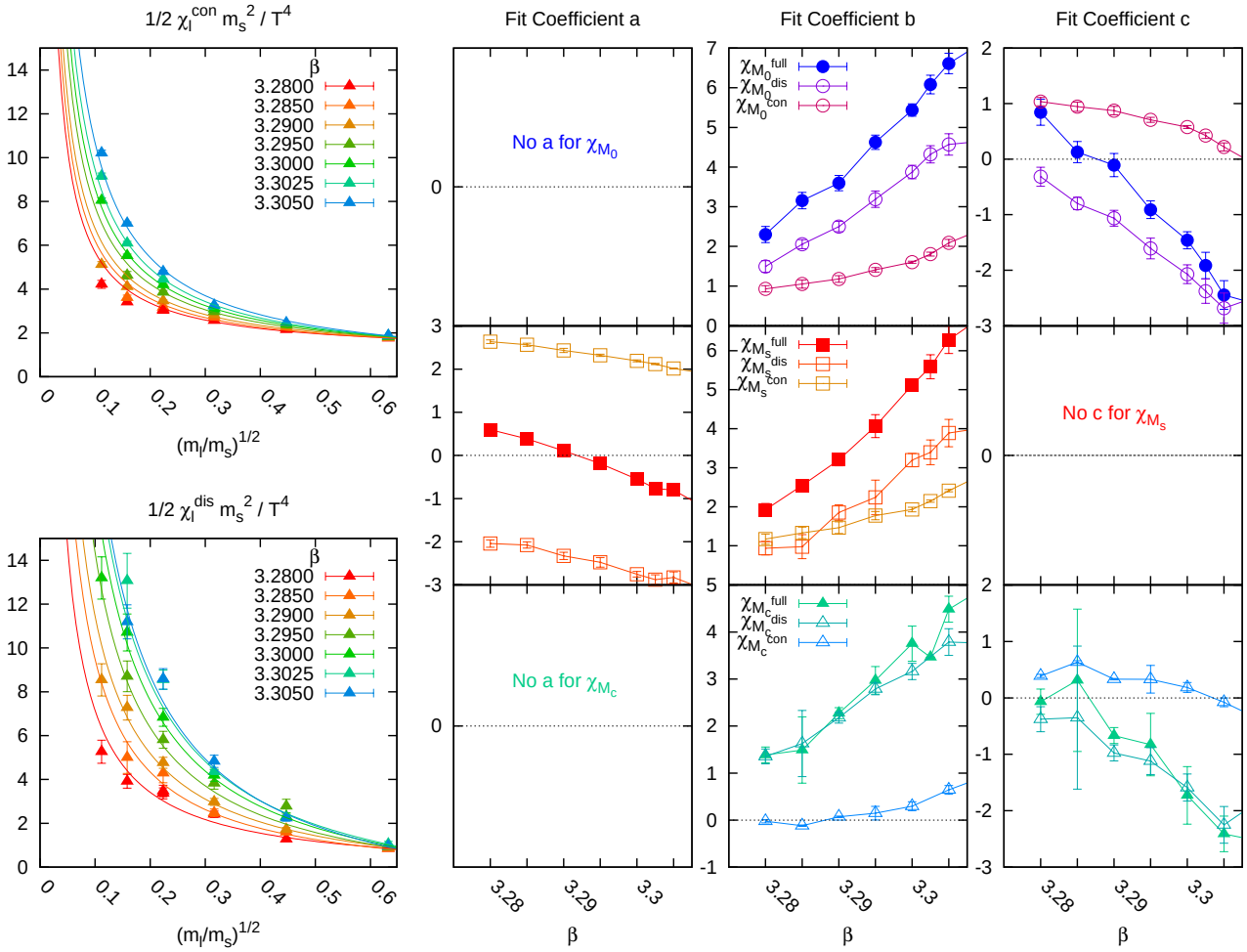

Figure 5.22: Comparison of fit coefficients for the susceptibilities ($N_\tau = 4$). On the left we show the 2=parameter fits for the connected and disconnected susceptibilities, on the right the results for the parameters are displayed, for M_0 (top), M_s (center) and M_c (bottom). The normalization allows direct comparison between the coefficients of the full susceptibilities and those of the condensates, Fig. 5.19.

The Goldstone analysis of the $N_\tau = 8$ susceptibility data suffers from the very limited mass range. The fits are not as well under control, hence we will not discuss them here in detail. One can see that the fit results for χ_{M_0} shown in Fig. 5.23 are comparable to those of $N_\tau = 4$ and with the $N_\tau = 8$ condensate fits. Remarkably, the constant $c_{\chi_{M_0^{\rm con}}} \simeq 4.2$ is close to the expected value $\tilde{c}^{(8)}_{\mathcal{U}\mathcal{N}} = 3.539$, and we find $b_{\chi_{M_0^{\rm con}}} \simeq b_{\chi_{M_0^{\rm dis}}}$ across the whole β region.

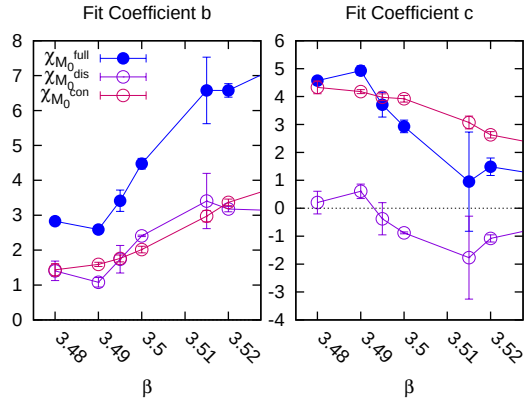

Figure 5.23: Fit coefficients for the χ_{M_0} susceptibilities ($N_\tau = 8$).

5.3.3 Estimate of Taste Breaking Effects in Chiral Observables

We have shown in the previous section that the Goldstone prefactors from the simplistic fit ansatz Eq. (5.3.2) already allows a physical interpretation. It might be useful to investigate, whether SχPT also gives reasonable predictions at finite temperature. In particular we want to understand how Goldstone modes in the connected susceptibility begin to cancel and eventually vanish in the continuum limit. Since the statistical errors of the connected susceptibility are quite small, we attempt to estimate by a joint fit ansatz the magnitude of taste splittings.

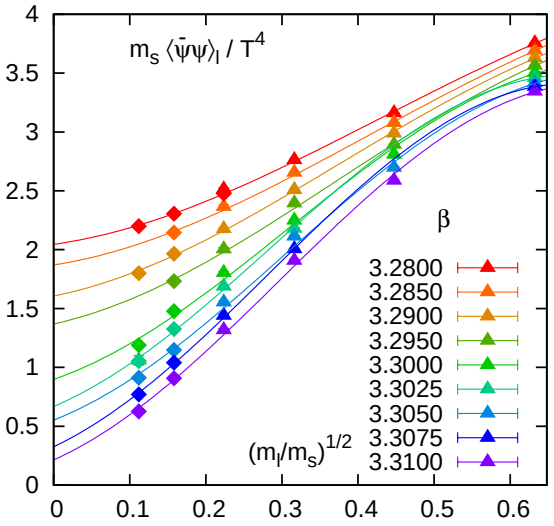

Figure 5.24: Goldstone multibranch fit for chiral condensate and connected/disconnected susceptibility, including an effective taste splitting Δ. The full susceptibility is indicated as small arrows, visualized as the derivative.

We also expect contributions from other heavy modes such as kaons and the eta. They are hard to discriminate from taste breaking, as they both show up as additional constants within the square root of the GMOR expression for the pseudoscalar meson masses, e.g. $\mathring{M}_K \sim \sqrt{H+1}$, $\mathring{M}_{\pi,t} \sim \sqrt{H + \Delta_t a^2/m_s}$. Only by a comparison of lattices with different lattice spacings one can hope to distinguish those constants independent of the lattice spacing from the taste splittings $\sim a^2$. This will be attempted in the next section. Here we will perform a simpler fit, neglecting the other pseudoscalar mesons for the moment, and discuss only $N_\tau = 4$.

It is impossible to fit all parameters which arise in the chiral condensate and the bubble term expressions for the susceptibilities according to SχPT. However, by assuming that in all taste channels apart from $t = P$ the taste violations are of the same magnitude, $\Delta_t = \Delta_{\text{eff}}$ for $t = \text{I}, \text{V}, \text{A}, \text{T}$, and assuming that hairpin diagrams in the I,V,A channels do not play a major role, one can make use of the following effective parameterization of taste violations which can be fitted to our data. Only taking the pion modes into account, the corresponding ansätze for the light chiral condensate and the chiral susceptibilities are

$$\Pi_{M_0}(H,\beta) = a(\beta) + b(\beta)\left[\frac{1}{12}H^{1/2} + \frac{11}{12}\left((H+\Delta)^{1/2} - \Delta^{1/2}\right)\right] +, c(\beta)H \tag{5.3.16}$$

$$\Pi_{\chi^{\text{full}}_{M_0}}(H,\beta) = \frac{b(\beta)}{2}\left[\frac{1}{12}H^{-1/2} + \frac{11}{12}\left((H+\Delta)^{-1/2}\right)\right] + c(\beta), \tag{5.3.17}$$

$$\Pi_{\chi^{\text{dis}}_{M_0}}(H\beta) = \frac{b(\beta)}{2}\left[\frac{1}{24}H^{-1/2} + \frac{23}{24}\left((H+\Delta)^{-1/2}\right)\right] + c^{\text{dis}}(\beta), \tag{5.3.18}$$

$$\Pi_{\chi^{\text{con}}_{M_0}}(H\beta) = \frac{b(\beta)}{2}\left[\frac{1}{24}H^{-1/2} - \frac{1}{24}\left((H+\Delta)^{-1/2}\right)\right] + c^{\text{con}}(\beta), \tag{5.3.19}$$

where $\Delta = \Delta_{\text{eff}} a^2/M_S^2$. The subtraction of $\sqrt{\Delta}$ in Eq. (5.3.16) ensures that the value of a, i.e. the chiral condensate in the chiral limit, is not affected by the value of Δ. If $\Delta = 0$, we recover the former fit ansatz, valid in the continuum limit. The coefficient $z_{\text{PS}} = 1/12$ is the weight for the true Goldstone boson in the pseudoscalar taste channel, and $z_{\text{NPS}} = 11/12$ is the weight for all the other taste channels. They are fixed by the relations $z_{\text{PS}} + z_{\text{NPS}} = 1$ and $z_{\text{PS}} : z_{\text{NPS}} = 1 : 11$, as discussed in Sec. 4.4.5. We performed a multibranch fit, i.e. a joint fit of the condensate and susceptibility data. The result for the condensate is shown in Fig. 5.3.3. Note that in contrast to the previous fits,

the same b is fitted in all chiral observables, and only $c = c^{\rm dis} + c^{\rm con}$ is additive. From the fit we obtain $\Delta = 0.3(1)$, which translates to $\Delta_{\rm eff} a^2 = 200(70)$ MeV on the $N_\tau = 4$ lattice. This should correspond to the average pion mass on this coarse lattice in the chiral limit. We expect that for $N_\tau = 8$ this additional unphysical mass term is reduced by a factor 4.

5.3.4 SχPT Fits of Chiral Observables

We now turn to the more refined full SχPT fit which includes kaon and eta modes, as they also contribute to the quark mass dependence of chiral observables. We have performed a joint fit of the chiral observables, M_0, $\chi^{\rm con}_{M_0}$, $\chi^{\rm dis}_{M_0}$ and $M_{0,s}$, $\chi^{\rm con}_{M_{0,s}}$, $\chi^{\rm dis}_{M_{0,s}}$ for both $N_\tau = 4$ and $N_\tau = 8$. According to the results of SχPT, Sec. 4.4.5, which are summarized in Tab. 4.3, the fit ansätze for the condensates are

$$\mathcal{F}_{M_0}(H,\beta) = a(\beta)\left\{1 + b(\beta)\left(4\mathcal{I}_\pi(H) + 2\mathcal{I}_K(H) - \mathcal{I}_K(H) + \frac{1}{3}\mathcal{I}_\eta(H)\right)\right\}, \\ + K_{1,l}(\beta)(2H+1) + K_{2,l}(\beta)H \tag{5.3.20}$$

$$\mathcal{F}_{M_{0,s}}(H,\beta) = a(\beta)\left\{1 + b_s(\beta)\left(4\mathcal{I}_\pi(H) + 2\mathcal{I}_K(H) - \mathcal{I}_K(H) + \frac{1}{3}\mathcal{I}_\eta(H)\right)\right\} \\ + K_{1,s}(\beta)(2H+1) + K_{2,s}(\beta), \tag{5.3.21}$$

and for the susceptibilities they are

$$\mathcal{G}_{\chi^{\rm con}_{M_0}}(H,\beta) = \frac{a(\beta)b(\beta)}{2}\left(2\mathcal{T}'_{\pi\pi}(H) + \mathcal{T}'_{KK}(H) - 2\mathcal{I}'_{\pi\pi}(H) + \frac{2}{3}\mathcal{I}'_{\pi\eta}(H)\right) + K_{2,l}(\beta) + K_3 H, \tag{5.3.22}$$

$$\mathcal{G}_{\chi^{\rm dis}_{M_0}}(H,\beta) = \frac{a(\beta)b(\beta)}{2}\left(\mathcal{T}'_{\pi\pi}(H) + \frac{1}{2}\mathcal{I}'_{\pi\pi}(H) - \frac{1}{3}\mathcal{I}'_{\pi\eta}(H) + \frac{1}{18}\mathcal{I}'_{\eta\eta}(H)\right) + K_{1,l}(\beta) - \frac{1}{2}K_3 H, \tag{5.3.23}$$

$$\mathcal{G}_{\chi^{\rm con}_{M_{0,s}}}(H,\beta) = \frac{a(\beta)b_s(\beta)}{2}\left(2\mathcal{T}'_{KK}(H) + \mathcal{T}'_{SS}(H) - 4\mathcal{I}'_{SS}(H) + \frac{8}{3}\mathcal{I}'_{S\eta}(H)\right) + K_{2,s}(\beta), \tag{5.3.24}$$

$$\mathcal{G}_{\chi^{\rm dis}_{M_{0,s}}}(H,\beta) = \frac{a(\beta)b_s(\beta)}{2}\left(\mathcal{T}'_{SS}(H) + 2\mathcal{I}'_{SS}(H) - \frac{8}{3}\mathcal{I}'_{S\eta}(H) + \frac{8}{9}\mathcal{I}'_{\eta\eta}(H)\right) + K_{1,s}(\beta), \tag{5.3.25}$$

where the functions $\mathcal{T}_P(H)$,$\mathcal{T}'_P(H)$ and $\mathcal{I}_P(H)$,$\mathcal{I}'_P(H)$ are defined as follows:

$$\mathcal{T}_P(H) = \frac{1}{16}M_P^2(H) + \frac{15}{16}\left(\sqrt{M_P^2(H)+\Delta} - \sqrt{\Delta}\right), \tag{5.3.26}$$

$$\mathcal{T}'_{PQ}(H) = \frac{1/16}{M_P(H)+M_Q(H)} + \frac{15/16}{\sqrt{M_P^2(H)+\Delta}+\sqrt{M_Q^2(H)+\Delta}}, \tag{5.3.27}$$

$$\mathcal{I}_P(H) = \sqrt{M_P^2(H)+\Delta_{\rm I}}, \qquad \mathcal{I}'_{PQ}(H) = \frac{1}{\sqrt{M_P^2(H)+\Delta_{\rm I}}+\sqrt{M_Q^2(H)+\Delta_{\rm I}}}, \tag{5.3.28}$$

$$M_\pi(H) = \sqrt{H}, \qquad M_K(H) = \sqrt{(H+1)/2}, \qquad M_\eta(H) = \sqrt{(H+2)/3}.. \tag{5.3.29}$$

All observables are 1-flavor normalized. The terms $\mathcal{T}_P$ and $\mathcal{T}'_{PP}$ sum over all taste channels, whereas $\mathcal{I}_P$ and $\mathcal{I}'_{PP}$ are only the iso-singlet contribution which results from the partial fraction expansion of the disconnected meson propagators, as discussed in Sec. 4.4.5. In this fit ansatz we assume that in the Goldstone region, all modes $\hat{\mu}_{P,t}$, $\hat{\mu}_{PQ,t}$ with $P,Q \in \{\pi, K, \eta\}$ as defined in Eq. (4.4.39) are essentially of the form

$$\hat{\mu}_{P,t} \sim T\mathring{M}_{P,t}, \qquad \hat{\mu}_{PQ,t} \sim T/(\mathring{M}_{P,t} + \mathring{M}_{Q,t}), \tag{5.3.30}$$

β	a	b	$K_{1,l}$	$K_{2,l}$	$K_{1,s}$	$K_{2,s}$
3.2800	1.66(3)	2.40(20)	-3.21(23)	-1.56(33)	3.00(22)	1.73(30)
3.2850	1.45(4)	3.19(31)	-3.76(30)	-2.13(41)	3.44(28)	2.12(36)
3.2900	1.05(3)	5.14(42)	-4.34(30)	-2.86(41)	3.98(28)	2.61(36)
3.4800	3.70(8)	0.77(7)				
3.4900	3.19(7)	0.90(8)	-3.52(27)	7.57(36)	3.72(23)	-1.93(31)
3.4950	2.96(8)	0.98(9)				

β-indep.	coeffs.
b_S	0.31(2)
Δ	0.28(3)
$K_3^{(N_\tau=4)}$	0.27(9)
$K_3^{(N_\tau=8)}$	2.60(22)

Table 5.8: Fit results for multibranch fit of all pseudoscalar meson modes and taste breaking term, inspired by SχPT.

where the temperature is more or less constant. We note that deviations from this fit ansatz are expected since (a) the taste splittings Δ_t take in general very different values, (b) we have neglected the effect of hairpin diagrams due to non-zero couplings δ_V, δ_A, (c) the coupling which accounts for the 't Hooft vertex $\delta_I = 4m_0^2/3$ was set to infinity, such that the η' remains heavy, and (d) we have neglected higher order terms $\mathcal{O}\left(T, \mathring{M}_{P,t}^3\right)$. Although we have attempted to take into account these effects and in general obtain improved fits, the results lack systematics as there are too many fit parameters involved.

The taste splittings Δ and Δ_I are assumed to be independent of the temperature in the transition region. Here we will present only results for $\Delta = \Delta_I$, which simplifies the fit ansatz even further. In contrast, the fit coefficients a,b, $K_{1,q}$ and $K_{2,q}$ are temperature dependent, hence for each β value we have one fit variable. We only considered values below β_c, for $N_\tau = 4$ we chose $\beta = 3.28$, $\beta = 3.285$ and $\beta = 3.29$ and for $N_\tau = 8$ we chose $\beta = 3.48$, $\beta = 3.49$ and $\beta = 3.495$, to ensure that we only expect true GS scaling. $K_{1,q}$ is the coefficient for the valence quark mass, whereas $K_{2,q}$ is the coefficient for the sum of the sea quark masses. Actually one would expect $K_{1,l} = K_{1,s}$ and $K_{2,l} = K_{2,s}$, but the approximations in the above fit ansätze generate a large number of additional linear terms which interfere with the physical linear terms. It is therefore not possible to estimate the linear terms or even the UV-divergent contribution with the above fit ansatz. It was also necessary to include a linear term for the light connected and disconnected susceptibilities of opposite sign (thus no quadratic term arises in the light condensate), again to account for fit artifacts. We have ensured that all these modifications do not interfere with the determination of Δ. We have only included the quark masses with $H \leq 1/5$ in the fit, but it is also possible to account for the larger quark masses by including cubic terms in the condensates. Those fits result in a similar value for Δ, although they are less under control.

The result of the above fit is given in Tab. 5.8 and shown in Fig. 5.26. Also here, a value of $\Delta \simeq 0.3$ is favored. In order to understand the systematics of these fits, we have checked the dependence of the fits on various additional parameters, e.g. we have $\Delta \neq \Delta_I$, where we obtain that Δ is somewhat smaller than Δ_I, but still in the range $0.15 < \Delta_I < 0.3$. In the above fit we have forced $\Delta_{\text{eff}}^{(N_\tau=4)}/\Delta_{\text{eff}}^{(N_\tau=8)} = 4$. We observe that the joint fit is consistent with this expectation: although a fit of the ratio as an additional fit variable yields $\Delta_{\text{eff}}^{(N_\tau=4)}/\Delta_{\text{eff}}^{(N_\tau=8)} \simeq 2.1(8)$ rather than 4, the reduced $\chi^2 = 7.13$ is not much smaller than for the fit with a fixed ratio, which yields $\chi^2 = 7.21$.

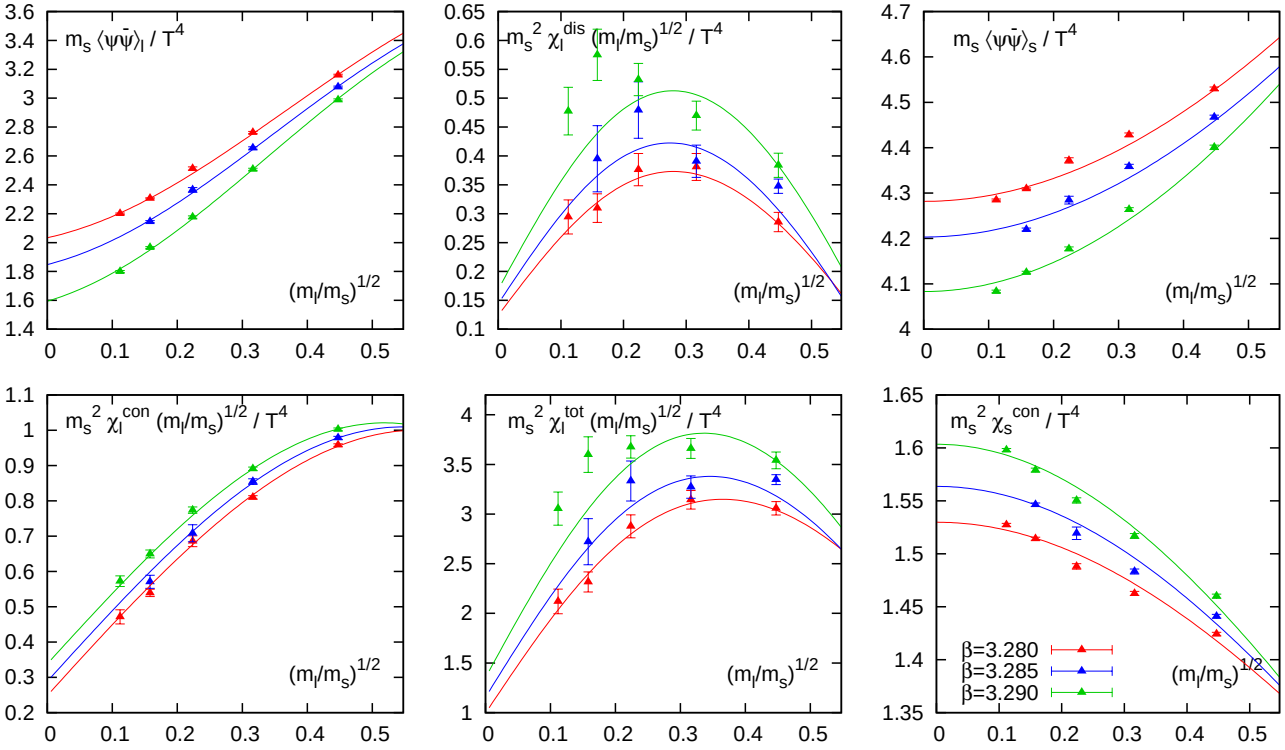

Figure 5.25: Multibranch fit of effective taste breaking term Δ_{eff} in the Goldstone region for $N_\tau = 4$, according to fit ansatz Eq. (5.3.29)

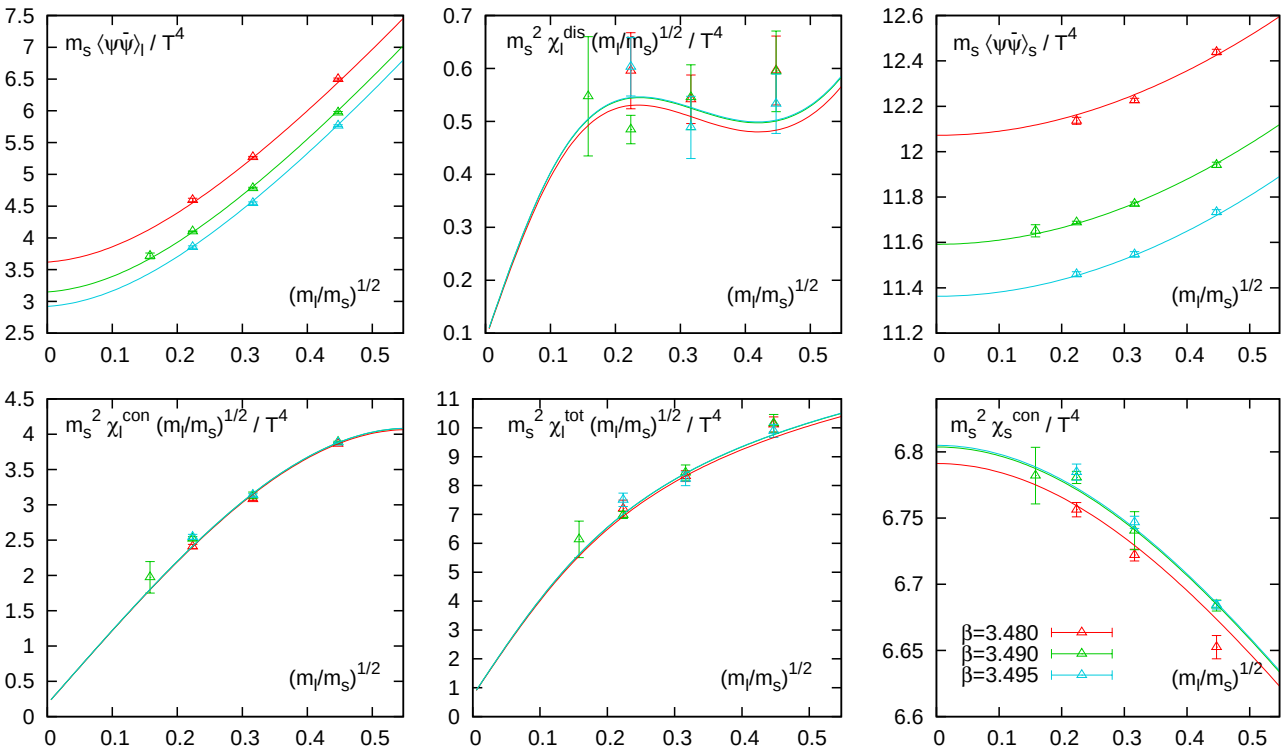

Figure 5.26: Multibranch fit of effective taste breaking term Δ in the Goldstone region for $N_\tau = 4$, according to fit ansatz Eq. (5.3.29)

5.4 The Universality Class

5.4.1 Binder Cumulant

One of the simplest methods to determine the universality class of a second order transition is to calculate the Binder cumulant of the order parameter at the critical coupling. For the light quark chiral condensate it is defined as

$$B_4 \equiv \frac{\left\langle (\delta\bar{\psi}\psi)^4 \right\rangle_{\beta_c}}{\left\langle (\delta\bar{\psi}\psi)^2 \right\rangle^2_{\beta_c}}, \qquad \delta\bar{\psi}\psi = \bar{\psi}\psi - \left\langle \bar{\psi}\psi \right\rangle . \tag{5.4.1}$$

As we expect to approach the universal value only in the chiral limit, we are confronted with the situation that the Binder cumulant takes a universal value different from the value often quoted in the literature, i.e. the value valid for a temperature driven transition strictly at $H = 0$. One can only recover this value in simulations without an external symmetry breaking field, which is possible in O(N) spin models, but not in LQCD. Hence one needs to consider a refinement, which takes into account that the quark masses break the rotation invariance of the O(N)-symmetric field, as was already discussed in in Sec. 3.3.3, results in a new value of the Binder cumulant. For O(2), the value we eventually want to compare with is $B_4^r = 1.863(3)$.

The Binder cumulant in lattice QCD has usually been measured with the contributions of the disconnected graphs only. It is a priori not clear whether this will guarantee the fastest convergence to the universal value as we go to the chiral limit. To check this, we include the connected contributions as well. We expand the fourth moment of the fluctuation:

$$\begin{aligned}
\left\langle (\delta\bar{\psi}\psi)^4 \right\rangle &= \left\langle \bar{\psi}(x)\psi(x)\bar{\psi}(y)\psi(y)\bar{\psi}(z)\psi(z)\bar{\psi}(w)\psi(w) \right\rangle - 4\left\langle \bar{\psi}(x)\psi(x)\bar{\psi}(y)\psi(y)\bar{\psi}(z)\psi(z)\left\langle \bar{\psi}\psi \right\rangle \right\rangle \\
&\quad + 6\left\langle \bar{\psi}(x)\psi(x)\bar{\psi}(y)\psi(y)\left\langle \bar{\psi}\psi \right\rangle^2 \right\rangle - 4\left\langle \bar{\psi}(x)\psi(x)\left\langle \bar{\psi}\psi \right\rangle^3 \right\rangle + \left\langle \bar{\psi}\psi \right\rangle^4 \\
&\equiv \xi^{(0)}_{\bar{\psi}\psi} + \xi^{(1)}_{\bar{\psi}\psi} + \xi^{(2)}_{\bar{\psi}\psi} + \xi^{(3)}_{\bar{\psi}\psi} + \xi^{(4)}_{\bar{\psi}\psi}
\end{aligned} \tag{5.4.2}$$

After Wick contraction we find:

$$\begin{aligned}
\xi^{(0)}_{\bar{\psi}\psi} =& 6\left\langle \bar{\psi}\overbrace{(x)\psi(x)\bar{\psi}(y)\psi(y)\bar{\psi}(z)\psi(z)\bar{\psi}(0)\psi(0)} \right\rangle + 8\left\langle (\bar{\psi}\psi)\bar{\psi}\overbrace{(x)\psi(x)\bar{\psi}(y)\psi(y)\bar{\psi}(0)\psi(0)} \right\rangle \\
&+ 3\left\langle \left(\bar{\psi}\overbrace{(x)\psi(x)}\bar{\psi}\overbrace{(0)\psi(0)}\right)^2 \right\rangle + 6\left\langle (\bar{\psi}\psi)^2\bar{\psi}\overbrace{(x)\psi(x)}\bar{\psi}\overbrace{(0)\psi(0)} \right\rangle + \left\langle (\bar{\psi}\psi)^4 \right\rangle ,
\end{aligned} \tag{5.4.3}$$

$$\begin{aligned}
\xi^{(1)}_{\bar{\psi}\psi} =& -4\left[2\left\langle \bar{\psi}\overbrace{(x)\psi(x)\bar{\psi}(y)\psi(y)\bar{\psi}(0)\psi(0)} \right\rangle \left\langle \bar{\psi}\psi \right\rangle \right. \\
&\left. + 3\left\langle (\bar{\psi}\psi)\bar{\psi}\overbrace{(x)\psi(x)}\bar{\psi}\overbrace{(0)\psi(0)} \right\rangle \left\langle \bar{\psi}\psi \right\rangle + \left\langle (\bar{\psi}\psi)^3 \right\rangle \left\langle \bar{\psi}\psi \right\rangle \right] ,
\end{aligned} \tag{5.4.4}$$

$$\xi^{(2)}_{\bar{\psi}\psi} = 6\left[\left\langle \bar{\psi}\overbrace{(x)\psi(x)}\bar{\psi}\overbrace{(0)\psi(0)} \right\rangle \left\langle \bar{\psi}\psi \right\rangle^2 + \left\langle (\bar{\psi}\psi)^2 \right\rangle \left\langle \bar{\psi}\psi \right\rangle^2 \right] , \tag{5.4.5}$$

$$\xi^{(3)}_{\bar{\psi}\psi} + \xi^{(4)}_{\bar{\psi}\psi} = -3\left\langle \bar{\psi}\psi \right\rangle^4 . \tag{5.4.6}$$

We can collect the contributions of fully disconnected graphs:

$$\xi^{\text{disc.}}_{\bar{\psi}\psi} = \left[\left\langle (\bar{\psi}\psi)^4 \right\rangle - 4\left\langle (\bar{\psi}\psi)^3 \right\rangle \left\langle \bar{\psi}\psi \right\rangle + 6\left\langle (\bar{\psi}\psi)^2 \right\rangle \left\langle \bar{\psi}\psi \right\rangle^2 - 3\left\langle \bar{\psi}\psi \right\rangle^4 \right] . \tag{5.4.7}$$

The contributions of the fully disconnected graphs are:

$$B_4^{\text{disc}} \equiv \frac{\xi^{\text{disc}}_{\bar{\psi}\psi}|_{\beta_c}}{(\chi^{\text{disc}}_{\bar{\psi}\psi}|_{\beta_c})^2} . \tag{5.4.8}$$

We checked whether also the connected diagrams contribute to the universal behavior, however, it turned out that the value of B_4 becomes even larger (see Fig. 5.27 right, the full B_4 corresponds to the $N_{\rm f} = 2$ value, $B_4^{\rm disc}$ corresponds to the limit $N_{\rm f} \to \infty$ such that all (partially) connected contributions become suppressed).

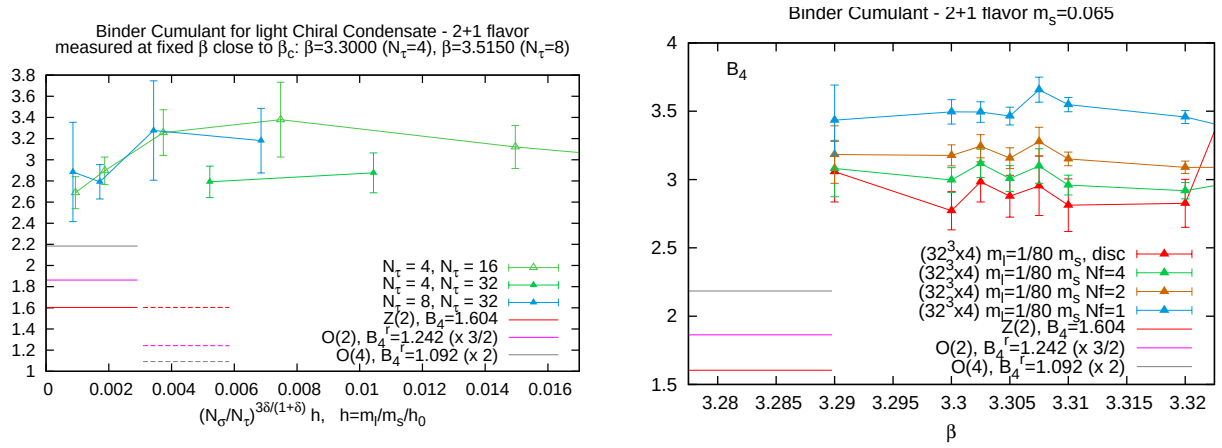

Figure 5.27: Binder cumulant (disconnected parts) along the critical line (left) and as a function of β (right) for the smallest quark mass $H = 1/80$, where it is compared with the definition containing connected contributions. Due to the poor statistics, it does not exhibit a clear minimum.

The (fully disconnected) Binder cumulants shown in the left of right Fig. 5.27 is limited by statistics. We have checked that an increase of RNVs did not lower the measured values for B_4^r. We still seem to be far in the crossover region, where $B_4 = 3$ is expected. However, it is not inconceivable that the Binder cumulant will approach the O(2) value in the chiral limit. We conclude that at the present stage, the Binder cumulant can not be used to predict the universality class.

5.4.2 Magnetic Equation of State for the Chiral Condensates

In this section we provide evidence for O(N) universality of $N_{\rm f} = 2+1$ QCD with a physical strange quark mass. This is achieved via the magnetic equation of state (MEoS). We will also determine the critical temperature and the QCD invariant quantity z_0 which allows to calculate the slope of the pseudo-critical line.

Fit $\mathcal{SD}_0$: Neglecting Deviations From Scaling

First we determine $\beta_{\rm c}$ and h_0, t_0 without taking into account deviations from scaling coming from the regular part of the free energy. For this purpose we only fit the smallest quark masses to the scaling function f_G. The fit was obtained via the MEoS:

$$\mathcal{SD}_0: \qquad M(t,h) = f_G(th^{-1/\beta\delta})h^{1/\delta}, \tag{5.4.9}$$

the O(N) scaling functions have been introduced and discussed in detail in Sec. 3.3.1. The fit results are shown in Fig. 5.28, where we compare the three order parameters M_0, M_s and M_c for $N_\tau = 4$, taking into account only the masses $H = 1/40$ and $H = 1/80$ in the fit. We also show the conjugate representation in terms of the thermal version of the MEoS (TEoS) given by $M(t,h) = |t|^\beta f_T(ht^{-\beta\delta})$, which focuses on the low- and high-temperature behavior. The cumulants Δ_{M_0} also shown involves the susceptibility and hence suffers from poor statistics (see next section).

We find that the O(2) scaling function describes the order parameters very well. We only observe that the smallest mass $H = 1/80$ deviates somewhat from the scaling function at values around $z \approx 2$. However, as can be seen in the TEoS plot of the same data (center of 5.28), in the limit

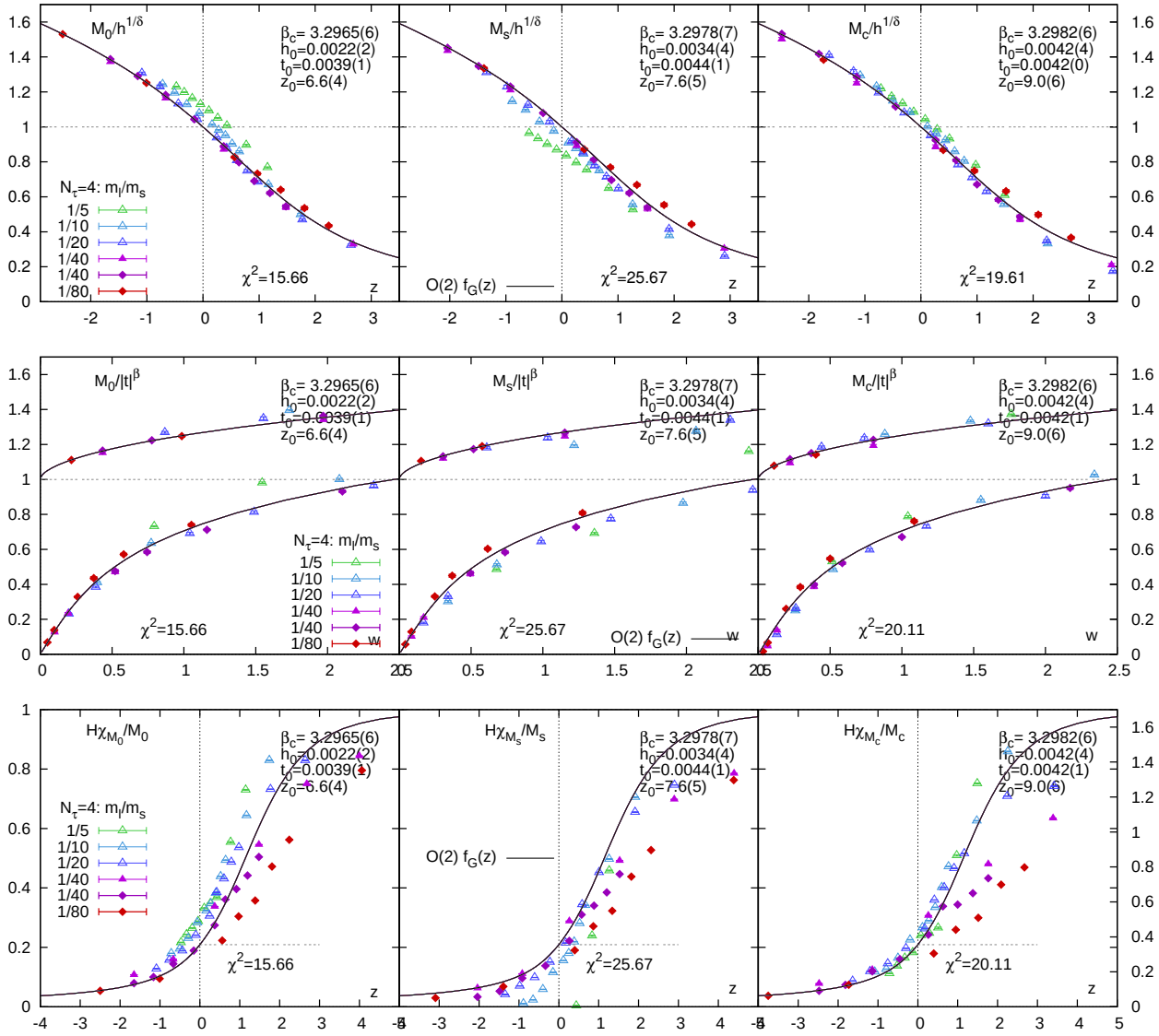

Figure 5.28: Fits for order parameters M_i $(i = 0, s, c)$ to the scaling function $f_G(z)$ via the magnetic equation of state (only the masses $m_l = 1/80, 1/40 m_s$ are included into fit), in three different representations: fit of the rescaled order parameter $M_i/h^{1/\delta}$ (top), $M_i/|t|^{\beta}$ (center) and the cumulant Δ_i (bottom).

$z \to \infty$, corresponding to $w = |z|^{-\beta\delta} \to 0$ on the high-temperature branch, the data are well behaved again. We speculate that the origin of this mismatch is related to the contribution of the connected susceptibility to the slope of the chiral condensate. Note that for all order parameters M_i scaling deviations (SD) become substantial for $H \geq 1/10$. Whereas the SD for M_0 have the tendency to pull the data for large quark masses above f_G, the SD for M_s pull the data below f_G.

We only show O(2) scaling plots, but we have fitted all data also to the Z(2) and O(4) scaling function, see Tab. 5.9. The fits to the models O(2), O(4) and Z(2) give similar χ^2, and similar β_c. Thus it is not possible on this basis to distinguish between the universality classes.

The scale invariant quantity $z_0 = t_0^{-1} h_0^{1/\beta\delta}$ takes different values, in the range $6.6 \lesssim z_0 \lesssim 10.3$. This constant will be of special interest, as it allows to determine the pseudo-critical line, and in the continuum limit it will only depend on the strange quark mass: $z_0 = z_0(m_s) + \mathcal{O}\left(a^2\right)$, and hence it is a QCD-specific quantity.

In Tab. 5.9, all fit results for $N_\tau = 4$ are summarized, where we have compared different fit ranges (explained in the next section). In a second step, we have enforced that all order parameters M_i give the same critical coupling and z_0, as it should not depend on the choice of the order parameter — they may only differ in the crossover region. By this procedure we obtain very different predictions for β_c and z_0 depending on the underlying universality class. We observe that both β_c and z_0 become smaller as N in O(N) grows (Z(2) = O(1)). The value $\beta_c = 3.293(1)$ for O(4) seems unreasonably small, as we observe Goldstone scaling at $\beta = 3.295$. The best fit provides O(2) with $\beta = 3.2952(3)$ and $z_0 = 5.4(2)$.

$N_\tau = 4$					
O(N)	OP	$\tilde{H}$	χ^2	β_c	z_0
O(1)	M_0	3/140	17.3	3.2971(4)	7.6(3)
O(1)	M_0	2/120	14.3	3.2971(5)	7.5(4)
O(1)	M_0	1/80	10.2	3.2974(6)	7.2(5)
O(1)	M_s	3/140	19.9	3.2992(4)	9.3(4)
O(1)	M_s	2/120	20.1	3.2983(6)	8.5(5)
O(1)	M_s	1/80	18.4	3.2979(7)	7.9(7)
O(1)	M_c	3/140	25.9	3.2986(4)	10.3(5)
O(1)	M_c	2/120	22.4	3.2981(6)	9.7(7)
O(1)	M_c	1/80	30.6	3.2979(12)	9.0(15)
O(2)	M_0	3/140	13.8	3.2967(4)	6.8(2)
O(2)	M_0	2/120	15.5	3.2965(6)	6.6(4)
O(2)	M_0	1/80	5.9	3.2962(5)	6.3(3)
O(2)	M_s	3/140	22.6	3.2989(4)	8.3(4)
O(2)	M_s	2/120	25.3	3.2979(7)	7.6(5)
O(2)	M_s	1/80	12.2	3.2971(7)	6.9(5)
O(2)	M_c	3/140	18.1	3.2986(4)	9.5(4)
O(2)	M_c	2/120	19.6	3.2982(6)	9.0(6)
O(2)	M_c	1/80	27.4	3.2974(12)	8.1(12)
O(4)	M_0	3/140	18.9	3.2954(6)	6.7(3)
O(4)	M_0	2/120	25.7	3.2947(10)	6.4(5)
O(4)	M_0	1/80	4.3	3.2939(5)	5.9(3)
O(4)	M_s	3/140	35.0	3.2980(6)	8.2(4)
O(4)	M_s	2/120	39.1	3.2967(11)	7.4(7)
O(4)	M_s	1/80	8.4	3.2954(7)	6.6(4)
O(4)	M_c	3/140	13.7	3.2984(3)	9.8(3)
O(4)	M_c	2/120	20.2	3.2980(7)	9.4(7)
O(4)	M_c	1/80	24.7	3.2967(13)	8.2(12)

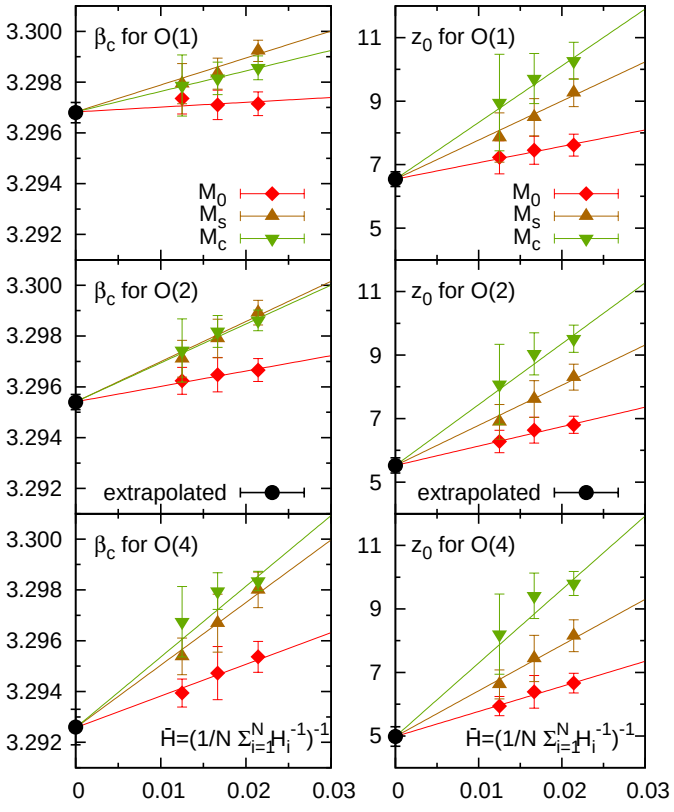

Table 5.9: Fit results for MEoS fits to $N_\tau = 4$ data without considering scaling deviations, cuts for fit mass range are at $H = 1/80$ ($\bar{H} = 1/80$), $H = 1/40$ ($\bar{H} = 1/60$), and $H = 1/20$ ($\bar{H} = 3/40$).

Fits SD_1, SD_3: Taking Into Account Deviations from Scaling

Since we have seen SD in the data, as a next step we will attempt to account for those by the following fits, based on the symmetries of the regular free energy:

$$\mathcal{SD}_1: \qquad M(t,h) = f_G(th^{-1/\beta\delta})h^{1/\delta} + a_t(T-T_c)/T_cH + b_1H, \tag{5.4.10}$$

$$\mathcal{SD}_3: \qquad M(t,h) = f_G(th^{-1/\beta\delta})h^{1/\delta} + a_t(T-T_c)/T_cH + b_1H + b_3H^3. \tag{5.4.11}$$

The deviations do not know about critical scaling, hence these terms do not include normalization factors h_0, t_0. These fit ansätze also account for the larger quark masses which we include in the fits. This also allows to compare with results from the $N_\tau = 8$ lattice, for which small quark masses are not available. The question we may ask: is the mass range $1/20 \geq H$ ($1/40 \geq H$) good enough to determine β_c, t_0 and h_0? The answer is: yes, for $N_\tau = 4$, the values for β_c and z_0 can be recovered within errors. We assume that this should also hold for $N_\tau = 8$. When comparing $N_\tau = 4$ and $N_\tau = 8$ fits, we also neglected the smallest quark mass H=1/80 for $N_\tau = 4$. To quantify the mass ranges considered, we introduce the following mass average which encodes the fit range used:

$$\tilde{H} = \left(\frac{1}{N}\sum_{i=1}^{N} H_i^{-1}\right)^{-1}, \qquad H_i \in \{1/80, 1/40, 1/20, 1/10, 1/5, 2/5\}. \tag{5.4.12}$$

Since the mass ratios increase by factors of 2, $\tilde{H}$ uniquely denotes a specific subset of the masses. This mass parameter will be used to plot fit parameters and allows to talk of the chiral limit.

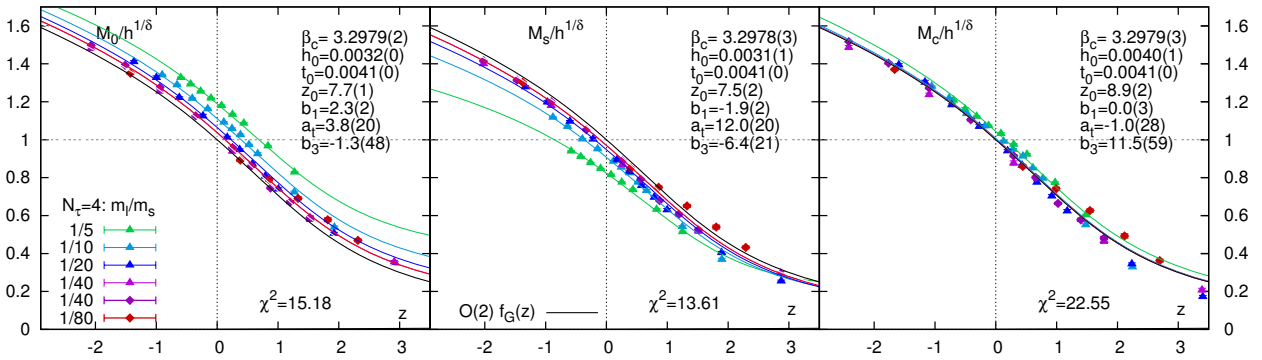

Figure 5.29: Fit to the scaling function by taking into account regular part from the free energy (scaling deviations). The full mass range is fitted here.

First we consider fits in the mass range $\tilde{H}/5 = (80+40+20+10+5)^{-1}$ as shown in Fig. 5.29. We observe that $\beta_c = 3.2979(3)$ agrees for all order parameters and also agrees with β_c from M_s fitted without scaling deviations. This is a remarkable finding, which may indicate that including the regular part may even improve to find the best estimate for β_c and z_0. For all three fits, also h_0 agrees exactly, only t_0 takes a different value.

We note that $b_1 = 2.3(2)$ for M_0 is larger than the expected value $\tilde{c}^{(4)}_{\mathcal{U}\mathcal{V}}$ for $N_\tau = 4$. But the temperature dependent term a_t, which may account for $c_2(T)$ from Eq. (5.2.18), is also quite large, although it has a huge error. Surprisingly, and in contrast with the findings of the Goldstone fits, M_s does not have a vanishing linear term, but $b_1 = -1.9(2)$. Instead, M_c now has a vanishing linear term, $b_1 = 0.0(3)$, although it was not vanishing in the Goldstone fits. It seems that in M_s, more than just the linear term was subtracted, because the scaling deviations now approach the scaling function from below, whereas in M_c the subtraction seems to work well.

We now come to a direct comparison of $N_\tau = 4$ and $N_\tau = 8$ data, based on the mass subset $\tilde{H}/4 = (40+20+10+5)^{-1}$, as shown in Fig. 5.30. We can clearly see that also this range suffices

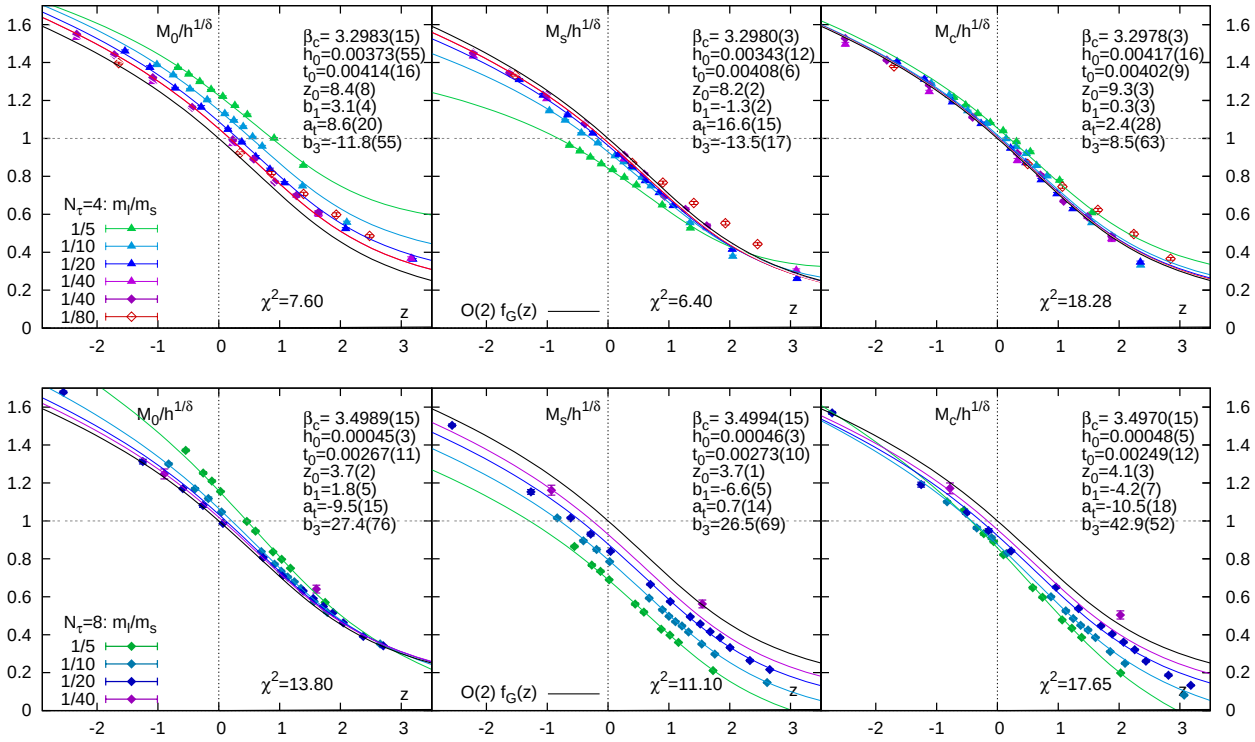

Figure 5.30: Comparison of MEoS fits for $N_\tau = 4$ (top) and $N_\tau = 8$ (bottom), according to fit ansatz $\mathcal{SD}_3$, with mass range excluding $m_l = 1/80 m_s$ for better comparison

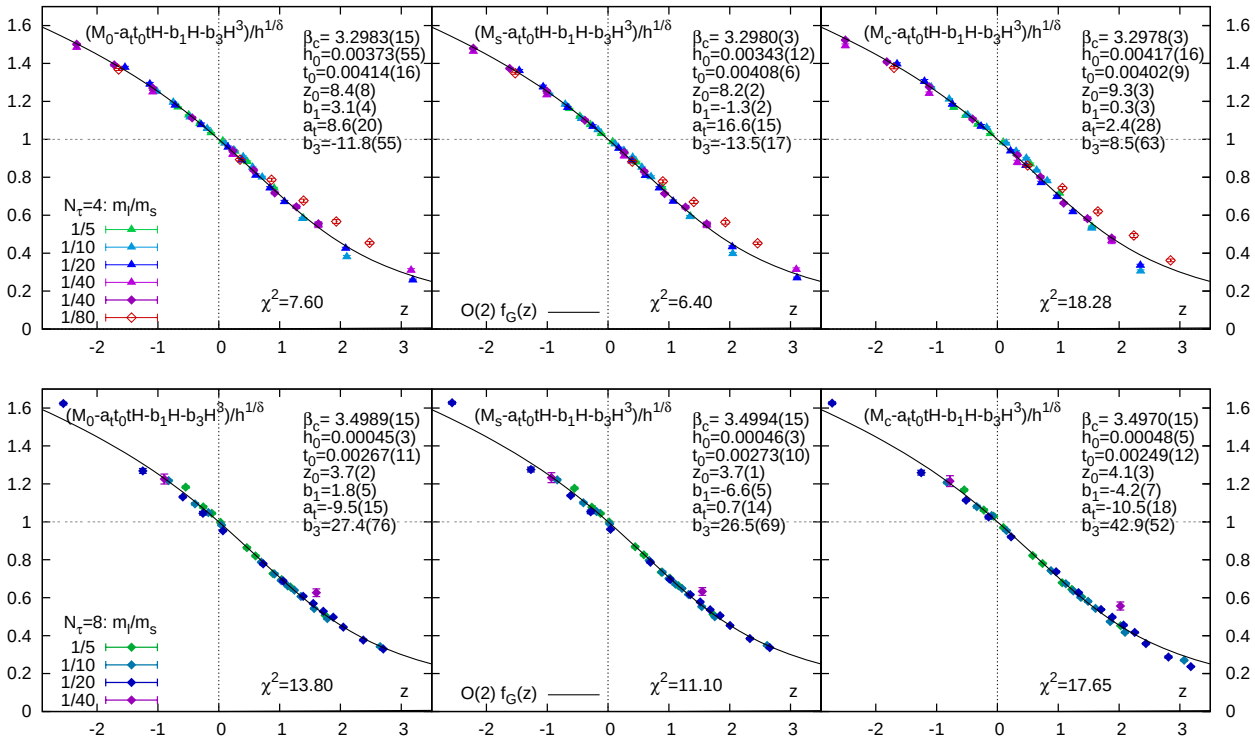

Figure 5.31: Comparison of MEoS fits for $N_\tau = 4$ (top) and $N_\tau = 8$ (bottom), according to fit ansatz $\mathcal{SD}_3$, with regular part subtracted.

to extract $\beta = 3.2979(3)$. The determination of the critical coupling via the MEoS turns out to be a robust result, which is a remarkable finding. We observe that $b_1 = 2.9(2)$ became larger for M_0 ($N_\tau = 4$). For $N_\tau = 8$, the results vary for the different M_i but we may conclude that $3.497 \lesssim \beta_c \lesssim 3.500$. Also these fits work surprisingly well. For z_0 we obtain an estimate $3.7 \lesssim z \lesssim 4.1$. It is remarkable that the difference between z_0 for $N_\tau = 4$ and $N_\tau = 8$ mainly stems from a very different value of h_0, whereas t_0 is of the same order. In all fits, b_3 has a large error, which may also effect the other fit variables.

We have also fitted the condensate data without a cubic term, all fit results can be found in the App. C.3, Tab. C.3 and Tab. C.3.

Magnetic Equation of State for Full Susceptibilities

We will now compare the above fits with the full susceptibilities, which are expected to be described by the scaling function

$$\chi^{\text{full}}(t,h) = \frac{1}{h_0} h^{1/\delta-1} f_\chi(t h^{-1/\beta\delta}), \qquad f_\chi(z) = \frac{1}{\delta}\left(f_G(z) - \frac{z}{\beta}\frac{d}{dz} f_G(z)\right). \tag{5.4.13}$$

In principle, O(2) and O(4) scaling should be distinguishable in f_χ for lattice data, however, the statistics is not sufficient. For a better comparison, we have already subtracted the fitted regular part to match the data with the scaling function. The general observation is that for all order parameters, the peak is too low for the smallest quark masses:

For $N_\tau = 4$, M_0 and M_s reach the asymptotic form of the scaling function already for $z < 0$ and $z > 4$. The asymptotic of behavior for M_c is not as good. This may be a signal for the missing contribution of the connected part.

For $N_\tau = 8$, the asymptotic behavior is worse, which might be just due to the fact that no small masses are available here. Interestingly, the data in the peak region of M_s show a nice convergence in the chiral limit.

Contributions to Scaling Function from Connected and Disconnected Part

We now want to reconsider the important question: does the *lattice* connected part contribute to the scaling function? The first answer is: no. If we assume to find O(2) or O(4) scaling, the connected part should not contribute to f_χ at fixed z, because in models with these symmetries, the $\mathrm{U_A}(1)$ symmetry will not be (effectively) restored and as a consequence, χ_l^{con} will not diverge as $h^{1/\delta-1}$ on the critical line. Note that at fixed z, as one goes to the chiral limit $h \to 0$, one also has to send $|t| \to 0$ and will run out of the Goldstone regime. Hence, the fact that χ_l^{con} shows Goldstone scaling does not imply by itself that it contributes to the scaling function at some finite z.

Nevertheless, we pose this question despite we expect that this should not be the case in the continuum theory. It may well be that the continuum limit is spoiled for the connected part (apart from $c_{\mathcal{UV}}$), which may produce an unphysical divergence in the chiral limit, just as we found an unphysical Goldstone divergences due to taste breaking. A critical divergence of χ_l^{con} at β_c could be e.g. explained if at least in one taste channels the delta meson mass m_δ^2 drops to zero as it is not sensitive to topological charges. It is well known that rooted staggered fermions do not account correctly for the vacuum structure as they do not obey the index theorem.

Hence we should take indications for a divergence of χ_l^{con} seriously. We now consider the data. In order to discuss the connected and disconnected contributions separately, one has to decide how to subtract the scaling deviations. We will assume that the UV-divergent term is the main contribution to the linear term and hence the linear term will be solely subtracted from the connected part. Since all constants a_t, b_1, b_3 from the M_0 fit are positive, we will be even more conservative and subtract

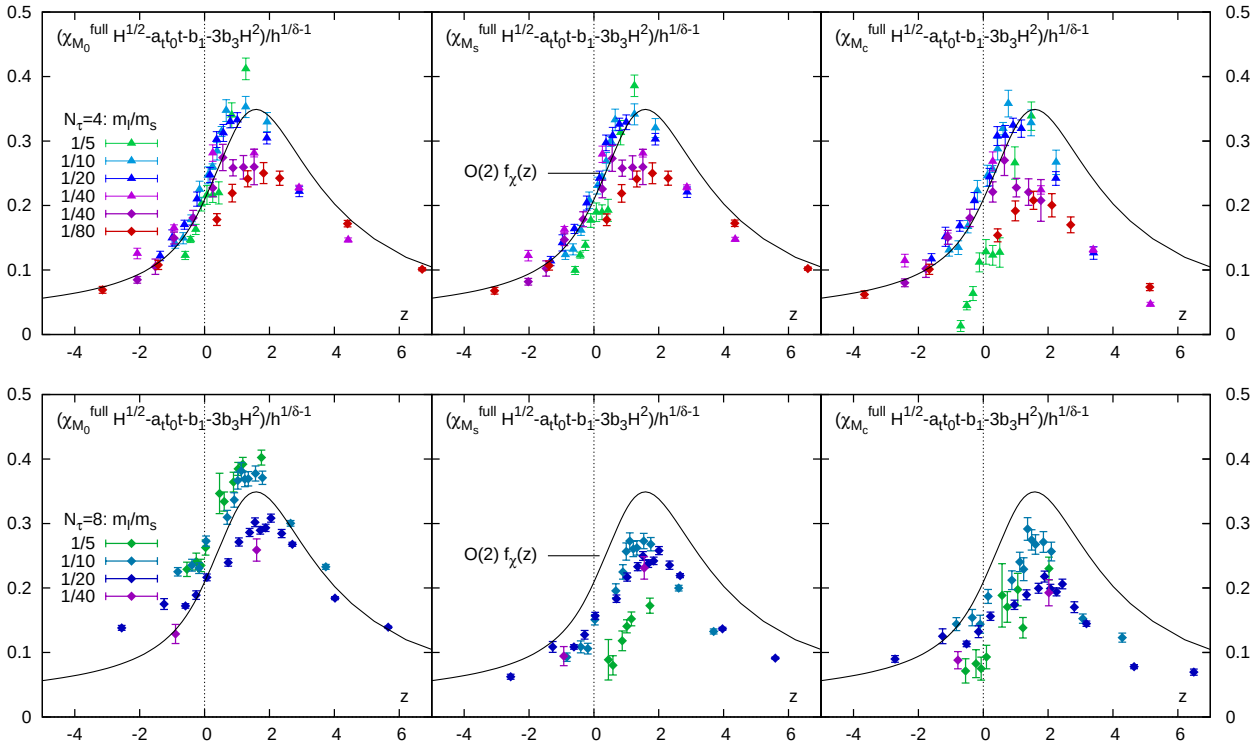

Figure 5.32: The chiral susceptibilities for M_0 (left), M_s (center) and M_c (right) compared to the scaling function $f_\chi(z)$, both for $N_\tau = 4$ (top) and $N_\tau = 8$ (bottom).

the whole regular term from the connected part in order to minimize it. We will then investigate whether $\chi_l^{\rm con} h^{1/\delta-1}$ remains finite despite all these subtraction.

The result is seen in Fig. 5.33: The $N_\tau = 4$ data indicate that $\chi_l^{\rm con}$ is large for $z > 2$ and does not seem to vanish in the mass region considered. In contrast, $\chi_l^{\rm dis}$ is significantly too low. However, it would be premature to say that this tendency persists in the chiral limit.

The $N_\tau = 8$ data are even more ambiguous, because despite the subtraction, there is a significant linear term in the connected part. The data now seem to indicate that $\chi_l^{\rm con}$ vanishes in the chiral limit. In contrast, the disconnected part remains finite, but does not grow either.

Identification of Goldstone Modes

The thermal version of the magnetic equation of state (TEoS), based on the scaling function $f_T^{\pm}(w)$ with $w = |z|^{-\beta\delta}$ (for details see Sec. 3.3.1), yields an alternative depiction of $f_G(z)$ which is suited to identify the Goldstone contributions, which are located in the low temperature branch $f_T^-(w)$ in the limit $w \to 0$. This can be seen in Fig. 5.34 and 5.4.2, where we have fitted all masses $H \leq 2/5$ for $N_\tau = 4$ to the TEoS:

$$M(t,h) = f_T^{\pm}(w)|t|^\beta + a_t(T - T_{\rm c})/T_{\rm c}H + b_1 H + b_3 H^3. \tag{5.4.14}$$

The fit results are of course very similar to the MEoS fits. The advantage of this alternative representation is that $w = h|t|^{-\beta\delta}$ can be rescaled to $H^{1/2}$, which allows a direct comparison with the Goldstone fits in the previous section. In Fig. 5.34 (bottom), one can easily recognize the straight lines for $3.28 \leq \beta \leq 3.29$. The corresponding rescaled susceptibilities in Fig. 5.4.2 (bottom) $\chi_{M_i} H^{1/2}$ remain finite in the Goldstone region, whereas $\beta = 3.30$, which is closest to $\beta_{\rm c}$, diverges stronger. Above $\beta_{\rm c}$, all branches tend to zero in the chiral limit as they are not truly divergent.

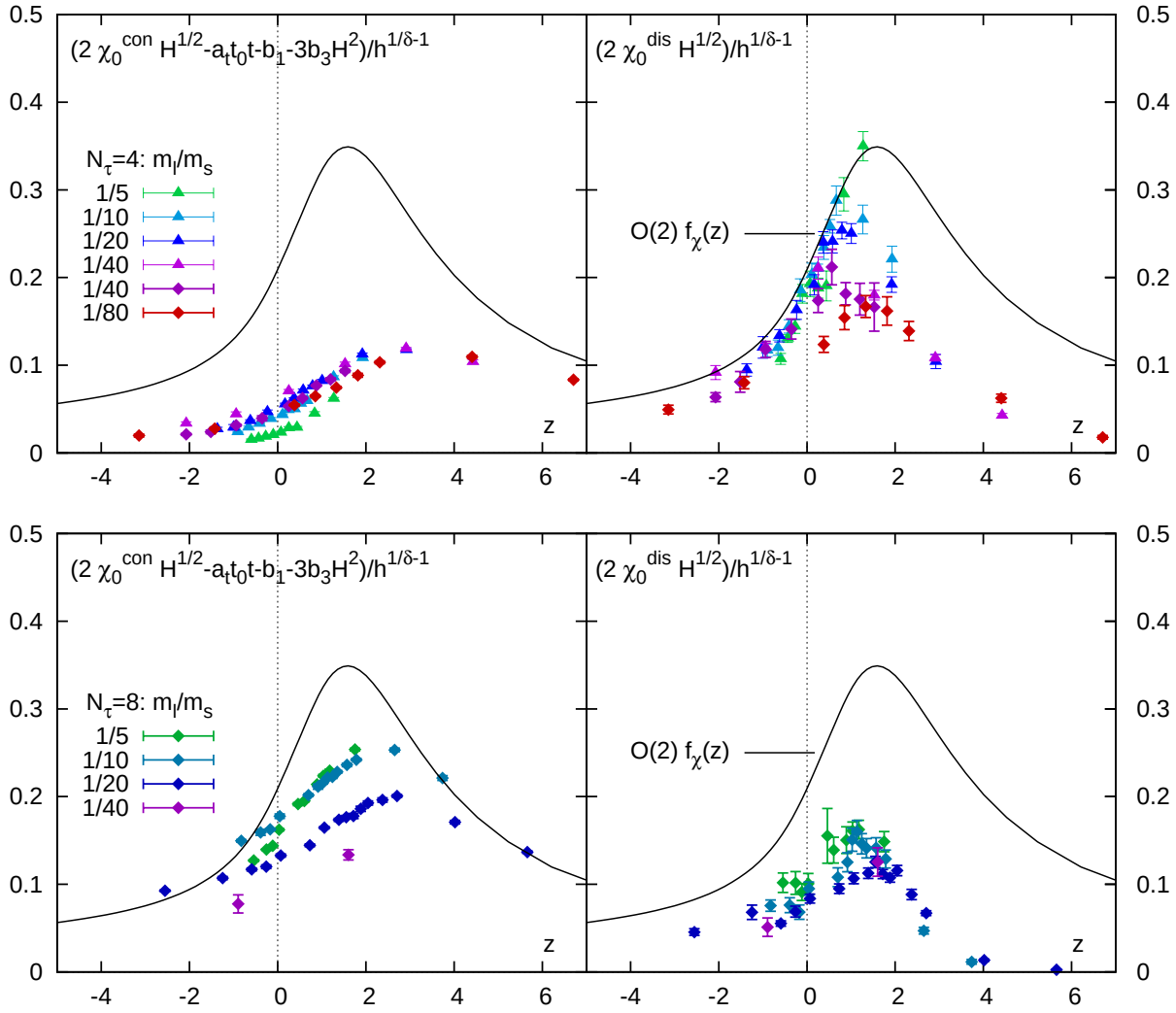

Figure 5.33: Connected susceptibility (left) and disconnected susceptibility (right) both for $N_\tau = 4$ (top) and $N_\tau = 8$ (bottom).

Joint Fits of Order Parameters

In the previous sections we have fitted the order parameter M_i separately and studied the chiral limit $\tilde{H} \to 0$. In the chiral limit, the results for β_c and z_0 should become independent of the choice of the order parameter, only the regular part of the order parameters differs. Hence we have applied a multibranch fit to extract the jointly fitted β_c and z_0, and only a_t, b_1 and b_3 remain distinct for each M_i. The result is shown in Fig. 5.36, we can see that the jointly fitted values are somewhat larger than the chiral extrapolated values from Tab. 5.9.

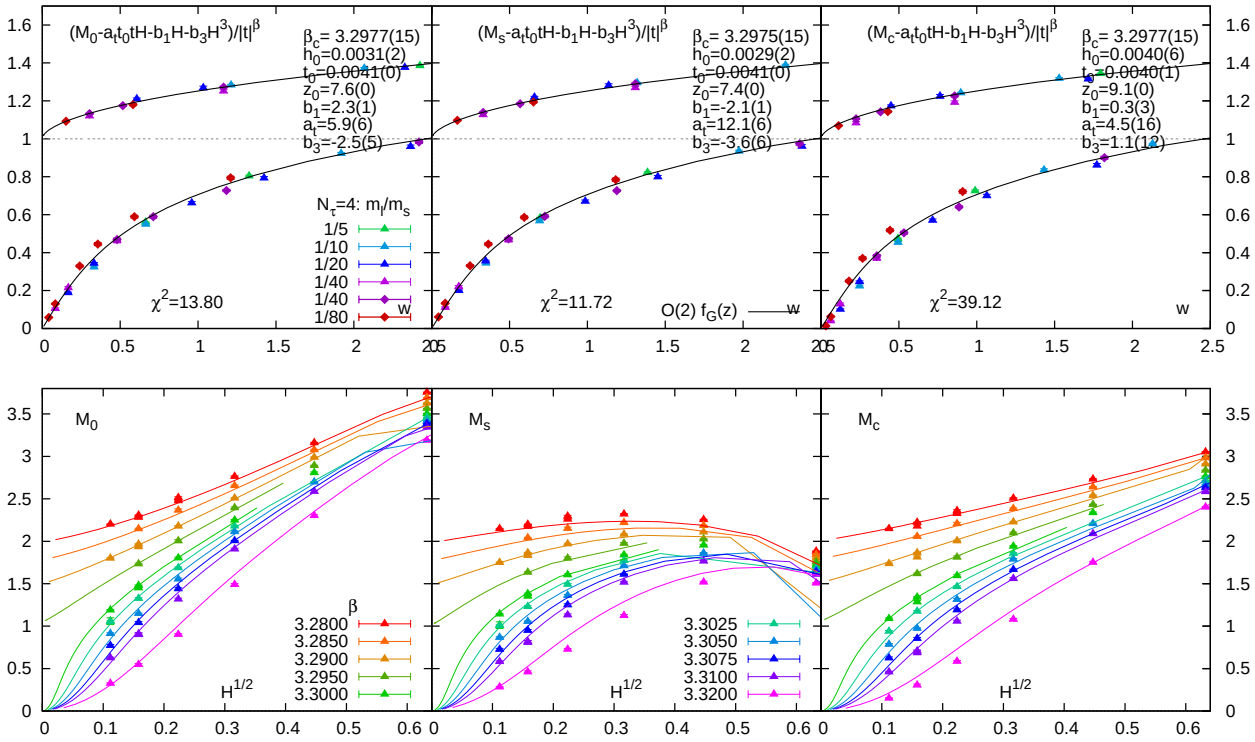

Figure 5.34: Fit of the order parameters M_0, M_s, M_c to $f_T^{\pm}(w)$ according to the TEoS fit Eq. (5.4.14) (top), and rescaled results (bottom)

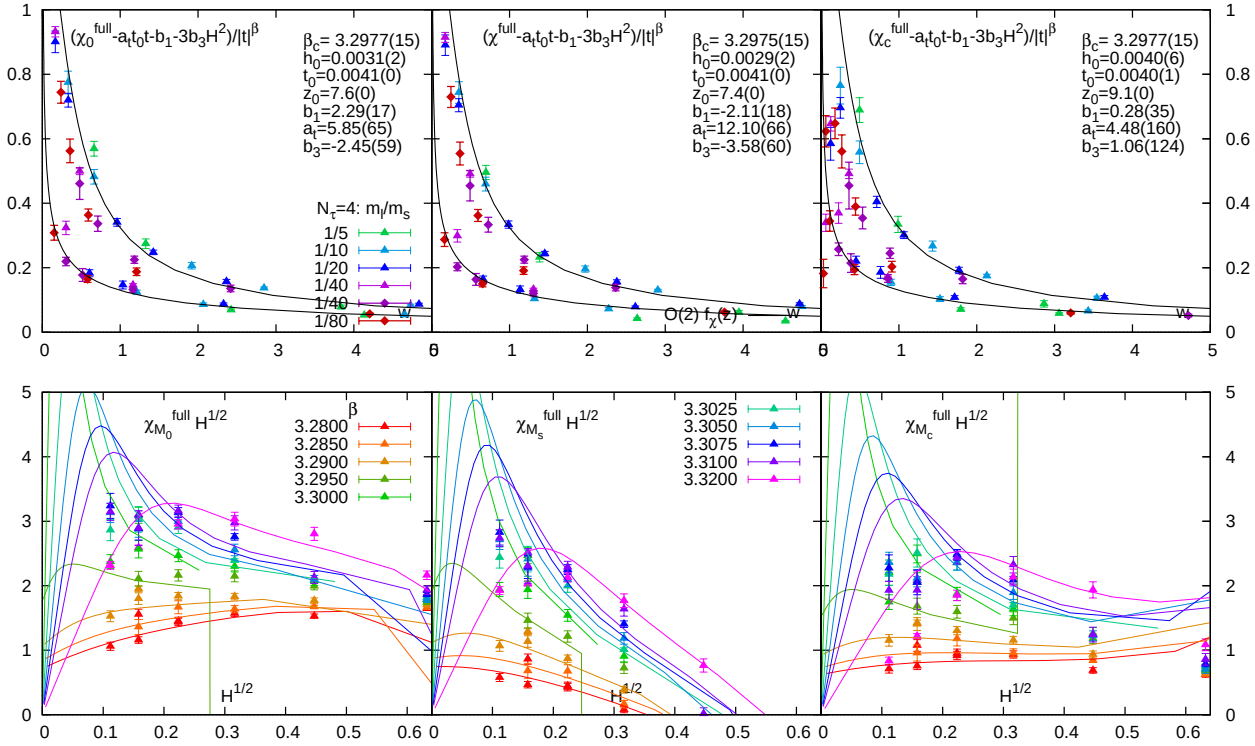

Figure 5.35: Comparison of the TEoS fits above with the susceptibilities χ_{M_0}, χ_{M_s}, χ_{M_c}.

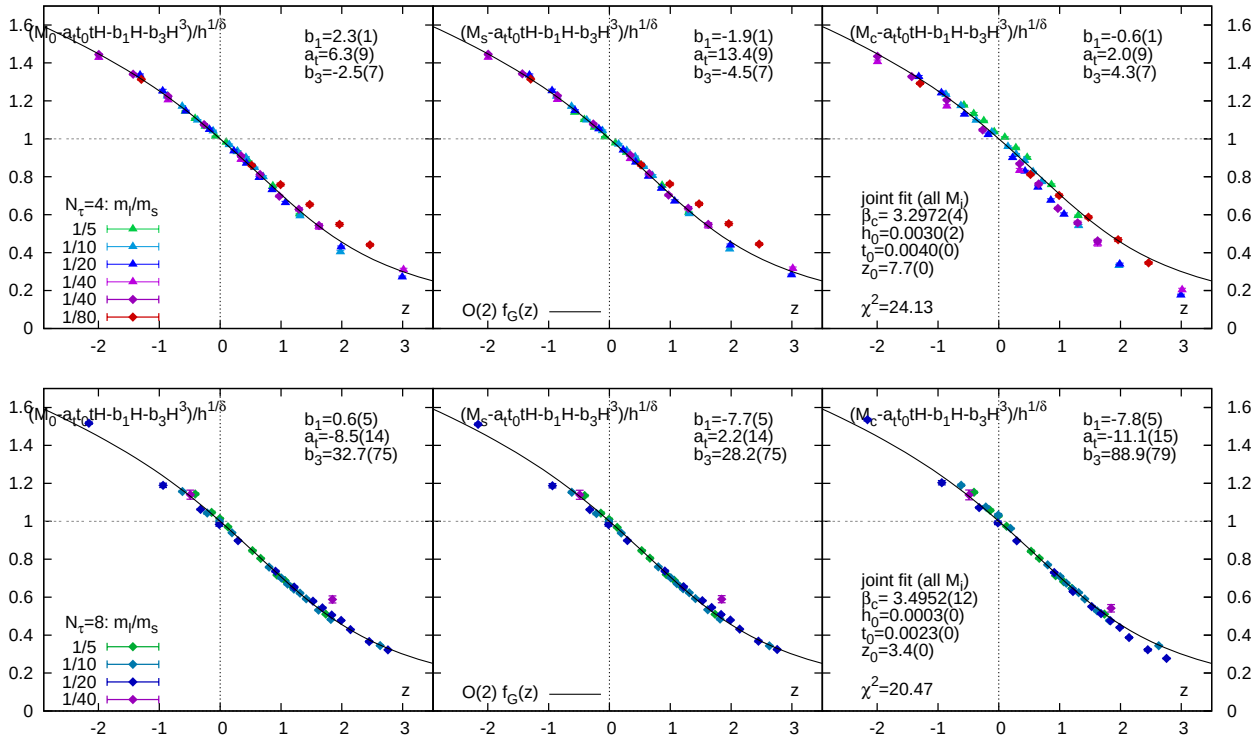

Figure 5.36: Multibranch fit of the order parameters M_0, M_s, M_c to $f_G(z)$ according to the MEoS. By this, an average value of β_c and z_0 can be extracted.

Exclusion of Ising Scaling

The last aspect we want to address in this scaling analysis is the exclusion of Z(2). Despite the fact that we are not able to distinguish O(2) scaling from O(4) scaling, and also Z(2) scaling is not to be ruled out, one may think of other methods which can give indications whether the tricritical point is below the physical strange quark mass or not. In the following we want to show that at least Z(2) scaling with a mass not much smaller than $m_l = 1/80 m_s$ is ruled out. If m_l^c exists at physical strange quark mass, it must be very small.

We have replaced in the above fits $H \to H - H_c$ and determined the quality of the fit by $\chi^2/d.o.f.$ The result for $N_\tau = 4$ is shown in Fig. 5.37. We find that the fits become worse as $H_c = m_l^c/m_s$ becomes large. The minimal χ^2 is indeed found for $H_c = 0$. This is true for fits including and excluding the cubic term. Unfortunately, at the present stage the same analysis is not yet possible for $N_\tau = 8$.

We note that for finite m_l^c, the chiral condensate is not the adequate order parameter any more. Instead, the true order parameter is obtained by mixing the chiral condensate with the energy density [75]:

$$\tau = \beta - \beta_c + A(m - m_l^c), \qquad (5.4.15)$$

$$\xi = m - m_l^c + B(\beta - \beta_c). \qquad (5.4.16)$$

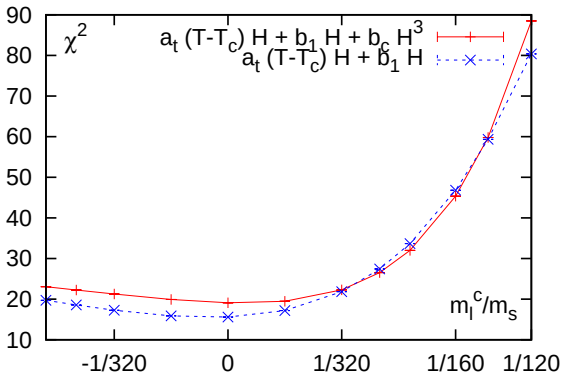

Figure 5.37: Exclusion of Ising Scaling for large quark masses $m_l^c/m_s > 1/160$ via comparison of χ^2.

5.4.3 The pseudo-critical line

The slope of the pseudo-critical line

The scaling analysis has shown that the physical point is already strongly influenced by critical scaling as scaling deviations are small. A precise determination of the pseudo-critical line may also improve on estimates of the pseudo-critical temperature for physical quark masses.

N_τ	z_0	β_c	$(T_c r_0)_{0,m_s,N_\tau}$
4	7.7(8)	3.2979(12)	0.4635(18)
8	3.6(6)	3.4975(45)	0.4132(78)

Table 5.10: Estimates from the fit values for the O(2) scaling analysis.

The slope of the pseudo-critical line, the constant $\breve{A}$ in Eq. (5.2.47), can be specified in terms of the QCD constant $z_0 = t_0^{-1} h_0^{1/\beta\delta}$ and the peak position z_p of the scaling function f_χ. In practice, to establish such a relation one needs to assume that the function $r_0/a(\beta)$ does not depend on the quark masses, which was shown to be a good approximation [25]. For small but finite h, the pseudo-critical coupling is given by:

$$t_{\rm pc} = z_p h^{1/\beta\delta} \qquad \Longrightarrow \qquad \frac{T_{\rm pc} - T_c}{T_c} = t_{\rm pc} t_0 = \frac{z_p}{z_0} H^{1/\beta\delta}, \tag{5.4.17}$$

$$(T_{pc} r_0)_{\hat{m}_l, \hat{m}_s, N_\tau} = (T_c r_0)_{0,m_s,N_\tau} \left(1 + \frac{z_p}{z_0} H^{1/\beta\delta}\right). \tag{5.4.18}$$

With $z_p = 1.56(10)$ for O(2), and the values of z_0, β_c as given in Tab. 5.10, we find by comparing with the coefficients of Eq. (5.2.47):

$$\breve{A}_{N_\tau} = (T_c r_0)_{0,m_s,N_\tau} \frac{z_p}{z_0} = \begin{cases} 0.094(18) & N_\tau = 4 \\ 0.179(46) & N_\tau = 8 \end{cases}, \tag{5.4.19}$$

which for both cases is consistent with the values $\breve{A}_{N_\tau}$ we obtained from the pseudo-critical coupling of the full susceptibility $\beta_{\rm pc}^{\rm full}$, see Tab. 5.5. However, we still do not find that $\breve{A}_{N_\tau}$ is independent of N_τ and we have speculated in Sec. 5.2.4 that this may be due to small differences in the physical quark masses for $N_\tau = 4$ and $N_\tau = 8$. In fact, since we know the mass dependence of $\breve{A}_{N_\tau} = A(M_S r_0)^{2/\beta\delta}$ with A constant by definition, z_0 is quark mass dependent as

$$z_0(m_s) = z_p A^{-1} (T_c r_0)_{0,m_s,\infty} (M_S r_0)^{-2/\beta\delta}, \tag{5.4.20}$$

where $M_S r_0$ is known from zero temperature measurements for a given $\hat{m}_s$. If one wanted to keep the physical m_s constant along the pseudo-critical line, one would need to adjust $\hat{m}_s$ accordingly. In order to estimate the size of the change we use the function $m_s a(\beta) = 10 m_l r_0(\beta)/(r_0/a(\beta))$ and we obtain $\hat{m}_s(\beta_c) = 0.072$ for $N_\tau = 4$ and $\hat{m}_s(\beta_c) = 0.026$ for $N_\tau = 8$. We find that our choice $\hat{m}_s = 0.065$ for $N_\tau = 4$ is somewhat too small, as it corresponds to a strange quark mass having 90% of its physical value, resulting in a 5% lighter mass for M_S.[12] In the next section we will determine the dependence of $z_0(m_s)$ on m_s via reweighting and find it to be strong.

We conclude this section by giving an estimate for the pseudo-critical temperature for physical quark masses. It is useful to use the kaon mass $M_K = 497$ MeV as a reference instead. Based on the approximation $H \sim 0.52(M_{\pi,5}/M_K)^2$ in the vicinity of the physical mass, we obtain

$$\frac{T_{pc}(M_{\pi,5}) - T_c}{T_c} = 0.68 \frac{z_p}{z_0} \left(\frac{M_{\pi,5}}{M_K}\right)^{2/\beta\delta}. \tag{5.4.21}$$

For $N_\tau = 4$ we find $0.68 z_p/z_0 \sim 0.15(5)$ and for $N_\tau = 8$ we find $0.68 z_p/z_0 \sim 0.20(8)$. Hence the prefactor is not large, and we conclude that the dependence of T_{pc} on $M_{\pi,5}$ is weak.

[12] This estimate is based on the assumption $M_S \sim \hat{m}_s^{1/2}$, but note that M_S may be too heavy to be subject to GMOR.

Reweighting in m_l and m_s at fixed H

In order to refine our study of the strange quark mass dependence, we reweight in the strange quark mass and in the light quark mass by keeping the quark mass ratio H fixed. The situation is illustrated in Fig. 5.38. We applied reweighting in a range $0.85 \lesssim m_s^{\rm rew} \lesssim 1.15$. Then we repeated the scaling analysis for the reweighted order parameters. Since the results of reweighting for the connected susceptibility are not as satisfactory as for the condensates, we will do the scaling analysis only for the reweighted order parameters M_0 and M_s.

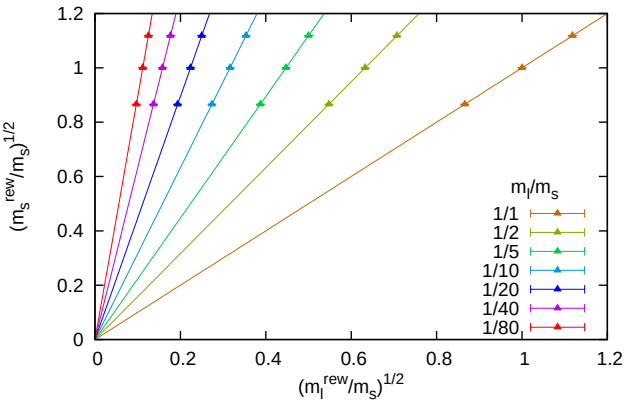

Figure 5.38: Range of quark masses along the lines in m_l and m_s to which reweighting has been applied, marked by dots.

We observe that z_0 increases for decreasing m_s (both $N_\tau = 4$ and $N_\tau = 8$). Hence the pseudo-critical line T_{pc} will have a weaker dependence on $M_{\pi,5}$ as we go further to the chiral limit. The new parameters taken at $m_s^{\rm rew}$ according to the LCP value are $z_0 = 6.11(86)$ for $N_\tau = 4$ and $z_0 = 3.78(24)$ for $N_\tau = 8$.

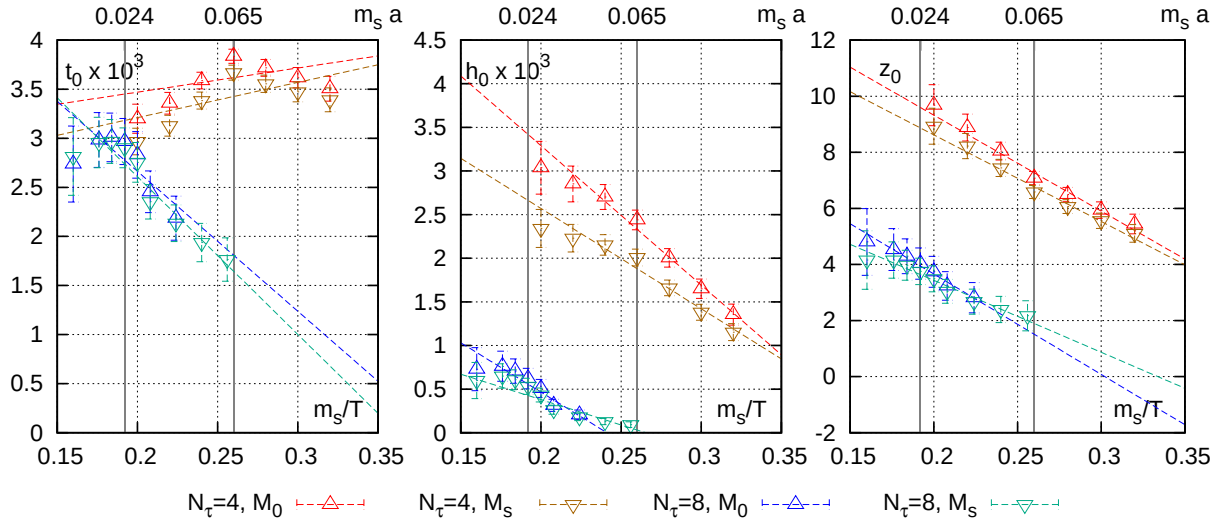

Figure 5.39: Results for the MEoS fits after reweighting in the quark masses at fixed H: t_0 (left) has different tendencies for $N_\tau = 4$ and $N_\tau = 8$, h_0 (center) and z_0 (right) are observed to increase as we decrease m_s. Red data are for $N_\tau = 4$, blue data for $N_\tau = 8$.

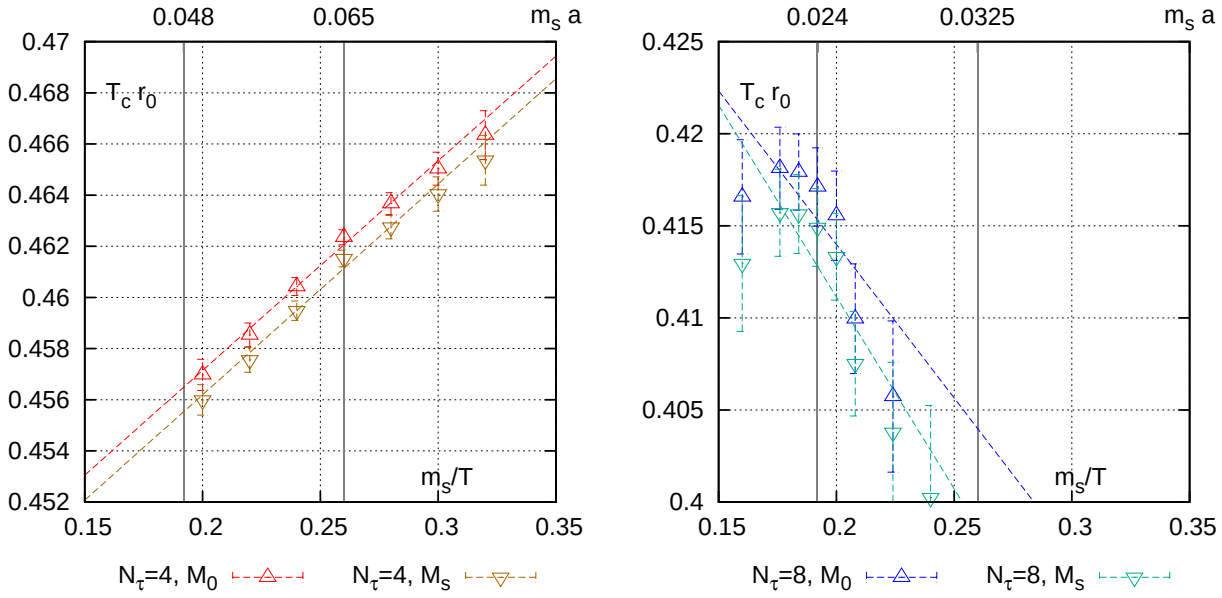

Figure 5.40: Results for the MEoS fits after reweighting in the quark masses at fixed H: For $N_\tau = 4$ (left), the critical temperature is observed to decrease as we decrease m_s. For $N_\tau = 8$ (right), the data are not conclusive yet.

5.4.4 The critical line at finite density

As we have discussed in the introduction, the location of the physical point w.r.t. the critical line is of importance also for QCD at non-zero density: The critical line extends to a critical surface which may hit the physical point at some critical chemical potential μ_c. Hence we are interested in the μ-dependence of the critical temperature. We make use of the Taylor expansion method described in Sec. 2.4. We emphasize that it is not granted whether a chiral critical point really exists. The critical line for finite density is characterized by

$$t(\mu_l) = \frac{1}{t_0}\left(\frac{T-T_c}{T_c} + \kappa_\mu \left(\frac{\mu_l}{T}\right)^2\right) + \mathcal{O}\left((\mu_l/T)^4\right) \tag{5.4.22}$$

with μ_l the light quark chemical potential. In the chiral limit, μ_l does not break chiral symmetry explicity, hence it will only influence the reduced temperature. Therefore, the critical line for finite density is characterized by the condition $t(\mu_l) = 0$.

The coefficient κ_μ, which gives the slope of the critical line at lowest order, can be determined on the lattice from the Taylor coefficient $c_2^{\bar\psi\psi}$, which is proportional to the thermal susceptibility χ_t, see Eq. (3.3.31):

$$c_2^{\bar\psi\psi} \equiv \left.\frac{\partial^2 M}{\partial(\mu_l/T)^2}\right|_{\mu_l=0} = \frac{\kappa_\mu}{t_0 T_c} h^{(\beta-1)/\beta\delta} f_G'(z). \tag{5.4.23}$$

Hence $c_2^{\bar\psi\psi}$ can be used to determine κ_μ. Our group, the RBC-Bielefeld-GSI collaboration, is currently measuring this coefficient. It has already been calculated for $N_\tau = 4$. The preliminary result was obtained by a fit to the O(2) scaling function $f_G'(z)$, with h_0 and t_0 as determined in the previous section, and we yield $\kappa_\mu = 0.035(1)$. The fit is shown in Fig. 5.41. We have started to measure $c_2^{\bar\psi\psi}$ for selected values in the peak region for $N_\tau = 8$ as well, but we have not analyzed the data yet.

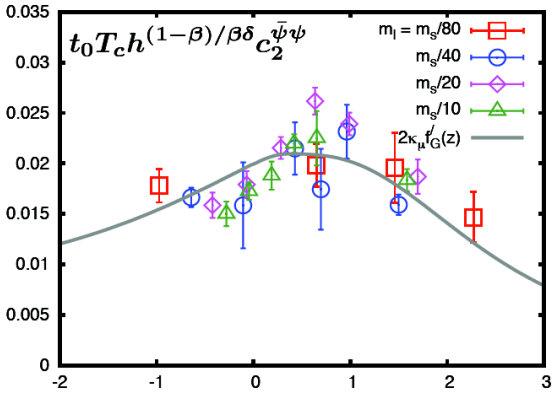

Figure 5.41: Fit of the rescaled thermal susceptibility to the scaling function. Thanks to S. Mukherjee for providing the data.

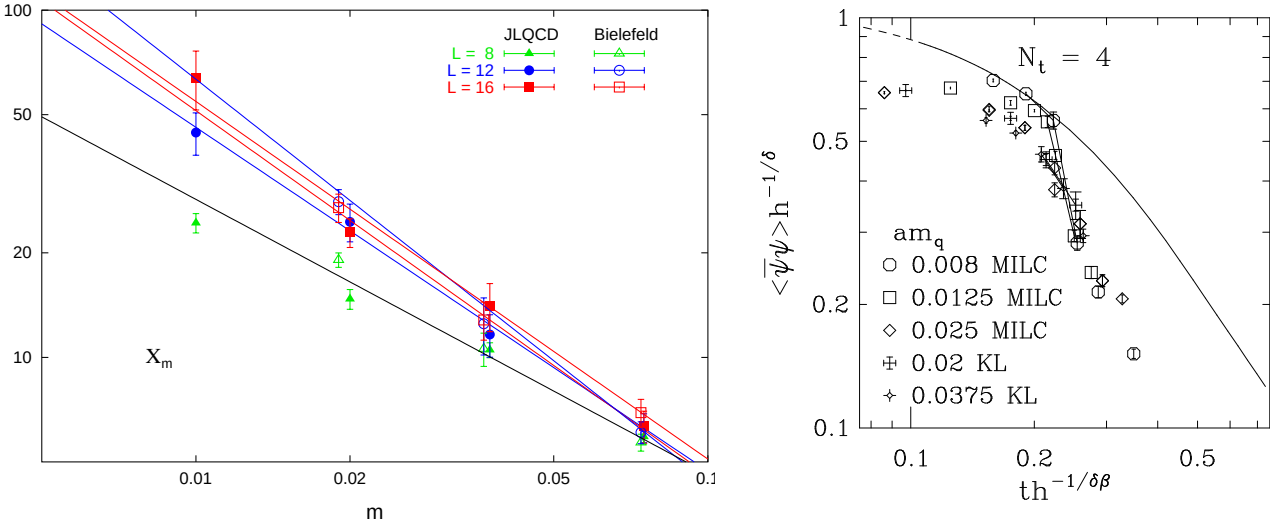

Figure 5.42: Scaling plots for $N_{\rm f} = 2$ which test for O(4) scaling, left: comparison of JLQCD data and Bielefeld data on the divergence of the chiral susceptibility (taken from [82]), right: chiral condensate data of the MILC collaboration fitted to the O(4) MEoS (taken from [11]).

5.5 Comparison with Literature and Conclusion

This work is the first investigation of the order of the chiral transition in the two flavor chiral limit for $N_{\rm f} = 2 + 1$ with a *physical strange quark mass* making use of improved staggered fermions.

We found evidence for O(N) scaling in the chiral limit and no signal for a first order transition. On the coarse lattice $N_\tau = 4$ we can exclude a first order transition with $m_l^c > 1/160 m_s$. We emphasize however again that it is not clear at all that the transition is of second order in the chiral limit. One might find a first order for all values of m_s and the tricritical point might not even exist. There is even the conceptual possibility that there exist more than one tricritical point, and O(4) scaling is found only for intermediate values of m_s, although this is unlikely to happen from what we know about the role of the anomaly.

We will now review the results from the literature and compare with our findings.

5.5.1 Universal scaling in $N_{\rm f} = 2$ QCD

Consistency of $N_{\rm f} = 2$ staggered fermion lattice data has been reported by Karsch and Laermann already in 1994 [73, 74]. Due to the lack of the strange quark mass, they introduce the symmetry breaking field as $H \equiv m_l/T$ and the reduced temperature $t \equiv \beta - \beta_c \simeq (T - T_{\rm c})/T_{\rm c}$. Their analysis is based on a rather small lattice $8^3 \times 4$ obtained via the R-algorithm. They find that the ratio $\chi_l^{\rm dis}/\chi_l^{\rm con}$ drops in the chiral limit, indicating that the connected part does not contribute to critical scaling. From the cumulant $\Delta = m_l \chi_l / \langle \bar{\psi}\psi \rangle_l$ they were also able to determine limits for the inverse critical exponent $0.21 < 1/\delta = 0.23 < 0.26$, which is almost consistent with the O(2) value $\delta = 0.2093$, but lacks the precision to distinguish this from other universality classes. In 1998, results for larger lattice volumes have been presented, $N_\sigma = 12, 16$ [82], but they do not find the larger lattices to agree wit O(2) or O(4) critical exponents.

The MILC collaboration [11] has investigated the chiral transition in 2000 by making use of the magnetic equation of state. They have checked explicity for the O(4) scaling and compared to the meanfield scaling function. They observe that scaling predictions become worse as they go to smaller masses compared to [74], and conclude that strong discrepancies w.r.t. critical exponents and the MEoS persist: if the chiral transition is second order with O(N) universality, the quark masses considered so far are not yet in the scaling region.

In contrast, the Pisa Group [31, 28] did not find evidence for a second order transition in their analysis of standard staggered fermions with two flavors. Their data on the specific heat seem to provide evidence for a first order transition. However, this evidence is not so much supported by their results on the chiral susceptibility, which are ambiguous and do not exclude a second order transition. Their analysis is based on a finite size scaling analysis, the lattice volumes are $N_\sigma = 16, 20, 24, 32$ and $N_\tau = 4$. They admit however that open questions remain: E.g. they do not find a double peak structure in the histograms of observables near the transition point and also lattice artifacts for this unimproved action may be problematic. Nevertheless they are confident to have the subtraction of the UV-divergent term under control.

In Japan, also simulations on the two flavor chiral transition with Wilson fermions have been performed, most notably the JLQCD collaboration [5], Iwasaki *et. al.* [70] and the CP-PACS Collaboration [1]. Since the chiral order parameter is obtained from chiral Ward identities, they have to determine renormalization constants for the quark mass and chiral observables. Despite these complications, they find almost perfect matching of the chiral condensate data with the O(4) magnetic equation of state. This is particularly remarkable since Wilson fermions break chiral symmetry explicity at non-zero lattice spacing and in contrast to staggered fermions, no residual symmetry survives. However, they have mainly analyzed data for $z > 0$.

5.5.2 Universal scaling in $N_\mathrm{f} = 2 + 1$ QCD

There has also been carried out a scaling analysis for $2 + 1$ flavors by de Forcrand and Philipsen, based on staggered fermions [46]. On lattices with temporal extent $N_\tau = 4$ they encounter a first order transition in the chiral limit and pin down the Ising critical line $m_s(m_l)$, which for a physical strange quark mass reaches a critical light quark mass m_l^c corresponding to a pion mass of $M_\pi^c = 130$ MeV. However, their result has to be considered as rather preliminary because they used standard staggered fermions without improvement, and they have observed that the first order region shrinks considerably on a finer lattice with $N_\tau = 6$. This shrinking has also been observed in the $N_\mathrm{f} = 3$ for improved staggered fermion simulations of the RBC-Bi collaboration, performed by Ch. Schmidt [75]. It is also expected that finite size effects are substantial because for the smallest quark mass at the pseudo-critical line they have $M_\pi L = 1.7$ (compare with our box size $M_\pi L = 3$).

5.5.3 Conclusion

In this analysis, we have established the Goldstone effect and critical O(N) scaling in QCD with 2+1 flavors in the staggered fermion formulation. We have compared predictions from continuum and staggered chiral perturbation theory with lattice data. We have also analyzed the ultraviolet divergent linear term in the condensate and predicted its value in the infinite volume limit to be $c_{\mathcal{UV}} = 1.5$, which proved to be broadly consistent with zero-temperature lattice data as well as finite temperature data. We stress that $c_{\mathcal{UV}}$ shows up as UV-divergent constant in the connected susceptibility only.

For the scaling analysis, we have mainly relied on the magnetic equation of state. Our data are compatible with the O(2) scaling function, and the fits to extract β_c and z_0 work remarkably well. The $N_\tau = 4$ data indicate that there is no first order transition for light quark masses above $H \simeq 1/160$, and if one presumes the Ising Z(2) universality class, the best fit is consistent with $H = 0$, indicating that there is no first order region. Moreover, O(2) scaling is preferred over Z(2) scaling, which gives reason to believe that the tricritical point m_s^tric is located below the physical strange quark mass. However, we were not successful to establish this finding also for the finer lattice, $N_\tau = 8$. We have determined the pseudo-critical line via the parameter z_0, and found agreement with the previous direct determination of the pseudo-critical line via scaling laws. z_0 seems to have a large cut-off dependence when comparing the results for $N_\tau = 4$ and $N_\tau = 8$. In particular, the pseudo-critical line becomes steeper in the continuum limit. We also find that z_0 decreases when

increasing the strange quark mass at fixed ratio H, making the pseudo-critical line steeper as one moves to the $N_{\rm f} = 2$ theory.

5.5.4 Outlook

We have covered a broad range of light quark masses and have observed O(N) scaling in many observables, nevertheless there also remain some puzzles, e.g. why the Binder cumulant is still close to the Gaussian value. One would like to go further into the chiral limit, but it is unlikely that we will persue this program in near future with the p4fat3 action on these rather course lattices, because generating the data will be too expensive and the pay-off may be rather small. Instead, our collaboration might redo a scaling analysis with another action (most likely HISQ), once a considerable range of light quark masses is available.

At present, the data set for $N_\tau = 8$ can be easily improved by generating more data below $\beta = 3.515$ for $H = 1/40$. In contrast to the $N_\tau = 4$ data, the fit results for both $\beta_{\rm c}$ and z_0 do not show a systematic behavior with the cut-off mass so far, and the chiral extrapolations have to be considered as rather preliminary. Also, it is not yet possible to exclude Ising universality at some finite mass for $N_\tau = 8$. These measurements may allow to attempt a more reliable continuum limit of the parameters of our scaling analysis.

Another open issue is the location of the tricritical point. While not ruling out, our analysis does not give evidence for a tricritical point at or above the physical strange quark mass. It would be interesting to repeat the analysis at various smaller strange quark masses or even follow the critical line once it is detected in e.g. three flavor simulations.

An important, still unresolved issue is the divergence of the connected susceptibility. Our data did exclude the hypothetical possibility that the connected part might contribute to the scaling function. It will be interesting to see what the quark mass dependence of the connected part will be with other improved actions such as the HISQ action. The strong divergence of $\chi_l^{\rm con}$ might as well be a lattice artifact of the p4fat3 action, or even be related to rooting. To clarify this issue, a carefull analysis of $\mathrm{U_A}(1)$ symmetry restoration is needed as well.

Acknowledgments

Many people have helped me to conduct research on this subject, and have supported me in various ways. I am especially grateful to my supervisor, Prof. Dr. Edwin Laermann, for his assistance and support during my PhD thesis. It has been a great pleasure to discuss my work with him, I am thankful for his guidance and patience.

I also owe deep gratitude to Prof. Dr. Karsch, in particular for providing me with generous computing time at the NewYork Blue and for inviting me to BNL twice. I appreciated the stimulating discussions with him, which enormously helped to put this project forward. I like to thank as well Prof. Dr. Jürgen Engels for pointing out some less obvious aspects of O(N) models and for providing me with Monte Carlo data on the O(4) model.

I thank Christian Schmidt, Swagato Mukherjee and Wolfgang Söldner for many fruitful discussions, and also for helping to solve problems related to the machines and simulation software. I would like to thank all my present and former office colleagues, in particular Hengtong Ding and Chuan Miao, for the friendly atmosphere in the office, and for discussions on more general aspects of lattice QCD and data processing.

I want to express my gratitude to the people who supported me also emotionally: Most importantly, I want to thank my girlfriend Sabine Bönig for her permanent support and encouragement. I also like to thank Babak Soleymanzadeh and Marina Seikel for the breaks between work. Finally, I want to thank my parents for their encouragement.

This work has been supported by the Deutsche Forschungsgemeinschaft under grant GRK 881. I thank the graduate school Bielefeld for the financial support and for giving me the opportunity to attend various conferences and block courses during the last years.

Appendix A

O(N) Non-linear Sigma Model

A.1 Angular Distribution Integrals for Binder Cumulant

We summarize the calculation of the distribution integral relevant for the refined value of the Binder cumulant B_4^r. The idea goes back to Thomas Schulze, who described it in his PhD thesis [107]. We introduce generalized polar coordinates for the N-component unit vector $\boldsymbol{S} = (S_1, \dots S_N)$:

$$\begin{aligned} S_1 &= \sin\phi \sin\theta_1 \dots \sin\theta_{N-2}, \\ S_2 &= \cos\phi \sin\theta_1 \dots \sin\theta_{N-2}, \\ &\vdots \\ S_{N-1} &= \cos\theta_{N-2} \sin\theta_{N-2}, \\ S_N &= \cos\theta_{N-2}, \qquad\qquad \phi \in [0, 2\pi], \quad \theta_i \in [0, \pi]. \end{aligned} \tag{A.1.1}$$

We demand that $\boldsymbol{S}$ shall have the same probability density $f^N(x)$ in the interval $x \in [-1, 1]$ with $x = \cos\theta_N - 2$. The Jacobi determinant for the above coordinates can be calculated recursively:

$$J_N(\phi, \theta_1, \dots, \theta_{N-2}) = J_{N-1}(\phi, \theta_1, \dots, \theta_{N-3}) \sin^{N-2}\theta_{N-2}, \tag{A.1.2}$$

hence the variable θ_{N-2} is distributed proportional to $\sin^{N-2}\theta_{N-2}$:

$$\begin{aligned} f_N(x) &= C_N \int_0^\pi d\theta_{N-2} \sin^{N-2}\theta_{N-2} \delta\left(x - cos\theta_{N-2}\right) \\ &= C_N \int_{-1}^1 d\cos\theta_{N-2} \left(1 - \cos^2\theta_{N-2}\right)^{(N-3)/2} \theta_{N-2} \delta\left(x - cos\theta_{N-2}\right) \\ &= C_N \int_{-1}^1 dy \left(1 - y^2\right)^{(N-3)/2} \delta(x - y). \end{aligned} \tag{A.1.3}$$

The probability density has to be normalized:

$$C_N^{-1} = \int_0^\pi d\theta_{N-2} \sin^{N-2}\theta_{N-2} = \sqrt{\pi} \frac{\Gamma\left((N-1)/2\right)}{\Gamma\left(N/2\right)} = \frac{(N-3)!!}{(N-2)!!} \begin{cases} \pi & \text{for } N \text{ even} \\ 2 & \text{for } N \text{ odd} \end{cases}. \tag{A.1.4}$$

This results in the probability density

$$f_N(x) = \frac{(N-2)!!}{(N-3)!!} \left(1 - x^2\right)^{(N-3)/2} \begin{cases} 1/\pi & N \text{ even} \\ 1/2 & N \text{ odd} \end{cases}. \tag{A.1.5}$$

This formula is valid for $N \geq 2$, given the definitions $(-1)!! = 1$ and $0!! = 1$.

Appendix B

Chiral Perturbation Theory

B.1 Dimensional and Cut-off Regularization

B.1.1 Scalar Loop Integrals

The following d dimensionsal scalar field integrals in Euclidean space are evaluated via dimensional regularization [105]:

$$\begin{aligned} I_\alpha(M,\mu,d) &\equiv \mu^{4-d}\int_0^\infty \frac{d^dp}{(2\pi)^d}\frac{1}{(p^2+M^2)^\alpha} = \mu^{4-d}\frac{\Omega_d}{(2\pi)^d}\int_0^\infty \frac{p^{d-1}dp}{(p^2+M^2)^\alpha} \\ &= \mu^{4-d}\frac{2\pi^{d/2}}{\Gamma(d/2)}\frac{1}{(2\pi)^d}M^{-2\alpha}\int_0^\infty \frac{p^{d-1}dp}{(p^2/M^2+1)^\alpha} \\ &= \frac{\mu^{4-d}}{(4\pi)^{d/2}\Gamma(d/2)}M^{d-2\alpha}\int_0^\infty \frac{t^{d/2-1}dt}{(t+1)^\alpha} \end{aligned} \tag{B.1.1}$$

with $t \equiv p^2/M^2$. By making use of the Beta function

$$B(x,y) = \int_0^\infty \frac{t^{x-1}dt}{(1+t)^{x+y}} = \frac{\Gamma(x)\Gamma(y)}{\Gamma(x+y)}, \tag{B.1.2}$$

which is convergent for $x>0$ and $y>0$, we obtain

$$I_\alpha(M,\mu,d) = \frac{\mu^{4-d}M^{d-2\alpha}}{(4\pi)^{d/2}}\frac{\Gamma(\alpha-d/2)}{\Gamma(\alpha)}, \tag{B.1.3}$$

$$I_1(M,\mu,4-\epsilon) = \frac{\mu^\epsilon M^{2-\epsilon}}{(4\pi)^{2-\epsilon/2}}\Gamma(-1-\epsilon/2), \qquad I_2(M,\mu,4-\epsilon) = \frac{\mu^\epsilon M^{-\epsilon}}{(4\pi)^{2-\epsilon/2}}\Gamma(-\epsilon/2) \tag{B.1.4}$$

$$I_1(M,\mu,3) = -\frac{\mu M}{4\pi}, \qquad I_2(M,\mu,3) = \frac{\mu}{2\pi M}. \tag{B.1.5}$$

These integrals appear in the calculation of the Goldstone effect, Sec. 3.2.2. The μ-dependence of the three-dimensional integrals is usually dropped, as dimensional regularization can not account for power divergences.

The divergences of the four-dimensional integrals can be rewritten as explicit logarithms by making use of $a^x = \exp(\log(a)x) = 1+\log(a)x+\mathcal{O}\left(x^2\right)$:

$$\begin{aligned} I_1(M,\mu,4-\epsilon) &= \frac{M^2}{(4\pi)^2}\left[1+\frac{\epsilon}{2}\log\left(\frac{4\pi\mu^2}{M^2}\right)+\mathcal{O}\left(\epsilon^2\right)\right]\left(\frac{-2}{\epsilon}\right) \\ &\quad\times\left(1+\frac{\epsilon}{2}+\mathcal{O}\left(\epsilon^2\right)\right)\left(\Gamma(1)+\frac{\epsilon}{2}\Gamma'(1)+\mathcal{O}\left(\epsilon^2\right)\right) \\ &= \frac{M^2}{(4\pi)^2}\left[-\frac{2}{\epsilon}+\gamma_E-1-\log(4\pi)+\log\left(\frac{M^2}{\mu^2}\right)+\mathcal{O}(\epsilon)\right] \end{aligned} \tag{B.1.6}$$

with $\gamma_E = \Gamma'(1) \simeq 0.5772$.

This can be readily compared to cut-off regularization

$$I_\alpha(M,\Lambda,d) = \int_0^\Lambda \frac{d^dp}{(2\pi)^d}\frac{1}{(p^2+M^2)^\alpha} = \frac{\Omega_{d-1}}{(2\pi)^d}\int_0^\Lambda \frac{p^{d-1}dp}{(p^2+M^2)^\alpha}, \tag{B.1.7}$$

$$\begin{aligned} I_1(M,\Lambda,4) &= \frac{1}{8\pi^2}\frac{1}{2}(\Lambda^2 - M^2\log\left(\Lambda^2/M^2+1\right)) \\ &\simeq \frac{1}{16\pi^2}(\Lambda^2 - M^2\log\left(\Lambda^2/M^2\right)), \end{aligned} \tag{B.1.8}$$

$$\begin{aligned} I_2(M,\Lambda,4) &= \frac{1}{8\pi^2}\frac{1}{2}\left(\frac{M^2}{\Lambda^2+M^2} - \log\left(\Lambda^2/M^2+1\right) - 1\right) \\ &\simeq -\frac{1}{16\pi^2}\left(1+\log\left(\Lambda^2/M^2\right)\right), \end{aligned} \tag{B.1.9}$$

$$I_1(M,\Lambda,3) = \frac{1}{2\pi^2}(\Lambda - M\arctan(\Lambda/M) \simeq \frac{\Lambda}{2\pi^2} - \frac{M}{4\pi}, \tag{B.1.10}$$

$$I_2(M,\Lambda,3) = \frac{1}{2\pi^2}\frac{1}{2}\left(-\frac{\Lambda}{\Lambda^2+M^2} + \frac{\arctan\Lambda/M}{M}\right) \simeq -\frac{1}{4\pi^2} + \frac{1}{8\pi M}, \tag{B.1.11}$$

where the approximations are valid for $\Lambda \gg M$. Here we also encounter logarithmic divergences in four dimensions and power divergences in three dimensions.

B.1.2 Renormalization

We noted that it is possible to absorb the one-loop divergences by the renormalziation of the low energy constants L_i and high energy constant H_2 of the effective chiral Lagrangian. The coefficients of the renormalizations prescriptions [51]

$$L_i = L_i^r + \Gamma^i\lambda, \qquad H_2 = H_2^r + \tilde{\Gamma}^2\lambda \tag{B.1.12}$$

$$\lambda = \frac{\mu^{d-4}}{(4\pi)^2}\left\{\frac{1}{d-4} - \frac{1}{2}\left(\log(4\pi) - \gamma_E + 1\right)\right\}. \tag{B.1.13}$$

are given in Tab. B.1. The renormalized coefficients depend on the scale μ:

$$L_i^r(\mu_2) = L_i^r(\mu_1) + \frac{\Gamma_i}{(4\pi)^2}\log\left(\frac{\mu_1}{\mu_2}\right). \tag{B.1.14}$$

The scale dependence of the coefficients and the finite part of the loop integrals compensate such that physical observables are scale independent.

Γ_1	Γ_2	Γ_3	Γ_4	Γ_5	Γ_6	Γ_7	Γ_8	$\tilde{\Gamma}_2$
$\frac{3}{32}$	$\frac{3}{16}$	0	$\frac{1}{8}$	$\frac{3}{8}$	$\frac{11}{144}$	0	$\frac{5}{48}$	$\frac{5}{24}$

Table B.1: Coefficients for the renormalization of the low-/high-energy constants $L_i = L_i^r + \Gamma_i\lambda$, $H_2 = H_2^r + \tilde{\Gamma}_2\lambda$ in chiral perturbation theory for three non-degenerate flavors [51].

B.1.3 Ultraviolet Divergence in Chiral Condensate

In Sec. 5.2.3 we have calculated the ultraviolet divergent term $c_{\mathcal{UV}}/a^2$ from the free fermi gas. In fact, it stems from the following loop integral:

$$\begin{aligned} \left\langle\bar{\psi}\psi\right\rangle_q^{\mathrm{UV}} =& \nu_f\,\mathrm{Tr}\int\frac{d^4k}{(2\pi)^4}\frac{\not{k}+m}{k^2+m^2} = -\nu_f\frac{8\pi^2}{(2\pi)^4}m\int_0^{\pi/a}\frac{k^3dk}{k^2+m^2} \\ =& m\frac{\nu_f}{4\pi^2}\left\{(\pi/a)^2 - m^2\log\left(\frac{(\pi/a)^2}{m^2}+1\right)\right\} \simeq m\frac{\nu_f}{4a^2} = N_{\mathrm{f}}c_{\mathcal{UV}}m/a^2 \end{aligned} \tag{B.1.15}$$

with $\nu_f = 2N_{\rm c}N_{\rm f}$. Now we want to demonstrate that the contact term indeed shows up in the connected susceptibility. The connected part to lowest order is the following loop integral with two insertions:

$$\begin{aligned}\chi^{\rm con,UV} =& \nu_f \,\mathrm{Tr} \int \frac{d^4k}{(2\pi)^4} \frac{\not{k}+m}{k^2+m^2} \frac{-\not{k}+m}{k^2+m^2} = -\nu_f \frac{8\pi^2}{(2\pi)^4} \int_0^{\pi/a} \frac{k^2-m^2}{(k^2+m^2)^2} k^3 dk \\ =& \frac{\nu_f}{4\pi^2} \left\{ (\pi/a)^2 - 3m^2 \log\left(\frac{(\pi/a)^2}{m^2}+1\right) + 2 - \frac{2m^4}{(\pi/a)^2+m^2} \right\} \simeq \frac{\nu_f}{4a^2} = N_{\rm f} c_{\mathcal{UV}}/a^2\end{aligned} \tag{B.1.16}$$

where we have used that $\mathrm{tr}\,\not{k}^2 = 4k^2$. We obtain the same result as before, which proves our hypothesis. Note that the above integrals are also approximately valid for staggered fermions, as the staggered denominator is dominated by the physical pole in the continuum limit, $\sum_\mu \sin^2(p_\mu/2)/a^2 + m^2 \simeq p^2 + m^2$. Note also that both the lattice condensate $\left\langle \mathrm{tr}\, M^{-1} \right\rangle$ and lattice connected part $\left\langle -\mathrm{tr}\, M^{-2} \right\rangle$ are indeed normalized with a factor $N_{\rm c}N_{\rm f}$.

Also in the bosonic integrals we find the same contact term, provided that the cut-off is $2\pi/a$, as the mesons are composed of two quarks, each of them carrying a momentum up to π/a: On the lattice in 4 dimensions, the contact term contribution to the Goldstone boson propagator is:

$$G_\pi(x) = \nu_b I_1(M, 2\pi/a, 4) \approx \frac{\nu_b}{4a^2} - \frac{1}{4\pi^2} M^2 \log\left((2\pi/a)^2/M^2\right) \tag{B.1.17}$$

Now, usually $\nu_b = 2N_{\rm f}^2 - 1$ when we consider chiral aspects, but UV-divergences are also present in the massive states such as the η'. The Goldstone bosons also carry intrinsic color (and anti-color), hence also a factor $N_{\rm c}$ is comprehensible.

B.2 Chiral Perturbation Theory to One Loop

In this section we present calculations in chiral perturbation theory based on the paper by Gasser and Leutwyler from 1985 [51], who provide a general framework for computations with an arbitrary number of flavors. We will discuss how to calculate the chiral condensate and how to derive the connected and disconnected susceptibility.

B.2.1 The $\mathfrak{su}(N)$ Lie Algebra

In the defining or fundamental representation the generators t^a are represented by $N \times N$ matrices, which are conventionally normalized by the condition

$$t^a t^b = \frac{1}{2N}\delta_{ab}\mathbb{1}_N + \frac{1}{2}\sum_{c=1}^{N^2-1}(if_{abc} + d_{abc})t^c, \tag{B.2.1}$$

where f_{abc} and d_{abc} are the antisymmetric and symmetric structure constants. As a consequence, the (anti-)commutators are

$$\left[t^a, t^b\right] = i\sum_{c=1}^{N^2-1} f_{abc}t^c, \qquad \left\{t^a, t^b\right\} = \frac{1}{N}\delta_{ab} + \sum_{c=1}^{N^2-1} d_{abc}t^c. \tag{B.2.2}$$

and also the following relations among the structure constants are implied:

$$\sum_{c,e=1}^{N^2-1} f_{ace}f_{bce} = N\delta_{ab}, \qquad \sum_{c,e=1}^{N^2-1} d_{ace}d_{bce} = \frac{N^2-4}{N}\delta_{ab}. \tag{B.2.3}$$

The quadratic casimir operator $C_2(N)$ in the fundamental representation is defined by

$$\sum_{a=1}^{N^2-1} t^a t^a = C_2(N)\mathbb{1}_N, \qquad C_2(N) = \frac{N^2-1}{2N}. \tag{B.2.4}$$

The generators also satisfy the following completeness relation for arbitrary $N \times N$ matrices A,B:

$$\sum_{a=1}^{N^2-1} \operatorname{tr}(\lambda^a A \lambda^a B) = -\frac{2}{N}\operatorname{tr}(AB) + 2\operatorname{tr} A \operatorname{tr} B. \tag{B.2.5}$$

We also give the symmetric structure constants for $\mathfrak{su}(3)$ which we will need below:

$$\begin{aligned} d_{118} = d_{228} = d_{338} = -d_{888} &= \frac{1}{\sqrt{3}} \\ d_{448} = d_{558} = d_{668} = d_{778} &= -\frac{1}{2\sqrt{3}} \\ d_{146} = d_{157} = -d_{247} = d_{256} = d_{344} = d_{355} = -d_{366} = -d_{377} &= \frac{1}{2}. \end{aligned} \tag{B.2.6}$$

B.2.2 The Chiral One-Loop Generating Functional

The chiral partition function up to 1-loop is composed of the pieces

$$\mathcal{Z} = \mathcal{Z}_1 + \mathcal{Z}_2 + \mathcal{Z}_A + \mathcal{Z}_{\text{1-loop}}, \qquad \mathcal{Z}_1 = \int d^dx \mathcal{L}^{(2)}, \qquad \mathcal{Z}_2 = \int d^dx \mathcal{L}^{(4)}, \tag{B.2.7}$$

where $\mathcal{Z}_A$ captures the $\mathrm{U_A}(1)$ anomaly which we will neglect here. We focus on the one-loop generating functional $\mathcal{Z}_{\text{1-loop}}$. We will consider the fields in the neigborhood of the classical solution

$$\bar{U} = u^2, \qquad U = u\left(\mathbb{1} + i\boldsymbol{\phi} - \frac{1}{2}\boldsymbol{\phi}^2 \ldots\right)u, \qquad \boldsymbol{\phi} = \phi^i\lambda^i = \phi_P\lambda_P \tag{B.2.8}$$

In contrast to SU(2) or the O(N) models, where the sigma mode is given by the condition $\sigma^2 = F_0^2 - \boldsymbol{\pi}^2$, the expression for the sigma mode in general $\mathrm{SU}(N_\mathrm{f})$ non-linear sigma models is more complicated due to non-vanishing symmetric structure constants, and it also involves the quark mass matrix $\mathcal{M}$:

$$\sigma = B_0\left(u\mathcal{M}u + u^\dagger\mathcal{M}u^\dagger\right) \tag{B.2.9}$$

The sigma mode as defined here has another mass dimension than the pseudo-scalar meson fields ϕ_P as it is not possible to eliminate $\mathcal{M}$ at this stage. The quark mass matrix aligns the field u just as the external field H does in O(N) models. In the ground state, where $u = \bar{U} = \mathbb{1}$, the sigma mode acquires the vacuum expectation value and can be identified with the chiral condensate:

$$\left\langle\bar{\psi}\psi\right\rangle_q = F_0^2\frac{\partial}{\partial m_q}\langle\sigma\rangle = B_0F_0^2. \tag{B.2.10}$$

Before we will come to the more specific case of $N_\mathrm{f} = 3$ non-degenerate flavors, we will outline the general structure of the 1-loop generating functional, as discussed in detail in [51]. It is defined via the Gaussian integral

$$e^{i\mathcal{Z}_{\text{1-loop}}} = \int[D\boldsymbol{\phi}]\exp\left(\frac{i}{2}F_0^2\int d^dx\sum_{a,b=1}^{N_\mathrm{f}^2-1}\phi^a\lambda^aD^{ab}\phi^b\lambda^b\right) = N_\mathrm{f}(\det D)^{-1/2} \tag{B.2.11}$$

with the differential operator

$$D^{ab} = \partial^2 + \hat{\sigma}^{ab}, \qquad \hat{\sigma}^{ab} = \frac{1}{4}\,\mathrm{tr}\left(\left\{\lambda^a, \lambda^b\right\}\sigma\right) \tag{B.2.12}$$

where $\hat{\sigma}^{ab}$ is the flavor tensor which specifies how the sigma mode couples to the pseudoscalars. The 1-loop contribution can then be expressed as follows:

$$\begin{aligned}\mathcal{Z}_{\text{1-loop}} &= \frac{1}{2} i \log\det D \qquad\qquad (B.2.13)\\ &= \frac{F_0^2}{4}\left\{-\frac{1}{d}\,\mathrm{Sp}\,\mathbb{1} + \frac{1}{4\pi(d-2)}\int d^dx\,\mathrm{Sp}\,\hat{\sigma} - \frac{1}{(4\pi)^2(d-4)}\int d^dx d^dy\,\mathrm{Sp}\left(\tfrac{1}{2}\hat{\sigma}^2\right)\ldots\right\},\end{aligned}$$

where Sp denotes the trace in the $(N_\mathrm{f}^2-1)\times(N_\mathrm{f}^2-1)$ dimensional space. The poles of the full differential operator D at $d = 0, 2, 4, \ldots$ stem from UV-divergences. Evaluation of the trace yields:

$$\begin{aligned}\mathrm{Sp}\,(\hat{\sigma}) = \sum_{a=1}^{N_\mathrm{f}^2-1}\hat{\sigma}^{aa} &= \frac{1}{4}\sum_{a=1}^{N_\mathrm{f}^2-1}\mathrm{tr}\,(\{\lambda^a,\lambda^a\}\,\sigma) = \sum_{a=1}^{N_\mathrm{f}^2-1}\mathrm{tr}\left(\frac{1}{N_\mathrm{f}}\delta^{aa}\sigma + \sum_{c=1}^{N_\mathrm{f}^2-1} d_{aac}\frac{\lambda^c}{2}\sigma\right)\\ &= \frac{N_\mathrm{f}^2-1}{N_\mathrm{f}}\,\mathrm{tr}\,\sigma, \qquad\qquad (B.2.14)\end{aligned}$$

where we have used the fact that $\sum_{a=1}^{N^2-1} d_{aac} = 0$, which can be seen by combining Eq. (B.2.1) and Eq. (B.2.4). In order to calculate $\mathrm{Sp}\left(\frac{1}{2}\hat{\sigma}^2\right)$, we make use of the following identity obtained from the completeness relation in Eq. (B.2.5):

$$\sum_{a=1}^{N_\mathrm{f}^2-1}\mathrm{tr}\,(\lambda^a A)\,\mathrm{tr}\,(\lambda^a B) = 2\,\mathrm{tr}\,(AB) - \frac{2}{N_\mathrm{f}}\,\mathrm{tr}\,A\,\mathrm{tr}\,B \tag{B.2.15}$$

With this one obtains:

$$\begin{aligned}\mathrm{Sp}\left(\tfrac{1}{2}\hat{\sigma}^2\right) &= \frac{1}{2}\sum_{a,b=1}^{N_\mathrm{f}^2-1}\hat{\sigma}^{ab}\hat{\sigma}^{ba} = \frac{1}{32}\sum_{a,b}\mathrm{tr}\left(\left\{\lambda^a,\lambda^b\right\}\sigma\right)\mathrm{tr}\left(\left\{\lambda^b,\lambda^a\right\}\sigma\right)\\ &= \frac{1}{2N_\mathrm{f}^2}\sum_{a,b=1}^{N_\mathrm{f}^2-1}\delta^{ab}\,(\mathrm{tr}\,\sigma)^2 + \frac{1}{2N_\mathrm{f}}\sum_{a,b=1}^{N_\mathrm{f}^2-1}\delta^{ab}\sum_{c=1}^{N_\mathrm{f}^2-1} d_{aac}\,\mathrm{tr}\,\sigma\,\mathrm{tr}\,(\lambda^c\sigma) + \frac{1}{8}\sum_{a,b,c,d=1}^{N_\mathrm{f}^2-1} d_{abc}d_{abd}\,\mathrm{tr}\,(\lambda^c\sigma)\,\mathrm{tr}\left(\lambda^d\sigma\right)\\ &= \frac{N_\mathrm{f}^2-1}{2N_\mathrm{f}^2}\,(\mathrm{tr}\,\sigma)^2 + \frac{1}{2N_\mathrm{f}}\sum_{a,c=1}^{N_\mathrm{f}^2-1} d_{aac}\,\mathrm{tr}\,\sigma\,\mathrm{tr}\,(\lambda^c\sigma) + \frac{1}{8}\sum_{c,d=1}^{N_\mathrm{f}^2-1}\frac{N_\mathrm{f}^2-4}{N_\mathrm{f}}\delta_{cd}\,\mathrm{tr}\,(\lambda^c\sigma)\,\mathrm{tr}\,(\lambda^c\sigma)\\ &= \frac{N_\mathrm{f}^2-1}{2N_\mathrm{f}^2}\,(\mathrm{tr}\,\sigma)^2 + \frac{N_\mathrm{f}^2-4}{8N_\mathrm{f}}\left(2\,\mathrm{tr}\,\sigma^2 - \frac{2}{N_\mathrm{f}}(\mathrm{tr}\,\sigma)^2\right)\\ &= \frac{N_\mathrm{f}^2+2}{4N_\mathrm{f}^2}\,(\mathrm{tr}\,\sigma)^2 + \frac{N_\mathrm{f}^2-4}{4N_\mathrm{f}}\,\mathrm{tr}\,\sigma^2, \qquad\qquad (B.2.16)\end{aligned}$$

where we have used Eq. (B.2.3) and Eq. (B.2.15). After substituting Eq. (B.2.9) we obtain

$$\mathrm{Sp}\,(\hat{\sigma}) = \frac{N_\mathrm{f}^2-1}{N_\mathrm{f}}B_0\,\mathrm{tr}\left(\mathcal{M}\bar{U} + \bar{U}^\dagger\mathcal{M}\right) \tag{B.2.17}$$

$$\mathrm{Sp}\left(\tfrac{1}{2}\hat{\sigma}^2\right) = \frac{N_\mathrm{f}^2+2}{4N_\mathrm{f}^2}B_0^2\left(\mathrm{tr}\left(\mathcal{M}\bar{U} + \bar{U}^\dagger\mathcal{M}\right)\right)^2 + \frac{N_\mathrm{f}^2-4}{4N_\mathrm{f}}B_0^2\,\mathrm{tr}\left(\mathcal{M}\bar{U}\mathcal{M}\bar{U} + \bar{U}^\dagger\mathcal{M}\bar{U}^\dagger\mathcal{M} + 2\mathcal{M}\mathcal{M}\right). \tag{B.2.18}$$

The traces can not be evaluated in general as the solution $\bar{U}$ to the classical EoM will usually deviate from unity. For that purpose a physical basis has to be introduced, which we will do in the next section for the special case $N_\mathrm{f} = 3$. Here, we will give the result for the chiral condensate and the chiral susceptibility for the degenerated case $\mathcal{M} = m\mathbb{1}$. With

$$\Sigma = B_0 F_0^2 \left(\bar{U} + \bar{U}^\dagger\right), \qquad \mathrm{tr}\,(\mathcal{M}\Sigma) = m\,\mathrm{tr}\,\Sigma \tag{B.2.19}$$

the chiral condensate obtained from Eq. (B.2.14) via the direct derivative w.r.t. m

$$\begin{aligned}\langle 0|\bar{\psi}\psi|0\rangle &= -\frac{1}{V}\frac{\partial}{\partial m}\mathcal{Z}_{\text{1-loop}} = -\frac{1}{V}\frac{\partial}{\partial m}\int d^dx \left\{\frac{F_0^2}{4(4\pi)(d-2)}\,\mathrm{Sp}\,\hat{\sigma}\right\} \\ &= -\frac{1}{4(4\pi)(d-2)}\frac{N_\mathrm{f}^2-1}{N_\mathrm{f}}\langle \mathrm{tr}\,\Sigma\rangle + \mathcal{O}(m)\end{aligned} \tag{B.2.20}$$

Likewise for the chiral susceptibility

$$\begin{aligned}\chi &= -\frac{1}{V}\frac{\partial^2}{\partial m^2}\mathcal{Z}_{\text{1-loop}} = -\frac{1}{V}\frac{\partial^2}{\partial m^2}\int d^dx d^dy \left\{\frac{F_0^2}{4(4\pi)^2(d-4)}\,\mathrm{Sp}\left(\tfrac{1}{2}\hat{\sigma}\right)\right\} \\ &= \frac{V}{16F_0^2(4\pi)^2(d-4)}\left(\frac{N_\mathrm{f}^2+2}{N_\mathrm{f}^2}\left\langle(\mathrm{tr}\,\Sigma)^2\right\rangle + \frac{N_\mathrm{f}^2-4}{N_\mathrm{f}}\left\langle\mathrm{tr}\left(\Sigma^2\right)\right\rangle\right)\end{aligned} \tag{B.2.21}$$

we are able to identify the disconnected part (first term) and connected part (second term) of the susceptibility.

B.2.3 The Gell-Mann matrices in Physical Mass Basis

We will now turn to $N_\mathrm{f} = 3$ non-degenerate flavors. With the definition $K_0^+ \equiv K^0$, $K_0^- \equiv \bar{K}^0$ we calculate the anti-commutators of the Gell-Mann matrices in the physical basis:

$$\{\lambda_{\pi^+}, \lambda_{\pi^-}\} = -\left\{(d_{118}+d_{228})\lambda^8 + \tfrac{2}{3}\mathbb{1}\right\} = -\tfrac{1}{\sqrt{3}}\lambda_\eta - \tfrac{2}{3}\mathbb{1} \tag{B.2.22}$$

$$\{\lambda_{K^+}, \lambda_{K^-}\} = -\left\{(d_{448}+d_{558})\lambda^8 + (d_{443}+d_{553})\lambda^3 + \tfrac{4}{3}\mathbb{1}\right\} = -\tfrac{1}{\sqrt{3}}\lambda_\eta - \tfrac{1}{2}\lambda_{\pi^0} - \tfrac{4}{3}\mathbb{1} \tag{B.2.23}$$

$$\{\lambda_{K_0^+}, \lambda_{K_0^-}\} = -\left\{(d_{668}+d_{778})\lambda^8 + (d_{663}+d_{773})\lambda^3 + \tfrac{4}{3}\mathbb{1}\right\} = -\tfrac{1}{\sqrt{3}}\lambda_\eta + \tfrac{1}{2}\lambda_{\pi^0} - \tfrac{4}{3}\mathbb{1} \tag{B.2.24}$$

$$\{\lambda_{K^\pm}, \lambda_{\pi^0}\} = \mp\sqrt{2}\left\{d_{434}\lambda^4 \pm \lambda_{535}\lambda^5\right\} = \lambda_{K^\pm} \tag{B.2.25}$$

$$\{\lambda_{K_0^\pm}, \lambda_{\pi^0}\} = \mp\sqrt{2}\left\{d_{636}\lambda^6 \pm \lambda_{737}\lambda^7\right\} = -\lambda_{K_0^\pm} \tag{B.2.26}$$

$$\{\lambda_{\pi^\pm}, \lambda_{\eta}\} = \mp\sqrt{2}\left\{d_{181}\lambda^1 \pm \lambda_{282}\lambda^2\right\} = \tfrac{2}{\sqrt{3}}\lambda_{\pi^\pm} \tag{B.2.27}$$

$$\{\lambda_{K^\pm}, \lambda_{\eta}\} = \mp\sqrt{2}\left\{d_{484}\lambda^4 \pm \lambda_{585}\lambda^5\right\} = -\tfrac{1}{\sqrt{3}}\lambda_{K^\pm} \tag{B.2.28}$$

$$\{\lambda_{K_0^\pm}, \lambda_{\eta}\} = \mp\sqrt{2}\left\{d_{686}\lambda^6 \pm \lambda_{787}\lambda^7\right\} = -\tfrac{1}{\sqrt{3}}\lambda_{K_0^\pm} \tag{B.2.29}$$

$$\{\lambda_{\pi^\pm}, \lambda_{K^\mp}\} = -\left\{(d_{146}+d_{256})\lambda^6 \pm i(d_{157}-d_{247})\lambda^7\right\} = \sqrt{2}\lambda_{K_0^\pm} \tag{B.2.30}$$

$$\{\lambda_{\pi^\pm}, \lambda_{K_0^\pm}\} = \pm\left\{(d_{164}-d_{274})\lambda^4 \pm i(d_{175}+d_{265})\lambda^5\right\} = -\sqrt{2}\lambda_{K^\pm} \tag{B.2.31}$$

$$\{\lambda_{K^\pm}, \lambda_{K_0^\mp}\} = \pm\left\{(d_{461}+d_{571})\lambda^1 \pm i(d_{562}-d_{472})\lambda^2\right\} = -\sqrt{2}\lambda_{\pi^\pm} \tag{B.2.32}$$

$$\{\lambda_{\pi^0}, \lambda_{\pi^0}\} = 2d_{338}\lambda^8 + \tfrac{2}{3}\mathbb{1} = \tfrac{2}{\sqrt{3}}\lambda_\eta + \tfrac{2}{3}\mathbb{1} \tag{B.2.33}$$

$$\{\lambda_{\pi^0}, \lambda_{\eta}\} = 2d_{383}\lambda^3 = \tfrac{2}{\sqrt{3}}\lambda_{\pi^0} \tag{B.2.34}$$

$$\{\lambda_{\eta}, \lambda_{\eta}\} = 2d_{888}\lambda^8 + \tfrac{2}{3}\mathbb{1} = -\tfrac{1}{\sqrt{3}}\lambda_\eta + \tfrac{2}{3}\mathbb{1} \tag{B.2.35}$$

With these anti-commutators, the tree-level masses $\mathring{M}_P^2 = B_0\,\mathrm{tr}\left(\mathcal{M}\lambda_P\lambda_P^\dagger\right)$ given explicitly in Eqs. (4.2.10-4.2.10) are readily obtained. Note that $\lambda_{p^\pm}^\dagger = -\lambda_{p^\mp}$ of the charged particles $p^\pm \in$

$\{\pi^\pm, K^\pm\}$ and $\lambda_P^\dagger = \lambda_P$ for the neutral particles $P^\pm \in \{\pi^\pm, K^\pm\}$. We have explicity given the diagonal matrices as their non-vanishing trace will give contribution to the chiral condensate:

$$\{\lambda_{\pi^\pm}, \lambda_{\pi^\pm}^\dagger\} = 2\begin{pmatrix} 1 & 0 & 0 \\ 0 & 1 & 0 \\ 0 & 0 & 0 \end{pmatrix}, \quad \{\lambda_{K^\pm}, \lambda_{K^\pm}^\dagger\} = 2\begin{pmatrix} 1 & 0 & 0 \\ 0 & 0 & 0 \\ 0 & 0 & 1 \end{pmatrix}, \quad \{\lambda_{K_0^\pm}, \lambda_{K_0^\pm}^\dagger\} = 2\begin{pmatrix} 0 & 0 & 0 \\ 0 & 1 & 0 \\ 0 & 0 & 1 \end{pmatrix},$$
$$\{\lambda_{\pi^0}, \lambda_{\pi^0}^\dagger\} = 2\begin{pmatrix} 1 & 0 & 0 \\ 0 & 1 & 0 \\ 0 & 0 & 0 \end{pmatrix}, \quad \{\lambda_\eta, \lambda_\eta^\dagger\} = \tfrac{2}{3}\begin{pmatrix} 1 & 0 & 0 \\ 0 & 1 & 0 \\ 0 & 0 & 4 \end{pmatrix} \tag{B.2.36}$$

B.2.4 Non-degenerate Calculations for $N_\mathrm{f} = 3$

We re-express the 1-loop generating functional in the new basis:

$$\mathcal{Z}_{\text{1-loop}} = \tfrac{1}{2} i \ln\det D = \tfrac{1}{2} i \ln\det D_0 + \tfrac{1}{4} i \operatorname{Tr}\left(D_0^{-1}\bar{\sigma}\right) - \tfrac{1}{4} i \operatorname{Tr}\left(D_0^{-1}\bar{\sigma}D_0^{-1}\bar{\sigma}\right) + \ldots, \tag{B.2.37}$$
$$D = D_0 + \bar{\sigma}, \quad D_{0,PQ} = \delta_{PQ}(\partial^2 + \mathring{M}_P^2), \quad \bar{\sigma}_{PQ} = \frac{1}{4}\operatorname{tr}\left(\{\lambda_P, \lambda_Q^\dagger\}\sigma\right) - \delta_{PQ}\mathring{M}_P^2, \tag{B.2.38}$$

where Tr denotes the trace in flavor and position space. The term $\operatorname{Tr}\left(D_0^{-1}\bar{\sigma}\right)$ contains all tadpole graphs (loops with one point insertion), D_0^{-1} is given by the scalar propagator $\Delta_P(x)$. Evaluation of the trace yields:

$$\begin{aligned}
\operatorname{Sp} D_0^{-1}\bar{\sigma} =& \sum_{P=1}^{8} \Delta_P(0)\bar{\sigma}_{PP} = \sum_{P=1}^{8} \Delta_P(0)\left(\frac{1}{4}\operatorname{tr}\left(\left\{\lambda_P, \lambda_P^\dagger\right\}\sigma\right) - \mathring{M}_P^2\right) \\
=& \frac{1}{4}\sum_{P=1}^{8} \Delta_P(0)\operatorname{tr}\left(\left\{\lambda_P, \lambda_P^\dagger\right\}\mathcal{M}(\bar{U} + \bar{U}^\dagger - 2\mathbb{1})\right) \\
=& \frac{1}{2}\left((m_u + m_d)(\Delta_{\pi^+}(0) + \Delta_{\pi^-}(0) + \Delta_{\pi^0}(0)) + (m_u + m_s)(\Delta_{K^+}(0) + \Delta_{K^-}(0))\right. \\
&\left. + (m_d + m_s)(\Delta_{K_0^+}(0) + \Delta_{K_0^-}(0)) + \tfrac{1}{3}(m_u + m_d + 4m_s)\Delta_\eta(0)\right)
\end{aligned} \tag{B.2.39}$$

This yields the contributions to the chiral condensates, as given in Eqs. (4.2.30-4.2.32).

In principle, it is straight forward to proceed and calculate the next order of the 1-loop generating functional, where one can exploit the identity

$$\sum_{PQ} \bar{\sigma}_{PQ}\bar{\sigma}_{QP} = \operatorname{Sp}\hat{\sigma}^2 - 2\sum_P \left(\mathring{M}_P^2\bar{\sigma}_{PP} - \mathring{M}_P^4\right), \tag{B.2.40}$$

however, the calculation is somewhat lengthy and we have already obtained the result via SχPT, so we will not discuss it here.

B.3 Additional Calculations in SχPT

B.3.1 Continuum Effective Action

Up to order $\mathcal{O}\left(a^2\right)$, the continuum effective action for staggered fermions, which describes quarks and gluons with momenta much below the cut-off $p \ll \pi/a$, is given by [85]:

$$\mathcal{L}_{\text{eff}} = \mathcal{L}^2 + a^2(\mathcal{L}^3_{\text{glue}} + \mathcal{L}^3_{\text{bilin}} + \mathcal{L}^3_{\text{FF(A)}} + \mathcal{L}^3_{\text{FF(B)}}), \tag{B.3.1}$$

$$\mathcal{L}^{(2)} = \frac{1}{2}\,\text{Tr}\,F_{\mu\nu}F_{\mu\nu} + \bar{Q}(\not{D} + \mathcal{M})Q, \qquad \not{D} = \sum_\mu (\gamma_\mu \otimes \mathbb{1})D_\mu, \tag{B.3.2}$$

$$\mathcal{L}^{(3)}_{\text{glue}} \sim \text{Tr}(D_\mu F_{\mu\nu} D_\rho F_{\rho\nu}) + \sum_{\mu\nu\rho}\text{Tr}(D_\mu F_{\nu\rho} D_\mu F_{\nu\rho}) + \sum_{\mu\nu}\text{Tr}(D_\mu F_{\mu\nu} D_\mu F_{\mu\nu}), \tag{B.3.3}$$

$$\begin{aligned}\mathcal{L}^{(3)}_{\text{bilin}} \sim{}& \bar{Q}(\not{D})^3 Q + \sum_\mu \bar{Q}(D_\mu^2 \not{D} + \not{D} D_\mu^2)Q + \sum_\mu \bar{Q} D_\mu \not{D} D_\mu Q + \sum_\mu \bar{Q}(\gamma_\mu \otimes \mathbb{1}) D_\mu^3 Q \\ &+ m\bar{Q}(\not{D})^2 Q + \sum_\mu m\bar{Q} D_\mu^2 Q + m^2 \bar{Q}\not{D} Q + m^3 \bar{Q} Q,\end{aligned} \tag{B.3.4}$$

$$\begin{aligned}\mathcal{L}^{(3)}_{\text{FF(A)}} \sim{}& [S\times A] + [S\times V] + [A\times S] + [V\times S] + [P\times V] + [P\times A] \\ &+ [V\times P] + [A\times P] + [T\times V] + [T\times A] + [V\times T] + [A\times T] \\ &+ ([S\times S] - [P\times P]) + ([S\times P] - [P\times S]) + ([S\times T] - [P\times T]) \\ &+ ([T\times S] - [T\times P]) + ([V\times V] - [A\times A]) + ([V\times A] - [A\times V]),\end{aligned} \tag{B.3.5}$$

$$\begin{aligned}\mathcal{L}^{(3)}_{\text{FF(B)}} \sim{}& [T_\mu \times V_\mu] + [T_\mu \times A_\mu] + [V_\mu \times T_\mu] + [A_\mu \times T_\mu] \\ &+ ([V_\mu \times V_\mu] - [A_\mu \times A_\mu]) - \frac{1}{4}([V\times V] - [A\times A]) \\ &+ ([V_\mu \times A_\mu] - [A_\mu \times V_\mu]) - \frac{1}{4}([V\times A] - [A\times V]),\end{aligned} \tag{B.3.6}$$

where the first letter indicates the spin structure while the second letter denotes the taste. This notation is shortcut for the product of quark bilinears, e.g.

$$[T\times V] \equiv \sum_{\mu<\nu}\sum_\rho \bar{Q}(y)(\gamma_{\mu\nu}\otimes\xi_\rho)Q(y)\bar{Q}(y)(\gamma_{\mu\nu}\otimes\xi_\rho)Q(y), \tag{B.3.7}$$

where γ is a spin matrix and ξ is a taste matrix. In $\mathcal{L}^{(3)}_{\text{FF(A)}}$, the Lorentz and taste indices are contracted separately, whereas in $\mathcal{L}^{(3)}_{\text{FF(B)}}$ the contractions lead to a correlation between spins and tastes. The latter do not contribute to the matching with the chiral effective potential because this would demand the inclusion of derivatives. The remaining symmetries of the particular terms of the staggered fermion Lagrangian are summarized in Tab. (4.2). The operators in $\mathcal{L}^{(3)}_{\text{glue}}$, $\mathcal{L}^{(3)}_{\text{bilin}}$ and $\mathcal{L}^{(3)}_{\text{FF(A)}}$ are mapped onto the effective potential $\mathcal{V}(U)$ given in Eq. 4.4.3 [85]. Consider e.g. operators with spin structure V or A, i.e. linear combinations of $[V\times F]$ and $[A\times F]$ with F denoting the taste, which consist of terms of the form

$$\mathcal{O}_F = \pm\sum_\mu \left(\bar{Q}_R(\gamma_\mu\otimes F_R)Q_R \pm \bar{Q}_L(\gamma_\mu\otimes F_R)Q_L\right)^2. \tag{B.3.8}$$

The operator $\mathcal{O}_F$ has to be invariant under chiral transformations, hence it is required that

$$F_L \to L F_L L^\dagger, \qquad F_R \to R F_R R^\dagger. \tag{B.3.9}$$

The operators of $\mathcal{V}$ are then composed of all operators which are chiral singlets, quadratic in F and parity invariant. After the matching, one sets $F_L = F_R = F$. Likewise one proceeds with spin structures S, P or T to end up with the effective potential $\mathcal{V}(U)$ The coefficients $C_k, C_{k'}$ are all of the order of Λ_{QCD}.

B.3.2 The Disconnected Meson Propagator

The partial fraction expansion of the disconnected propagator is given by

$$\left\langle \phi^t_{gs,fr}(-k)\phi^t_{f'r',g's'}(k)\right\rangle_{\text{dis}} = -\delta_{rs}\delta_{r's'}\delta_{fg}\delta_{f'g'}\delta_t\left(\frac{g^t_\pi}{k^2+m_{\pi,t}}+\frac{g^t_\eta}{k^2+m_{\eta,t}}+\frac{g^t_{\eta'}}{k^2+m_{\eta',t}}\right). \quad \text{(B.3.10)}$$

The residues are given by

$$\begin{aligned} g^t_\pi &= \frac{m^2_{S,t}-m^2_{\pi,t}}{(m^2_{\eta,t}-m^2_{\pi,t})(m^2_{\eta',t}-m^2_{\pi,t})} = \frac{1}{2n_{\text{r}}\delta_t},\\ g^t_\eta &= \frac{m^2_{S,t}-m^2_{\eta,t}}{(m^2_{\pi,t}-m^2_{\eta,t})(m^2_{\eta',t}-m^2_{\eta,t})}, \qquad g^t_{\eta'} = \frac{m^2_{S,t}-m^2_{\eta',t}}{(m^2_{\pi,t}-m^2_{\eta',t})(m^2_{\eta,t}-m^2_{\eta',t})} \end{aligned} \quad \text{(B.3.11)}$$

for $f,g,f'g' \in \{u,d\}$,

$$\begin{aligned} g^t_S &= \frac{m^2_{\pi,t}-m^2_{S,t}}{(m^2_{\eta,t}-m^2_{S,t})(m^2_{\eta',t}-m^2_{S,t})} = \frac{1}{n_{\text{r}}\delta_t},\\ g^t_\eta &= \frac{m^2_{\pi,t}-m^2_{\eta,t}}{(m^2_{S,t}-m^2_{\eta,t})(m^2_{\eta',t}-m^2_{\eta,t})}, \qquad g^t_{\eta'} = \frac{m^2_{\pi,t}-m^2_{\eta',t}}{(m^2_{S,t}-m^2_{\eta',t})(m^2_{\eta,t}-m^2_{\eta',t})} \end{aligned} \quad \text{(B.3.12)}$$

for $f,g,f'g' = s$ and

$$g^t_\eta = \frac{1}{(m^2_{\eta',t}-m^2_{\eta,t})} = -g^t_{\eta'} \quad \text{(B.3.13)}$$

for $f,g \in \{u,d\}, f'g' = s$. The identity for g^t_π and g^t_S is exact, whereas g^t_η and $g^t_{\eta'}$ can be expanded in δ_t, which implies

$$Z_t = m^2_{S,t} - m^2_{U,t} - n_r\delta_t + \frac{4n_r\delta_t}{m^2_{S,t}-m^2_{U,t}} + \mathcal{O}\left((\delta_t)^3\right) \quad \text{(B.3.14)}$$

and gives for $X,Y = U,D$:

$$g^t_\eta = -\frac{1}{2n_{\text{r}}\delta_t} + \frac{n_{\text{r}}\delta_t}{(m^2_{S,t}-m^2_{U,t})^2} + \mathcal{O}\left((n_r\delta_t)^2\right), \qquad g^t_{\eta'} = -\frac{n_{\text{r}}\delta_t}{(m^2_{S,t}-m^2_{U,t})^2} + \mathcal{O}\left((n_r\delta_t)^2\right) \quad \text{(B.3.15)}$$

and in the case $X,Y = S$:

$$g^t_\eta = -\frac{2n_{\text{r}}\delta_t}{(m^2_{S,t}-m^2_{U,t})^2} + \mathcal{O}\left((n_r\delta_t)^2\right), \qquad g^t_{\eta'} = -\frac{1}{n_{\text{r}}\delta_t} + \frac{2n_{\text{r}}\delta_t}{(m^2_{S,t}-m^2_{U,t})^2} + \mathcal{O}\left((n_r\delta_t)^2\right). \quad \text{(B.3.16)}$$

In the isosinglet taste channel, large m_0 implies

$$\frac{1}{Z_I} = \frac{1}{m_0^2} + \frac{1}{3}\frac{m^2_{S,t}-m^2_{U,t}}{m_0^4} + \mathcal{O}\left(m_0^{-6}\right). \quad \text{(B.3.17)}$$

Hence we obtain for $X,Y = U,D$:

$$g^I_\pi = \frac{3}{2m_0^2}, \qquad g^I_\eta = -\frac{1}{2m_0^2} - \frac{2}{3}\frac{m^2_{S,t}-m^2_{U,t}}{m_0^4} + \mathcal{O}\left(m_0^{-6}\right), \quad \text{(B.3.18)}$$

$$g^I_{\eta'} = -\frac{1}{m_0^2} + \frac{2}{3}\frac{m^2_{S,t}-m^2_{U,t}}{m_0^4} + \mathcal{O}\left(m_0^{-6}\right), \quad \text{(B.3.19)}$$

for $X,Y = S$:

$$g^I_S = \frac{3}{m_0^2}, \qquad g^I_\eta = -\frac{2}{m_0^2} + \frac{4}{3}\frac{m^2_{S,t}-m^2_{U,t}}{m_0^4} + \mathcal{O}\left(m_0^{-6}\right), \quad \text{(B.3.20)}$$

$$g^I_{\eta'} = -\frac{1}{m_0^2} - \frac{4}{3}\frac{m^2_{S,t}-m^2_{U,t}}{m_0^4} + \mathcal{O}\left(m_0^{-6}\right), \quad \text{(B.3.21)}$$

and for $X = U, D; Y = S$:

$$g_\eta^I \;=\; \frac{1}{m_0^2} + \frac{1}{3}\frac{m_{S,t}^2 - m_{U,t}^2}{m_0^4} + \mathcal{O}\left(m_0^{-6}\right) \;=\; -g_{\eta'}^I. \tag{B.3.22}$$

B.3.3 Bubble Terms Involving the Strange Quark

$$\begin{aligned}
B_{ss;ss}^{\mathrm{con}}(0) &= \mathcal{N}\sum_k \Bigg[-4n_{\mathrm{r}} \sum_{t=I,4V,4A} \frac{1}{k^2+m_{S,t}^2}\delta_t \left(\frac{g_S^t}{k^2+m_{S,t}^2} + \frac{g_\eta^t}{k^2+m_{\eta,t}^2} + \frac{g_{\eta'}^t}{k^2+m_{\eta',t}^2}\right) \\
&\quad + n_{\mathrm{r}}^2 \sum_{t=1}^{16} \left(\frac{2}{k^2+m_{K,t}^2}\frac{1}{k^2+m_{K,t}^2} + \frac{1}{k^2+m_{S,t}^2}\frac{1}{k^2+m_{S,t}^2}\right)\Bigg] \\
&= \mathcal{N}\Bigg[-4\hat{\mu}_{SS,I} - \frac{4m_0^2}{3}\left(g_\eta^I\hat{\mu}_{S\eta,I} + g_{\eta'}^I\hat{\mu}_{S\eta',I}\right) - 4\sum_{t=V,A}\left(4\hat{\mu}_{SS,t} + 4n_{\mathrm{r}}\delta_t\left(g_\eta^t\hat{\mu}_{S\eta,t} + g_{\eta'}^t\hat{\mu}_{S\eta',t}\right)\right) \\
&\quad + n_{\mathrm{r}}^2\sum_{t=1}^{16}\left(2\hat{\mu}_{KK,t} + \hat{\mu}_{SS,t}\right)\Bigg],
\end{aligned} \tag{B.3.23}$$

$$\begin{aligned}
B_{ss;ss}^{\mathrm{dis}}(0) &= \mathcal{N}\sum_k \left[n_{\mathrm{r}}^2\sum_{t=1}^{16}\frac{1}{\left(k^2+m_{S,t}^2\right)^2} + 2n_{\mathrm{r}}^2\sum_{t=I,4V,4A}\delta_t^2\left(\frac{g_S^t}{k^2+m_{\pi,t}^2} + \frac{g_\eta^t}{k^2+m_{\eta,t}^2} + \frac{g_{\eta'}^t}{k^2+m_{\eta',t}^2}\right)^2\right] \\
&= \mathcal{N}\Bigg[n_{\mathrm{r}}^2\sum_{t=1}^{16}\hat{\mu}_{SS,t} + 2\hat{\mu}_{SS,I} + \frac{4m_0^2}{3}\left(g_\eta^I\hat{\mu}_{S\eta,I} + g_{\eta'}^I\hat{\mu}_{S\eta',I}\right) \\
&\quad + \frac{2m_0^4}{9}\left((g_\eta^I)^2\hat{\mu}_{\eta\eta,I} + (g_{\eta'}^I)^2\hat{\mu}_{\eta'\eta',I} + 2g_\eta^I g_{\eta'}^t\hat{\mu}_{\eta\eta',I}\right) \\
&\quad + 4\sum_{t=V,A}\left(2\hat{\mu}_{SS,t} + 2n_{\mathrm{r}}\delta_t\left(g_\eta^t\hat{\mu}_{S\eta,t} + g_{\eta'}^t\hat{\mu}_{S\eta',t}\right)\right. \\
&\quad \left. + 2n_{\mathrm{r}}^2\delta_t^2\left((g_\eta^t)^2\hat{\mu}_{\eta\eta,t} + (g_{\eta'}^t)^2\hat{\mu}_{\eta'\eta',t} + 2g_\eta^t g_{\eta'}^t\hat{\mu}_{\eta\eta',t}\right)\right)\Bigg],
\end{aligned} \tag{B.3.24}$$

$$\begin{aligned}
B_{ss;ss}^{\mathrm{full}}(0) &= \mathcal{N}\Bigg[-2\hat{\mu}_{SS,I} - 4\sum_{t=V,A}\left(2\hat{\mu}_{SS,t} + 2n_{\mathrm{r}}\delta_t\left(g_\eta^t\hat{\mu}_{S\eta,t} + g_{\eta'}^t\hat{\mu}_{S\eta',t}\right)\right) \\
&\quad + n_{\mathrm{r}}^2\sum_{t=1}^{16}\left(2\hat{\mu}_{KK,t} + 2\hat{\mu}_{SS,t}\right) + \frac{2m_0^4}{9}\left((g_\eta^I)^2\hat{\mu}_{\eta\eta,I} + (g_{\eta'}^I)^2\hat{\mu}_{\eta'\eta',I} + 2g_\eta^I g_{\eta'}^I\hat{\mu}_{\eta\eta',I}\right) \\
&\quad + 4\sum_{t=V,A}\left(2n_{\mathrm{r}}^2\delta_t^2\left((g_\eta^t)^2\hat{\mu}_{\eta\eta,t} + (g_{\eta'}^t)^2\hat{\mu}_{\eta'\eta',t} + 2g_\eta^t g_{\eta'}^t\hat{\mu}_{\eta\eta',t}\right)\right)\Bigg],
\end{aligned} \tag{B.3.25}$$

$$\begin{aligned}
B_{ll;ss}^{\mathrm{dis}}(0) &= \mathcal{N}\sum_k \left[n_{\mathrm{r}}^2\sum_{t=1}^{16}\frac{1}{\left(k^2+m_{K,t}^2\right)^2} + 2n_{\mathrm{r}}^2\sum_{t=I,4V,4A}\delta_t^2\left(\frac{g_\eta^t}{k^2+m_{\eta,t}^2} + \frac{g_{\eta'}^t}{k^2+m_{\eta',t}^2}\right)^2\right] \\
&= \mathcal{N}\Bigg[n_{\mathrm{r}}^2\sum_{t=1}^{16}\hat{\mu}_{KK,t} + \frac{2m_0^4}{9}\left((g_\eta^I)^2\hat{\mu}_{\eta\eta,I} + (g_{\eta'}^I)^2\hat{\mu}_{\eta'\eta',t} + 2g_\eta^I g_{\eta'}^I\hat{\mu}_{\eta\eta',t}\right) \\
&\quad + 4\sum_{t=V,A}\left(2n_{\mathrm{r}}^2\delta_t^2\left((g_\eta^t)^2\hat{\mu}_{\eta\eta,t} + (g_{\eta'}^t)^2\hat{\mu}_{\eta'\eta',t} + 2g_\eta^t g_{\eta'}^t\hat{\mu}_{\eta\eta',t}\right)\right)\Bigg] \;=\; B_{ll;ss}^{\mathrm{full}}(0).
\end{aligned} \tag{B.3.26}$$

Appendix C

Tables

C.1 Chiral Condensate and Susceptibility Data

β	$\langle\bar{\psi}\psi\rangle_l$	$\chi_l^{\rm con}$	$\chi_l^{\rm dis}$	$\langle\bar{\psi}\psi\rangle_s$	$\chi_s^{\rm conn}$	$\chi_s^{\rm disc}$	# traj.
$N_\sigma^3 \times N_\tau = 32^3 \times 8$, $m_l a = 0.0048000$							
3.4800	0.0547(1)	2.51(0)	0.39(4)	0.1047(0)	1.931(2)	0.22(2)	7350
3.4900	0.0503(1)	2.52(0)	0.39(4)	0.1005(1)	1.940(1)	0.20(2)	7560
3.4950	0.0486(1)	2.52(0)	0.35(3)	0.0988(0)	1.941(0)	0.19(2)	7900
3.5000	0.0433(1)	2.62(0)	0.38(4)	0.0886(0)	2.007(2)	0.19(1)	4370
3.5150	0.0364(2)	2.70(1)	0.59(11)	0.0802(1)	2.040(1)	0.27(4)	6720
3.5200	0.0345(1)	2.71(0)	0.53(5)	0.0784(1)	2.043(2)	0.23(2)	6470
3.5300	0.0305(1)	2.78(0)	0.57(5)	0.0749(0)	2.056(1)	0.25(2)	24900
3.5350	0.0291(0)*	2.78(1)	0.61(3)*	0.0735(0)*	2.057(1)	0.24(1)*	4850
3.5375	0.0280(0)*	2.82(2)	0.64(4)*	0.0725(0)*	2.065(5)	0.26(1)*	4890
3.5400	0.0274(0)*	2.82(2)	0.62(4)*	0.0719(0)*	2.063(5)	0.24(1)*	5280
3.5425	0.0264(0)*	2.83(3)	0.72(4)*	0.0710(0)*	2.062(8)	0.29(1)*	4460
3.5450	0.0258(0)*	2.81(2)	0.61(3)*	0.0704(0)*	2.055(4)	0.25(1)*	5390
3.5475	0.0246(0)*	2.85(2)	0.65(3)*	0.0694(0)*	2.063(4)	0.25(1)*	4720
3.5500	0.0239(0)*	2.84(1)	0.46(2)*	0.0687(0)*	2.067(3)	0.19(1)*	5540
3.5525	0.0233(1)	0.00(0)	0.60(4)	0.0681(0)	0.000(0)	0.25(1)	22540
3.5550	0.0223(1)	2.86(1)	0.59(5)	0.0671(0)	2.074(3)	0.24(2)	23420
3.5600	0.0208(0)	2.84(1)	0.56(4)	0.0657(0)	2.074(3)	0.24(1)	31380
3.5700	0.0184(1)	0.00(0)	0.47(5)	0.0632(1)	0.000(0)	0.22(2)	9250

Table C.1: Mean values, errors and statistics of chiral observables for large quark masses for $N_\tau = 8$. Data marked with * were calculated at LLNL.

β	$\langle\bar{\psi}\psi\rangle_l$	χ_l^{con}	χ_l^{dis}	$\langle\bar{\psi}\psi\rangle_s$	χ_s^{conn}	χ_s^{disc}	# traj.
$N_\sigma^3 \times N_\tau = 32^3 \times 8$, $m_l a = 0.0006000$							
3.4900	0.0313(3)	3.62(40)	1.01(20)	0.0981(2)	1.969(6)	0.12(4)	1900
3.5150	0.0151(4)	5.63(22)	2.47(31)	0.0770(2)	2.099(4)	0.35(5)	5430
$N_\sigma^3 \times N_\tau = 32^3 \times 8$, $m_l a = 0.0012000$							
3.4800	0.0387(2)	3.13(3)	0.77(9)	0.1022(1)	1.961(1)	0.23(2)	8400
3.4900	0.0345(0)	3.27(3)	0.63(3)	0.0984(0)	1.968(1)	0.20(1)	33720
3.4950	0.0325(1)	3.31(4)	0.78(7)	0.0965(0)	1.970(1)	0.23(2)	11550
3.5000	0.0278(1)	3.56(3)	0.95(5)	0.0862(0)	2.043(1)	0.23(1)	32520
3.5100	0.0234(1)	3.74(3)	1.08(6)	0.0840(0)	2.039(2)	0.22(1)	30070
3.5150	0.0195(1)	4.16(3)	1.21(7)	0.0774(0)	2.090(1)	0.22(1)	30520
3.5200	0.0172(1)	4.32(3)	1.28(6)	0.0757(0)	2.096(1)	0.25(1)	40020
3.5225	0.0161(1)	0.00(0)	1.43(7)	0.0748(0)	0.000(0)	0.28(1)	50050
3.5250	0.0150(0)	4.49(3)	1.27(5)	0.0740(0)	2.103(1)	0.23(1)	50900
3.5275	0.0141(0)	0.00(0)	1.22(5)	0.0732(0)	0.000(0)	0.22(1)	50930
3.5300	0.0126(1)	4.69(5)	1.32(6)	0.0722(0)	2.107(2)	0.26(1)	50250
3.5350	0.0107(1)	4.77(7)	1.01(6)	0.0704(0)	2.106(4)	0.23(2)	18390
3.5400	0.0093(0)	4.78(4)	0.76(3)	0.0691(0)	2.116(2)	0.20(1)	47980
3.5600	0.0046(0)	3.95(4)	0.15(1)	0.0559(0)	2.192(2)	0.15(1)	11660
3.5850	0.0029(0)	2.98(3)	0.03(0)	0.0479(1)	2.180(1)	0.14(3)	8200
$N_\sigma^3 \times N_\tau = 32^3 \times 8$, $m_l a = 0.0024000$							
3.4800	0.0444(1)	2.83(1)	0.50(4)	0.1029(0)	1.951(1)	0.21(1)	10870
3.4900	0.0403(1)	2.88(4)	0.50(5)	0.0991(0)	1.957(4)	0.21(2)	13850
3.4950	0.0383(1)	2.88(1)	0.45(5)	0.0972(1)	1.959(1)	0.16(2)	6840
3.5000	0.0340(1)	3.04(3)	0.63(4)	0.0872(0)	2.028(2)	0.20(1)	10070
3.5150	0.0265(1)	3.24(2)	0.71(7)	0.0785(0)	2.070(1)	0.21(2)	10110
3.5200	0.0244(1)	0.00(0)	0.82(7)	0.0768(0)	0.000(0)	0.22(2)	11810
3.5225	0.0232(1)	3.36(2)	0.99(8)	0.0758(0)	2.076(2)	0.28(2)	29460
3.5250	0.0222(1)	3.45(2)	1.05(8)	0.0750(0)	2.084(2)	0.29(2)	23310
3.5275	0.0214(1)	3.42(2)	0.96(7)	0.0743(0)	2.079(2)	0.26(2)	24200
3.5300	0.0203(1)	3.47(1)	0.93(7)	0.0734(0)	2.085(2)	0.25(1)	26040
3.5325	0.0193(1)	3.50(2)	0.94(7)	0.0725(0)	2.088(2)	0.24(1)	20290
3.5350	0.0182(1)	3.53(2)	0.93(7)	0.0716(0)	2.090(2)	0.26(2)	28110
3.5375	0.0171(1)	3.55(2)	0.85(5)	0.0708(0)	2.094(4)	0.25(1)	29570
3.5400	0.0163(1)	0.00(0)	0.85(6)	0.0700(0)	0.000(0)	0.25(2)	22970
3.5425	0.0156(1)	3.59(1)	0.79(5)	0.0693(0)	2.097(1)	0.24(1)	25050
3.5450	0.0149(1)	3.60(2)	0.60(4)	0.0686(0)	2.100(2)	0.19(1)	15060
3.5500	0.0115(2)	3.72(2)	0.50(6)	0.0603(1)	2.170(3)	0.18(1)	8200
3.5600	0.0089(0)	3.56(2)	0.31(2)	0.0562(0)	2.182(1)	0.20(1)	9510
3.5700	0.0076(0)	3.29(1)	0.20(2)	0.0529(0)	2.183(1)	0.17(2)	20300
3.5850	0.0060(1)	2.95(3)	0.08(1)	0.0483(1)	2.178(3)	0.12(2)	4610

Table C.2: Mean values, errors and statistics of chiral observables for small quark masses for $N_\tau = 8$.

β	$\langle\bar{\psi}\psi\rangle_l$	χ_l^{con}	χ_l^{dis}	$\langle\bar{\psi}\psi\rangle_s$	χ_s^{conn}	χ_s^{disc}	# traj.
$N_\sigma^3 \times N_\tau = 32^3 \times 4$, $m_l a = 0.0008125$							
3.2800	0.1322(3)	3.90(16)	2.43(24)	0.2575(1)	1.412(1)	0.47(4)	18730
3.2900	0.1082(4)	4.73(12)	3.95(34)	0.2454(1)	1.477(1)	0.63(5)	20070
3.3000	0.0715(4)	7.44(11)	6.10(44)	0.2294(1)	1.575(1)	0.63(4)	18830
3.3025	0.0633(6)	8.46(13)	7.61(67)	0.2261(2)	1.593(1)	0.77(7)	15810
3.3050	0.0548(6)	9.44(12)	8.23(61)	0.2226(2)	1.613(1)	0.90(7)	15850
3.3075	0.0463(7)	10.83(21)	7.97(79)	0.2191(2)	1.635(2)	0.81(9)	11640
3.3100	0.0376(5)	12.31(14)	6.85(53)	0.2156(1)	1.656(1)	0.70(6)	15850
3.3200	0.0195(4)	12.98(17)	3.07(23)	0.2054(2)	1.706(2)	0.57(4)	10380
3.3300	0.0111(2)	10.48(11)	0.88(10)	0.1968(1)	1.745(1)	0.40(4)	6850
$N_\sigma^3 \times N_\tau = 32^3 \times 4$, $m_l a = 0.0016250$							
3.2800	0.1386(2)	3.15(5)	1.81(14)	0.2590(1)	1.400(1)	0.42(3)	21080
3.2850	0.1289(4)	3.34(10)	2.31(33)	0.2536(1)	1.430(1)	0.40(5)	9290
3.2900	0.1181(3)	3.80(6)	3.36(26)	0.2479(1)	1.460(1)	0.62(5)	20940
3.2950	0.1041(4)	4.28(16)	4.02(32)	0.2410(2)	1.502(3)	0.71(6)	15490
3.3000	0.0888(4)	5.10(6)	4.95(39)	0.2336(1)	1.543(1)	0.74(6)	20550
3.3025	0.0797(5)	5.63(8)	6.04(57)	0.2295(2)	1.568(2)	0.89(9)	16870
3.3050	0.0690(4)	6.47(6)	5.17(35)	0.2249(1)	1.599(1)	0.69(5)	21280
3.3075	0.0625(7)	6.89(10)	5.00(51)	0.2218(3)	1.614(2)	0.63(7)	6570
3.3100	0.0545(7)	7.45(9)	4.74(78)	0.2183(3)	1.633(2)	0.72(14)	7370
$N_\sigma^3 \times N_\tau = 16^3 \times 4$, $m_l a = 0.0016250$							
3.2800	0.1380(7)	3.77(12)	2.12(13)	0.2593(3)	1.401(2)	0.44(3)	21180
3.2900	0.1165(7)	4.47(12)	3.10(17)	0.2475(3)	1.462(2)	0.55(3)	27440
3.3000	0.0880(10)	5.74(11)	5.35(38)	0.2337(4)	1.541(3)	0.76(6)	40000
3.3050	0.0688(10)	7.11(10)	5.83(40)	0.2252(4)	1.599(3)	0.82(7)	42000
3.3100	0.0533(11)	8.14(13)	4.88(30)	0.2182(4)	1.636(3)	0.63(4)	24910
3.3200	0.0334(7)	9.05(8)	2.95(14)	0.2075(3)	1.692(2)	0.51(3)	25050
3.3300	0.0202(4)	8.16(9)	1.09(6)	0.1975(3)	1.740(2)	0.39(3)	14870
$N_\sigma^3 \times N_\tau = 16^3 \times 4$, $m_l a = 0.0032500$							
3.2800	0.1510(6)	2.83(6)	1.56(11)	0.2627(3)	1.376(2)	0.40(2)	15280
3.2850	0.1421(9)	2.93(10)	1.98(20)	0.2575(5)	1.405(5)	0.49(5)	13260
3.2900	0.1308(5)	3.20(3)	2.20(11)	0.2510(2)	1.433(2)	0.50(2)	45080
3.2950	0.1204(9)	3.56(7)	2.69(17)	0.2454(4)	1.469(4)	0.60(4)	19110
3.3000	0.1083(6)	3.88(3)	3.16(18)	0.2388(3)	1.504(2)	0.64(3)	41050
3.3050	0.0933(7)	4.43(5)	3.97(21)	0.2312(3)	1.551(3)	0.76(4)	39960
3.3100	0.0792(7)	4.82(5)	4.12(18)	0.2239(3)	1.586(3)	0.77(3)	42890
3.3200	0.0542(6)	5.88(4)	3.16(14)	0.2107(2)	1.668(2)	0.66(3)	44490
3.3300	0.0375(5)	6.13(3)	1.72(13)	0.2003(3)	1.722(2)	0.48(3)	25150

Table C.3: Mean values, errors and statistics of chiral observables for small quark masses for $N_\tau = 4$.

β	$\langle\bar{\psi}\psi\rangle_l$	χ_l^{con}	χ_l^{dis}	$\langle\bar{\psi}\psi\rangle_s$	χ_s^{conn}	χ_s^{disc}	# traj.
$N_\sigma^3 \times N_\tau = 16^3 \times 4$, $m_l a = 0.0065000$							
3.2800	0.1660(4)	2.37(1)	1.11(6)	0.2661(2)	1.352(1)	0.37(2)	27550
3.2850	0.1595(5)	2.50(2)	1.14(8)	0.2619(2)	1.371(2)	0.38(2)	19150
3.2900	0.1507(4)	2.60(1)	1.37(7)	0.2562(2)	1.402(2)	0.43(2)	30160
3.2950	0.1439(5)	2.74(2)	1.77(12)	0.2519(3)	1.424(2)	0.53(3)	24880
3.3000	0.1351(5)	2.85(1)	1.94(12)	0.2464(2)	1.452(2)	0.57(3)	36100
3.3050	0.1269(5)	3.01(4)	2.23(12)	0.2414(3)	1.471(5)	0.63(3)	40230
3.3100	0.1146(6)	3.22(4)	2.74(15)	0.2343(3)	1.515(5)	0.74(4)	40440
3.3150	0.1007(6)	3.53(3)	3.09(15)	0.2262(3)	1.555(4)	0.81(4)	45570
3.3200	0.0895(6)	3.80(2)	2.53(15)	0.2197(3)	1.597(3)	0.65(4)	33360
3.3300	0.0666(8)	4.29(2)	2.10(14)	0.2061(4)	1.678(3)	0.62(4)	18060
$N_\sigma^3 \times N_\tau = 16^3 \times 4$, $m_l a = 0.0130000$							
3.2800	0.1899(3)	1.98(0)	0.59(3)	0.2722(2)	1.317(1)	0.28(1)	20050
3.2900	0.1795(4)	2.07(0)	0.79(4)	0.2645(2)	1.350(1)	0.34(1)	21040
3.3000	0.1687(5)	2.18(1)	1.06(7)	0.2565(3)	1.387(3)	0.45(3)	18880
3.3050	0.1621(4)	2.27(1)	1.03(6)	0.2518(2)	1.413(4)	0.43(2)	32170
3.3100	0.1555(6)	2.31(1)	1.05(9)	0.2470(4)	1.429(2)	0.44(3)	16580
3.3200	0.1383(6)	2.55(2)	1.67(10)	0.2354(3)	1.492(4)	0.64(4)	28740
3.3250	0.1295(4)	2.72(3)	1.81(9)	0.2295(2)	1.530(13)	0.68(3)	54840
3.3300	0.1186(5)	2.81(1)	1.92(9)	0.2222(3)	1.566(2)	0.72(3)	50000
$N_\sigma^3 \times N_\tau = 16^3 \times 4$, $m_l a = 0.0260000$							
3.2800	0.2256(2)	1.62(0)	0.39(2)	0.2812(1)	1.267(1)	0.24(1)	20310
3.2900	0.2180(2)	1.66(0)	0.42(2)	0.2747(2)	1.290(1)	0.25(1)	23950
3.3000	0.2105(3)	1.71(0)	0.45(2)	0.2683(2)	1.314(2)	0.27(1)	15330
3.3050	0.2054(3)	1.73(0)	0.44(3)	0.2642(2)	1.331(1)	0.27(1)	22550
3.3100	0.2010(3)	1.76(1)	0.57(4)	0.2605(2)	1.346(4)	0.34(2)	20170
3.3200	0.1916(4)	1.82(0)	0.67(4)	0.2528(3)	1.378(1)	0.39(2)	20030
3.3300	0.1807(4)	1.90(0)	0.74(6)	0.2440(3)	1.417(2)	0.41(3)	23380
$N_\sigma^3 \times N_\tau = 32^3 \times 4$, $m_l a = 0.0032500$							
3.2800	0.1488(2)	0.00(0)	1.61(13)	0.2615(1)	0.000(0)	0.46(3)	20000
$N_\sigma^3 \times N_\tau = 16^3 \times 4$, $m_l a = 0.0008125$							
3.3000	0.0627(25)	0.00(0)	7.64(94)	0.2279(9)	0.000(0)	0.71(10)	6690
$N_\sigma^3 \times N_\tau = 8^3 \times 4$, $m_l a = 0.0008125$							
3.3000	0.0452(21)	0.00(0)	4.68(39)	0.2335(13)	0.000(0)	0.70(5)	25830
$N_\sigma^3 \times N_\tau = 8^3 \times 4$, $m_l a = 0.0016250$							
3.2800	0.1141(29)	0.00(0)	5.26(25)	0.2584(12)	0.000(0)	0.51(4)	38280
3.2900	0.0963(21)	0.00(0)	5.24(17)	0.2485(9)	0.000(0)	0.61(3)	40660
3.3000	0.0753(35)	0.00(0)	5.32(34)	0.2380(16)	0.000(0)	0.75(6)	40100
$N_\sigma^3 \times N_\tau = 8^3 \times 4$, $m_l a = 0.0032500$							
3.3000	0.0954(21)	0.00(0)	3.49(13)	0.2372(10)	0.000(0)	0.63(3)	30000

Table C.4: Mean values, errors and statistics of chiral observables for large quark masses and lattices for finite volume analysis for $N_\tau = 4$.

C.2 Goldstone Fit Results

	fit coeff. for $\mathcal{F}_{M_0}(H)$			fit coeff. for $\mathcal{F}_{M_s}(H)$			fit coeff. for $\mathcal{F}_{M_c}(H)$		
β	a	b	c	a	b	c	a	b	c
3.2800	1.87(1)	2.71(9)	0.40(8)	1.80(3)	3.30(16)	0.02(4)	1.95(0)	1.75(4)	0.00(4)
3.2850	1.64(0)	3.15(1)	0.13(1)	1.55(3)	3.88(10)	0.01(1)	1.74(1)	2.07(3)	-0.16(2)
3.2900	1.39(1)	3.60(5)	-0.12(4)	1.32(2)	4.25(11)	0.00(1)	1.45(1)	2.61(4)	-0.48(4)
3.2950	1.08(2)	4.27(9)	-0.53(8)	0.99(0)	5.01(2)	-0.00(0)	1.14(2)	3.22(9)	-0.84(7)
3.3000	0.65(4)	5.31(18)	-1.20(16)	0.58(2)	5.98(14)	-0.02(3)	0.67(5)	4.39(23)	-1.62(21)
3.3025	0.51(5)	5.44(21)	-1.22(20)	0.43(4)	6.21(17)	-0.02(4)	0.50(6)	4.58(27)	-1.68(25)
3.3050	0.26(6)	6.09(28)	-1.65(26)	0.19(5)	6.82(24)	-0.03(6)	0.24(7)	5.23(32)	-2.10(30)
3.3100	-0.08(5)	6.71(23)	-1.96(21)	-0.16(4)	7.48(19)	-0.02(4)	-0.16(6)	6.02(28)	-2.53(26)
3.3200	-0.46(5)	6.92(28)	-1.85(25)	-0.54(7)	7.70(35)	0.02(8)	-0.55(7)	6.03(35)	-2.22(32)
3.3300	-0.48(9)	5.78(62)	-0.65(70)	-0.54(10)	6.44(76)	0.28(32)	-0.48(11)	4.38(78)	-0.55(89)

Table C.5: Fit coefficients of the Goldstone fits for the order parameters M_0, M_s, M_c for $N_\tau = 4$

	fit coeff. for $\mathcal{F}_{M_0}(H)$			fit coeff. for $\mathcal{F}_{M_s}(H)$			fit coeff. for $\mathcal{F}_{M_c}(H)$		
β	a	b	c	a	b	c	a	b	c
3.4800	2.9(0)	2.5(0)	6.9(0)	2.8(0)	3.0(0)	1.6(0)	3.0(0)	1.0(0)	3.7(0)
3.4900	2.5(0)	2.6(2)	6.5(3)	2.5(0)	2.9(2)	1.4(1)	2.6(0)	1.2(2)	3.2(3)
3.4950	2.3(0)	2.5(0)	6.8(0)	2.2(0)	2.9(0)	1.6(0)	2.4(0)	1.2(0)	3.4(0)
3.5000	1.4(0)	5.6(0)	1.8(0)	1.4(0)	6.0(0)	-0.2(0)	1.5(1)	4.0(9)	-1.2(14)
3.5150	0.4(1)	6.8(7)	0.9(11)	0.3(1)	7.2(7)	-0.1(5)	0.2(1)	6.2(8)	-3.5(13)
3.5200	0.0(0)	7.5(0)	0.2(0)	-0.0(0)	7.9(0)	-0.3(0)	-0.1(0)	6.4(0)	-3.4(0)
3.5300	-0.7(0)	9.4(0)	-2.3(0)	-0.8(0)	9.7(0)	-1.3(0)	-0.9(0)	8.6(0)	-6.2(0)
3.5350	-0.6(0)	7.3(0)	1.3(0)	-0.7(0)	7.7(0)	0.3(0)	-0.7(0)	5.9(0)	-1.8(0)
3.5400	-0.5(0)	5.4(0)	3.8(0)	-0.5(0)	5.9(0)	1.2(0)	-0.6(0)	4.1(0)	0.6(0)

Table C.6: Fit coefficients of the Goldstone fits for the order parameters M_0, M_s, M_c for $N_\tau = 8$

C.3 Magnetic Equation of State Fit Results

			$N_\tau = 4$					$N_\tau = 8$			
O(N)	OP	$\tilde{H}$	χ^2	β_c	z_0	a_t	b_1	χ^2	β_c	z_0	a_t	b_1
O(1)	M_0	0.086	18.0	3.2973(15)	8.8(11)	2.0(3)	6.1(30)	18.4	3.5020(18)	4.8(7)	4.0(5)	-13.1(16)
O(1)	M_0	0.053	11.3	3.2986(5)	9.2(5)	2.1(1)	6.3(19)	18.0	3.5024(17)	4.8(7)	4.1(4)	-13.0(15)
O(1)	M_0	0.032	19.6	3.2978(5)	8.2(4)	2.2(1)	-1.6(23)	-	-	-	-	-
O(1)	M_s	0.086	9.5	3.2997(15)	9.7(14)	-1.9(3)	15.8(28)	13.2	3.4997(18)	4.4(6)	-4.6(4)	-4.1(15)
O(1)	M_s	0.053	9.8	3.2975(7)	8.6(6)	-2.1(2)	10.1(22)	13.2	3.5001(17)	4.4(6)	-4.5(4)	-4.0(14)
O(1)	M_s	0.032	17.1	3.2977(5)	8.0(4)	-2.2(1)	6.3(23)	-	-	-	-	-
O(1)	M_c	0.086	17.2	3.2965(19)	9.8(18)	0.4(4)	1.4(42)	24.0	3.4961(27)	4.9(12)	-1.8(7)	-15.0(25)
O(1)	M_c	0.053	14.2	3.2977(7)	10.2(8)	0.7(2)	0.1(27)	24.0	3.4967(25)	4.9(11)	-1.7(7)	-15.1(25)
O(1)	M_c	0.032	17.4	3.2982(4)	10.0(6)	0.7(1)	-2.9(28)	-	-	-	-	-
O(2)	M_0	0.086	13.3	3.2959(16)	7.6(9)	1.8(3)	9.4(26)	13.9	3.5001(18)	4.0(6)	3.5(5)	-9.5(14)
O(2)	M_0	0.053	12.4	3.2967(6)	7.5(4)	2.0(1)	6.7(18)	13.7	3.5005(17)	4.0(5)	3.5(5)	-9.4(14)
O(2)	M_0	0.032	16.9	3.2975(4)	7.5(3)	2.1(1)	3.8(21)	-	-	-	-	-
O(2)	M_s	0.086	6.4	3.2970(17)	7.9(11)	-2.5(3)	18.4(25)	10.3	3.4982(18)	3.7(4)	-5.1(4)	-0.8(13)
O(2)	M_s	0.053	6.3	3.2968(6)	7.6(4)	-2.4(1)	14.5(19)	10.3	3.4986(17)	3.7(4)	-5.0(4)	-0.8(13)
O(2)	M_s	0.032	14.2	3.2973(4)	7.2(3)	-2.4(1)	11.2(21)	-	-	-	-	-
O(2)	M_c	0.086	14.4	3.2954(21)	8.6(15)	0.2(4)	5.5(39)	21.3	3.4949(30)	4.1(10)	-2.2(8)	-11.8(24)
O(2)	M_c	0.053	11.9	3.2976(6)	9.3(6)	0.6(2)	5.8(25)	21.4	3.4955(28)	4.2(9)	-2.1(7)	-11.9(23)
O(2)	M_c	0.032	15.4	3.2982(4)	9.3(5)	0.7(1)	3.5(26)	-	-	-	-	-
O(4)	M_0	0.086	5.6	3.2943(11)	7.3(5)	1.5(2)	14.6(17)	11.2	3.4966(21)	3.6(5)	2.5(6)	-4.5(14)
O(4)	M_0	0.053	5.8	3.2960(4)	7.7(2)	1.9(1)	14.5(12)	11.1	3.4971(20)	3.6(5)	2.6(6)	-4.5(14)
O(4)	M_0	0.032	17.3	3.2968(4)	7.6(3)	1.9(1)	11.8(20)	-	-	-	-	-
O(4)	M_s	0.086	2.2	3.2941(12)	7.2(5)	-3.0(2)	22.1(16)	9.4	3.4947(22)	3.3(4)	-6.1(6)	3.9(13)
O(4)	M_s	0.053	2.2	3.2954(4)	7.4(2)	-2.8(1)	21.3(12)	9.4	3.4952(21)	3.4(4)	-6.0(5)	3.9(13)
O(4)	M_s	0.032	14.0	3.2964(5)	7.2(3)	-2.7(1)	18.5(20)	-	-	-	-	-
O(4)	M_c	0.086	9.0	3.2950(17)	8.8(11)	0.1(3)	12.1(31)	19.3	3.4917(38)	3.7(9)	-3.1(10)	-6.8(25)
O(4)	M_c	0.053	7.9	3.2972(5)	9.6(5)	0.5(1)	13.7(20)	19.5	3.4928(35)	3.8(9)	-2.9(9)	-6.9(24)
O(4)	M_c	0.032	13.2	3.2980(4)	9.7(4)	0.7(1)	12.2(23)	-	-	-	-	-

Table C.7: Fits of the order parameter to the O(N) scaling functions, linear terms from regular part included ($\mathcal{SD}_1$).

			$N_\tau = 4$						$N_\tau = 8$					
O(N)	OP	H	χ^2	β_c	z_0	a_t	b_1	b_3	χ^2	β_c	z_0	a_t	b_1	b_3
O(1)	M_0	0.086	14.0	3.2981(5)	9.2(3)	2.3(6)	6.6(30)	-2.5(87)	15.1	3.4996(15)	4.2(2)	1.6(6)	-12.2(16)	35.0(82)
O(1)	M_0	0.053	11.8	3.2981(2)	9.0(2)	2.9(2)	2.8(19)	-8.9(48)	15.0	3.4997(15)	4.2(2)	1.6(6)	-12.3(15)	35.6(82)
O(1)	M_0	0.032	18.5	3.2980(2)	8.3(2)	2.3(2)	-1.6(22)	-1.2(53)	-	-	-	-	-	-
O(1)	M_s	0.086	12.0	3.2981(5)	9.1(3)	-1.8(6)	14.6(28)	-6.9(89)	12.9	3.4999(15)	4.1(2)	-6.8(5)	-1.9(14)	35.0(77)
O(1)	M_s	0.053	10.1	3.2981(2)	8.9(1)	-1.3(2)	11.3(18)	-13.4(45)	12.7	3.4999(15)	4.1(2)	-6.9(5)	-1.9(14)	35.6(76)
O(1)	M_s	0.032	16.3	3.2980(2)	8.2(1)	-1.8(2)	6.9(20)	-6.1(50)	-	-	-	-	-	-
O(1)	M_c	0.086	31.6	3.2976(9)	10.0(7)	-0.6(8)	-0.4(51)	18.8(126)	30.3	3.4989(15)	4.8(4)	-5.3(9)	-10.4(23)	60.9(119)
O(1)	M_c	0.053	23.4	3.2979(4)	10.2(4)	0.4(3)	-3.6(31)	5.3(68)	29.8	3.4989(15)	4.8(4)	-5.3(9)	-10.4(23)	61.6(118)
O(1)	M_c	0.032	29.3	3.2979(3)	9.6(3)	0.0(3)	-7.8(31)	11.7(67)	-	-	-	-	-	-
O(2)	M_0	0.086	8.9	3.2980(4)	8.4(2)	2.7(4)	10.4(24)	-7.0(68)	13.9	3.4989(15)	3.7(2)	1.8(5)	-9.5(15)	26.7(77)
O(2)	M_0	0.053	7.4	3.2980(2)	8.3(1)	2.9(2)	8.3(16)	-10.0(38)	13.8	3.4989(15)	3.7(2)	1.8(5)	-9.5(15)	27.4(76)
O(2)	M_0	0.032	15.2	3.2979(2)	7.7(1)	2.3(2)	3.8(20)	-1.3(48)	-	-	-	-	-	-
O(2)	M_s	0.086	7.4	3.2980(4)	8.2(2)	-1.5(4)	18.2(23)	-10.8(69)	11.5	3.4993(15)	3.7(2)	-6.5(5)	0.8(14)	26.0(70)
O(2)	M_s	0.053	6.1	3.2980(1)	8.2(1)	-1.2(2)	16.7(14)	-14.3(35)	11.4	3.4994(15)	3.6(1)	-6.6(5)	0.8(14)	26.6(70)
O(2)	M_s	0.032	13.3	3.2979(2)	7.6(1)	-1.8(2)	12.2(19)	-6.1(45)	-	-	-	-	-	-
O(2)	M_c	0.086	22.8	3.2976(8)	9.2(5)	-0.3(7)	4.8(45)	14.0(105)	22.5	3.4993(15)	4.3(3)	-4.6(7)	-7.9(21)	50.4(99)
O(2)	M_c	0.053	18.3	3.2978(3)	9.3(3)	0.3(3)	2.4(28)	8.5(63)	22.1	3.4994(15)	4.3(3)	-4.7(7)	-7.9(20)	51.0(98)
O(2)	M_c	0.032	22.5	3.2979(3)	8.9(2)	0.0(3)	-1.0(28)	11.5(59)	-	-	-	-	-	-
O(4)	M_0	0.086	3.6	3.2979(3)	8.6(1)	3.1(3)	15.9(16)	-12.1(43)	16.9	3.4968(15)	3.5(2)	1.6(6)	-5.4(18)	21.0(85)
O(4)	M_0	0.053	3.6	3.2979(1)	8.7(1)	3.0(1)	16.8(11)	-11.3(26)	16.7	3.4968(15)	3.5(2)	1.5(6)	-5.4(17)	22.0(84)
O(4)	M_0	0.032	15.7	3.2978(2)	8.0(1)	2.3(2)	12.0(21)	-1.5(49)	-	-	-	-	-	-
O(4)	M_s	0.086	2.9	3.2979(2)	8.4(1)	-1.3(3)	23.3(14)	-14.0(42)	15.0	3.4980(15)	3.5(2)	-6.5(6)	4.8(16)	18.3(78)
O(4)	M_s	0.053	3.2	3.2979(1)	8.6(0)	-1.2(1)	25.0(11)	-15.4(25)	14.7	3.4981(15)	3.5(2)	-6.5(5)	4.9(16)	19.0(77)
O(4)	M_s	0.032	14.5	3.2978(2)	7.9(1)	-1.8(2)	20.2(20)	-6.3(48)	-	-	-	-	-	-
O(4)	M_c	0.086	12.1	3.2976(5)	9.7(3)	0.2(5)	12.5(34)	8.1(75)	17.5	3.4976(15)	4.1(2)	-4.7(6)	-4.3(19)	45.3(90)
O(4)	M_c	0.053	9.3	3.2978(2)	9.9(2)	0.6(2)	12.5(20)	3.0(43)	17.2	3.4976(15)	4.1(2)	-4.7(6)	-4.2(19)	46.2(89)
O(4)	M_c	0.032	15.1	3.2979(2)	9.4(2)	0.1(2)	9.1(24)	10.3(49)	-	-	-	-	-	-

Table C.8: Fits of the order parameter to the O(N) scaling functions, linear and cubic terms regular part included ($\mathcal{SD}_3$).

List of Figures

List of Tables

Bibliography

[1] A. Ali Khan *et al.* [CP-PACS Collaboration]. *Phys. Rev. D* **63** (2001) 034502
"Phase structure and critical temperature of two flavor QCD with renormalization group improved gauge action and clover improved Wilson quark action"

[2] C. R. Allton *et. al. Phys. Rev. D* **66** (2002) 074507
"QCD thermal phase transition in the presence of a small chemical potential"

[3] C. R. Allton *et. al. Phys. Rev. D* **71** (2005) 054508
"Thermodynamics of two flavor QCD to sixth order in quark chemical potential"

[4] S. Aoki *et al.* [JLQCD Collaboration]. *Phys. Rev. D* **57** (1998) 3910
"Scaling study of the two-flavor chiral phase transition with the Kogut-Susskind quark action in lattice QCD"

[5] S. Aoki *et al.* [JLQCD Collaboration]. *Nucl. Phys. B (Proc. Suppl.)* **63** (1998) 397
"Finite-temperature chiral transitions in QCD with the Wilson quark action"

[6] C. Aubin and C. Bernard. *Phys. Rev. D* **68** (2003) 034014
"Pion and kaon masses in staggered chiral perturbation theory"

[7] C. Aubin and C. Bernard. *Phys. Rev. D* **68** (2003) 074011
"Pseudoscalar decay constants in staggered chiral perturbation theory"

[8] C. Aubin *et al. Phys. Rev. D* **70** (2004) 094505
"Light hadrons with improved staggered quarks: Approaching the continuum limit"

[9] C. Aubin and C. Bernard. *Phys. Rev. D* **73** (2006) 014515
"Staggered chiral perturbation theory for heavy-light mesons"

[10] R. J. Baxter. *Academic Press Limited, London* (1982)
"Exactly Solved Models in Statistical Physics"

[11] C. Bernard *et al.* [MILC Collaboration]. *Phys. Rev. D* **61** (2000) 054593
"Critical behavior in $N_t = 4$ staggered fermion thermodynamics"

[12] C. Bernard *et al.* [MILC Collaboration]. *Phys. Rev. D* **71** (2005) 034504
"QCD thermodynamics with three flavors of improved staggered quarks"

[13] C. Bernard *et al. Phys. Rev. D* **75** (2007) 094505
"QCD equation of state with 2+1 flavors of improved staggered quarks"

[14] C. Bernard, C. DeTar, Z. Fu and S. Prelovsek. *Phys. Rev. D* **76** (2007) 094504
"Scalar meson spectroscopy with lattice staggered fermions"

[15] K. Binder. *Z. Phys. B - Cond. Matt.* **43** (1981) 119
"Finite Size Scaling Analysis of Ising Model Block Distribution Functions"

[16] K. Binder. *Phys. Rev. Lett.* **47** (1981) 693
"Critical Properties from Monte Carlo Coarse Graining and Renormalization"

[17] H. W. J. Blöte, E. Luijten and J. R. Heringa *J. Phys. A: Gen.* **28** (1995) 6289
"Ising universality in three dimensions: a Monte Carlo study"

[18] H. W. J. Blöte, J. R. Heringa, M. M. Tsypin *Phys. Rev. E* **62** (2000) 77
"Three-dimensional Ising model in the fixed magnetization ensemble: A Monte Carlo study"

[19] S. Borsanyi *et al. arXiv:hep-lat/1005.3508v1* (2010)
"Is there still any T_c mystery in lattice QCD?"

[20] E. Brézin, D. J. Wallace and K. G. Wilson. *Phys. Rev. B* **7** (1973) 232
"Feynman-Graph Expansion for the Equation of State near the Critical Point"

[21] F. R. Brown *et al. Phys. Rev. Lett.* **65** (1990) 2491
"On the existence of a phase transition for QCD with three light quarks"

[22] W. E. Caswell. *Phys. Rev. Lett.* **33** (1974) 244
"Asymptotic Behavior of Non-Abelian Gauge Theories to Two-Loop Order"

[23] M. Cheng *et al.* (RBC-Bielefeld). *Phys. Rev.* **D74** (2006) 054507
"The transition temperature in QCD"

[24] M. Cheng *et al.*, *Phys. Rev. D* **77** (2008) 014511
"The QCD equation of state with almost physical quark masses"

[25] M. Cheng *et al.* Phys. Rev. D **81** (2010) 054504
"Equation of state for physical quark masses"

[26] M. A. Clark and A. D. Kennedy. *Nucl. Phys. B (Proc. Suppl.)* **129** (2004) 850
"The RHMC Algorithm for 2 Flavors of Dynamical Staggered Fermions"

[27] J. Cleymans, H. Oeschler, K. Redlich and S. Wheaton. *Phys. Rev. C* **73** (2006) 034905
"Comparison of chemical freeze-out criteria in heavy-ion collisions"

[28] G. Cossu, C. Bonati, M. D'Elia, A. Di Giacomo and C. Pica. *PoS* **204** (2008)
"A test of first order scaling in $N_{\rm f} = 2$ QCD: a progress report"

[29] M. Creutz. *Cambridge University Press* (1983)
"Quarks, Gluons and Lattices"

[30] M. Creutz. *Phys. Lett. B* **649** (2007) 230
"Chiral anomalies and rooted staggered fermions"

[31] M. D'Elia, A. Di Giacomo and C. Pica. *Phys. Rev. D* **72** (2005) 114510
"Two Flavor QCD and Confinement"

[32] C. E. DeTar and U. M. Heller. *Eur. Phys. J. A* **41** (2009) 405
"QCD thermodynamics from the lattice"

[33] S. Duane, A. D. Kennedy, B. J. Pendleton and D. Roweth. *Phys. Lett. B* **195** (1987) 216
"Hybrid Monte Carlo"

[34] G. Ecker, J. Gasser, A. Pich and E. de Rafael. *Nucl. Phys. B* **321** (1989) 311
"The Role of Resonances in Chiral Perturbation Theory"

[35] J. Engels, S. Holtmann, T. Mendes, T. Schulze. *Phys. Lett. B* **492** (2000) 219
"Equation of State and Goldstone-mode effects of the three-dimensional O(2) model"

[36] J. Engels and T. Mendes. *Nucl. Phys. B* **572** (2000) 289
"Goldstone-mode effects and scaling function for the three-dimensional O(4) model"

[37] J. Engels, S. Holtmann, T. Mendes and T. Schulze. *Phys. Lett. B* **514** (2001) 299
"Finite-size-scaling functions for 3d O(4) and O(2) spin models and QCD"

[38] A. Cucchieri, J. Engels, S. Holtmann, T. Mendes and T. Schulze. *J. Phys. A: Math. Gen.* **35** (2002) 6517
"Universal amplitude ratios from numerical studies of the three-dimensional O(2) model"

[39] J. Engels, L. Fromme, M. Seniuch. *Nucl. Phys. B* **655** [FS] (2003) 277 "Numerical equation of state and other scaling functions from an improved three-dimensional Ising model"

[40] J. Engels, L. Fromme and M. Seniuch. *Nucl. Phys. B* **675** (2000) 533
"Correlation lengths and scaling functions in the three-dimensional O(4) model"

[41] J. Engels, S. Holtmann and T. Schulze. *Nucl. Phys. B* **724** (2005) 357 "Scaling and Goldstone effects in a QCD with two flavours of adjoint quarks"

[42] S. Ejiri, F. Karsch, E. Laermann, C. Miao, S. Mukherjee, P. Petreczky, C. Schmidt, W. Soeldner and W. Unger. *et al. Phys. Rev. D* **80** (2009) 094505
"Magnetic equation of state in (2+1)-flavor QCD"

[43] A. M. Ferrenberg and R. H. Swendsen. *Phys. Rev. Lett.* **61** (1988) 2635
"New Monte Carlo technique for studying phase transitions"

[44] A. M. Ferrenberg and R. H. Swendsen. *Phys. Rev. Lett.* **63** (1989) 1195
"Optimized Monte Carlo data analysis"

[45] E. Follana *et al. Phys. Rev. D* **75** (2007) 054502
"Highly improved staggered quarks on the lattice, with applications to charm physics"

[46] P. de Forcrand and O. Philipsen. *JHEP 0701* (2007) 077
"The chiral critical line of $N_{\rm f} = 2 + 1$ QCD at zero and non-zero baryon density"

[47] A. Frommer. *Nucl. Phys. B (Proc. Suppl.)* **53** (1997) 120
"Linear systems solvers - recent developments and implications for lattice computations"

[48] V. Furman and Y. Shamir. *Nucl. Phys. B* **439** (1995) 54
"Axial symmetries in lattice QCD with Kaplan fermions"

[49] J. Gasser and H. Leutwyler. *Phys. Rep.* **87** (1982) 77
"Quark Masses"

[50] J. Gasser and H. Leutwyler. *Ann. Phys.* **158** (1984) 142
"Chiral Perturbation Theory to One Loop"

[51] J. Gasser and H. Leutwyler. *Nucl. Phys. B* **250** (1985) 465
"Chiral Perturbation Theory: Expansion in the Mass of the Strange Quark"

[52] J. Gasser and H. Leutwyler. *Phys. Lett. B* **184** (1987) 83
"Light Quarks at Low Temperatures"

[53] J. Gasser and H. Leutwyler. *Phys. Lett. B* **188** (1987) 477
"Thermodynamics of Chiral Symmetry"

[54] J. Gasser and H. Leutwyler. *Nucl. Phys. B* **307** (1988) 763
"Spontaneously broken symmetries: Effective lagrangians at finite volume"

[55] S. Gavin, A. Gocksch and R. D. Pisarski. *Phys. Rev. D* **49** (1994) 3079
"QCD and the chiral critical point"

[56] M. Gell-Mann, R. J. Oakes and B. Renner. *Phys. Rev.* **175** (1968) 2195
"Behavior of Current Divergences under SU3xSU3"

[57] P. Gerber and H. Leutwyler. *Nucl. Phys. B* **321** (1989) 387
"Hadrons Below the Chiral Phase Transition"

[58] J. Goldstone, A. Salam and S. Weinberg. *Phys. Rev.* **172** (1962) 965
"Broken Symmetries"

[59] S. Gottlieb, W. Liu, D. Tousssaint, R. L. Renken and R. L. Sugar. *Phys. Rev. D* **35** (1987) 2531
"Hybrid-molecular-dynamics algorithm for the numerical simulation of quantum chromodynamics"

[60] A. Gray *et al. Phys. Rev. D* **72** (2005) 094507
"Y spectrum and m_b from full lattice QCD"

[61] R. B. Griffiths. *Phys. Rev.* **158** (1967) 176
"Thermodynamic Functions for Fluids and Ferromagnets near the Critical Point"

[62] D. J. Gross and F. Wilczek. *Phys. Rev.* **30** (1973) 1343
"Ultraviolet behavior of non-abeilan gauge theories"

[63] H. E. Haber. *Phys. Rev. Lett.* **46** (1981) 1497
"Thermodynamics of an Ultrarelativistic Ideal Bose Gas"

[64] H. E. Haber and H. A. Weldon. *Phys. Rev. D* **25** (1982) 502
"Finite-temperature symmetry breaking as Bose-Einstein condensation"

[65] M. Hasenbusch. *Phys. Lett. B* **519** (2001) 177
"Speeding up the hybrid-Monte Carlo algorithm for dynamical fermions"

[66] P. Hasenfratz and H. Leutwyler. *Nucl. Phys. B* **343** (1990) 241
"Goldstone Boson Related Finite Size Effects in Field Theory and Critical Phenomena with O(N) Symmetry"

[67] B. Sturm, U. M. Heller and F. Karsch. *Phys. Rev. D* **60** (1999) 114502
"Improved staggered fermion actions for QCD thermodynamics"

[68] S. Holtmann. *PhD Thesis* (2004)
"Goldstone-mode effects and critical behaviour of QCD with 2 light quark flavours"

[69] I. Horváth, A. D. Kennedy and S. Sint. *Nucl. Phys. B* **73** (1999) 834
"A New Exact Method for Dynamical Fermion Computations with Non-Local Actions"

[70] Y. Iwasaki, K. Kanaya, S. Kaya and T. Yoshié. *Phys. Rev. Lett.* **78** (1997) 179
"Scaling of chiral order parameter in two-flavor QCD"

[71] B. Jegerlehner. *hep-lat/9612014)* (1996)
"Krylov space solvers for shifted linear systems"

[72] L. P. Kadanoff. *Physics* **2** (1966) 263
"Scaling laws for Ising models near T_c"

[73] F. Karsch. *Phys. Rev. D* **49** (1994) 3791
"Scaling of pseudocritical couplings in two flavor QCD"

[74] F. Karsch and E. Laermann. *Phys. Rev. D* **50** (1994) 6954
"Susceptibilities, the specific heat and a cumulant in two flavor QCD"

[75] F. Karsch, E. Laermann and Ch. Schmidt. *Phys. Lett. B* **520** (2001) 41
"The chiral critical point in 3-flavour QCD"

[76] L. H. Karsten and J. Smit. *Nucl. Phys. B* **183** (1981) 103
"Lattice Fermions: Species Doubling, Chiral Invariance and the Triangle Anomaly"

[77] G. W. Kilcup and S. R. Sharpe *Nucl. Phys. B* **283** (1987) 493
"A Tool Kit For Staggered Fermions"

[78] J. Kogut and L. Susskind. *Phys. Rew. D* **11** (1975) 11
"Hamiltonian formulation of Wilson's lattice gauge theories"

[79] J. B. Kogut and D. K. Sinclair. *Phys. Rev. D* **70** (2004) 094501
"Finite temperature transition for 2-flavor lattice QCD at finite isospin density"

[80] J. B. Kogut and D. K. Sinclair. *Phys. Rev. D* **73** (2006) 074512
"Evidence for O(2) universality at the finite temperature transition for lattice QCD with 2 flavours of massless staggered quarks"

[81] H. A. Kramers and G. H. Wannier. *Phys. Rev.* **60** (1941) 252
"Statistics of the Two-Dimensional Ferromagnet. Part I"

[82] E. Laermann. *Nucl. Phys. Proc. Suppl.* **63** (1998) 895
"Thermodynamics using Wilson and staggered quarks"

[83] E. Laermann, A. Francis, S. Fröhlich and S. Mukherjee. *PoS (Lattice 2008)* **193** (2008)
"Recent results on screening masses"

[84] M. Le Bellac. Cambridge University Press (1996)
"Thermal Field Theory"

[85] W. Lee and S. R. Sharpe. *Phys. Rev. D* **60** (1999) 114503
"Partial flavor symmetry restoration for chiral staggered fermions"

[86] B. W. Lee. *Documents on Modern Physics* (1972) Gordon and Breach Science Publishers
"Chiral Dynamics"

[87] H. Leutwyler. *Phys. Lett. B* **189** (1987) 197
"Energy Levels of Light Quarks Confined to a Box"

[88] H. Leutwyler. *Nucl. Phys. B (Proc. Suppl.)* **4** (1988) 248
"QCD: Low Temperature Expansion and Finite Size Effects"

[89] M. Marchi and E. Meggiolaro. *Nucl. Phys. B* **665** (2003) 425
"Reviewing the problem of the U(1) axial symmetry and the chiral transition in QCD"

[90] Ulf-G. Meißner. *Rep. Prog. Phys.* **56** (1993) 903
"Recent developments in chiral perturbation theory"

[91] C. Miao. *PhD Thesis* (2008)
"The QCD equation of state at high temperature and small density from the lattice"

[92] C. J. Morningstar and M. Peardon. *Phys. Rev. D* **60** (1999) 034509
"Glueball spectrum from an anisotropic lattice study"

[93] S. Naik. *Nucl. Phys. B* **316** (1989) 238
"On-shell improved lattice action for qcd with suskind fermions and asymptotic freedom scale"

[94] Y. Nambu and G. Jona-Lasinio. *Phys. Rew.* **122** (1961) 345
"Dynamical Model of Elementary Particles Based on an Analogy with Superconductivity"

[95] R. Narayanan and H. Neuberger. *Phys. Rev. Lett.* **71** (1993) 3251
"Chiral fermions on the lattice"

[96] H. B. Nielsen and M. Ninomiya. *Phys. Lett. B* **105** (1981) 219
"No go theorem for regularizing chiral fermions"

[97] L. Onsager. *Phys. Rev.* **65** (1981) 117
"Crystal Statistics. I. A Two-Dimensional Model with an Order-Disorder Transition"

[98] K. Orginos, D. Toussaint and R. L. Sugar [MILC Coll]. *Phys. Rev. D* **60** (1999) 054503
"Variants of fattening and flavor symmetry restoration"

[99] A. Peikert, B. Beinlich, A. Bicker, F. Karsch and E. Laermann. *Nucl. Phys. Proc. Suppl.* **63** (1998) 895
"Staggered fermion actions with improved rotational invariance"

[100] R. D. Pisarski and F. Wilczek. *Phys. Rev. D* **29** (1984) 338
"Remarks on the chiral phase transition in chromodynamics"

[101] H. D. Politzer. *Phys. Rev.* **30** (1973) 1346
"Reliable perturbative results for strong interactions"

[102] S. Prelovsek. *Phys. Rev. D* **73** (2006) 014506
"Effects of staggered fermions and mixed actions on the scalar correlator"

[103] K. Rajagopal and F. Wilczek. *Nucl. Phys. B* **399** (1993) 395
"Static and dynamic critical phenomena at a second order QCD phase transition"

[104] H. J. Rothe. *World Scientific Lecture Notes in Physics Vol.* **74** (2005)
"Lattice Gauge Theories"

[105] S. Scherer. *MKPH-T-02-09* (2002)
"Introduction to Chiral Perturbation Theory"

[106] Ch. Schmidt *et. al. Nucl. Phys. B (Proc. Suppl.)* **119** (2003) 517
"The quark mass and μ dependence of the QCD chiral critical point"

[107] T. Schulze. *PhD Thesis* (2004)
"Goldstone-Effekte und Skalenfunktion in der QCD mit zwei leichten adjungierten Quark-Flavours"

[108] E. Seiler. *arXiv:hep-th/0312015v1* (2003)
"The Case Against Asymptotic Freedom"

[109] J. C. Sexton and D. H. Weingarten. *Nucl. Phys. B* **380** (1992) 665
"Hamiltonian evolution for the hybrid Monte Carlo algorithm"

[110] A. V. Smilga and J. Stern. *Phys. Lett. B* **318** (1993) 531
"On the spectral density of Euclidean Dirac operators in QCD"

[111] A. V. Smilga and J. J. M. Verbaarschot. *Phys. Rev. D* **54** (1996) 1087
"Scalar susceptibility in QCD and the multiflavor Schwinger model"

[112] R. Sommer. *Nucl. Phys. B* **411** (1994) 839
"A new way to set the energy scale in lattice gauge theories and its application to the static force and α_s in SU(2) YangMills theory"

[113] E. J. Squires. *Rep. Prog. Phys.* **42** (1979) 1187
"Remarks on the chiral phase transition in chromodynamics"

[114] K. Symanzik. *Nuc. Phys. B* **226** (1983) 187
"Continuum Limit and Improved Action in Lattice Theory"

[115] G. 't Hooft. *Phys. Rev. D* **14** (1976) 3432
"Computation of the Quantum Effects due to a Four-Dimensional Pseudoparticle"

[116] E. Vicari. *PoS LAT2007* **023** (2007)
"Critical Phenomena and renormalization-group flow of multi-parameter Φ^4 field thoeries"

[117] D. J. Wallace and R. K. P. Zia. *Phys. Rev. B* **12** (1975) 5340-5342
"Singularities induced by Goldstone modes"

[118] F. J. Wegner. *J. Math. Phys.* **12** (1971) 2259
"Duality in Generalized Ising Models and Phase Transitions without Local Order Parameters"

[119] K. G. Wilson. *Phys. Rev. B* **4** (1971) 3174
"Renormalization Group and Critical Phenomena. I. Renormalization Group and the Kadanoff Scaling Picture"

[120] K. G. Wilson. *Phys. Rev. B* **4** (1971) 3184
"Renormalization Group and Critical Phenomena. II. Phase-Space Cell Analysis of Critical Behavior"

[121] K. G. Wilson and M. E. Fisher. *Phys. Rev. Lett.* **28** (1972) 240
"Critical Exponents in 3.99 Dimensions"

[122] K. G. Wilson. *Phys. Rev. Lett.* **28** (1972) 548
"Feynman-Graph Expansion for Critical Exponents"

[123] K. G. Wilson and J. Kogut. *Phys. Rep.* **12** (1974) 75
"The Renormalization Group and the ϵ Expansion"

[124] K. G. Wilson. *Phys. Rev. D* **10** (1974) 2445
"Confinement of Quarks"

[125] K. G. Wilson. *New Phenomena in Subnuclear Physics A, Plenum Press, New York* (1974) 69
"Proceedings of the First Half of the 1975 International School of Subnuclear Physics, Erice, Sicily"

[126] R. J. Zinn Justin. *Clarendon Press, Oxford* (1989)
"Quantum Field Theory and Critical Phenomena"